The Role Of Superficial Geology In Controlling Groundwater Recharge In Drylands

Emanuel Zarate

Supervisor: Dr. Mark Cuthbert

Department of Earth and Environmental Sciences
Cardiff University

This dissertation is submitted for the degree of
Doctor of Philosophy

Cardiff October 2023

Summary

Groundwater is often the principal and most reliable source of water in drylands. Improved understanding and quantification of groundwater recharge is critical to water security in these regions. The structure and hydraulic properties of superficial geology likely plays an important role in governing the spatiotemporal complexity of groundwater recharge in drylands. However, these hydraulic processes are poorly understood and/or quantified. To elucidate the role superficial geology plays in controlling groundwater recharge, a combination of analyses and interpretation of field data, synthesis of literature and numerical simulations were performed. Conceptual models of groundwater recharge were developed from the results of geophysical surveys conducted in semi-arid Tanzania and combined hydrometric and geophysical investigations from an ephemeral stream in semi-arid Australia. The field investigations show that (1) 'windows' of superficial sand deposits occurring within layers of clay underlying intermittent rivers and ephemeral streams (IRES) provide pathways for potential focused recharge (2) these deposits act as collectors and stores that redistribute infiltrated water to zones of active faulting and/or similar permeable pathways, enabling recharge to the regional water-table and (3) a combination of the permeability contrast between these deposits and surrounding geology, and their volume controls this redistribution. The findings from the two field sites were combined with literature on drylands to propose a new framework for understanding recharge in drylands. The new framework groups recharge controls into a hierarchy of processes that encapsulate their role in converting rainfall to recharge. A series of numerical simulations were conducted using a distributed model representing an idealised IRES system with heterogeneous geology. The results quantify the sensitivity of geological and climatic controls on IRES systems predominant in the framework. This framework provides a 'springboard' for more accurately mapping, quantifying, and forecasting groundwater recharge in drylands with variable geology.

Declaration

I hereby declare that except where specific reference is made to the work of others, the contents of this dissertation are original and have not been submitted in whole or in part for consideration for any other degree or qualification in this, or any other university. This dissertation is my own work and contains nothing which is the outcome of work done in collaboration with others, except as specified in the Author contributions (below) and Acknowledgements. This dissertation contains fewer than 80,000 words including appendices, bibliography, footnotes, tables and equations.

Author contributions

Chapter 2 has been published as:
Zarate, E., Hobley, D., MacDonald, A.M., Swift, R.T., Chambers, J., Kashaigili, J.J., Mutayoba, E., Taylor, R.G. and Cuthbert, M.O., 2021. The role of superficial geology in controlling groundwater recharge in the weathered crystalline basement of semi-arid Tanzania. Journal of Hydrology: Regional Studies, 36, p.100833.

In Tanzania, field support was provided by Edmund Mutayoba.

Chapter 3 is to be submitted for publication as: Zarate, E., Andersen, M. S.,Rau, G. C.,Acworth, R. I.,Rutlidge, H.,MacDonald, A. M., Cuthbert, M.O. How alluvial storage controls spatiotemporal water balance partitioning in intermittent and ephemeral stream systems

Geophysical data analysed and presented in Chapter 3 was collected by Dr. Mark Cuthbert and Prof. Ian Acworth.
Hydrometric data was provided by Dr. Martin Andersen from UNSW with thanks.

While both papers have multiple co-authors, the data analysis, conceptual model development, and writing of the manuscript was entirely my own work. The co-authors offered recommendations and feedback on the manuscript and on emergent issues during the analysis, which did not exceed the usual assistance given from supervisors.

Emanuel Zarate
October 2023

Acknowledgements

I would like to think of my PhD as one big adventure. As I reach the terminus point of my journey, I can't help but reminisce about all the wonderful people that I've met, and have helped me, along the way.

Over the past 4 years, Mark has been my supervisor, but in reality he has been much more than this. Mark's enthusiasm, conceptual brilliance and eye for detail has been instrumental in guiding me through this work, and is an inspiration as an aspiring hydrogeologist. He's always been there when I needed a hand, a pick me up or some encouragement. I honestly couldn't have asked for a better supervisor, and more importantly, I'm grateful to have gained a lifelong friend.

Thank you to Alan MacDonald for his constant support throughout the thesis, his encyclopedic knowledge of African hydrogeology, and his company in Tanzania and Edinburgh. Looking forward to going mountain biking together again!

A big thank you to Dan Hobley for his mentorship and co-supervision during the start of the thesis, and a big thank you to Adrian Chappell for stepping up and filling in as co-supervisor midway through my PhD. His geomorphic expertise has been instrumental, and I always learnt something new and exciting every time I spoke with Adrian.

At the BGS, Jon Chambers geophysical knowledge was a great addition to the Tanzania work, and a big thank you to Russel Swift for putting up with my stupid questions, and his logistical wizardry in getting geophysical equipment to Tanzania.

During my time in Tanzania, I would like to thank Richard Taylor and David Seddon for showing me the ins and outs of the Makutapora research, and to Catherine Mwihimbo for being my guide in the wellfield. A big thank you to the wellfield staff that helped me during my fieldwork, to Abdulla for driving me around, and to Edmund for his company and field support.

My time in Australia was the highlight of my PhD, and this was all down to the people that welcomed me there. Thank you to Martin Andersen, whom in aussie terms can best be defined as a 'bloody legend', for being the most welcoming host. I enjoyed our fireside chats, and Martins knowledge of the Maules Creek catchment has been invaluable. Thank you to all the staff at UNSW who helped with various forms of data collection and interpretation:

To Fang Bian, who, during lockdown, while we were at home, was braving the floods/fires and wildlife to collect data from Middle Creek. To Helen Routlidge and Gabriel Rau for our discussions and insights into the data, and to Ian Acworth for collecting and supporting in interpretation of the geophysical data.

A big shout out to the PhD community at UNSW, particularly Nadav, Katie, Margot and Dan for 'showing me the ropes' and getting me outside and introduced me to a lovely bunch of climbing people. Thank you to Stefano, Raimundo and Killian for showing me what peak surfing prowess looks like, Hiruni, for introducing me to ogalos, Fred for letting me touch his beard, and to Reilly, Aditiya, Tom, Maryam and Kate who all made me feel so welcome. Big mention to the Narabeen locals, Cutting and the two Chazzas for making me feel like I was in living in London with the beach. Finally, thank you to Hugo, the definition of a soul surfer, and one of the nicest people I've ever met. See you soon in the line-up boys.

I would not have been in Cardiff if it wasn't for McGuckin, so thanks John for your craic over the years! To the cohort I started this journey with: Ana, Erin and Ben. It's been a long time coming but it's been wonderful to share these experiences with you. Thanks to Charlie for his company during our weekly rounds of golf and a big thank you to Ernest, Panton, Aiden, Lizzo, Freddy and Max for making my time in Cardiff an absolute blast and for being such great friends during my time here.

A big thank you to Andres Quichimbo for letting me pick his modelling brain, and for helping me with my salsa dancing.

To all my friends at home: Thanks, Swart for keeping me company in Cardiff, enjoyed our board game sessions, to the Kuzi gang: Adam, Charlie, Yas and Yamin, and to Nico for moving to the UK just to hang out with me

Thank you to my parents, George and Josefina, who I dedicate this PhD to. Their love and support over the years has been a constant source of warmth. Last but not least I couldn't have completed this thesis without my best friend and partner in crime Cara – thanks for putting up with me, always being there for me, making me smile when I'm down.

I would like to dedicate this thesis to my loving parents ...

Table of contents

List of figures

List of tables

Chapter 1

Introduction

1.1 Background and motivation

1.1.1 Drylands and groundwater

Drylands (subhumid to hyper-arid regions) cover 45% of the earth's surface (Prăvălie, 2016) and support a population of around 2 billion people, 90% of whom live in low-or middle-income countries (UN, 2017). Characterized by large atmospheric water demands and temperature contrasts (Cherlet et al., 2018), surface water is often seasonally or perennially absent in drylands (Wheater et al., 2008). Due to its widespread distribution and relative resilience to climate variability, groundwater is often the only viable source of freshwater in these regions (Cuthbert et al., 2017; Dai, 2013; Feng and Fu, 2013; Huang et al., 2016).

Demands on dryland groundwater resources are likely to increase in the coming decades (Gleeson et al., 2012; Taylor, 2014; Wada et al., 2010) due to rising population (DESA, 2017), human activity (C. Chen et al., 2019; Wada et al., 2013) and climate change (Abel et al., 2020; Berdugo et al., 2020; J. Huang et al., 2017; Taylor et al., 2013a). These additional abstractions could lead to the unsustainable development of groundwater, and thus the understanding and quantification of groundwater recharge in dryland areas is a key uncertainty for current and future groundwater management (Gleeson et al., 2020; Keshavarzi et al., 2017; Meixner et al., 2016).

1.1.2 Groundwater recharge in drylands

Global and continent scale models of recharge that exist in the literature (e.g. P. Döll and Fiedler, 2008) have proved useful in providing a first estimate of the likely magnitude

of groundwater recharge. However, these models omit key dryland-specific hydrological processes in their computation (J. Huang et al., 2017; Quichimbo et al., 2021), and have been shown to be unreliable at predicting long-term patterns of groundwater recharge when compared to ground-based estimates (West et al., 2023), and variations in terrestrial water storage measured using GRACE (Scanlon et al., 2018).

Recent continental to global scale analyses (MacDonald et al., 2021; Moeck et al., 2020; Mohan et al., 2018) have highlighted broad associations between groundwater recharge and both climate and land-cover characteristics but provide limited insight to the recharge processes themselves (Jasechko and Taylor, 2015; MacDonald et al., 2021). These knowledge gaps are most acute in drylands, due to their unique hydrological characteristics (Cuthbert et al., 2019b; Somaratne and Smettem, 2014).

Groundwater recharge in drylands occurs through two main mechanisms: *diffuse* and *focused recharge*. These processes have seen many iterations of varying definitions and nomenclature in the literature. For example, an important synthesis of conceptual models for groundwater recharge was proposed by Lloyd, 1986 based upon observations of processes in various arid zones including northern Chile and the Middle East. These processes are illustrated in Figure 1.1 and form much of the basis for recharge studies by later workers (J J de Vries and Simmers, 2002; Scanlon et al., 2006).

Lerner et al., 1990 and Simmers, 2003 use the term direct recharge to refer to any recharge occurring diffusively over large areas due to infiltration from precipitation which has become synonymous conceptually to the mechanism of *diffuse recharge* (Healy and Scanlon, 2010). In contrast, the term indirect recharge refers to recharge that is more focused spatially as a result of losses from a surface water body which has become synonymous to the mechanism of *focused recharge* (Healy and Scanlon, 2010). Lerner et al., 1990 also distinguish two types of indirect recharge mechanisms: (i) localised recharge, to describe the recharge from ponded water bodies, in the absence of well-defined channels and (ii) indirect recharge to describe the recharge processes through the beds of surface water courses.

Following Healy and Scanlon, 2010, I use the term *focused recharge* to refer to any recharge which involves ponded or flowing surface-water that subsequently infiltrates to the water table. For any other recharge which is more widely distributed in the landscape I use the term *diffuse recharge*, to refer to any recharge that results from precipitation flowing vertically through the unsaturated zone to the water table.

Many field studies have yielded important insights into dryland-specific recharge processes (de Vries and Simmers, 2002; Simmers, 1997). Scanlon et al., 2006 reviewed 140 such recharge studies in dryland regions from all continents and noted the significant contribution

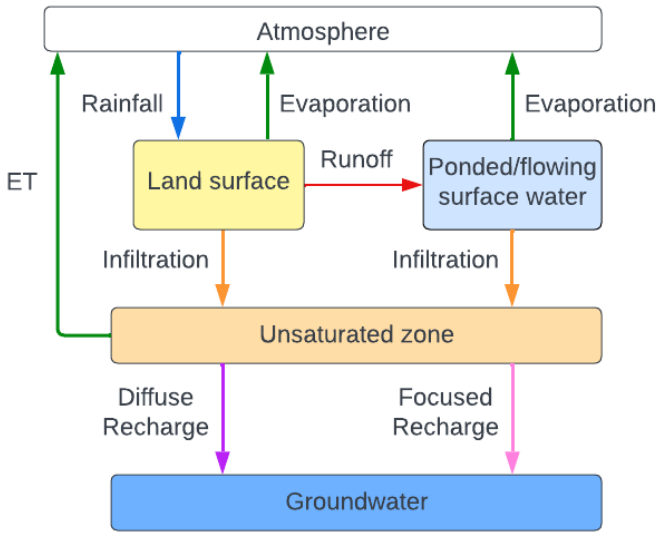

Fig. 1.1 Current understanding of recharge process in drylands

of focused recharge from ephemeral streams and fractured systems in accounting for the spatial variability in recharge rates. This was elaborated by Shanafield and Cook 2014, whose review of transmission losses in intermittent rivers and ephemeral streams systems (termed IRES in this thesis, after Messager et al., 2021), highlighted the importance of these systems in delivering focused recharge to dryland aquifers. More recently (Cuthbert et al., 2019) used multi-decadal groundwater level timeseries in conjunction with local knowledge to develop site specific conceptual models which allowed the authors to demonstrate the dominance of episodic, focused recharge processes with increasing aridity in sub-Saharan Africa.

In a recent review of groundwater recharge and climate change in the western United States, Meixner et al., 2016 hypothesised that, while focused recharge may increase due to potential changes in the magnitude and frequency of extreme precipitation events, the lack of understanding of the dominant controls behind this process creates difficulty in predicting this response. Yet, despite its present and future importance, the spatio-temporal controls on focused groundwater recharge in drylands, and their sensitivity to environmental change, are currently poorly understood (Acworth et al., 2016; Cuthbert et al., 2019a; Scanlon et al., 2006; Taylor et al., 2013a; Wheater et al., 2010)

Assessing the controls on groundwater recharge in drylands, and particularly with respect to focused recharge, has proven challenging. Many of the common methods used for monitoring and data collection in perennial river systems are not appropriate in dryland

IRES, where monitoring infrastructure (if present) often fails or is destroyed due to the flashy and extreme nature of runoff events (Acworth et al., 2016b; El Khalki et al., 2020; Pilgrim et al., 1988; Shanafield et al., 2021). These challenges have slowed the development and understanding of the physical processes that underpin the various fluxes and interactions between surface water and groundwater in drylands (Cuthbert et al., 2019b; Green et al., 2011).

1.1.3 Superficial geology and recharge

One such factor, the geometry and hydraulic properties of superficial deposits, has been shown to moderate potential recharge to underlying bedrock aquifers in temperate climates (Griffiths et al., 2011; Misstear et al., 2009) and local-scale configurations of these deposits provide recharge pathways through high permeability layers (Cuthbert et al., 2009). In drylands, heterogeneities in the hydraulic properties and structure of superficial deposits have been hypothesised to influence the subsurface dynamics of groundwater recharge to deeper aquifers (Acworth et al., 2020; Dvory et al., 2016; Goodrich et al., 2018; Rau et al., 2017). For example, marked temporal and spatial variability in the hydraulic conductivities of floodplain and streambed deposits has been shown to control on surface-groundwater interactions within dryland IRES (Costa et al., 2013; Dahan et al., 2008a; Flinchum et al., 2020; McCallum et al., 2014). Within such systems, there is growing literature that highlight the importance transmission losses in contributing to groundwater recharge (Shanafield et al., 2021) and subsurface heterogeneity has been demonstrated to play a key role in controlling subsurface flow and streamflow generation (Costigan et al., 2016; Gutiérrez-Jurado et al., 2019; Newman et al., 2006).

Several studies have shown the influence of bedrock geology as a major control on subsurface hydrologic flow paths (Huntington and Niswonger, 2012; Nimmo et al., 2017; Owen and Dahlin, 2005), and other studies have shown that contrasting layers of superficial deposits promote subsurface flow by restricting vertical flow and favouring the development of a perched aquifer (Bourke et al., 2021; Maxwell and Kollet, 2008; Villeneuve et al., 2015). As such, the magnitude and/or timing of *actual recharge* to the water table may differ considerably from the distribution of infiltrated water that has percolated below the root zone, which I refer to in this thesis as *potential recharge* (Callegary et al., 2007). Furthermore, *actual recharge* may occur as bypass flow via preferential pathways: macropores, fractures, faults which 'bypass' the storage of variably saturated porous matrix materials (Beven, 2012).

However, while these studies have highlighted the role of superficial geology in recharge and subsurface distribution, very few have combined quantitative detailed observations of

superficial geological structure with long term hydrometric monitoring with the goal of better classifying and quantifying the to better understand how configurations of superficial geology can control the spatiotemporal complexity in groundwater recharge processes in these regions. Without this process understanding, it is impossible to quantify the sensitivity of these processes to environmental and anthropogenic change in drylands with varying geology. This is the major research gap identified from the literature which this thesis addresses. Within each chapter of the thesis, a deeper and more specific consideration of the literature on each sub-theme is presented, and within, which the research was carried out.

1.2 Scope and Objectives

This PhD thesis therefore aims to better understand and quantify the role of superficial geology in controlling groundwater recharge in drylands. To address the shortcomings in existing literature identified above, I set the following specific objectives:

- **Objective 1**: To make detailed quantitative observations of superficial geological structure in drylands to better understand the likely flowpaths and processes controlling dryland groundwater recharge.
- **Objective 2**: To elucidate how configurations of superficial geology control the variability of water balance partitioning in dryland IRES.
- **Objective 3**: To produce a conceptual model, applicable to a wide range of dryland settings, that illustrates how superficial geology controls groundwater recharge between and within dryland catchments.
- **Objective 4**: To quantify the sensitivity of focused recharge in dryland IRES to variations in superficial geology and to changes in environmental conditions.

1.3 Thesis Outline

To achieve these objectives, I have structured the thesis into the following six chapters:

- **Chapter 1** (current chapter) provides the introduction, context, objectives of the present research, and the structure of the thesis.
- **Chapter 2** addresses **Objective 1** by presenting the results of a series of geophysical investigations using Electrical Resistivity Tomography (ERT) to determine the

geometry and inter-relationships between superficial deposits, underlying geology and fracture systems in the intensively monitored and pumped groundwater system in the Makutapora wellfield, central Tanzania. Based on these results, a series of local-scale conceptual hydrogeological models were produced and collated to generate a 3D conceptual model of groundwater recharge to the wellfield.

- **Chapter 3** addresses **Objective 2** by combining a new and unusually rich set of streamflow and groundwater observations from the Maules Creek Catchment, New South Wales (NSW), Australia, with targeted geophysical characterisation of the subsurface, to elucidate how configurations of superficial geology surrounding dryland IRES control the variability in streamflow and groundwater responses. A conceptual model of water balance partitioning with varying geology, that is applicable to a wide range of dryland settings, is also presented in this chapter.

- **Chapter 4** addresses **Objective 3** by utilizing the findings of Chapters 2 and 3, with a synthesis of current literature to propose a novel conceptual model of groundwater recharge in drylands that identifies controls on focused and diffused recharge, with an emphasis on the role of superficial geology, and groups them into a hierarchy of processes that encapsulates their role in converting rainfall into recharge. Based on this model, I group these controls based on their likelihood of occurrence within a geomorphic model to explore variations of recharge processes within the catchment.

- **Chapter 5** addresses **Objective 4** by presenting the results of a series of 3-D numerical simulations using a physically based distributed model to better understand the sensitivity of water balance components within an idealised IRES system to changes in geological controls and climate forcing.

- **Chapter 6** presents a summary, general conclusions of the thesis, and recommendations for future research.

Chapter 2

The role of superficial geology in controlling groundwater recharge in the weathered crystalline basement of semi-arid Tanzania

2.1 Introduction

Groundwater supports livelihoods and poverty alleviation throughout sub-Saharan Africa (Braune and Xu, 2010; Cobbing and Hiller, 2019; Gaye and Tindimugaya, 2019), particularly in semi-arid regions (Xu and Beekman, 2019), and groundwater use is increasing in rural (Baguma et al., 2017) and urban areas (Lapworth et al., 2017; Thompson et al., 2000). These trends are anticipated to continue due to population growth (UN, 2017), urbanisation (Saghir and Santoro, 2018), increased agricultural use (Villholth, 2013), changes to agricultural activity (MacDonald et al., 2012) and climate change (Pörtner et al., 2022).

The Makutapora wellfield is presently the sole source of Dodoma's municipal and industrial water supply and in 2016 supplied the city with an average of 50,000 m^3 day^{-1} of freshwater (DUWASA, 2017). Groundwater abstraction in the wellfield has increased from 0.1 to 1.5 million m^3 per month and, despite having exceeded previous estimates of its maximum sustainable yield, groundwater levels are currently higher than they were in the 1990s and roughly the same as they were prior to development (Seddon, 2019). Long-term groundwater level data from the wellfield indicates that intensive groundwater abstraction is replenished on a decadal timescale by episodic recharge events during exceptional seasonal

rainfalls associated with El Niño events, interrupting multi-annual recessions in groundwater levels (Cuthbert et al., 2019b; Kolusu et al., 2019; Taylor et al., 2013b).

Perceptions regarding the predominant process by which groundwater recharge to the Makutapora wellfield occurs have changed over time. Groundwater recharge was initially considered to be primarily diffuse (Nkotagu, 1996; Shindo, 1989) with soil macropores transmitting the majority of infiltrating water through the unsaturated zone (Shindo, 1990). More recently, through empirical analyses of long term groundwater and stream stage monitoring observations at the wellfield, Seddon et al., 2021 and Taylor et al., 2013b have shown hydrometric evidence of focused recharge from intensive rainfall within the wellfield. However, these studies provide little insight into the potential physical processes and flowpaths that could transmit surface water to groundwater systems via focused recharge processes.

The objectives of this chapter are thus to explore the potential physical basis for groundwater recharge by determining the geometry and inter-relationships between superficial deposits, underlying geology, and fracture systems in the intensively monitored and pumped groundwater system of the Makutapora wellfield in the Little Kinyasungwe River Catchment of central Tanzania. This system comprises a weathered and fractured crystalline basement aquifer system that is overlain in part by low permeability smectitic clays and, despite intensive groundwater abstraction, is replenished on a decadal timescale by episodic recharge events (Taylor et al., 2013b). To accomplish this, I conducted a series of geophysical investigations using Electrical Resistivity Tomography (ERT) and, in conjunction with borehole data and field observations (see Fig. A1), identified various geoelectrical structures and correlated these with interpreted subsurface lithology. Based on these findings, I present a series of local- and basin-scale conceptual models that identify multiple potential recharge pathways, illustrating how superficial geology may control focused recharge in the Little Kinyasungwe River Catchment. Although my study was not designed to quantitatively determine the relative proportions of diffuse and focused recharge in the Little Kinyasungwe River Catchment, my conceptual models provide a first step in quantifying recharge in the study area in the future, and I propose these models will be transferable to other dryland regions globally.

2.2 Methods

2.2.1 Site description

The Makutapora Wellfield, situated within the Little Kinyasungwe River Catchment (Figure 2.1), is underlain by the fractured crystalline basement of the Dodoma craton in central Tanzania (Kashaigili et al., 2003) and is approximately 20 km north of the capital city, Dodoma. The catchment occupies an area of 698 km^2 upstream of the Chihanga flow gauge located (Figure 2.1) at the catchment outlet and forms the upper section of the River Wami Basin. (Shindo, 1989).

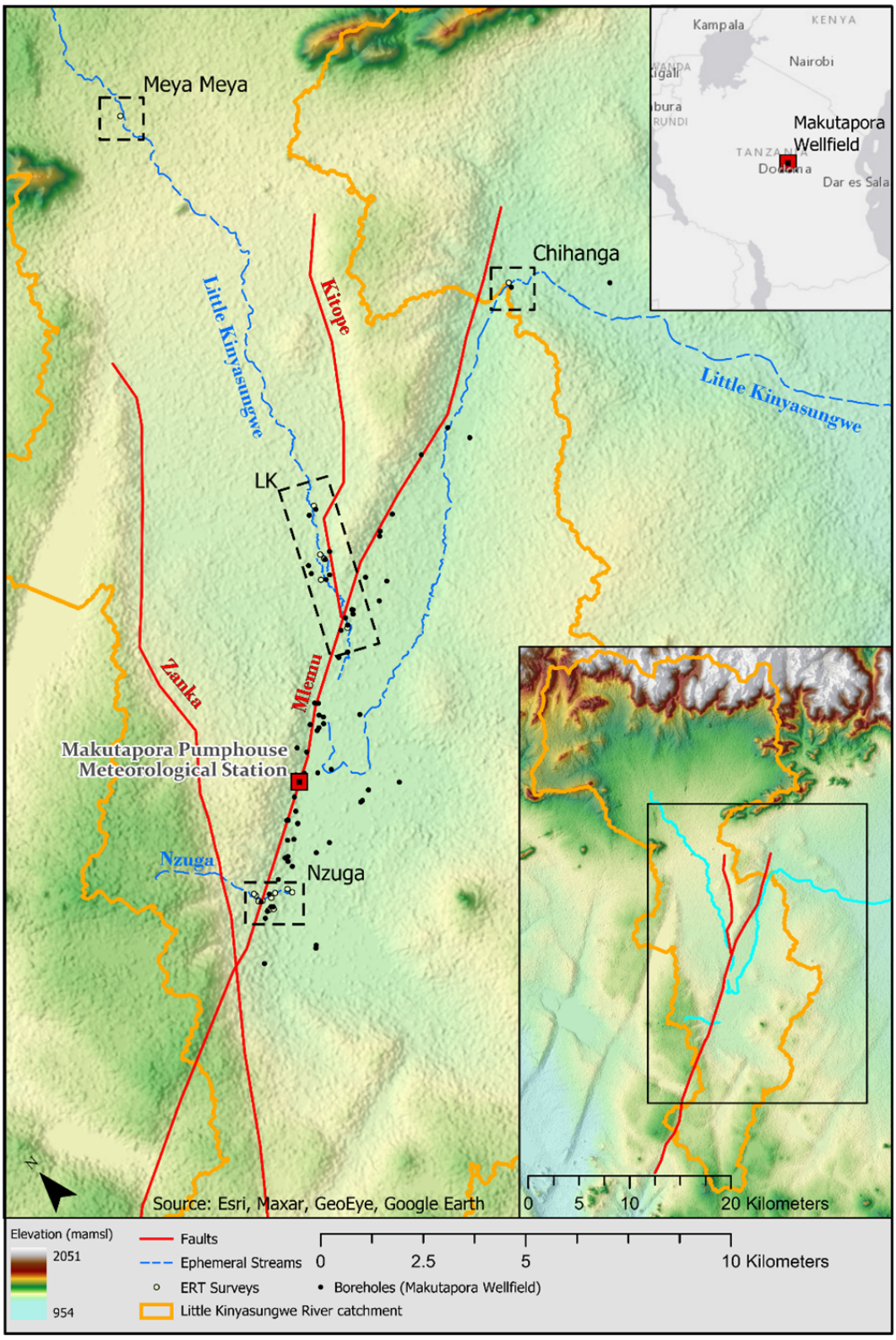

Fig. 2.1 The Makutapora Wellfield with NASA Shuttle Radar Topography Mission data (30 m resolution) Digital Elevation Model (NASA, METI, AIST, Japan Spacesystems, US/Japan ASTER Science Team, 2019) overlain. Location of study sites outlined in black and location of wellfield within greater Little Kinyasungwe River catchment (inset). Catchment was delineated using the Digital Elevation Model (DEM). Major faults in the study area are labelled and name and position as mapped by current literature (Rwebugisa, 2008; Shindo, 1990)

The climate is semi-arid and characterized by distinct wet and dry seasons. Average air temperatures are 23 °C, with highs ranging from 26.5 °C to 30.5 °C in July-October, and lows from 13.6 °C to 18.8 °C in Nov-June (WMO, 2020). Average annual precipitation is 550 mm at Makutapora Meteorological Station (Figure 2.1), 99% of which falls in a single wet season from December to April (Seddon, 2019; Taylor et al., 2013b). Short-lived observations in the catchment suggest that precipitation in the upland areas may be greater than on the floor of the catchment (Onodera et al., 1995; Seddon et al., 2021a). There have been several estimates of potential evapotranspiration in Makutapora (Fawley, 1958; Kashaigili et al., 2003; Onodera et al., 1995; Shindo, 1990, 1989), the most recent being 2120 mm·yr-1, based on 3 non-consecutive years of data recorded between 2003 and 2006 at the Makutapora Meteorological Station (Seddon, 2019).

The catchment is underlain by basement rocks comprised of Precambrian synorogenic granites and migmatite biotite gneiss of the Dodoma Basement Superterrane (De Pauw et al., 1983; Kabete et al., 2012; Ministry of Water, 1976), with more intrusive ultrabasic complexes of amphibolite and quartzo-feldspathic gneisses with biotite outcropping within the wellfield and Meya Meya regions (Figure 2.1). Metamorphosed rocks are also present in the region and amphibole schists crop out in a belt of inselbergs surrounding Meya Meya (Julian et al., 1963).

Apart from outcrops at the topographic highs of the Chenene Hills (Kashaigili, 2010) or along channels of ephemeral streams (Hayashi, M., & Chiba, 1994), these basement rocks are generally covered by a deeply weathered regolith (50-100m thick) of fractured saprock, saprolite, and pedolitic products of Neogene age at varying stages of chemical decomposition (Julian et al., 1963). Regolith composition varies throughout and is related to the mineralogy of the underlying parent rock.

The regolith is overlain by unconsolidated alluvial material consisting of detrital sands, gravels, and silts. (Kashaigili et al., 2003; Nkotagu, 1996). In the centre of the catchment and in the lowland areas of the wellfield depression, the regolith is overlain by layers of black, smectitic 'Mbuga' clay (Onodera et al., 1995). Such black smectitic clays often exist as valley infill in the rifted basins of central Tanzania (Bianconi and Borshoff, 1984). These are also typical of other semi-arid regions across the world in similar geological contexts (Oakes and Thorp, 1951), and have previously been associated with the presence of seasonal freshwater swamps in Makutapora (Wade and Oates, 1938).

Tectonic activity associated with the Manyara-Dodoma rift segment, a branch of the East African Rift system extending south across the Dodoma craton (Dawson, 2008), has left a complex network of faults in the study area. These faults are expressed as linear features trending SW-NE & NW-SE across the topography of the region (Macheyeki et al.,

2008) as seen in Figure 2.1. The main faults that cross the study area, the Mlemu and Kitope, form a natural NW boundary to the Makutapora wellfield, which is situated along a distinct fault-bounded topographic lowland depression within the wider catchment, and there is evidence of further faulting north of the catchment (Kabete et al., 2012). The large-scale discontinuities and dense fracture networks associated with faults such as the Mlemu are the defining hydrogeological feature of Makutapora, giving rise to anomalously high transmissivities of 400 to 4000 m^3 day^{-1} within the wellfield, and producing high well yields in boreholes proximal to the faults (Maurice et al., 2019; Rwebugisa, 2008).

2.2.2 Geophysical Methods

Data acquisition, processing, and inversion

Geophysical techniques have received increasing attention in recent years due to their non-destructive character and ability to provide information on subsurface features over large areas (Binley et al., 2015; Parsekian et al., 2015; Singha, 2017). Among the available techniques, electrical resistivity tomography (ERT) was chosen for this study for its ability to map and characterise superficial deposits for hydrological interpretation (e.g. Gourry et al., 2003; Andersen and Acworth, 2009; Cuthbert et al., 2009; Clifford and Binley, 2010; Cassidy et al., 2014; Gourdol et al., 2018).

In this study an AGI SuperSting R8 resistivity meter (http://www.agiusa.com) was used in dipole-dipole configuration. This configuration made efficient use of the instrument's multichannel capability and provided good lateral and vertical resolution. A 64-electrode array with dipole sizes (a) of a=6 and a=8, and dipole separations (n*a) with n=1 to 8 were used, and combinations of long (>3 m) electrode spacings used in areas where penetration depth was important, while shorter (2 m) electrode spacings used in areas where high resolution targets were to be delineated (see Table S1 for detailed survey set-up parameters)

Areas close to and parallel with roads or overhead power cables were avoided to minimize interference from other electrical signals or man-made disturbances of the subsurface. Dry and hard-ground conditions necessitated the use of saltwater to improve electrode contact resistance, and scrub vegetation commonly had to be removed to ensure the lines were able to maintain precise, straight-line orientations. Start and end points of sections were located using a GPS (Garmin eTrex 10) to <5 m uncertainty and orientated by taking a compass bearing. The relative elevations of the topographic variations along each line were measured using a Leica Disto D410 with a vertical accuracy of 1 mm.

Each apparent resistivity measurement was made in normal ρ_n and reciprocal ρ_r configuration (LaBrecque et al., 1996) with the measurement value used defined as the mean of these two measurements, ρ_m. The percentage standard error in this mean, referred to here as the reciprocal error, e, is defined as:

$$e = 100 \left(\frac{|\rho_r - \rho_n|}{(\rho_r - \rho_m)} \right) \tag{2.1}$$

Negative apparent resistivity data points were removed, and measurements with reciprocal errors greater than 5% were filtered out. This filtered dataset was inverted using the RES2DINV (Geotomo Software) algorithm (Loke, 2001). A least squares data constraint was used that minimizes the error between the observed and calculated apparent resistivity values, and a limit of 4 iterations was set to avoid model over-fitting. A robust model constraint, incorporating topographic variations, was selected over a least squared inversion constraint since it is known to better resolve sharp geological boundaries expected within the study area (Loke et al., 2003). In this case, it was important to delineate the boundaries between the superficial deposits, in-situ regolith, and zones bounded by normal faulting. Inverted data are presented as resistivity model sections (Edwards, 1977) and used in the interpretation of geoelectric layers and subsurface lithology.

Intepretation of resistivity models

Due to the smoothing and non-uniqueness inherent in fitting 3D geological structure to 2D resistivity models (Aizebeokhai and Singh, 2013; Dahlin et al., 2007), independent data were used to aid interpretation and to assist in identifying layer boundaries in the images. Boreholes with lithological data proximal to survey lines were collated from the Tanzanian Ministry of Water in Dodoma (Table A2) and superimposed onto these sections to correlate resistivity layers and lithological observations. In addition, field observations were used to constrain the resistivity ranges for superficial deposits observed at the ground surface. Sharp discontinuities seen in the resistivity sections were corroborated with field observations of faulted zones and regions of faulting inferred from analysing topographical data from STRM 30m DEM of the study area (NASA, METI, AIST, Japan Spacesystems, US/Japan ASTER Science Team, 2019).

Water content and temperature variations are known to affect subsurface resistivity (Brunet et al., 2010) but these effects were not considered in the interpretation of geological layers since they are greatly outweighed by contrasts in resistivity due to lithological variation (mostly clays), which are the focus of this chapter. Further, geophysical surveys were

undertaken in the middle of the dry season (June-July) when variations in soil moisture content and temperature between the dates of individual surveys were minimal.

Forward modelling using the RES2DMOD software (Loke, 2002) was used to identify and rule out various unexpected features found in some of the inversions to decide whether they should be interpreted as 'true' variations in subsurface resistivity. Firstly, several inversions at the Nzuga (Figures A.4, A.9-A.12), LK (Fig. A.15, A.17), Meya Meya (Fig. A.18) and Chihanga (Fig. A.19) sites show low resistivity zones underlying regions of high ($> 250\ \Omega$ m) resistivity at the surface. Secondly, I observe many sections at Nzuga (Fig. A.9-A.11) and Meya Meya sites (Fig. A.19) which have decreasing resistivity with depth underlying shallower zones of $> 40\ \Omega$ m resistivity (See Section 2.3.1 for further discussion).

Using the field site profile characteristics of the Nzuga 8 survey (Fig. A.10), a simplified two-layer synthetic model of the subsurface was developed for the forward modelling exercise. The top layer for the model was defined as 0-2.5 m with a resistivity of 40 Ω m, and the bottom layer from 2.5 to 30 m with a resistivity of 20 Ω m (Fig. A.20). Two regions 10 m wide and 3 m thick with high, 1000 Ω m, resistivities were then added to the model to examine the effects of pockets of high resistivity material (Fig. A.21). The synthetic results indicate that these low resistivity features underlying high resistivity zones (circled in black in Figure A.21) occur despite the attempts to minimise the number of iterations and are thus anomalous features. Further synthetic results indicate that sections with decreasing resistivity with depth were indeed true features that cannot be re-created without adding decreasing resistivity layers with depth in my forward models.

Survey locations

A total of 17 ERT surveys were conducted in June and July 2019 at four locations within the study area. These areas are shown in Figure 2.1, and a map of survey lines at each study site are shown inset within Figures 2.2-2.5. These locations were chosen to be representative of the various catchment areas that surround the wellfield as described for each site below. Three sites (Meya Meya, LK and Chihanga) are situated on the Little Kinyasungwe River, which comprises 75% of the catchment area draining into the Makutapora wellfield depression.

Meya Meya, the furthest upstream survey site, is located approximately 20 km upstream from the Makutapora wellfield. This location was chosen for one survey (Figure 2.6 and A.18) to coincide with the long-term stream gauge monitoring taking place at the site (Seddon et al., 2021). This gauge measures the inflow of the Little Kinyasungwe River into the next downstream study site (LK). The purpose of surveys in this area is to

provide geological context to streamflow patterns recorded here and the geological structure comprising upland 'pediplain' areas that surround the wellfield (Shindo 1989).

The site 'LK' was chosen for 5 surveys (Figures A13-17) to constrain the geological configuration underneath the Little Kinyasungwe River as it enters the wellfield depression. This site is bounded by the Kitope fault to the East and is situated in a lowland area covered by Mbuga Clay and silts. In seasons with particularly high precipitation, these lowland regions can experience overland flow and inundation during the wet season (Fig. A2).

The Chihanga site represents the furthest downstream survey site on the Little Kinyasungwe River and was chosen for one survey (Figure 2.5 and A19). Like Meya Meya, it was chosen to constrain the geological conditions as the stream exits the wellfield depression into the downstream Hombolo basin.

The fourth site is in the vicinity of the ephemeral Nzuga stream and lies on the North-Western edge of the wellfield. This site was chosen for 10 surveys (Figure 2.2 and A3-12). The Nzuga stream crosses the Zanka and Mbuga faults before terminating in the wellfield depression, forming an alluvial fan. Spot gauging within the stream has shown that ephemeral streamflow does not always reach the depression and is instead thought to be lost by leakage from the stream channel into underlying and surrounding superficial deposits (Shindo 1990). Such 'headwater channels' (Sutfin et al., 2014a) are common throughout the region in the transition slopes between upland and lowland areas and comprises approximately 25% of the catchment area flowing into the catchment.

2.3 Results and discussion

2.3.1 Resistivity units

Integrating the results of the 17 ERT surveys (Figures A3-19) with interpreted borehole log information (Table A2) and outcrop field observations (Figure A1), I defined five main resistivity units in the catchment, and associated inferred lithologic properties and depositional settings as follows:

a) Deposits of coarse sand (>250 Ω m) and silts (20-160 Ω m)

b) Transported smectitic clays (<10 Ω m)

c) Cemented pedolitic soils (30-80 Ω m)

d) Smectite-rich saprolite (15-30 Ω m)

e) Weathered saprock (110 - 450 Ω m)

These layers correspond to the idealised weathering profile of tropical soils above crystalline basement rocks described in the literature (Dewandel et al., 2006; Fookes, 1997; Taylor and Eggleton, 2001; Taylor and Howard, 1999; Wright and Burgess, 1992) and fall within a corresponding range of resistivties for weathered products of mafic origin containing 2:1 clays established for similar geological provinces (Anudu et al., 2014; Barongo and Palacky, 1991; Beauvais et al., 1999; Belle et al., 2019; Ritz et al., 1999; Robineau et al., 2007). The presence or absence of the different layers in the profile varies from location to location in the study area, which I interpret due to local variations in rock type and structure, topography and rates of sediment erosion and deposition.

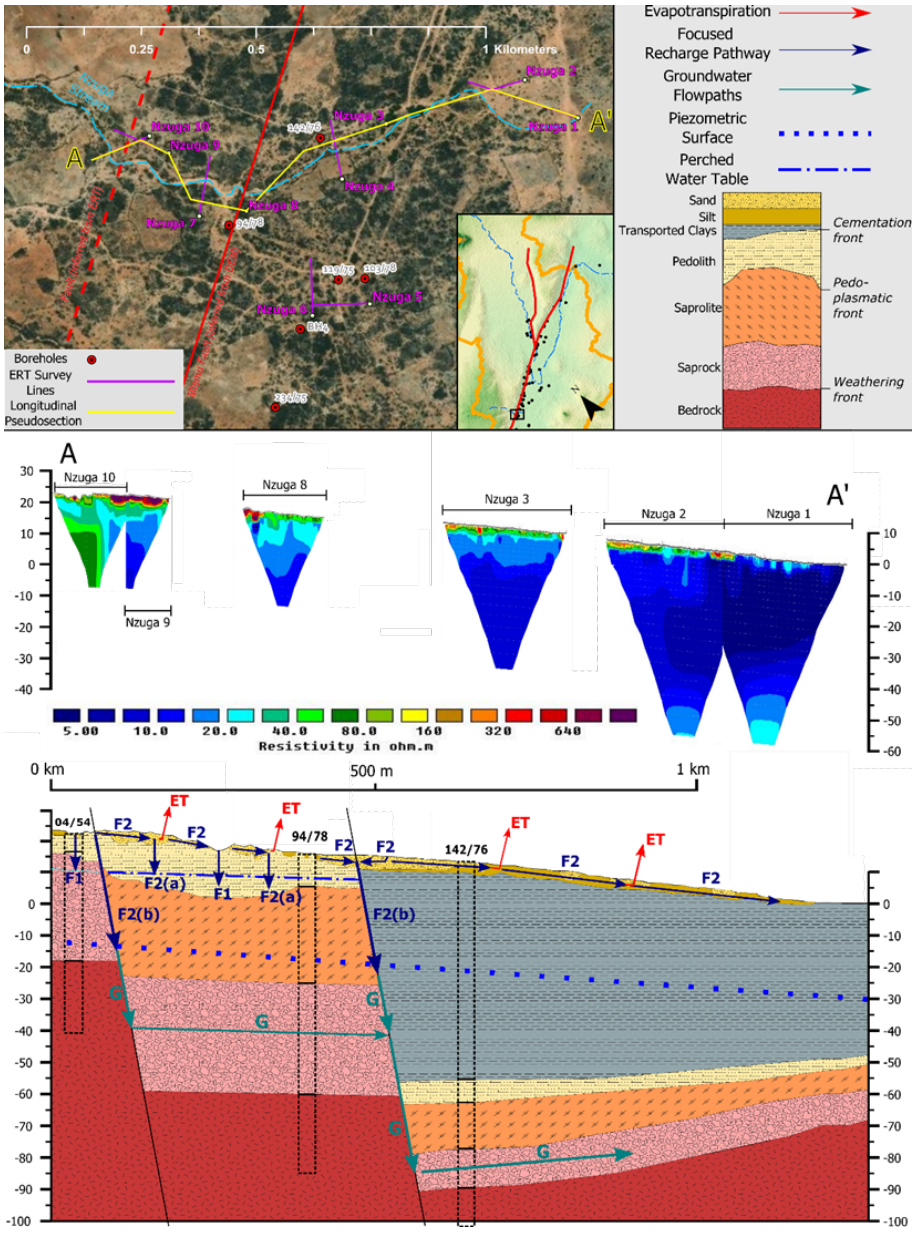

Fig. 2.2 Nzuga study site - with map of ERT surveys (top), combined longitudinal geoelectric section of the study site (middle) and interpreted geological structure and conceptual model (bottom). Interpreted borehole logs (Table A2) superimposed in black. Labels and arrows drawn correspond to recharge pathways outlined in in section 2.3.2. Consult Figure A27 for individual borehole lithologies and water levels.

The topmost layer **(a)** comprises sand of variable grain sizes ranging from coarse to fine (See Figures A1 3c) with resistivities >250 Ω m, set amongst silts with resistivities of 20-160 Ω m. Sand is 0.5-4 m thick and is present but often discontinuous at all the study sites. Continuous <0.5m thick layers of sand were directly observed within the dry

streambeds of the Nzuga (Figures 2.2,A6, 9, 12), and Little Kinyasungwe River at Meya Meya (Fig. A18), LK (Figures A15, 17) and Chihanga (Figures A19).

Thicker layers of sand are particularly prominent at the Nzuga site, where they exist as 1-4 m thick deposits in and around the banks of the Nzuga (Figures A5, 9-12), and smaller 1-2 m thick deposits in Little Kinyasungwe (Figures A15, 17). Owing to their channel-like morphology, I interpret these sand deposits as abandoned ephemeral stream channel alluvial deposits. Silts often surround these pockets of coarser alluvium and are most commonly present as <0.5 m thin layers in the soil profile surrounding the Nzuga stream and Little Kinyasungwe River. However, thicker layers (1-2m) of these silts are particularly prominent in the alluvial fan of the Nzuga (Figures 2.3, A3, 4), and in the floodplain areas surrounding the Little Kinyasungwe River at the LK site (Figures 2.4, A13, 15, 17, and see Figure A1 5). I interpret these as overbank deposits from the existing or previous ephemeral stream network.Very low resistivity layers (<10 Ω m) (b) are present in every study area, and in outcrops that correspond with layers of black, smectitic 'Mbuga Clay' (see Figure A1 4). This clay layer is 30 m thick in the downstream reaches of the Nzuga stream where it meets the wellfield depression (Figures 2.3 and A3-5) and is also present as a 10-25 m thick layer below the Little Kinyasungwe River in the LK site (Figures 2.4 and A15-17).

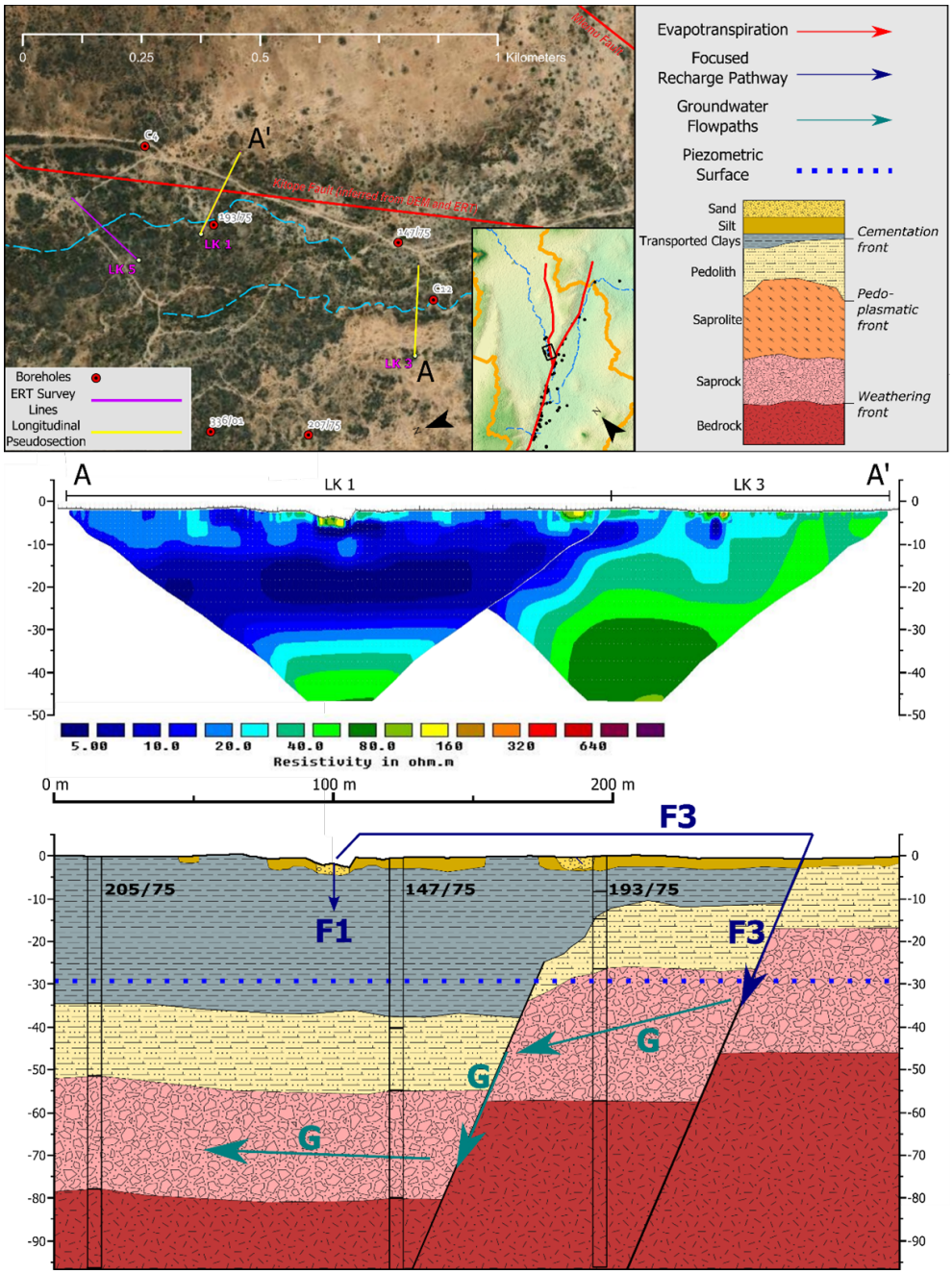

Fig. 2.3 LK study site - with map of ERT surveys (top), combined longitudinal geoelectric section of the study site (middle) and interpreted geological structure and conceptual model (bottom). Interpreted borehole logs (Table A2) superimposed in black. Labels and arrows drawn correspond to recharge pathways outlined in in section 2.3.2.Consult Figure A27 for individual borehole lithologies and water levels.

At the Meya Meya site, this low resistivity clay exists only as an isolated 0.5 m thick layer 40 m away from the Little Kinyasungwe River (Figure A19). More prominent 0.5-1 m thick

deposits of this clay can be seen surrounding but not underlying the Little Kinyasungwe River at the Chihanga site (Figures 2.5 and A19). I interpret these clay layers to be transported basin infill deposits in the downthrown side of Mlemu and Kitope faults at the Nzuga and LK sites, respectively. However, at Chihanga it is unclear whether these deposits are previous basin infill that has subsequently been cut through by the Little Kinyasungwe, or more recent over bank deposits.

Underlying these transported sediments, I observe a zone of approximately 80 Ω m (c) that crops out within the Nzuga streambed (see Figure A1 3b) but only upstream of the Mlemu Fault (Figs. 2.3 and A11-12), as well as within the streambed of the Little Kinyasungwe River at both the Meya Meya (see Fig. A1 1a) and Chihanga sites. This comprises quartz grains (1-4 mm) interbedded in a yellow to white fine sandy-clay matrix (see Figure A1 3a). At the Nzuga (Figures 2.3 and A9-12) and Meya Meya (Fig. A18) sites, the resistivity of this zone further decreases with depth, from approximately 80 to 30 Ω m.Comprising the uppermost in-situ cemented layer of my profile, I interpret this layer as a pedolith (or mottled zone), with a decrease in resistivity with depth suggesting a transition from 1:1 pedogenic clays to increasing proportion of 2:1 clays as the weathering profile moves below the water table and approaches the saprolite (Pal et al., 1989).

This transition is common in tropical profiles, and in the partial weathering of mafic materials, where 2:1 clays typically persist below the water table where less intense weathering processes in the saturated zone inhibits weathering of 2:1 clays to kaolinite (Taylor and Howard, 1999). At shallower depths above the water table, variable saturation can lead to micro-weathering environments that create lower pH and higher complexing agent concentrations that accelerate weathering to kaolinite (Dennis et al., 2009; Taylor and Howard, 1999).

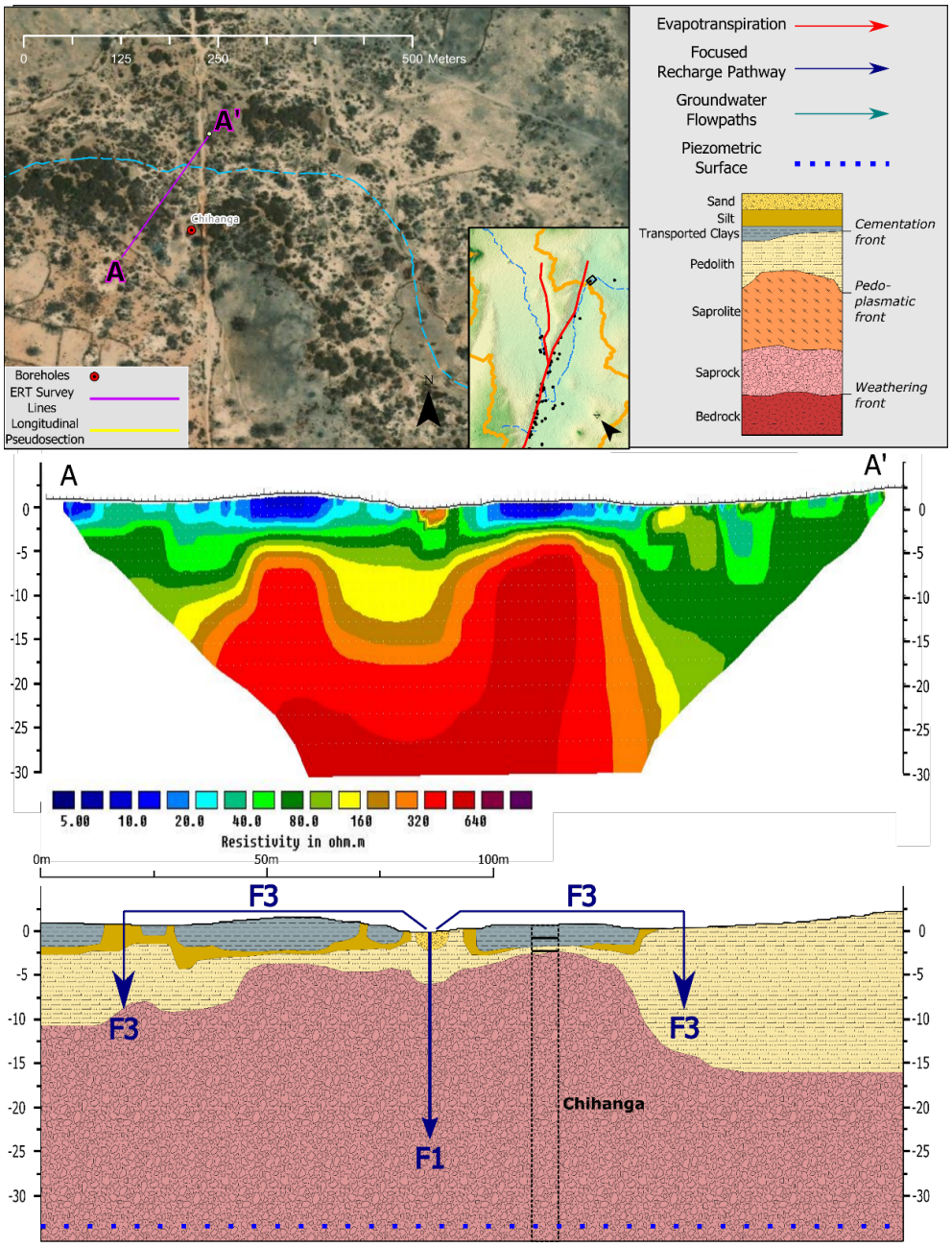

Fig. 2.4 Chihanga study site - with map of ERT surveys (top), combined longitudinal geoelectric section of the study site (middle) and interpreted geological structure and conceptual model (bottom). Interpreted borehole logs (Table A2) superimposed in black. Labels and arrows drawn correspond to recharge pathways outlined in in section 2.3.2. Consult Figure A27 for individual borehole lithologies and water levels.

At the Nzuga and Meya Meya sites, there is a continuous geoelectric gradient with depth as resistivities further decrease to 10-30 Ω m (Figures A9-11, A18). Based on interpretation of borehole data, I interpret this as a gradual transition from lower pedolith

to upper saprolite zone (d), with a resistivity of 10-30 Ω m typical of saprolites of smectitic composition seen in similar geological provinces (e.g. Pal et al., 1989; Taboada and Garcia, 1999; Robineau et al., 2007; Anudu, Essien and Obrike, 2014). This continuous decrease of resistivity is indicative of the boundary between the saprolite and pedolith, known as the pedoplasmatic front, which is characterized by a change in composition from pedogenic clays to more less weathered, lithic material (Stoops et al., 2018).

However, this 10-30 Ω m saprolitic layer is non-existent in the geoelectric sections at the LK and Chihanga sites (Figures 2.4 and 2.5). Instead, zones of 60-80 Ω m, interpreted as indicative of 1:1 pedolitic clays described earlier, are immediately underlain by higher resistivity zones of 110 - 450 Ω m, increasing with depth. This higher resistivity zone has been interpreted as zones of fractured bedrock or saprock (e) and distinguished from >250 Ω m zones of coarse sand seen at the surface, or saprolite composed of more 1:1 clays, using borehole lithological interpretations. This wide resistivity range of 110 - 450 Ω m is common in the saprock of crystalline basement systems because of the fractured nature of the saprock - fractures filled with water or decomposed clays from the saprolite create inherent inhomogeneities in the subsurface resistivity (Dewandel et al., 2006; Robineau et al., 2007).

Sharp discontinuities in resistivity seen at the Nzuga (Figures. 2.3 and A11-12) and LK site (Figures 2.4 and A13) are interpreted as zones of normal faulting and correspond to the Mlemu and Kitope faults, respectively. These discontinuities also correspond with zones of faulting identified from the DEM (see section 2.2.3) and are typically bounded on the downthrown side with infill of transported clays (i.e. layer b) in Figures 2.3 and 2.4.

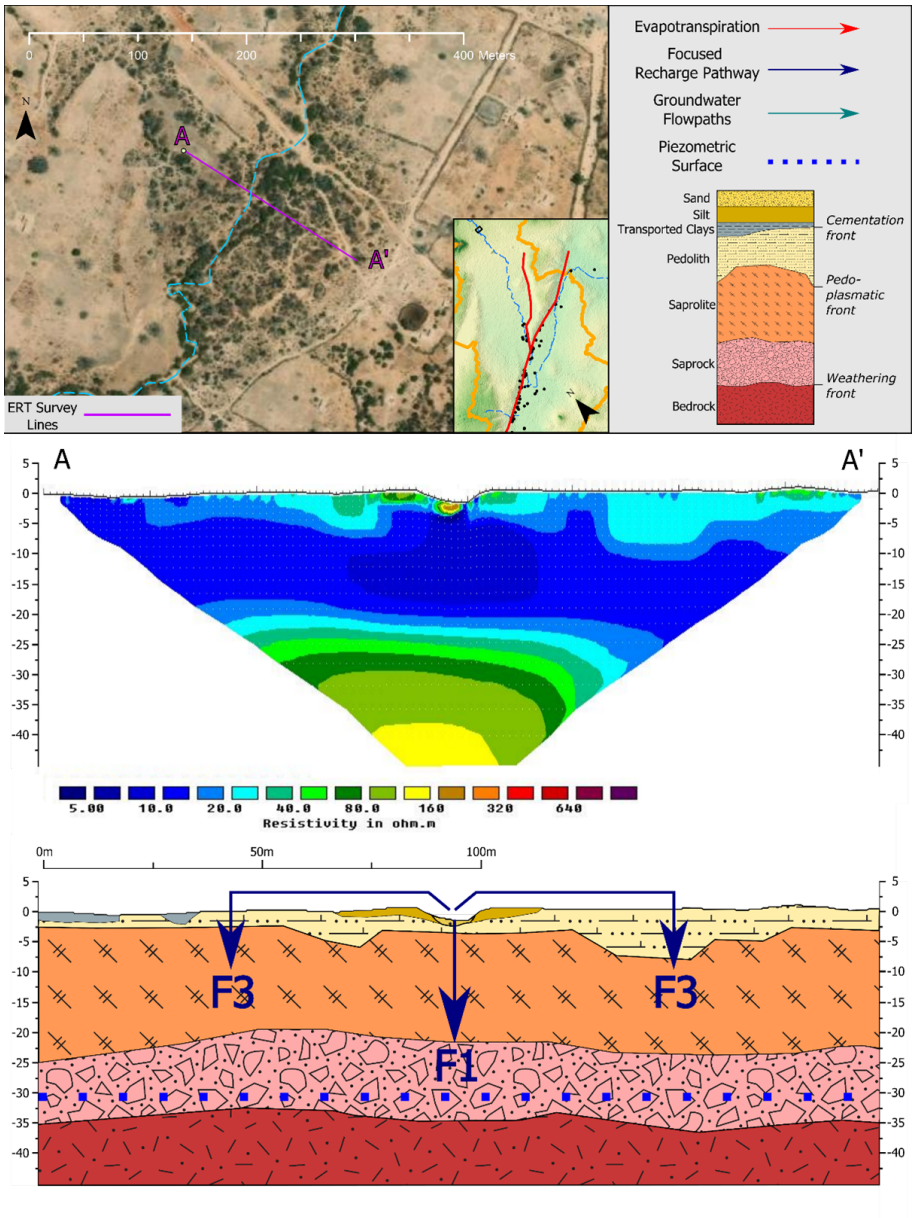

Fig. 2.5 Meya study site - with map of ERT surveys (top), combined longitudinal geoelectric section of the study site (middle) and interpreted geological structure and conceptual model (bottom). Interpreted borehole logs (Table A2) superimposed in black. Labels and arrows drawn correspond to recharge pathways outlined in in section 2.3.2. Consult Figure A27 for individual borehole lithologies and water levels.

2.3.2 Conceptual model

Based on the results and interpretation of the geoelectric data collected in the study area, a series of local-scale conceptual hydrogeological models of focused recharge at the Nzuga,

LK, Chihanga and Meya Meya sites have been produced. These are shown schematically in Figures 2.2-2.5 respectively, with interpreted borehole lithological data superimposed in black (where available) and focused pathways highlighted in dark blue.

These local-scale models were then collated, and in conjunction with borehole log information, used to produce a 3D conceptual model of the recharge processes (including diffuse processes) in the Makutapora wellfield, shown in Figure 6. Based on these models, I propose that the superficial (transported) deposits control recharge to the deeper bedrock aquifer system as follows:

F Focused recharge pathways:

- **F1** Ephemeral streams lose water into the underlying aquifer via sufficiently permeable intervening superficial deposits and/or weathered bedrock material. This potentially occurs at all study sites. Rates of recharge are likely controlled by the hydraulic properties of the underlying geology, in addition to the stream flow frequency and the depth to the water table (Quichimbo et al., 2020). The lithological characteristics of smectitic Mbuga clays (Figures 2.4 and A1 4) suggest these have low matrix hydraulic conductivities of the order of 1e-10 ms^{-1}, although that could be enhanced by one or two orders of magnitude if preferential flow pathways are prevalent (Crane et al., 2015; Timms et al., 2018). Conversely, streams on the Nzuga, Chihanga and Meya Meya sites (Figures 2.2, 2.4 and 2.5 respectively) directly overlie pedolitic soils, which are assumed to be more hydraulically conductive. The presence of thick layers of smectite clay rich saprolite underlying this pedolith at the Nzuga and Meya Meya sites however would restrict flow.
- **F2** Shallow permeable alluvial deposits collect ephemeral stream losses and runoff but due to the variable permeability of underlying materials, this water is stored and slowly redistributed in the subsurface. These shallow stores of water form local perched aquifer systems upstream of the Mlemu fault in the Nzuga site (Shindo 1990), and within pockets of thick alluvium in the overbank regions of the Little Kinyasungwe River at LK (observed in the field by the authors). Such groundwater may flow slowly longitudinally downslope via connected alluvial ribbons to:
  - **ET** discharge back to the atmosphere via evaporation either directly where shallow enough, or through transpiration from riparian vegetation
  - **F2(a)** flow into the deeper bedrock aquifer via more permeable 'windows' in the underlying superficial deposits or

F2(b) flow into the deeper bedrock aquifer via highly permeable fractures or fault zones interconnected to the underlying aquifer system (Bense et al., 2013)

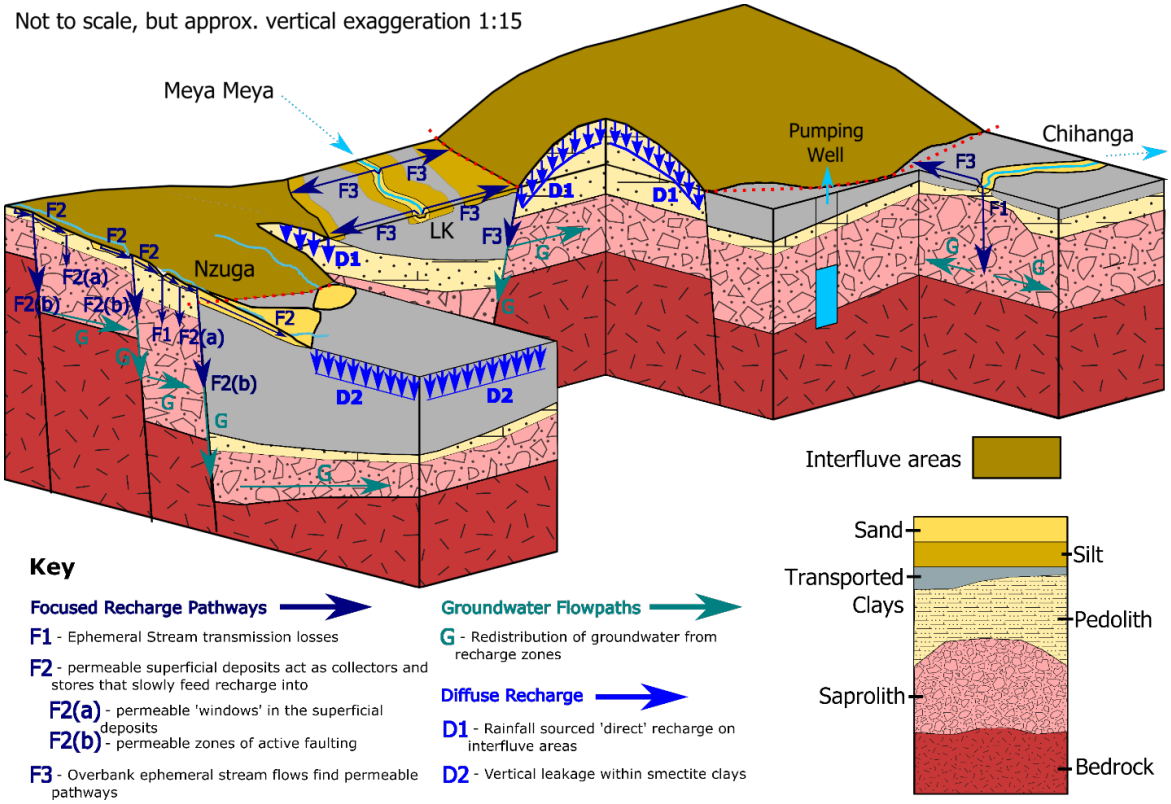

Fig. 2.6 Conceptual Model of the Makutapora wellfield showing configuration of superficial deposits and highlighting permeable pathways described in Section 2.3.2. Note that saprock and saprolite horizons have been grouped into 'saprolith' layer.

F3 Overbank ephemeral stream flows find permeable recharge pathways. Long term stream stage and groundwater relationships suggest that anomalously large rainfall events (and, as such, stream discharges) associated with El Niño events provide significant recharge to the Makutapora wellfield (Seddon et al., 2021). The Little Kingusygwe River, the main ephemeral stream that channels surface runoff to the wellfield, is often underlain by impermeable smectitic clays (Figure 2.3). However, stream stage data indicate these large rainfall events lead to overbank flows, and these flows may locate permeable pathways and faulted zones that bypass this impermeable clay and lead to greater groundwater recharge (Seddon et al., 2021). This recharge pathway is similar to the results of Lange (2005), who also found greater transmission losses with higher flow events attributed mainly to enhanced water losses in flooded overbank areas.

D Diffuse recharge:

D1 Rainfall-sourced diffuse recharge occurs when soil moisture deficits are overcome, or preferential flow pathways are activated through sufficiently permeable superficial deposits. One previously described mechanism which may be prevalent on the interfluve areas is enhanced recharge in the vicinity of abundant abandoned termite mounds (Shindo 1990).

D2 Vertical leakage through smectite clay deposits may be induced or increased by pumping in the underlying aquifer. Although the matrix hydraulic conductivity of the smectite clays are likely to be very low (see pathway **F1**), biological and weathering processes may compromise the hydraulic integrity of such deposits and allow more permeable syn-depositional macropores to accumulate deep into the formation and act as preferential flow networks that can be as deep as 30 m (Crane et al., 2015; Timms et al., 2018). This recharge flux via the lowland Mbuga clay may be low, but should not be discounted as a potential pathway for diffuse recharge into the bedrock aquifer system as it may occur over substantial areas.

G Redistribution of groundwater from recharge zones to the wellfield:

- High transmissivities in the faulted bedrock allow for quick redistribution of groundwater within the fractured aquifer system, capturing recharge from a wide range from the above pathways across the catchment. Pumping tests in the Makutapora Wellfield indicate transmissivities of 400 to 4000 m^2d^{-1}, much greater than typical weathered crystalline rock aquifer systems, that commonly range from 1 to 10 m^2d^{-1} (Bianchi et al., 2020). These anomalously high transmissivities arise from extensive faulting within the saprock (Maurice et al., 2019; Nkotagu, 1996). These fault systems in essence act as 'collectors' for groundwater recharged and stored in the regolith and weathered zone from both focused and diffuse sources as described.

2.3.3 Discussion and implications

In my study, the use of ERT has enabled a range of geometrical relationships to be defined among different geoelectric layers. The use of outcrop observations and borehole log information has then enabled lithological interpretations to be made from the geoelectric layers. At the Meya Meya site, borehole information was not available and robust lithological interpretations from the ERT data were only possible through the resistivity ranges of

subsurface layers ascertained from the other study sites in the catchment, together with outcrop observations within the streambed of the Little Kinyusungwe River at Meya Meya (Fig. A1). As such, the borehole logs and outcrop observations were critical to reducing the uncertainty in the conceptual models developed, and caution should be applied when interpreting ERT data in isolation in such environments.

My study was not designed to quantitatively determine the relative proportions of diffuse and focused recharge in the study site, but to identify potential recharge typologies. My conceptual models reveal several potential focused recharge pathways that are consistent with previous studies and where residence time indicators have suggested local recharge at Makutapora has a strong component of preferential flow following high-intensity rainfall events (Hayashi, M., & Chiba, 1994; Maurice et al., 2019; Onodera et al., 1995; Senguji, 1999; Shindo, 1990), and with the findings of Taylor et al. 2013 and Cuthbert et al. 2019b, which demonstrated that recharge at Makutapora occurs episodically following intensive precipitation, on average two or three times each decade over the last 60 years. This bias of recharge towards intensive precipitation has previously been indicated in hydrometric (Cuthbert et al., 2019b; Taylor et al., 2013b), stable isotope (Banks et al., 2020; Jasechko and Taylor, 2015; Vogel and Van Urk, 1975) and modelling (Eilers et al., 2007) studies in other semi-arid areas. As such, as projected decreases in mean annual precipitation are thought to lead to decreases in groundwater recharge in drylands (Jiménez Cisneros et al., 2014), increases in episodic recharge from more intensive precipitation events may offset these projections. However, caution is needed in such interpretations in the absence of local data on the exact nature of the recharge mechanisms, since local geological heterogeneity can in some cases lead to results that are contrary to this general expectation (Acworth et al., 2020).

The Nzuga study site was specifically chosen to represent smaller headwater streams that drain upper pediplain regions into the wellfield depression. Although these streams drain only 25% of the catchment area into the wellfield depression, my conceptual model from the Nzuga site (Figure 2.3) indicates that these streams may activate a greater proportion of recharge pathways than even the larger Little Kinyasungwe River, which is hypothesized to generate substantial recharge only in large precipitation events that lead to overbank flows (see Section 2.3.2). Therefore, while the Little Kinyasungwe River may be important in facilitating large recharge events, it may be possible that smaller streams provide a proportion of recharge in years between larger events by slowly 'drip feeding' recharge into the fault system.

As the population of Dodoma and other cities in drylands are set to increase the demand for freshwater in the coming decades (UN, 2017), it is possible that this increased

abstraction may lead to increased recharge in the study area. This may occur as increased pumping, and subsequent drawdown, leads to increased capture (Bredehoeft, 2002; Theis, 1940) as the cone of depression reaches further out. For example, this may increase the subsurface storage available in areas of previously shallow water table, thus activating new recharge pathways to collect recharge from an even wider area that may have otherwise been rejected. This increased recharge is difficult to quantify however, and future groundwater level monitoring at a wider range of distances from the wellfield may further elucidate the relative magnitude of diffuse recharge processes in my study site, and its uncertain relationship to focused recharge.

I propose that the study site acts as an analogue for the geological and climatological conditions in many other parts of sub-Saharan Africa, 40% of which are also underlain by weathered crystalline aquifers (A M MacDonald et al., 2012). These aquifers provide a vital source of reliable freshwater to over a quarter of a billion people in sub-Saharan Africa (Macdonald et al., 2008; Taylor and Tindimugaya, 2011), and groundwater abstraction to supply domestic water is expected to increase dramatically in the region (Braune and Xu, 2010; Taylor et al., 2009). Furthermore, indirect recharge from ephemeral streams (e.g. pathways F1, F2(a) and F2(b) described in Section 2.3.2) are likely prevalent in dryland alluvial settings of large global extent where ephemeral streams comprise >80% of the dryland river network (Levick et al. 2008; Sabater and Tockner 2010), and there is a growing body of literature using near-surface geophysics to that highlight the importance transmission losses and groundwater recharge in such dryland systems (e.g. Callegary et al., 2007; Shanafield et al., 2020). The study sites were chosen to represent a range of ephemeral stream geomorphologies observed in dryland regions (Sutfin et al., 2014a), excluding bedrock headwater channels which were difficult to access in my study region. Moreover, my models are directly applicable to dryland areas dominated by smectite clay (Acworth and Timms, 2003; Crane et al., 2015; Timms et al., 2019), the presence of which is typical of dryland regions across the world in mafic geological contexts (Oakes and Thorp, 1951).

Accurate quantification of recharge in dryland settings remains a challenge, with no widely applicable method currently available that can directly and accurately quantify the volume of rainwater that reaches the water table (Healy and Scanlon, 2010; Scanlon et al., 2002; Shanafield and Cook, 2014) despite multiple lines of evidence (Villeneuve et al., 2015). I believe my models provide a first step towards the quantification of recharge in drylands by shedding light on potential focused recharge pathways in the region which could be tested in the future using a variety of hydrogeological techniques. For example, soil moisture profiles placed proximal to areas of potential recharge have enabled the tracking of

deeper infiltration through multiple layers of varying geological characteristics in hyper-arid settings (Dahan et al., 2008b). Temperature tracing has also been used with great success to quantify shallow surface-groundwater interactions beneath ephemeral streams (Rau et al., 2017).

My models provide an informed physical basis for future 3-D numerical modelling of groundwater flow by incorporating superficial geological structure (Turner et al., 2015), and predicting responses to groundwater systems with variable geology to anthropogenic pressures and environmental change (Acworth et al., 2020). Further, this chapter provides a basis for improved understanding and management of the groundwater system in the Makutapora wellfield, and opens the door for improved efficacy and implementation of Managed Aquifer Recharge (MAR) in the future by providing a physical basis for recharge in the region (Dillon et al., 2019).

2.4 Conclusion

Few studies have made detailed observations of superficial geological structure in dryland regions. The use of the ERT method in conjunction with borehole logs and outcrop observations has enabled delineation of a variety of geometries and inter-relationships of superficial geology at four sites in the Makutapora wellfield, Tanzania. These data reveal lithologies and weathering profiles typical of tropical soils underlain by a crystalline basement complex, and permitted development of conceptual hydrogeological models of the study site. These models outline the role of superficial deposits in providing multiple potential pathways for focused groundwater recharge that bypass the low permeability smectite clay deposits that cover the wellfield. These pathways can be summarized as follows:

1. Superficial sand deposits act as collectors and stores that slowly feed recharge into zones of active faulting.

2. These fault zones provide permeable pathways enabling greater recharge to occur and rapid redistribution of recharge.

3. Windows within layers of smectitic clay underlying ephemeral streams may provide pathways for focused recharge via transmission losses.

4. Overbank flooding during high intensity precipitation events that inundate a greater area of the catchment, increases the probability of activating such permeable pathways.

My study was not designed to quantitatively determine the relative proportions of diffuse and focused recharge in the study site but does inform future monitoring at a more diverse

range of locations within, and peripheral to, the Makutapora wellfield that may further elucidate the relative magnitude of diffuse and focused recharge processes. Specifically, further monitoring of smaller streams, such as the Nzuga, is expected to better estimate the overall water balance.

The conceptual models I have developed provide a first step for improved understanding of groundwater recharge in drylands by providing a physical basis for how superficial geology controls recharge pathways and processes. These are critical to further understand and quantify for the purpose of improving groundwater management in response to climate and anthropogenic changes.

Chapter 3

How alluvial storage controls spatiotemporal water balance partitioning in intermittent and ephemeral stream systems

3.1 Introduction

Intermittent rivers and ephemeral streams (IRES) occur globally across all climates, with more than half of global channels drying periodically (Thibault Datry et al., 2016; Messager et al., 2021). In drylands (arid, semi-arid and sub-humid regions), these systems are more widespread and comprise >80% of the channel network (Datry et al., 2011; Levick et al., 2008). However the hydrology of these systems has historically been under-represented in published literature (Messager et al., 2021).

In both dryland and humid environments, IRES perform a variety of critical ecosystem services, including transport of biota, materials, nutrients, and water within the landscape (Acuña et al., 2017; Alan Yeakley et al., 2016; Datry et al., 2017) and host diverse aquatic and riparian ecosystems (T Datry et al., 2016; Katz et al., 2012). Ephemeral streamflow is often the primary source of surface water to these ecosystems (Stromberg and Merritt, 2016) and is crucial in maintaining their ecological health and diversity (Labbe and Fausch, 2000; Saccò et al., 2021).

Streamflow infiltration via the beds of IRES is a key pathway for replenishment of groundwater recharge in dryland regions (see Chapter 1, Cuthbert et al., 2019; Keppel and Renard, 1962; Wheater, 2008) through 'windows' of permeable alluvial deposits by

which potential focused recharge can occur (see Chapter 2). The geology surrounding these alluvial deposits likely varies longitudinally at the catchment scale. These heterogeneities will influence the subsurface partitioning of potential recharge within these systems, such that the distribution of potential recharge across the streambed may differ considerably from the actual recharge to the regional water table (Nimmo et al., 2017). However, characterization of the hydrogeological systems underlying non-perennial streams systems is rarely included in studies of stream hydrology, or if it is included, it is heavily simplified (Bourke et al., 2021).

Statistical analyses and hydrological modelling studies have included a parameter or index for bedrock (Richardson et al., 2020) or surface geology (Messager et al., 2021; Yu et al., 2019) in an effort to identify or account for the contribution of geology as a control on runoff and streamflow generation. However, these 2-dimensional data sets and derived indices are not able to capture the longitudinal heterogeneities that control groundwater flow and discharge to streams (Winter, 1999). There is a growing body of literature using near-surface geophysics to understand IRES dynamics (e.g. Bourke et al., 2021; Lorentz et al., 2020; Shanafield et al., 2020). However, these often lack information such as hydrometric data or spatial resolution to capture the complex spatial variation in streamflow and groundwater dynamics associated with water balance partitioning in IRES. Furthermore, while multi-year observations of groundwater dynamics in IRES exist, these have only been reported for few sites worldwide (e.g. Carling et al., 2012; Dahan et al., 2008a; Pool, 2005).

In this chapter, I 1) quantify variations in subsurface geology, stream stage and groundwater levels along an ephemeral stream system using a unusually rich monitoring site in the Maules Creek Catchment, New South Wales (NSW), Australia, (2) elucidate how configurations of superficial geology surrounding the stream control the variability in water balance partitioning and (3) generate a conceptual model of water balance partitioning in IRES with varying geology that is applicable to a wide range of dryland settings. My results help understand the consequence of changes to surface water-groundwater interactions (such as from river regulation, groundwater extractions and climate change) on biota, water quality, and water resources in drylands. This chapter also demonstrates the benefits of linking hydrological data with geophysical imaging to better understand flow paths through superficial deposits and surrounding deposits that can be widely applied to other areas.

3.2 Methods

3.2.1 Site description

The Maules Creek catchment is a semi-arid sub-catchment of the Namoi River in NSW, Australia. The catchment has been described in detail in previous studies (Andersen and Acworth, 2009; Cuthbert et al., 2016; McCallum et al., 2013; Rau et al., 2010; Rau et al., 2017) and is only briefly summarized here.

The catchment has a surface area of approximately 1,100 km^2 (study area in black line, Fig. 3.1b) and is located on the western slopes of the Great Dividing Range, south-east of the township of Narrabri. It is bound to the east by the New England Fold Belt and the Great Dividing Range, to the north by the Nandewar Range (and Mount Kaputar), to the south by the Leard State Forest and Gins Leap Gap, and to the west by a low ridge of hills that represent the edge of the Great Artesian Basin sediments. Middle Creek is an ephemeral tributary that drains approximately 106 km2 of the upper catchment, joining Maules Creek at Elfin Crossing, 250 m downstream from the Horsearm Creek confluence (Figure 3.1).

Rainfall is dominated by episodic frontal storms, the largest of which generally occurs in the summer months (December–February). Rainfall is also influenced by longer-term fluctuations in the El Niño Southern Oscillation Index (ENSO), with higher-than-average rainfalls in the positive phase (La Niña) and lower than average rainfalls in the negative phase (El Niño). Potential annual evapotranspiration (PET) is high and has been estimated as 1,200 mm in the Nandewar Range (Mt Lindesay), increasing to 1,800 mm in the lower altitudes (Turrawan) of the catchment (Mccallum et al., 2013).

A geological map of the catchment is shown in Figure 3.1c, and the geology of the catchment is summarized as follows. In the southern and western parts of the catchment the bedrock geology consists of Permian volcanic deposits of the Werrie Basalt formation. To the east, this formation is overlain by a sequence of Permian sedimentary deposits known as the Maules Creek formation, consisting of basal carbonaceous claystone, pelletoidal clay sandstone, minor coal, passing upwards into upward-fining cycles of sandstone, thinly bedded siltstone/sandstone, and coal. Towards the top of the formation, the stratigraphy becomes more conglomerate dominant. Excluding topographic highs and mafic intrusions (of the Nandewar Volcanic Complex), this bedrock is generally overlain by Tertiary and Quaternary alluvial deposits consisting of clays, sands, and gravels. The Mooki Thrust zone runs approximately north-south through the Eastern part of the catchment and defines the mountain front, separating the Permian bedrock and alluvial cover from Carboniferous headwaters consisting of meta-sediments and volcanic deposits of the Willuri Formation.

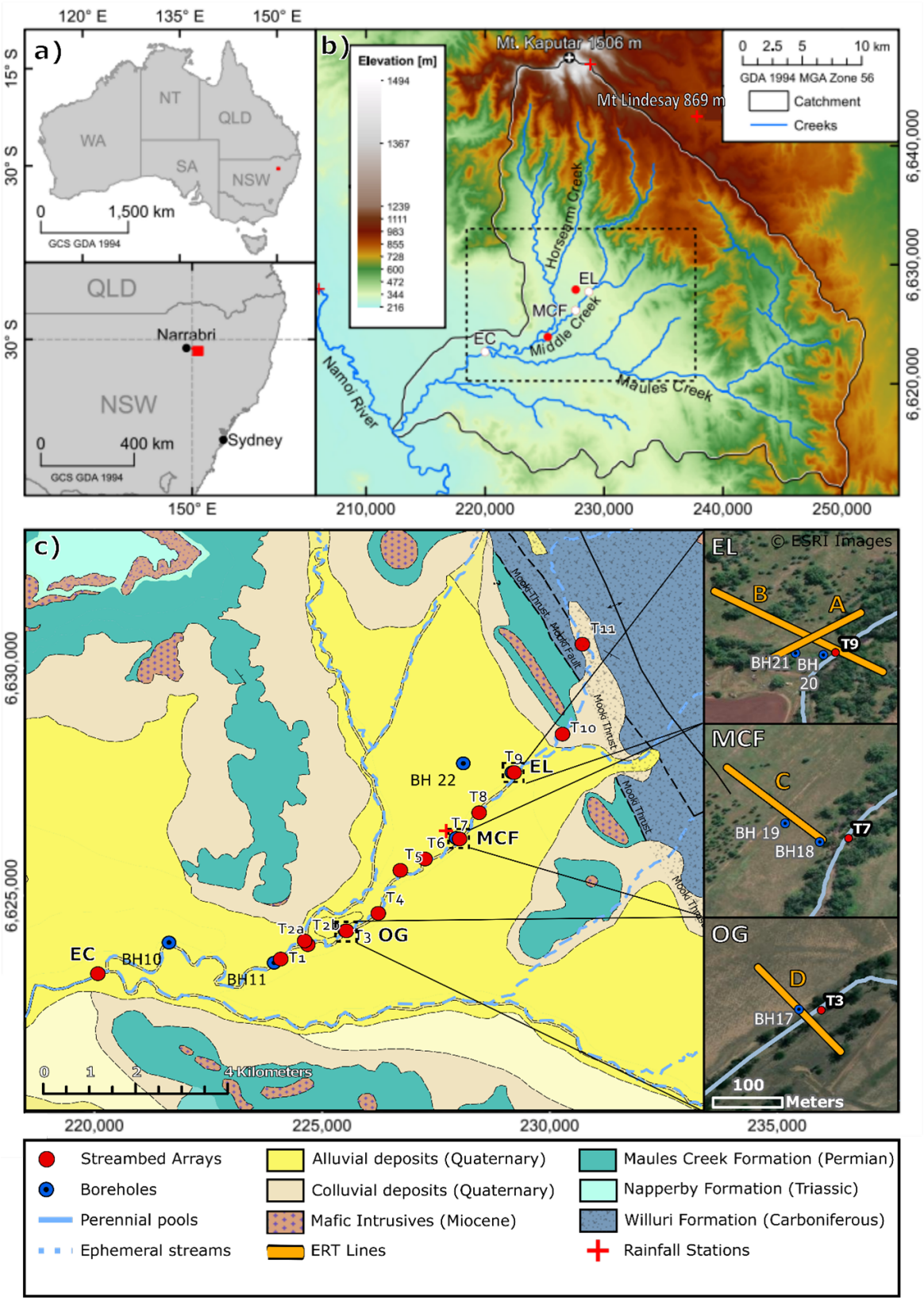

Fig. 3.1 Map showing a) Location of the Maules Creek catchment in relation to Australia and the state of New South Wales b) Catchment digital elevation map (DEM) with locations Mt Kaputar and Mt Lindesay meteorological stations. DEM used courtesy of Geoscience Australia c) Geological map centered around Middle Creek, with streambed array installations and boreholes. EL = East Lynne; MCF = Middle Creek Farm, OG = Old Glennelg; EC = Elfin Crossing d) Geophysical survey lines with line names shown inset. Map courtesy of Geoscience Australia.

Flow in Middle Creek is highly dependent on episodic frontal rainfall on the Nandewar Range that generates enough runoff in steep headwaters deliver high energy flows across the mountain front. These flows have cut 10-15 m deep channels into Quaternary sediments which form the alluvial plain. These channels are filled with a heterogeneous assemblage of boulders, cobbles, sands, and gravels that are substantially reworked by each major flow event, typical of alluvium in episodic high energy streams. Middle Creek, Horsearm Creek and Maules Creek form a system of such ephemeral channels.

Ephemeral flows in Middle Creek have been observed to extend all the way to the confluence with Horsearm Creek. Except under periods of prolonged drought, flow at Elfin Crossing is perennial, but ceases at some point between Elfin Crossing and the Namoi River because of losses to the underlying aquifer.

3.2.2 Monitoring of rainfall, groundwater, and stream stages/flows

The Maules Creek catchment has been well instrumented since 2009 funded by the Australian Government's National Collaborative Infrastructure Strategy (NCRIS). Stream stage and groundwater heads were monitored at four locations within the study site (with abbreviations used in Figures 3.1-3.8 in brackets): (1) East Lynne (EL), (2) Middle Creek Farm (MCF), (3) Old Glenelg (OG), and (4) Elfin Crossing (EC) (Fig 1). East Lynne is located 2.5 km downstream of the foothills that form the headwaters and is the most upstream site. Middle Creek Farm, Old Glenelg and Elfin Crossing are located a further 2 km, 3.5 km, and 5 km downstream respectively. East Lynne, Middle Creek Farm and Old Glenelg are located on Middle Creek, while Elfin Crossing is located at the confluence of Middle Creek and Maules Creek approx. 250m downstream from the confluence of Middle Creek and Horsearm Creek and is the most downstream site in my work.

Multi-level boreholes (BH 11, BH 17, BH 18 and BH 20 in Figure 3.1c) were installed adjacent to the ephemeral stream channel (distance within tens of meters) at the four sites, and piezometric heads were monitored at 15-minute intervals. The installation and setup of these boreholes is described by Cuthbert et al. (2016).

Stream stage was measured adjacent to boreholes at East Lynne, Middle Creek Farm and Old Glenelg using a using Solinst Levelogger pressure transducer at 15-minute intervals since June 2013. A digital camera placed at East Lynne has been capturing a record of flows in the creek since June 2012 and was used to determine the timing and approximate magnitude of the flow events that were not captured by the logger (Steam stage in red, Figure 3.2). Stream flow and stage at Elfin Crossing was taken from a permanent flow gauge established by the NSW Government (New South Wales Department of Primary Industries, 2014).Additional multilevel streambed arrays were installed at 12 different locations (T1-

T11) along Middle Creek (Fig 3.1c) to capture the water level of flow events occurring in a 60-day period from 20th March to 18th May 2016. Information on the details of this installation can be found in Rau et al. (2017).

Rainfall data was downloaded from the Australian Government Bureau of Meteorology (BoM) weather station directory for two locations: (1) Mt Kaputar National Park (BoM station #54151) and (2) Mt Lindesay Station (BoM station #54021, see Fig 1). Data from a full Campbell Scientific weather station installed next to BH19 at Middle Creek Farm was also used, representing rainfall on the alluvial plain. Most rainfall events were captured by the Mt Kaputar site and where rainfall data was missing, data from the Mt Lindesay and Middle Creek Farm were used to infill rainfall. For example, for the year 2020, the rainfall gauge at Mt Kaputar failed to record any rainfall, and from Mt Lindesay and Middle Creek Farm form the composite record for that year. Double mass analysis between Mt Kaputar and Mt Lindesay, and Mt Kaputar and Middle Creek Farm indicate that rainfall is closely correlated (r=0.99). This can be seen in Supplementary data (Figures A22 and A23).

3.2.3 Subsurface characterisation

Electrical resistivity surveys

Electrical resistivity tomography (ERT) was selected to map and characterise superficial deposits for hydrological interpretation (e.g. Chapter 2, Clifford and Binley, 2010; Cuthbert et al., 2009; Zarate et al., 2021).

ERT surveys were conducted at East Lynne, Middle Creek Farm and Old Glenelg sites using an ABEM SAS4000 Terrameter with an array of steel electrodes spaced 2.5m apart, and at various line lengths (see Figures 3.1d and 3.7). Topography was surveyed using a dumpy level. A map of the survey lines in relation to the study sites can be seen in Figure 3.1d. The Wenner electrode configuration was used to collect the data and the steel electrode locations were prepared using a saline mud solution to reduce surface resistance.

The data was inverted using the RES2DINV (Geotomo Software) algorithm (Loke, 2006) and a limit of 4 iterations was set to avoid model over-fitting. An absolute error data constraint was used that minimizes the error between the observed and calculated apparent resistivity values. A robust model constraint, incorporating topographic variations, was selected over a least squared inversion constraint since it is known to better resolve sharp geological boundaries expected within the study area (Loke et al., 2003). In this case, it was important to delineate the boundaries between the superficial deposits. Inverted data are presented as resistivity model sections (Edwards, 1977) and used in the interpretation of geoelectric layers and subsurface lithology.

Four ERT profiles were taken in April 2014, the locations of which are shown inset in Figure 1. Profiles B, C, and D are transects of Middle Creek at each of the study sites, while profile A is taken perpendicular to profile B, running parallel to the creek at East Lynne. Note that at Middle Creek Farm, steep bank conditions prevented the profile from crossing the creek, and profile C therefore terminates just before the creek bank (location of stream channel is drawn on profile for reference).

Geophysical well logging

GEOVISTA borehole logging equipment (Geovista, United Kingdom) was used in the deeper boreholes to establish profiles of bulk electrical conductivity and gamma-ray activity. Data were recorded at 10-mm intervals using an induction sonde (EM53) and a gamma-ray activity sonde.

Borehole lithological data, ascertained from drillers logs, were used to aid in interpretation and correlation of well log data and corresponding lithology. While these logs often contained ambivalent lithological descriptions such as: "sand coarse, some clay" or "clay sandy", due to the mixed nature of drill cuttings, they provide an insight into the range of possible lithologies contained within the quaternary sediments, which in turn were used in correlating the values obtained from downhole geophysical logging to values found in existing literature on the resistivity of sediments.

Slug testing

Slug tests were conducted by using a special device that seals the borehole and allows injecting compressed air to lower the pressure in the well by up to a few meters. After equilibration, the air was suddenly released through a valve and the re-equilibration (i.e., relaxation) of the water level was recorded at high resolution. The test was repeated for each of the bores to ensure representative results. A total of 9 slug tests were performed on five boreholes at each of the three study sites. The analytical solution by Hvorslev, 1951 was fitted to each of these datasets allowing averaging of the estimated sediment hydraulic conductivity values for each location.

3.3 Results

3.3.1 Hydrometric monitoring

Rainfall

A composite daily rainfall record from Mt Kaputar, Mt Lindesay and Middle Creek Farm meteorological stations are shown for the period 1/7/2012 – 1/12/2021 (Figure 3.2). The largest rainfall event occurred on 2/2/2013 for both sites in headwaters and was 149 mm/day and 150 mm/day for Mt Kaputar and Mt Lindesay respectively. On the alluvial plain, the largest rainfall event occurred on 20/02/2020 for Middle Creek Farm and was 99 mm/day.

Rainfall varies spatially across the catchment due to the orographic effect of the mountains and increases with elevation. The highest values of 824mm/year at Mt. Kaputar (1506 m AHD) and 679 mm at Mt Lindesay (869 m AHD) fall at the higher elevations (with both sites on the Nandewar Range), and the lowest values of 437 mm/year falling on the alluvial plain at Middle Creek Farm, (at 229 m AHD), only 19 km south Mt. Kaputar.

Streamflow responses

Stream stage hydrographs at the four sites from the period 1/7/2012 – 1/12/2021 are shown in Figure 3.2. These data, taken at 15-minute intervals, were averaged over 1-hour periods to aid in smoothing the data from barometric noise.

These data show that streamflow across all sites (except for Elfin Crossing, which is perennial) is highly episodic and responds to clustered periods of heavy rainfall that occur in the headlands (Figure 3.2). Not all these events lead to streamflow downstream however, and only events >66 mm/day generate enough streamflow to overcome channel transmission losses and appear at the furthest downstream site, Elfin Crossing.

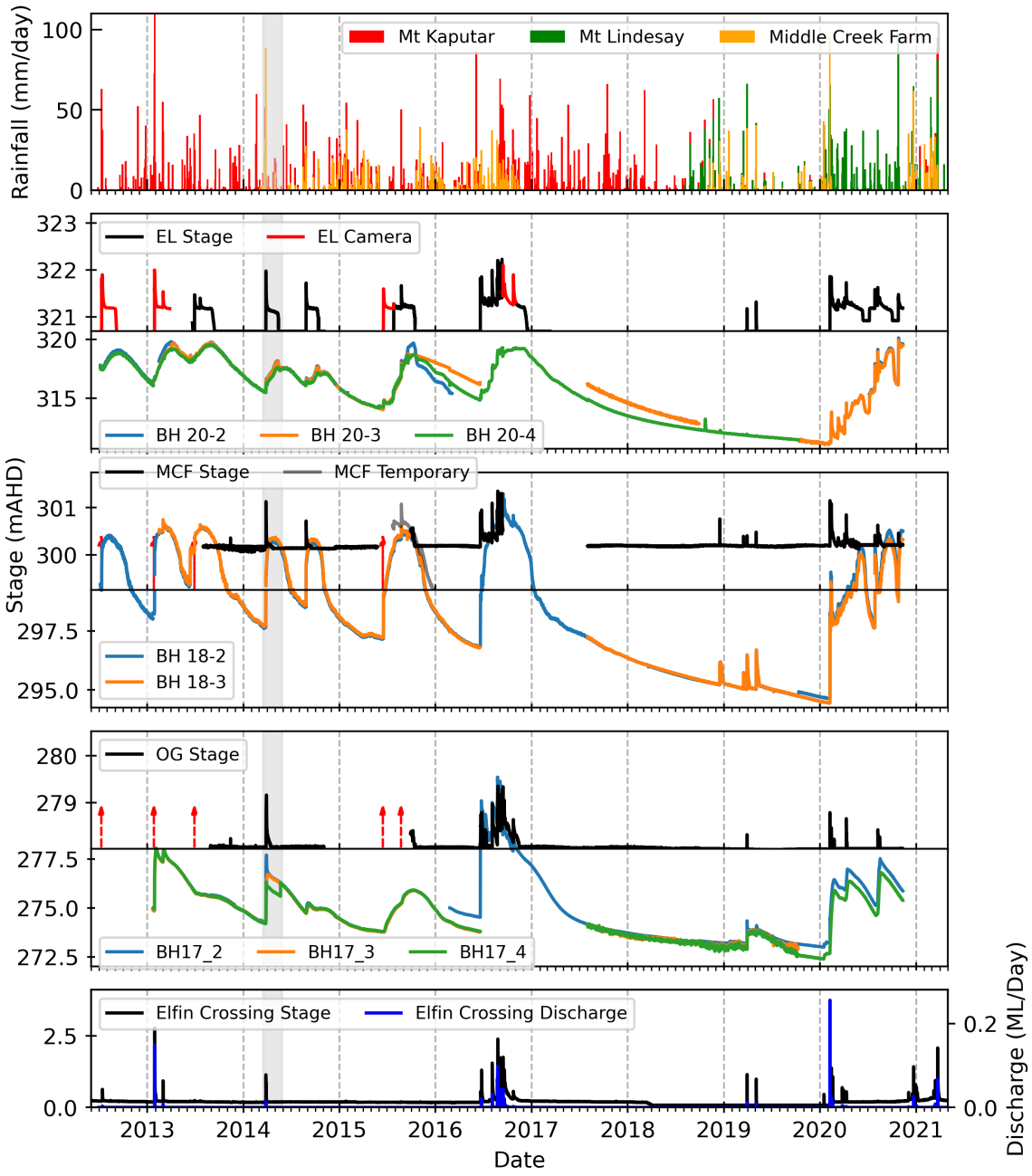

Fig. 3.2 Time series compilation of composite daily rainfall, stream stage hydrographs and groundwater heads. Stream stage and groundwater recorded at three study sites (East Lynne, Middle Creek Farm and Old Glennelg) were recorded at 15-minute intervals but averaged over 1-hour periods to aid in smoothing data from barometric noise. Red arrows denote streamflow events where there is missing data but can be inferred from the groundwater record. Shaded grey area denotes event captured in Figure 3.4. EL Camera denotes steam stage inferred from camera (see Section 3.2.2)

The highest recorded stage was in response to a large rain event occurring on the 25/08/2016. This event was not recorded by either rainfall gauge in the headwaters, however rainfall of 26.8 mm/day was recorded at Middle Creek Farm and was 26.8 mm (on 24/08/2016).

Streamflow events at East Lynne exhibit a gradual flattening of the hydrograph after the streamflow peak followed by a period of stable water level where the hydrograph exhibits a long 'shoulder' (Figure 3.3), and surface water is held within the channel at low flow rates. This behaviour is observed after every streamflow event in the study period, apart from two streamflow events occurring during the 2019 drought. A steady decline in water levels then follows this stable period, until streamflow finally ceases.

These streamflow events are shown in Figure 3.3, with each event plotted from their respective streamflow peaks and subsequent recessions (or until there is data available). Note that in cases where multiple streamflow peaks occur in a short space of time, the peak of the last streamflow event is used on the plot (See supplementary Figure S3 for plot containing previous events). When comparing each event, the length of the streamflow 'shoulders' after streamflow peaks remain remarkably consistent after every flow event in the time period ranging from 44 $\pm$ 3 days. This is despite large differences in stage (0.6 to 1.2 m) and flow (327 to 25523 ML/Day, at Elfin Crossing), and there is no correlation (pearson = -0.097) between the stream stage and duration of stable period at East Lynne (See Figure A24 for scatter plot).

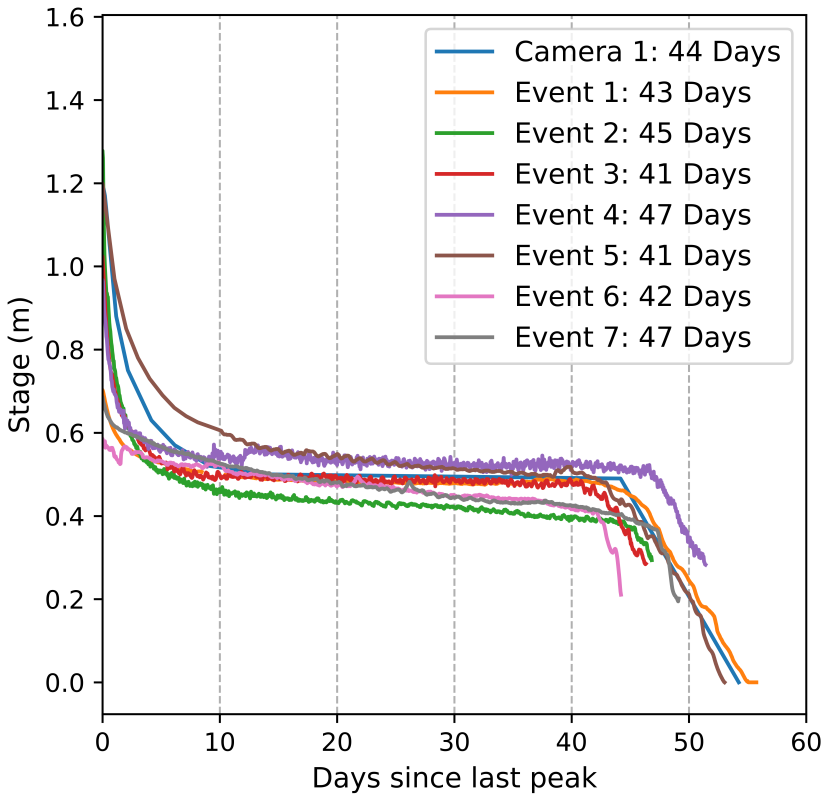

Fig. 3.3 Nested plot of streamflow hydrographs at East Lynne, plotted as days since last streamflow peak

When comparing the standard deviations (SD) to the mean values, the SD of the stream stages are a much greater % of the mean (SD = 28% of mean) than the SD% of the mean from the duration of streamflow (SD = 5.57% of mean), showing a much higher relative variance in the stage of streamflow events than the variance in duration of streamflow. Furthermore, the SD in flows at Elfin Crossing are a much greater % of the mean (SD = 138% of mean), since the stage discharge relationship is not linear (see Figure A25 for rating curve at Elfin Crossing), albeit Elfin Crossing integrates a much larger catchment than Middle Creek.

Similar behaviour cannot be confirmed at Middle Creek Farm however, as the logger was located at the end of a gravel bar and only captured the peak stage of each flow event. A streambed logger installed in a lower elevation within the streambed captured stage for August to December 2015 (MCF temporary shown in grey in Figure 3.2), and shows water

held in the channel for 35 days. In this instance, water held within the channel is due to groundwater levels rising above streambed elevation (see section 3.1.3).

At Old Glennelg the streamflow hydrograph rapidly declines after the streamflow peak, exhibiting short periods of flow before becoming dry within 3-4 days of rainfall cessation, with no extended stable flow periods as seen at East Lynne.

Elfin Crossing is generally perennial throughout the stage record due to a rise in the bedrock topography and a constriction of quaternary sediments at this site (Andersen 2009), only becoming dry in from March 2018 to Jan 2021, in response to a prolonged drought. The highest stream stage at Elfin Crossing was 4.29m, in response to the rainfall in January 2021.

Groundwater responses

Groundwater hydrographs are shown alongside stream stage at the four sites from the period 1/7/2012 – 1/12/2021 in Figure 3.2.

Heads varied between 0 and 8 m below ground level, with the thickness of the unsaturated zone generally increasing upstream. The groundwater responses are characterised by episodic rises that coincide with streamflow events along Middle Creek. Note that loading responses also occur at times of surface flows, as indicated by sudden increases in head in the groundwater hydrographs that correspond with onset of stream stage increases at the four sites. This is consistent with the variable lithology encountered during drilling, and the variability in formation hydraulic conductivity implied by slug testing, as described by Cuthbert et al., 2016 for a smaller number of events.

In general, following an ephemeral flow event there is an increase in vertical hydraulic gradients between piezometers at each borehole, followed by a more gradual re-equilibration of heads. These can be interpreted as being due to vertical, transverse, and longitudinal propagation of the pressure increase induced by streamflow losses to the underlying alluvium working over different characteristic timescales (Cuthbert et al., 2016). Vertical downward hydraulic gradients are initially induced near the creek which then dissipate on the time scale of days to weeks (for example, compare BH17_2 and BH17_4 in Figure 3.2). Longitudinal, down-catchment, gradients are apparent throughout the whole monitoring period suggesting they persist over longer time scales of years. These have an average gradient of 0.008 and indicate a general westward flow toward the Namoi River.

However, these groundwater responses vary at each study site. Heads in BH 20 (East Lynne) increase slowly in response to streamflow, peaking only when streamflow ceases at the site 44 $\pm$ 3 days after the streamflow peak. In BH18 (Middle Creek Farm), heads respond more rapidly to flow events and peak within 2-3 days of the streamflow peak.

These heads plateau and remain at the same head for a further 32 $\pm$ 2 days. Data from a temporary streambed logger installed at Middle Creek Farm for the period August to December 2015 show that water is held within the channel when groundwater levels remain above the streambed elevation. As such, surface water may be held within the stream for much longer than is seen in the stream hydrograph data at Middle Creek Farm, which only captures the peak of such flow events due its location on a gravel bar in the streambed. At BH17 (Old Glennelg), heads also rapidly increase in response to streamflow and peak within days of a flow event but fall much more quickly when streamflow ceases at the site 3-4 days after the streamflow peak.

These large fluctuations in heads interrupt long-term groundwater recessionary trends of various lengths, the steepness of which decreases downstream. During periods of prolonged no flow from Jan 2017 – Jan 2020, heads fell to 9m below the surface adjacent to the streambed at East Lynne, 6 m below at Middle Creek Farm, and 5m below at Old Glennelg.

Spatially detailed hydrological responses to a single runoff event (20th March to 18th May 2014)

To further examine the dynamics of streamflow variations along Middle Creek, data from 8 pressure loggers that recorded stream stage from 20th March to 18th May 2014 were plotted alongside nearby boreholes and are shown in Figure 3.4. This data is also presented in Rau et al., 2017, and illustrates the variation in stream hydrograph dynamics for one streamflow event at high spatial resolution but re-interpreted in light of additional data presented here. Site T9 is located at East Lynne, T7 at Middle Creek Farm and T3 and Old Glenelg (See Figure 3.1c for locations of pressure loggers). This flow event is also captured in time series compilation in Figure 3.2 and is shown in the shaded area in grey.

Streamflow hydrographs in this compilation behave differently for each array along the flow path (Fig 3.4). Arrays T11 and T10 exhibit the similar characteristics to long term streamflow behaviour seen at the East Lynne (T9) site (Figure 3.2). These upstream arrays (T11-T9) all show long hydrograph 'shoulders' (representing periods of stable water level) that increase downstream, from 22 days in T11 to 44 days at T9. Based on the long-term groundwater responses at T7 (Figure 3.2), it is likely that streamflow exists at a longer duration than indicated by the logger (which is situated on a bank with higher elevation than the bottom of the streambed) and water exists within the streambed at T7 for at least as long as T10. Downstream of T7, hydrograph shoulder lengths reduce substantially and exhibit rapid rises in groundwater levels 2 days after the streamflow peak, before quickly receding. Looking at the long-term trends (Figure 3.2), these dynamics

appear to be consistent in their shape and size during each runoff event, regardless of the size of rainfall event and subsequent runoff intensity (Figure 3.3).

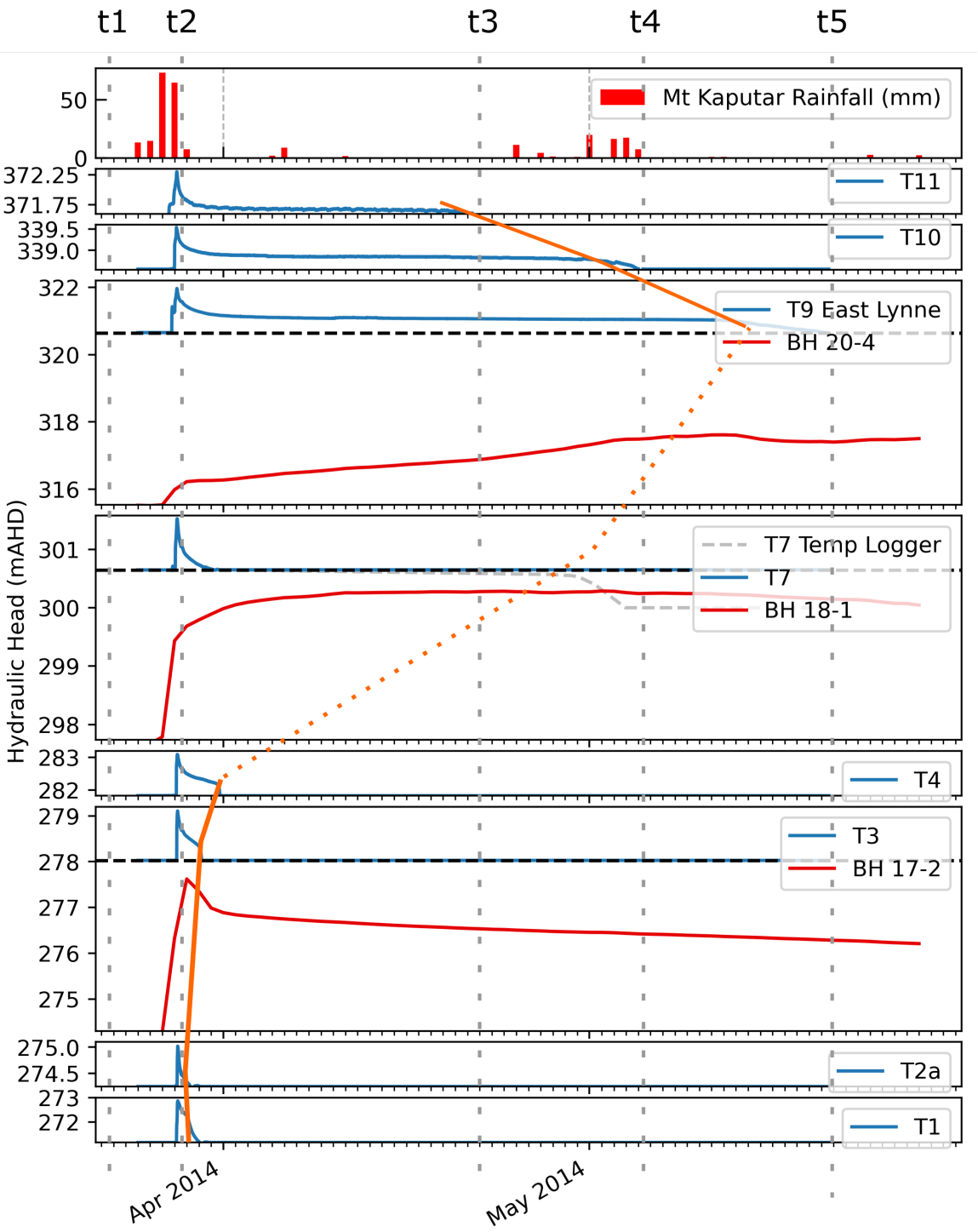

Fig. 3.4 Daily rainfall recorded at Mount Kaputar, hydraulic heads recorded by temporary streambed arrays installed along Middle Creek, including nearby groundwater heads. Dotted vertical lines indicate time periods described in section 3.3. Orange lines highlight increasing streamflow 'shoulders' from T11 to T9 and decreasing shoulders from T9 to T1. Note that as the streambed logger at T7 was situated on a bank, it does not capture full extent of streamflow and this shoulder is inferred by the dashed line. The data is reinterpreted from Rau et al., 2017.

3.3.2 Subsurface characterisation

Geophysical well logging

A total of 6 downhole geophysical logs were obtained in the period of April 2014 covering all three study sites (a list of boreholes and associated lithological logs where the downhole geophysical logs were preformed can be found in Table 3.1).

Integrating the results of the downhole geophysical logs with borehole log lithologies (as described in Section 3.2.3.2), four lithological groups were defined in the system using existing literature (Rubin and Hubbard, 2006) on the resistivity of sediments:

- Sands and gravels (>200 ohm m or <5mS/m)
- Interbedded sands and clays (200 to 50 ohm m or 5 to 20 mS/m)
- Clay dominated (50 to 20 ohm m or 20 to 50 mS/m)
- Bedrock (<20 ohm m or >50mS/m)

These interpretated lithological groups and conductivity ranges are shown superimposed onto the geophysical logs at each study site on Figures 3.5 and 3.6. Note that more detailed classification is made when describing the lithology of the Permian bedrock, where the exact interpretation from the drillers logs is used for each borehole (e.g., sandstone or shale)

In the uppermost Quaternary sediments, the gamma-logs have problems distinguishing between clay, sand, and gravel lithologies noted in the driller's logs. This effect was also observed in Andersen & Acworth, 2009, who hypothesised that the Quaternary sands and gravels of the Maules Creek catchment, derived from the volcanic Mt Kaputar complex, contain a very high potassium content.

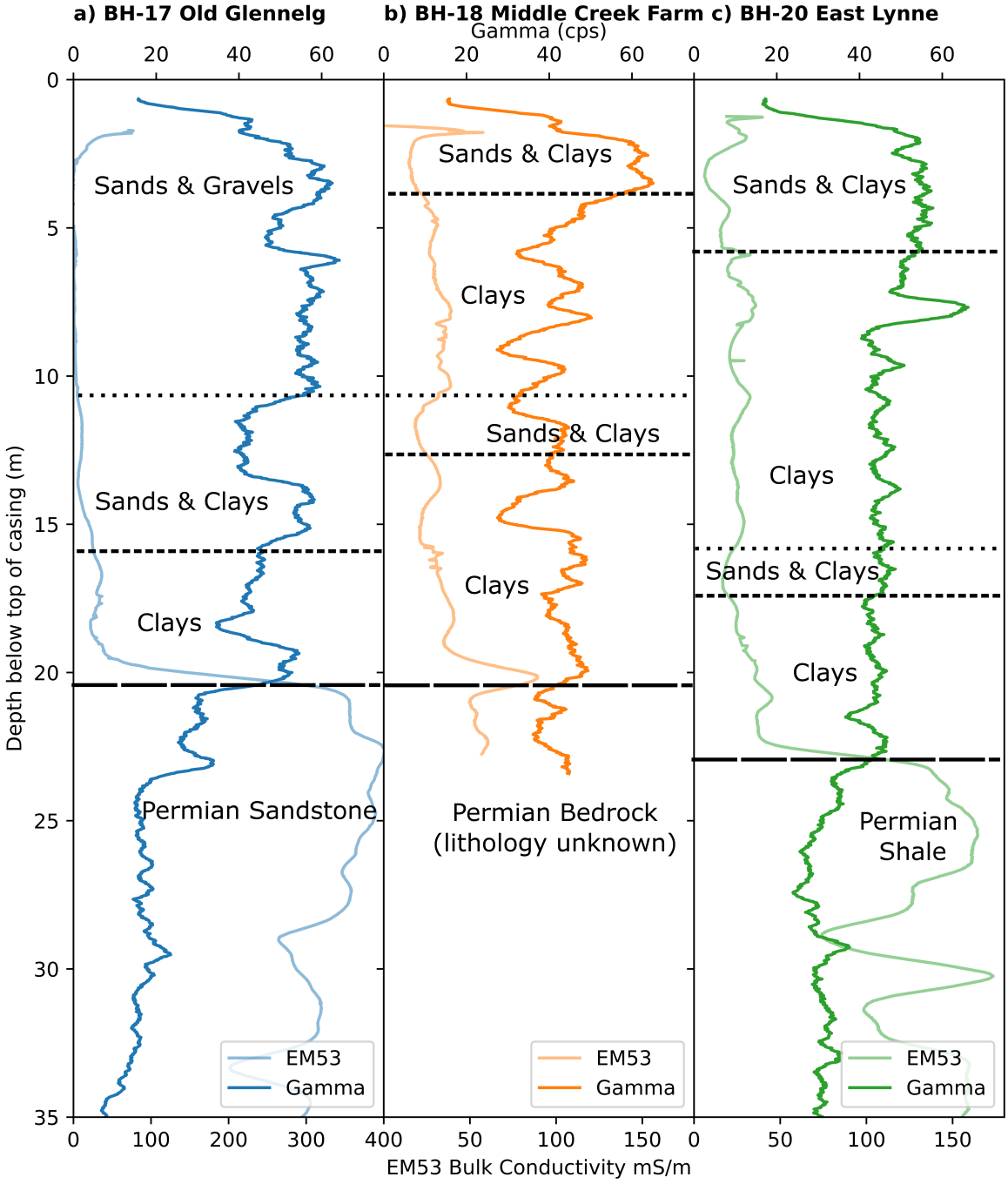

Fig. 3.5 Geophysical logs for boreholes at each of the three study sites. Lithological data taken from drill cuttings were used to aid in lithological interpretations of the data and these interpretations are superimposed. Note that BH18 was not drilled to the depth of the Permian bedrock and as such the interface and lithology here are unknown

As such, the total potassium content in the clay layers and the coarser alluvium would be very similar and therefore indistinguishable in the gamma logs. In this geological setting,

the gamma is a poor tool for distinguishing between the lithologies within the Quaternary alluvium.

However, the logs do show distinct decreases in gamma signal at deeper depths in BH17 (at 20 m) and BH20 (at 23 m), coincident with large increases in bulk electrical conductivity (EC) and a change from Quaternary sediments to Permian bedrock in the driller's logs. This decrease in gamma is likely representative of a change in lithology from potassium-rich Quaternary deposits to more potassium-deprived Permian (Maules Creek formation) bedrock beneath.

In contrast, the bulk EC shows clear differences between the boreholes in the uppermost Quaternary sediments. These differences are highlighted in Figure 3.6, where a smaller scale (0 to 80 mS/m) is used to distinguish lithologies at lower bulk EC typical of unconsolidated deposits. In the uppermost 12m, the sediments at BH 17 consist of low conductivity sands & gravels. These transition to sands with interbedded clays and finally clays before reaching the much higher conductivity Permian bedrock (sandstone, as noted in the drillers logs), which reaches conductivities of up to 400mS/m (see Fig 3.5). These very high conductivities are likely due to slightly saline nature of the deeper groundwater in the catchment.

In BH18 and BH20, the sediments consist of sands and clays in the uppermost 3m. After this point, the lithology is dominated by higher conductivity clays with possible layers of lower conductivity interbedded sands (at 11 m in BH18, and 17 m in BH20). In BH20 there is again a sharp increase in bulk EC (coincident with gamma decrease), signalling a transition into Permian bedrock (shales, in the drillers logs). Note that at BH18, both drillers' logs and geophysical well logs only extend to a depth of 23m, and as such this bedrock interface was not captured at this site.

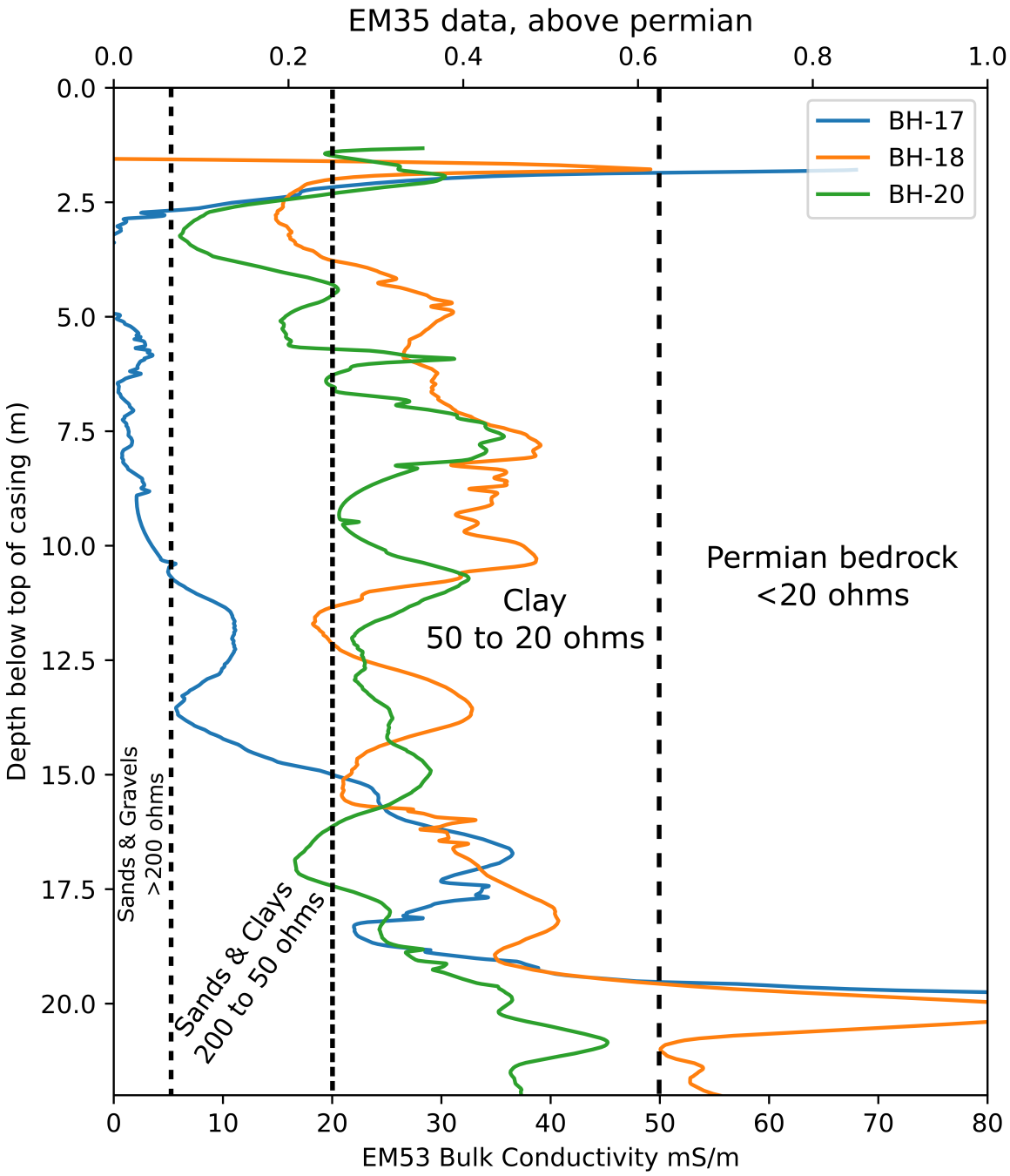

Fig. 3.6 EM53 Bulk Conductivity logs with smaller scale (0 to 80mS/m) to highlight variations in conductivity of quaternary sediments. Lithological interpretations with the aid of drill cuttings are superimposed alongside resistivities.

Electrical resistivity imaging

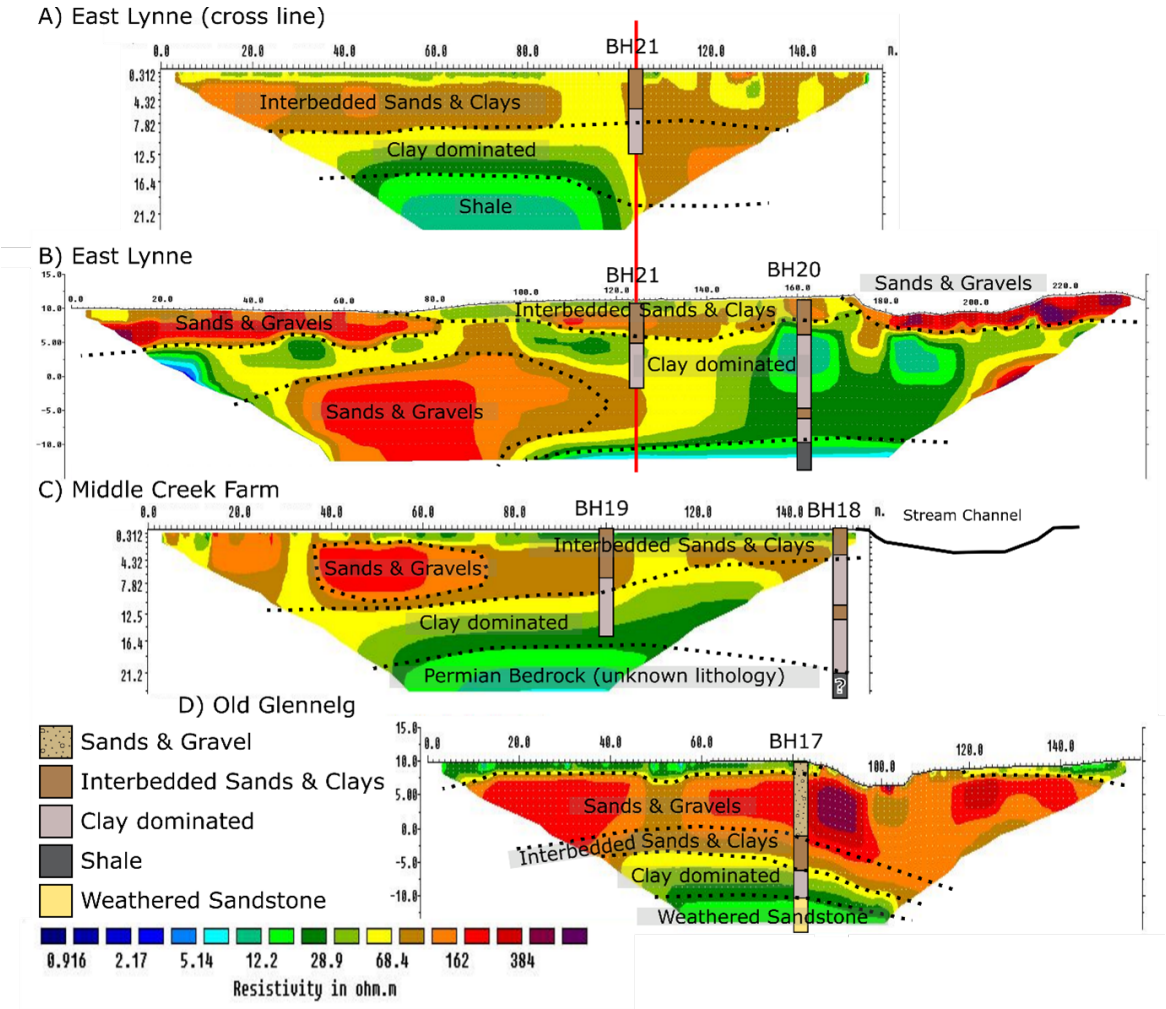

Fig. 3.7 Electrical resistivity images of transects taken at each study site. Locations of boreholes in relation to the lines are shown and lithological interpretations from section 3.2.1 superimposed onto the boreholes. Intersection point between lines a) and b) at East Lynne shown in red.

ERT profiles taken at each of the study sites, locations of which are shown inset in Figure 3.1, are shown in Figure 7. Boreholes with interpreted lithology based on combined data from geophysical well logging and drill cuttings (see section 3.3.2, Geophysical well logging) are superimposed. These were used to aid in interpretations of lithological layers described below.

The profiles taken at East Lynne show an upper zone of (3-5 m thick) with resistivity ranging from 70-300 Ohm m interpreted as sands & clays. In profile B, the alluvium surrounding the creek bed is apparent, exhibiting very high resistivities >300 Ohm m.

Pockets of these high resistivity alluvium appear to be present on the middle and left side of profile B and are interpreted as former channels. Below this zone, the profile becomes less resistive with depth, with resistivities falling between 10 and 50 Ohm m, as the lithology is interpreted to be clay dominated. At the very bottom of the profiles, the Permian shale bedrock begins to have an influence, with resistivity dropping below 10 Ohm m.

Middle Creek Farm exhibits a similar resistivity profile to East Lynne (lines A & B). A thin zone (0.5m to 1m thick) of low resistivity (15-30 Ohm m) material exists at the top of the profile. Below this, there exists a layer (5 – 8m thick) of higher resistivity (50-100 Ohm m) material, interpreted as sands and clays. Like profile b, a prominent pocket of high resistivity (>300 Ohm m) material is seen on the left side of the profile, 1m below the surface, indicating the presence of a former channel. At 10m, the lithology becomes less resistive and is interpreted to be clay dominated. At 20m depth, the resistivity again drops below 10 Ohm m as the low resistivity Permian bedrock affects the profile. Note that the presence of this bedrock is only interpreted here as drillers and geophysical well logs at this location do not extend this deep.

In profile D, a thin layer of low resistivity topsoil, like that in profile C, can be seen in as a continuous line 1-2 m thick extending across the profile. This line is interrupted at the stream channel by the presence of higher resistivity (200-300 Ohm m) streambed alluvium. However, it is difficult to distinguish the geometry of this alluvial material, as the underlying geology consists of similar high resistivity (150-350 Ohm m) materials, interpreted as sands and gravels. This layer of sands and gravels extends from 1 to 11m below the surface, before transitioning to a zone of lower resistivity (10-50 Ohm m) material interpreted as clay dominated and finally Permian sandstone bedrock (10 Ohm m) at a depth of 23 m. Pockets of higher resistivity (>300 Ohm m), as seen in profiles b and c, can also be seen in the sands and gravels on the left- and right-hand sides of profile d. These former channels exist at all three study sites, and satellite imagery confirms the continuity of the channels at the surface level. The continuity and geometry of the former channels at depth is unknown.

Aquifer testing

The slug testing results are shown in Table 3.1, as well as the lithology at each borehole interpreted in Section 3.3.2, Geophysical well logging. Due to difficulty pumping, possibly due to low conductivity of materials surrounding well screen, the test at BH 20_4 failed. Furthermore, possible high conductivity materials surrounding the screen at BH17_2 (interpreted as Sands and Gravels) prohibited getting enough pumping pressure to conduct a test at BH 17_2.

BH	Hydraulic Conductivity (m/d)	Depth to base of screen	Interpreted Lithology
17_2	High K inferred from low pumping pressure	13.5	Interbedded Sands and Clays
17_4	0.340	36.5	Permian Sandstone
18_2	0.470	12	Interbedded Sands and Clays
18_4	0.075	24	Permian Bedrock (lithology unknown)
19_1	0.017	11.5	Clay Dominated
19_2	0.039	23	Clay Dominated
20_2	0.021	12	Clay Dominated
20_4	Low K inferred from difficuly pumping	41	Permian Shales
21_2	0.003	13.5	Clay Dominated

Table 3.1 Hydraulic conductivity values of boreholes at various depths, obtained via slug testing. Interpreted lithology from Section 3.2.1 also added.

The results show low hydraulic conductivity sediments of 0.021m/day, interpreted as clay dominated, at depths of 12m at BH20_2, 2m away from the stream, at East Lynne. This hydraulic conductivity decreases to 0.003 m/day at BH21_2, which is a further 37m away. In the interpretation of downhole geophysical logs, sediments in boreholes at these depths were classified as clay dominated. However, the very low conductivities at BH21_2 suggest these sediments are more akin to pure homogenous clays, as opposed to clays with interbedded sands or silts as previously interpreted.

Sediments with similar conductivities (0.017 m/day) as BH_20 exist at the same depth (11.5 m) at BH19_1 at Middle Creek Farm but situated at 50 m away from the stream. Sediments increase in hydraulic conductivity closer to the stream at BH18 (which is situated 10m away from the stream) at the same depth, going from 0.017 to 0.470 m/d. These also correspond in a change in lithology from clays to interbedded sands and clays.

At greater depths (41m) the Permian sandstones at Old Glennelg exhibit conductivities of 0.340 m/day and are at the same order of magnitude as the sands and clays recorded at 12m at BH18_2. Conductivity decreases with depth at Middle Creek Farm, going from 0.470 m/d at 12m to 0.075 m/d at 24m. However, since drillers logs did not make it this far, lithology is unknown and can be interpreted as bedrock (see section 3.3.2).

3.3.3 An alluvial storage model for controlling water balance partitioning in Middle Creek

The results in Figures 3.2-3.4 illustrate the complex surface water-groundwater dynamics and water balance partitioning at Middle Creek. Based on these data, and the combined subsurface characterisation in Section 3.3.2, a hydrogeological conceptual model of the Middle Creek ephemeral stream system was developed (Figure 3.8) that seeks to elucidate the complex surface water - groundwater dynamics by way of variations in superficial geology at each site. Using time periods defined in Figure 3.4 (t1-t5), I propose that the superficial geology surrounding Middle Creek controls water balance partitioning as follows:

t1 Streamflow is non-existent in the creek and the groundwater system is in long term longitudinal recession. Large frontal storms generate orographic rainfall that quickly causes infiltration excess overland flow and large amounts of runoff are discharged across the mountain front. This is consistent with streamflow generation in dryland ephemeral streams, where, due to orographic effects, streamflow often begins in the mountain headwaters and upstream reaches of a catchment, and propagates downstream (Bull and Kirkby, 2002; Shanafield et al., 2021).

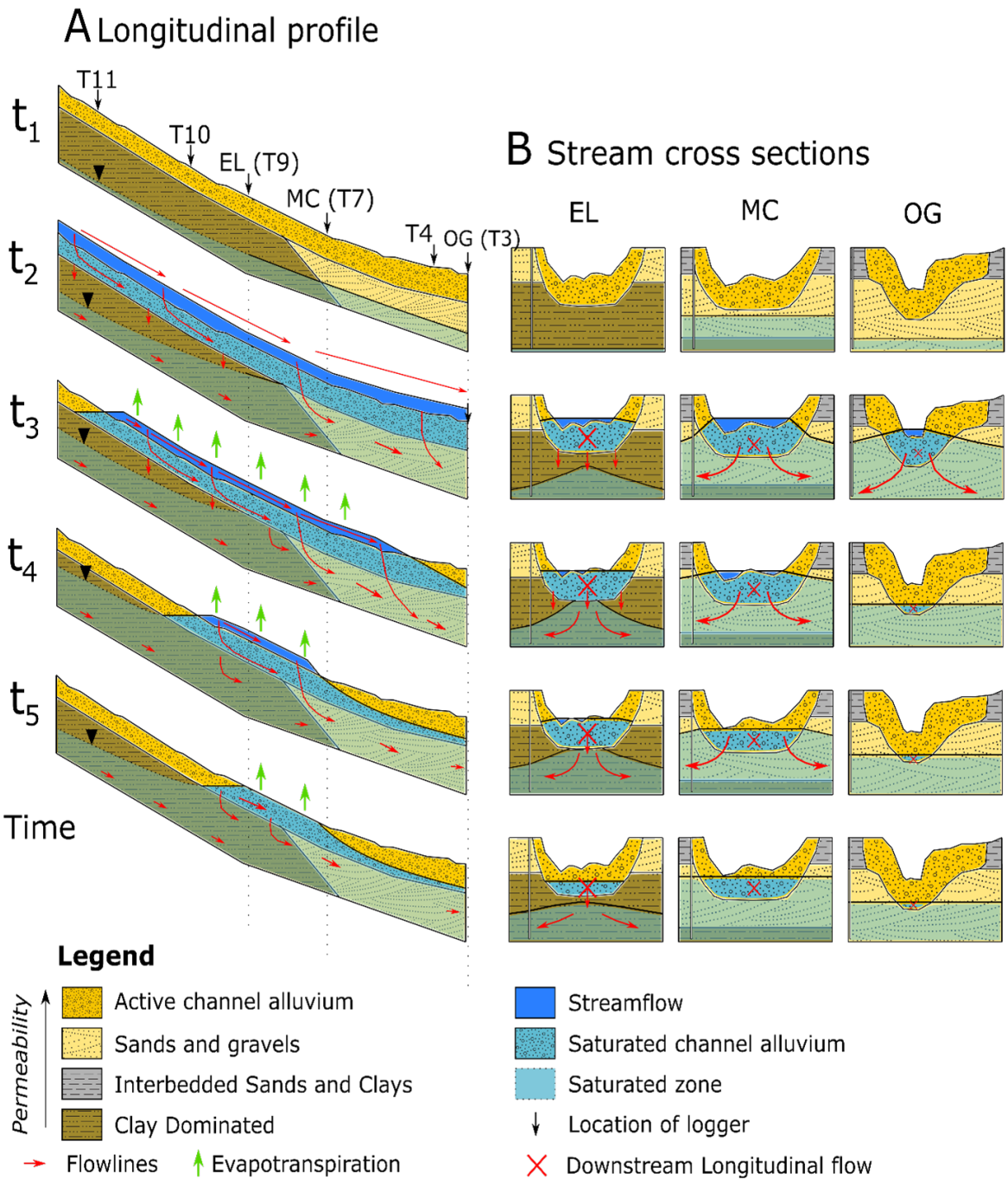

Fig. 3.8 Conceptual model of how superficial geological structure controls water balance partitioning and streamflow generations in Middle Creek.

t2 Runoff coalesces into ephemeral streams and the streamflow flood wave propagates downstream. As this runoff infiltrates the streambed, a perched groundwater mound saturates the streambed from the bottom upwards (Dahan et al., 2008b; Moulahoum,

2018; Wekesa et al., 2020) quickly filling the available 'alluvial storage' in the highly permeable alluvium (Telvari et al., 1998) and streamflow peaks in 1-2 days.

Upstream of Middle Creek Farm (T11-T7), the high 'permeability contrast' between alluvial material and surrounding low permeability (clay dominated) deposits slows the vertical infiltration of perched alluvial water. Groundwater mounding also occurs in the deeper aquifer beneath the alluvium, but its rise is slow due to the permeability contrast. Perched alluvial water is instead preferentially partitioned longitudinally downstream within the alluvium and manifests itself as streamflow from T11 to T7.

Rapid vertical infiltration occurs only when streamflow reaches higher permeability Quaternary sands and gravels downstream of Middle Creek Farm (T7) (and towards Old Glennelg (T3). Here infiltrating streamflow quickly fills the unsaturated zone between the water table and the stream and groundwater within the Quaternary deposits rises rapidly.

t3 Streamflow ceases at T11, but infiltrated water retained within the alluvium at T11 maintains longitudinal drainage downstream to T10 due to high permeability contrast between alluvium and underlying geology. This longitudinal drainage keeps downstream alluvial storage full, and due to the slope of the channel, manifests itself as flow within the streambed from T10 to T7.

Downstream of this site (T7-T1), higher permeability sands begin to dominate the sediments surrounding the alluvium and vertical flow is no longer slowed by high permeability contrasts. Vertical infiltration into these sediments becomes greater than the incoming flow from stored alluvial water, and the groundwater mound that has formed within the alluvium at these sites dissipates at a faster rate than upstream. The water table drops below the streambed faster, causing flow to cease at Old Glennelg.

t4 The duration of stable streamflow increases in duration downstream from T11-T9, owing to increased volumes of alluvial store (and therefore alluvial water flowing longitudinally) upstream of each site. Eventually streamflow only exists at East Lynne (T9), and streamflow duration peaks at 44 $\pm$ 3 days. In this period of stable streamflow, some water in the perched saturated alluvium continues to slowly infiltrate vertically and recharge the aquifer below, causing the deeper groundwater mound to grow.

In this period where extended durations of perched water exist within the alluvial store, evapotranspiration may also be maximised as riparian vegetation utilises this readily

available, shallow store of water. In some IRES evapotranspiration from this perched alluvial store can account for up to 100% of streamflow, and regional groundwater recharge is negligible (Bauer et al., 2006; Villeneuve et al., 2015).

t5 After 45 days, alluvial water storage upstream from T9 has been completely drained longitudinally and flow within the stream ceases. Stream becomes ephemeral once again. Eventually, the groundwater mound fully redistributes, and only long-term longitudinal groundwater recession occurs again.

3.4 Discussion

I consider the observations presented in this chapter to consist of an unusually rich dataset in both space and time, allowing an unprecedented insight into both IRES hydrodynamics and its control by the underlying geological structure.

My conceptual model outlines two dominant controls on water balance partitioning in intermittent rivers and ephemeral streams:

1. The permeability contrast between recent streambed alluvium and underlying (and surrounding) geology.

2. The volume of recent alluvium, which I call the 'alluvial store' at, and upstream, of the site. In areas of high permeability contrast (i.e., high permeability recent alluvium and lower permeability surrounding geology), restricted vertical infiltration into low conductivity materials allows for perched water and preferential longitudinal flow within recent alluvium, keeping alluvial stores downstream 'topped up' even when streamflow upstream has ceased. In areas of low contrast (i.e., high permeability recent alluvium surrounded by similar high permeability geology), perched water is unable to form, and instead streamflow is partitioned vertically to a greater extent, increasing soil moisture in the unsaturated zone, and recharging the water table within the high conductivity surrounding lithology.

The volume of recent alluvium at a particular site, and upstream of it, will also vary depending on stream order and position within the catchment (K L Jaeger et al., 2017). In channels located upstream, which drain a smaller area of catchment, there is not only a smaller alluvial store, but also less contributions in longitudinal flow due to a smaller volume of alluvial store upstream. In downstream reaches, which drain a greater extent of the catchment, also receive a greater volume of potential alluvial water from upstream reaches.

The dominant controls outlined in my conceptual model are widely transferable to other dryland catchments. High permeability contrasts between permeable alluvium and underlying low conductivity geology seen at East Lynne and Middle Creek Farm appear to be common features in dryland ephemeral streams worldwide (Acworth et al., 2020; Brunner et al., 2011; Goodrich et al., 2004; Lorentz et al., 2020; Rassam et al., 2006; Séguis et al., 2011; Shanafield et al., 2021; Villeneuve et al., 2015), and have been shown to control streamflow generation in dryland IRES (Bourke et al., 2021). At Old Glenelg, where there is a low permeability contrast, stream stage and groundwater responses are consistent with the dynamics of ephemeral streams where large unsaturated zones of several metres exist, and rapid vertical infiltration and recession occurs (Brunner et al., 2011; Quichimbo et al., 2020; Shanafield and Cook, 2014).

The partitioning of alluvial water into streamflow due to this contrast can be seen in the ephemeral sand rivers of southern Africa, where streamflow occurs via saturation excess only after the streambed 'alluvial store' has been filled (Dahlin and Owen, 1998; Hughes, 2008; Nord, 1985). This flow is consistent with the work of Lange et al., 1998, who found via artificial tracers that infiltrated streamflow within the alluvial store reappears on the surface due to the slope of the channel. In the crystalline basements of western Africa, Séguis et al., 2011 also found that alluvial stores of seasonal perched groundwaters are the major contributor to streamflow.

Perched alluvial water provides a valuable supply of accessible water for local people that is commonly exploited either by shallow pits dug in the sand or by well-points, infiltration galleries or collector wells in the river bank. (Hussey, 1997, Walker et al., 2018). Furthermore, this perched alluvial store has been shown to be enhanced by the construction of sand dams in southern Africa (Love et al., 2010). The alluvial store also allows more abundant and functionally diverse vegetation to develop in riparian areas (Shaw and Cooper, 2008). Water within this alluvial store is often consumed by trees and other vegetation (Bauer et al 2006). In some IRES where perched alluvial stores of water exist, evapotranspiration can account for up to 100% of streamflow, and regional groundwater recharge is negligible (Bauer et al., 2006; Villeneuve et al., 2015). In Australia, water within perched aquifer systems plays a crucial role in maintaining Eucalpytus camaldulensis trees (Cook et al., 2008).

At East Lynne, the stream stage hydrograph exhibits the longest period of flow, due to a combination of high permeability contrast and contributes from alluvial stores of water upstream (which in turn, flow longitudinally due to their own permeability contrasts). Thus, at Middle Creek, the combination of these two controls creates a 'goldilocks zone' of stream flow duration and perched water presence within the alluvium, maximising both

riparian water availability within the alluvium, and the potential for groundwater recharge due to the maximal persistence of this perched water. The two dominant controls from my conceptual model likely exist as a continuum in dryland catchments globally where these two controls interact and align, and I hypothesize that the combination of these two controls, the permeability contrast and size of alluvial store upstream, may create goldilocks zones where various components of the water balance (e.g., Evapotranspiration, groundwater recharge) are maximised.

While the results of this chapter share similarities with other sites that exhibit episodic groundwater recharge in response to high intensity rainfall events (Jasechko and Taylor, 2015; Lange, 2005; Owor et al., 2009; Seddon et al., 2021b; Taylor et al., 2013b), long term trends in streamflow characteristics and groundwater responses at East Lynne (Figure 3.2) indicate that groundwater recharge is limited by streamflow duration, which in turn, is independent of the size of rainfall and subsequent runoff event (Figure 3.3).

Since streamflow length is mediated by geological controls to 44$\pm$3 days, the largest recharge events in the catchment occur when multiple streamflow events are compounded, generating flow in the stream for much longer than 47 days. Although general climate forecasts for the region show that the mean annual rainfall will remain the same even though it is likely to arrive in more intense events (Taylor et al., 2013a), in Middle Creek, it may be the frequency of events that lead to more recharge and not the intensity of rainfall. This hypothesis should be tested in detail in further studies as it has implications for groundwater recharge and ecosystem functioning under changing climate and hydrological conditions in the future.

3.5 Conclusion

In this chapter, I examined variations in superficial geology and relationships between rainfall, streamflow, and groundwater in an ephemeral stream system in semi-arid Australia. I consider this data set to be unusually rich in both time and space. Spatially detailed responses to a single runoff event reveal that periods of highly stable stream-stage (following streamflow peaks) increase downstream to a maximum, before abruptly reducing further downstream. Long term hydrometric monitoring confirms that streamflow lasts 44$\pm$3 days after each streamflow peak and is independent of the size of the preceding streamflow peak.

A combination of downhole geophysical logging, near surface electrical resistivity imaging and slug testing were used to characterise the spatial and hydrogeological variation of the superficial geology surrounding the ephemeral stream. This revealed that Quaternary sedi-

ments surrounding the streambed alluvium transition from low permeability clay dominated sediments to higher permeability sands and gravels downstream.

Using these two datasets, I developed a generalized conceptual model of the ephemeral stream by way of variations in superficial geological structure around the stream elucidating the complexities in surface water-groundwater dynamics. I hypothesise that two dominant controls on water balance partitioning exist:

1. The permeability contrast between recent streambed alluvium and surrounding superficial geology.

2. The volume of recent alluvium at and upstream at a given location within the catchment.

High permeability contrasts between streambed alluvium and the surrounding superficial geology controls water balance partitioning within the stream by creating an 'alluvial store' of perched water within the streambed sediments that is partitioned longitudinally downstream within the alluvium. Longitudinal flow from alluvial volumes upstream manifests itself as streamflow and maintains the saturation of alluvium downstream. Where streambed alluvium intersects areas with lower permeability contrasts, alluvial water is more readily partitioned vertically. These two controls exist as a continuum within the catchment and likely intersect in any given dryland catchment to maximise the available water within the alluvium in both space and time, creating a 'goldilocks zone' that maximises riparian water availability and groundwater recharge potential.

My conceptual model provides a first step for improved understanding of water balance partitioning in dryland IRES. Future work will focus on the transferability of this conceptual model to other dryland catchments which have sufficient groundwater level data available, with the end goal of developing a process understanding of water balance partitioning within IRES that can be upscaled over broad areas and ungauged catchments. This would allow improved understanding of water availability and groundwater recharge under a changing climate.

Chapter 4

A new framework for understanding groundwater recharge processes in drylands

4.1 Introduction

The relationships between groundwater recharge and physical controls have long been of scientific and practical interest. Previous studies have identified climate, topography, geology, soil conditions, topography and vegetation as controls on diffuse recharge rates in drylands (J J de Vries and Simmers, 2002; Keese et al., 2005; Small, 2005a) and more recently there has been renewed interest in using ground-based estimates of groundwater recharge to gain insights into controls on recharge globally (e.g. Moeck et al., 2020; Mohan et al., 2018; West et al., 2022). However, these studies cover a broad spectrum of climates and recharge landscapes and focus on controls on diffuse recharge processes.

There is therefore a need for a conceptual model of groundwater recharge processes in drylands that incorporates the dominant climate and physiographic controls on both diffuse and focused recharge. These controls are distinct and differ from controls identified in humid regions, stemming from the fact that dryland regions exhibit key differences in the dominant hydrological processes that can greatly impact the water partitioning of arriving rainfall.

In Chapter 1, I highlighted the importance of groundwater in supporting current and future water supply in drylands and, in turn, the need to understand the processes that control groundwater recharge and its spatio-temporal distribution. In Chapter 2, I highlighted the role of superficial geology in providing pathways for focused recharge to

occur. In Chapter 3, I hypothesised the role of alluvial storage and permeability contrasts to redistribute this focused recharge in the sub-surface (and re-emerge as surface flow).

In this chapter, I make use of those key findings, and combine them with the latest literature to present a novel framework for understanding groundwater recharge in drylands. While other studies group recharge controls into independent variables (e.g. Moeck et al., 2020) or into distinct landscape domains (e.g. West et al., 2022) I group identified recharge controls into a hierarchy of processes that encapsulate their role in converting rainfall to recharge. Each process is governed by a set of climate or physiographic controls that exist as a continuum in the landscape and these controls can combine to produce predictable patterns of partitioning of the dryland water balance This novel framework for understanding dryland recharge includes four main processes as follows:

Climate: Rainfall is a first order control on available water for recharge and generating runoff. Aridity, the ratio of PET to precipitation, greatly impacts the partitioning of available water for recharge, and is thought to control dominance of diffuse or focused recharge processes (Cuthbert et al., 2019).

Concentration: Land surface characteristics interact with rainfall characteristics to enable the potential for diffuse recharge by focussing infiltration in time, or produce and concentrate runoff into topographical depressions, increasing the potential for focused recharge by concentrating water in space as infiltration from surface water bodies.

Delivery: Permeable pathways deliver this concentrated infiltration to perched (shallow) or deep water tables. Vegetation controls partitioning of this infiltration into evapotranspiration or potential recharge. A 'permeable pathway' is an area of sufficiently permeable subsurface soil or other superficial deposit which enables potential recharge to occur via the matrix or bypass flow mechanisms, or a combination of both, by linking a range of vertical and lateral pathways. These pathways can deliver potential recharge via:

1. Direct delivery to perched or deeper water tables via permeable pathways.
2. Indirect delivery via lateral re-distribution of perched water within certain configurations of superficial geology or permeable pathways in the subsurface, such that the spatiotemporal distribution of actual recharge may differ considerably from the distribution of potential recharge.

In Chapter 1, I explored the most current understanding of dryland recharge processes, which are summarised on Figure 1.1. The framework outlined in this chapter is summarised

in Figure 4.1, which builds upon Figure 1.1 by incorporating the findings of Chapters 2 and 3, and the processes described above. In section 4.2. the rationale for each process is examined in detail, and the controls within them, are explained in detail within the relevant sub-sections.

The controls outlined in Section 4.2 likely exist in specific ranges depending on their longitudinal (i.e., upstream to downstream) position in the catchment. Therefore, by using a geomorphic model of a generalized dryland catchment, I group these controls based on their likelihood of occurrence within this model (Section 4.3) to explore the efficacy of this framework in explaining the observed variability of dryland recharge processes at the catchment scale.

I then discuss the transferability of this framework in making generalised predictions of predominant recharge processes (i.e. diffuse versus focused) between differing dryland settings based on the differing combinations of controls (Section 4.4).

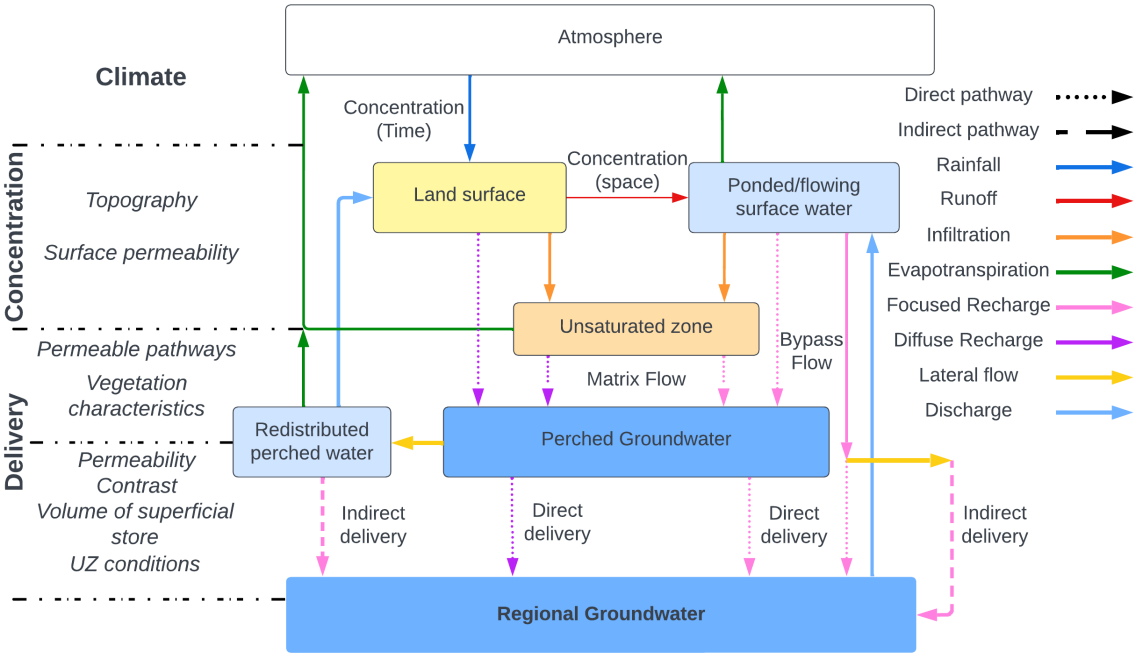

Fig. 4.1 Framework for understanding groundwater recharge in drylands. This figure builds upon Figure 1.1 (current understanding of dryland recharge processes) by incorporating the findings of Chapters 2 and 3. Key processes are shown in bold on the left hand side, and associated acting process domains shown with dashed black lines. Grouped controls are shown italicised and correspond with subheadings in Section 4.3. Note that discharge denotes both perched groundwater return flow to the surface (as both baseflow and surface runoff) or discharge into larger perennial bodies of water.

4.2 Processes and controls

4.2.1 Climate

Precipitation is a first order control on groundwater recharge, as it determines the quantity of water available to be partitioned into groundwater recharge (Stonestrom and Harrill, 2007). Studies in Africa show that long term average rainfall is strongly correlated with long term average (LTA) recharge (MacDonald et al., 2021). Globally, variability in both observed (Moeck et al., 2020) and modelled (P Döll and Fiedler, 2008) recharge are correlated with LTA rainfall.

The correlation between LTA rainfall and LTA recharge does not explain relationships on a shorter time scales as LTA rainfall smooths out the individual high and low years(MacDonald et al., 2021) and there are other climatic factors other than total amount of rainfall that exert an influence on recharge. For example, there are numerous studies that demonstrate that rainfall characteristics – rainfall intensity and spatio-temporal variability, play a crucial role in controlling groundwater recharge in drylands (e.g. Dawes et al., 2012; Dunkerley, 2012; Goni et al., 2021; Hu et al., 2019; Owor et al., 2009; Seddon et al., 2021; Vivoni et al., 2009).

Drylands are characterised by low LTA rainfall with high spatio-temporal variability (Aryal et al., 2020; Zoccatelli et al., 2019). Temporally, inter-annual and multi-decadal variations in precipitation impacts recharge rates (Kuss and Gurdak, 2014). For example, the El Niño–Southern Oscillation (ENSO) can lead to greatly reduced recharge rates in eastern and southern Africa (Kolusu et al., 2019), but may have the opposite effect in other parts of the world (Holman et al., 2009). Precipitation is often seasonal leading to episodic recharge concurrent with the strongest precipitation events (Crosbie et al., 2012; Wanke et al., 2008).

Dryland precipitation events are often short in duration and high in intensity (Zoccatelli et al., 2019), and this intensity has been shown to play a key role in controlling groundwater recharge (Dunkerley, 2012; French et al., 1996; Owor et al., 2009; Thomas et al., 2016) and runoff generation (Serrano-Notivoli et al., 2022). When occurring as convective rainstorms, these events exhibit a high degree of spatial variability (Singer and Michaelides, 2017) and cover discontinuous (and partial) areas of the catchment (Pilgrim et al., 1988). This 'spottiness' is an important aspect of dryland rainfall (Sharon, 1972) that has a significant impact on the catchments hydrological response (Sapriza-Azuri et al., 2015) by generating partial area runoff (Yair et al., 1978) resulting in a small proportion of catchment tributaries contributing streamflow to the mainstem for limited periods of time (S.-A. Chen et al., 2019). this reason, the spatial heterogeneity in rainfall is a significant determinant on the

spatial distribution of available precipitation input and thus recharge in drylands (Gee and Hillel, 1988).

In contrast to humid regions, where the LTA rainfall generally exceeds annual rates of potential evapotranspiration (PET), drylands are characterized by limited water availability and potential evapotranspiration that often exceeds LTA rainfall throughout the year (Wheater et al., 2008). This results in little downward movement of infiltrated water below the root zone (Gee et al., 1994), and means that groundwater recharge in drylands is more susceptible to near surface hydrological losses, leading to high soil moisture deficits, large unsaturated zones, and deep water tables (Pilgrim et al., 1988; Wheater et al., 2007).

These climatological conditions mean that recharge typically decreases with increasing PET (Brutsaert and Stricker, 1979; Kim and Jackson, 2012) and recharge in drylands largely depends on specific conditions which enable the concentration, or focussing, of water in time, such as a combination of rainfall events of sufficient intensity, and/or space such as the concentration of surface runoff. The spatial variability of these processes is in turn dependent on the heterogeneity in rainfall.

4.2.2 Concentration

Rainfall can be concentrated temporally and may exceed the potential evapotranspiration (PET) even though LTA rainfall is less than PET. Over small timescales such as days or weeks, the concentration of rainfall into a single large precipitation event or a series of events may yield significant diffuse recharge given favourable land surface conditions (Small, 2005b). This may occur on longer timescales with years of anomalously high rainfall. For example, in the dune covered Stampriet Basin in Namibia, where LTA rainfall is less than 250 mm per year, rainfall can be as high as 600 mm in some years—leading to significant diffuse recharge events (Stone and Edmunds, 2012).

Another mechanism for rainfall to overcome near surface hydrological losses is via the routing of overland flow to topographic depressions within the landscape, such as Intermittent Rivers and Ephemeral Streams (IRES) or seasonal ponds, where surface water is spatially concentrated in space. This concentrated runoff increases the potential for soil moisture deficits to be overcome, and focused recharge mechanisms to occur (Acworth et al., 2021; Favreau et al., 2009; Schreiner-McGraw et al., 2019; Sultan et al., 2000).

In addition, unsaturated zone thicknesses are often smaller beneath topographical depressions such as ponds and ephemeral streams, compared to surrounding areas (Izbicki et al., 2000), and concentration into these low-lying depressions increases the probability of infiltration overcoming unsaturated moisture deficits and become potential recharge.

In drylands, this concentration of runoff occurs mainly via infiltration excess (Hortonian) overland flow, due to a combination of rainfall events of sufficient magnitude and intensity, and favourable land surface conditions. These land surface conditions include topography and soil infiltration capacity. Each of these landscape controls are discussed in the subsections below.

Topography (slope)

Topography controls the movement of water across the land surface (Lerner et al., 1990). Topographical slope directly controls surface flow velocity which (in combination with surface permeability) determines runoff generation (Beven, 2011) by controlling the partitioning between runoff and infiltration into the subsurface (Liu and Singh, 2004).

Steeper slopes produce more runoff as water runs more rapidly off the surface during precipitation, reducing the residence time for infiltration. Inversely, gentler slopes produces slower runoff, allowing more time for infiltration (J J de Vries and Simmers, 2002; Díaz-Alcaide and Martínez-Santos, 2019). On smaller scales, soil roughness and microtopography within larger topographical features and slopes has been shown to control runoff generation by reducing runoff velocity (Bergkamp, 1998; Govers et al., 2000).

While steep slopes produce minimal recharge (Naves et al., 2021), they play an important role in the production of runoff that concentrates into topographic depressions (Allison et al., 1994; Cordery, 2004). For example, McKenna and Sala (2018) found that recharge beneath flat playas in the south-western United States is greater when the average slope of the catchment increases, due to the promotion of greater runoff onto the playa.

This concentration of runoff creates improved conditions for focused recharge in playas (De Vries et al., 2000) and IRES (e.g. Acworth et al., 2021; Cuthbert et al., 2016; Dahan et al., 2008; Manna et al., 2019; Villeneuve et al., 2015). These are landforms characteristic of dryland topography (Thomas, 2011) that have both been shown to contribute significantly to regional distributed groundwater recharge (Scanlon et al., 2006).

Surface permeability

By controlling infiltration rates, the permeability of surface soils and bedrock plays a critical role in the partitioning of rainfall into potential recharge via diffuse processes or runoff at the land surface (Bromley et al., 1997a; Issa et al., 2011). In low gradient catchments, surface permeability is the leading factor in controlling runoff generation (Gutiérrez-Jurado et al., 2019; Yair and Kossovsky, 2002).

Unconsolidated superficial soils or deposits display permeability ranges spanning many orders of magnitude. Those with larger fractions of coarser sediment with sufficiently interconnected large pore spaces are more permeable and support higher potential diffuse recharge rates than finer clay dominated soils (Small, 2005b). In a global scale meta-analysis of recharge estimates, Kim and Jackson (2012) show that on average sandy soils are 50% more efficient in converting water input into groundwater recharge than clay or silty soils. These results are corroborated in the analysis of Moeck et al., 2021, who found that the highest recharge occurs when soils have a sand fraction of 50–65%, a clay fraction of 25–35% and a silt fraction of 10–20%. As such, given a sufficient concentration of rainfall in time, significant diffuse recharge can occur over large areas of the dryland landscape covered by permeable soils, as observed in the dune covered Stampriet Basin in Namibia (Stone and Edmunds, 2012).

Conversely, lower recharge rates are found in clayey soils as the vertical percolation of water through the soil profile is restricted (Attandoh et al., 2013; Edmunds et al., 1992) and thus soil moisture is more exposed to evapotranspiration. Soil texture also plays a role, with recharge being typically greater in coarser versus finer textured soils (Cook and Kilty, 1992; Tao et al., 2021).

However, these observations ignore soil perturbations such as such as crusting, cementation and compaction that have a significant impact on infiltration and potential recharge rates. Whilst studies mostly find that soil crusting (Jacks and Traoré, 2014; Wakindiki and Ben-Hur, 2002), cementation (De Vries et al., 2000; Nash et al., 1994; Xu and Beekman, 2019) and compaction (Hamza and Anderson, 2005) reduce the permeability of soil layers and hence reduce groundwater recharge, the effects of deeply weathered soils known as laterites (Bonsor et al., 2014; Bromley et al., 1997b; Cuthbert and Tindimugaya, 2010) on recharge are much less clear.

While the potential for diffuse recharge is hampered by high intensity rainfall events falling on low permeability soils or bedrock, the combination of these factors can lead to a rapid exceedance of surface infiltration capacity, and lead to the production of (Hortonian) infiltration excess overland flow (Beven, 2002). For example, in the Sahel, land use change and clearing has caused crusting of slopes, lowering their surface permeability. This has caused increased recharge in the region, despite decreases in annual rainfall over the same period (Leblanc et al., 2008), by increasing runoff and increasing surface water concentration into temporary ponds and depressions (Favreau et al., 2009), and therefore enhanced focused recharge.

4.2.3 Delivery

In Chapters 2 and 3, I showed how local-scale configurations in the structure and hydraulic properties of superficial geology may allow surface water to escape ET by way of permeable geology or similar permeable pathways such as preferential flow through faults, macropores or fractures. In this thesis, such pathways are herein grouped into the term permeable pathways and is summarized in Figure 4.2.

While surface permeability mediates groundwater recharge by controlling the infiltration capacity of the surface, vegetation cover directly influences the amount of infiltrated water that percolates past the root zone and becomes potential recharge through the uptake of soil water by roots and subsequent evapotranspiration (ET) from leaves.

As such, the delivery of surface water to below the root zone (potential recharge) is mediated by the relationship between the rate at which permeable pathways can transmit water vertically and the depth and magnitude of evapotranspiration, which is determined by a combination of climate and vegetation cover. This relationship is discussed in the sub sections below.

Permeable pathways

As shown in Chapter 2, channelised runoff can percolate into deeper bedrock via more permeable 'windows' within the beds of IRES. These streambeds are typically characterized by alluvial deposits consisting of highly permeable coarse sands and gravels (Gee and Hillel, 1988), providing permeable pathways for focused recharge to occur (pathway 7 on Fig 4.2, Shanafield and Cook, 2014). These pathways are likely prevalent in dryland alluvial settings of large global extent where IRES comprise >80% of the dryland river network (Levick et al., 2008; Sabater and Tockner, 2009), and there is a growing that highlight the importance transmission losses and groundwater recharge in such dryland systems (Shanafield et al., 2021).

However, soil texture alone fails to recognise structural soil properties which enable infiltration via permeable pathways by way of preferential flow paths which bypass the soil matrix (Beven and Germann, 1982). Macropores in the soil structure or shrinkage cracks in expansive clays provide preferential flow paths that facilitate recharge in conditions which would otherwise be prohibitive by bypassing the soil matrix (pathway 6 on Fig 4.2, Beven and Germann, 1982; Cuthbert and Tindimugaya, 2010; Gates et al., 2008). For example, focused groundwater recharge via playa lakes are hypothesized to be due to rapid infiltration through cracks in the clay-lined floors (Gurdak and Roe, 2010).

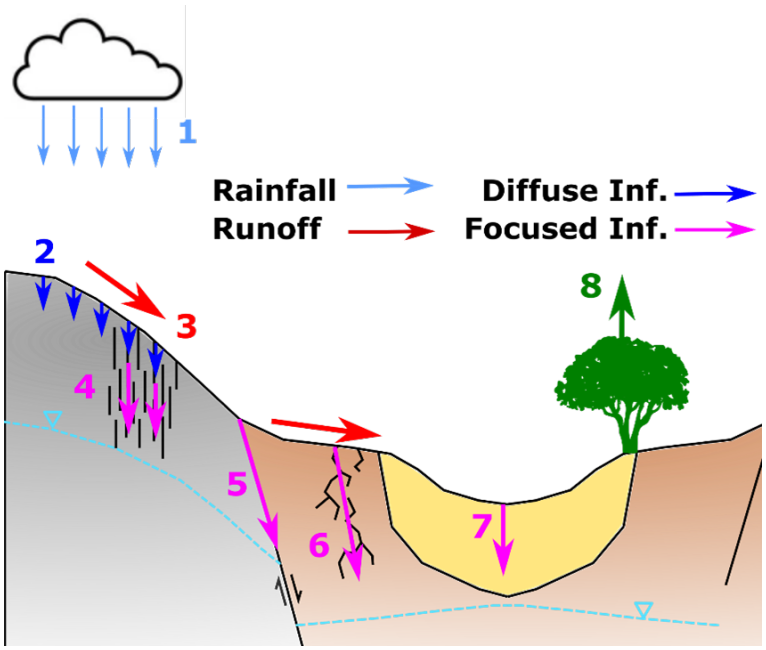

Fig. 4.2 A summary of permeable pathways for recharge. 1) Rainfall that falls directly onto land surface and infiltrates becomes 2) potential diffuse recharge or partitioned into 3) Runoff. Surface water may infiltrate through permeable pathways that permit bypass flow such as 4) Fractures 5) Faults 6) Soil macropores. 7) Surface water can also infiltrate through windows of permeability, most notably from IRES channel deposits. This infiltration can then percolate into deeper bedrock below, and this interaction is discussed in section 4.2.4 8) Vegetation controls partitioning of infiltration into potential recharge via evapotranspiration.

In bedrock, the presence of secondary permeability in the form of rock fracturing (Alazard et al., 2016; Manna et al., 2019; Rusagara et al., 2022; Salve et al., 2012) vertical conduits in karstic rock (Farid et al., 2014; Hartmann et al., 2017; Leketa et al., 2019) provide similar permeable pathways by way of bypass flow via preferential flow paths that increase the bulk permeability of the medium (pathway 4 on Fig 4.2). For example, mountain systems are often characterized by fractured bedrock that enables deep flow paths, leading to higher recharge in lower elevations at the mountain front or as spring discharge (Ajami et al., 2011; Smerdon et al., 2009).

Permeable pathways in the form of faults and faulted zones within the bedrock and distributed in the landscape act as complex conduit-barrier systems along which preferential flow may occur (Bense et al., 2013; Ren et al., 2019), and in a similar vein to soil macropores, bypass the unsaturated zone and deliver infiltration directly to the water table (Batlle-Aguilar et al., 2017). In Chapter 2, I show how geophysical delineation of fault systems distributed beneath superficial sandy deposits and in areas adjacent to ephemeral

stream channels provide permeable pathways for potential groundwater recharge to deeper aquifer to occur (pathway 5 on Fig 4.2). A greater density of these faults in a landscape setting may indicate a greater extent of fracturing in the rock below, increasing their bulk permeability and transmissivity (Maurice et al., 2019) and thus potential for infiltration and recharge (Oyarzún et al., 2019; Prasad et al., 2008).

Vegetation characteristics

Drylands regularly experience climate where evapotranspiration (ET) exceeds rainfall on multiple time scales. This evapotranspiration is spatially variable however, depending on vegetation cover and type (Sabathier et al., 2021; Warter et al., 2021).

Vegetation cover controls the efficiency by which permeable pathways can transmit infiltration as potential recharge (Kim and Jackson, 2012) through its control over transpiration, interception and soil evaporation fluxes (pathway 8 on Fig 4.3, Good et al., 2015; Gordon et al., 2005; Schlesinger and Jasechko, 2014). Studies often find groundwater recharge rates decline as vegetation cover increases (Boas and Mallants, 2022; Edmunds and Gaye, 1994; Gates et al., 2011). While infiltration capacity under vegetated cover can be enhanced by macropores by soil fauna and by roots (Bargués-Tobella et al., 2020; Burch et al., 1987; Owuor et al., 2016; Taniguchi, 1997). However, any gains in infiltration capacity are often offset by high evapotranspiration rates (Scanlon et al., 2005) that typically account for 90–95% of annual precipitation in drylands (Kurc and Small, 2004, Wilcox et al., 2003, Zhang et al., 2011), limiting the role of diffuse recharge (Taylor et al., 2013; Schreiner-McGraw et al., 2019).

For example, dense bush and tree savannah is believed to transpire much of the annual rainfall during the long dry season in the Kalahari desert, leading to very little recharge (De Vries et al., 2000). In Central Australia, runoff concentrated in the alluvial sediments of ephemeral streams are almost entirely consumed via evapotranspiration by riparian Eucalpytus camaldulensis trees (Cook et al., 1989). Thus, concentrated surface water within topographical depressions may be intercepted and taken up by vegetation given adequate vegetative cover. Owing to the widespread occurrence of riparian vegetation along IRES (Sandercock et al., 2007), this flux may form a large part of the dryland water balance.

Within areas of similar vegetation cover, vegetation characteristics such as rooting depth, leaf area, and phenology will affect the amount of infiltration that passes through the root zone (Cheng et al., 2021; Schenk and Jackson, 2002; Warter et al., 2021). For example, and the influence of rooting depth has been reported to depths of up to tens of meters within the unsaturated zone (Canadell et al., 1996; George et al., 1999). Desert

vegetation, such as the shrub Larrea (Creosotebush), have relatively deep root systems and transpire until soil water potential is highly negative (Pockman and Sperry, 2000). Furthermore, because desert plants are able to remove nearly all water from the top several meters of soil, it has been hypothesized that the transition to desert plant species at the end of the Pleistocene (approx. 10 kyr) is the cause of the shift to the lack of diffuse recharge processes observed at many sites in the southwest USA (Phillips, 1994; Small, 2005b; Walvoord et al., 2004). As such, for permeable pathways must penetrate at sufficient depth to transmit infiltration passed the root zone.

Conversely, land clearing, often for agricultural expansion, has been found to enhance groundwater recharge rates by reducing evapotranspiration (Scanlon et al., 2005) and this change from native vegetation to managed land use types often results in increases of recharge rates by one or two orders of magnitude (Scanlon et al., 2006). At sites in New Mexico and Nevada (Gee et al., 1994) found that water accumulated in deep lysimeters that were kept vegetation free, whereas deep percolation did not occur in lysimeters at the same sites with growing vegetation.

4.2.4 Direct or indirect delivery

Once surface geology and/or permeable pathways deliver infiltration into the subsurface as potential recharge, heterogeneities in the hydraulic properties and structure of superficial geology can cause potential recharge to collect at layer interfaces and to be redistributed longitudinally or laterally in the subsurface. As such, the spatiotemporal distribution of actual recharge to deeper water tables may differ considerably from the distribution of potential recharge (see Chapters 2 and 3).

This redistribution is an important component and understudied part of dryland hydrology (Nimmo et al., 2017), and in this section I propose within my framework a generalized model of subsurface distribution with differing geology that consists of unconsolidated superficial, alluvial cover (layer 1) underlain and surrounded by geology of differing permeability (layer 2).

This model is centred around configurations of geology in the close vicinity of IRES as: a) IRES are the main conduits of concentrated runoff in the dryland land surface b) alluvium within these systems are some of the largest and continuous deposits of superficial geology in drylands c) there is a growing body of literature using near surface geophysics to characterize the superficial geological structures in and around such systems (Callegary et al., 2007; Shanafield et al., 2020; Zarate et al., 2021)(e.g. Callegary et al., 2007; Shanafield et al., 2020, Zarate et al., 2021) d) IRES are a geomorphic feature prevalent in most dryland catchments (Tooth and Nanson, 2011).

In this model I distinguish between recharge to the perched groundwater, and recharge to deeper regional groundwater. I define the regional groundwater as groundwater that extends continuously across large areas, exists in, and is in hydraulic continuity with, multiple geology layers in multiple dimensions, and exists as the main groundwater source for local abstraction. This definition is closely correlated, and is consistent to, the description of regional groundwater in various contexts (e.g. Gleeson et al., 2016; Mádl-Szőnyi et al., 2022; Wallace and Renard, 1967).

Perched groundwater is defined by an underlying unsaturated zone separating the perched groundwater from the regional water table, significant seasonal variability (to the point that the water table may completely disappear in some periods) and lateral confinement or discontinuity, such that they exist primarily within the layers of superficial deposits or near surface geology. The formation and temporal continuity of this perched groundwater depends on the permeability contrast between the perching layer and underlying geology. I also note depending on the volume of the superficial store or deposit, these perched aquifers can become local aquifers that are utilized for groundwater abstraction.

Furthermore, the depth of the regional groundwater, which I simplify as water table depth, controls the thickness of the unsaturated zone between the perched and regional water table such that at shallow water table depths, the perched and regional water tables can be in hydraulic continuity with each other. In this case, potential recharge percolates directly to the regional water table.

I propose that there are three main controls on the redistribution of potential recharge in the subsurface: The permeability contrast between the streambed superficial store of alluvium and the surrounding geology, the volume of the superficial store, and the unsaturated zone characteristics below the perched groundwater. These controls are discussed in turn in the subsections below.

Permeability contrast

I define permeability contrast as the ratio of permeability between layer 1 and layer 2. A high permeability contrast between can layers can limit vertical unsaturated flow (Miller and Gardner, 1962; Nimmo et al., 2002) and cause perched water to collect at the layer interface (e.g. Bourke et al., 2020; Hamilton et al., 2005; Knighton and Nanson, 2000). Due to the formation of perched groundwater, I distinguish in my framework that permeable pathways can deliver potential recharge into either perched groundwater in layer 1 or to the deeper regional groundwater situated in the underlying geology (See Fig 4.3b), depending on the permeability contrast between the two layers. When this process occurs directly below the

flux of potential recharge from the surface, I make the distinction that the recharge process (diffuse or focused) occurs through direct delivery (see Fig 4.1).

In an ephemeral stream in Central Australia, Villeneuve et al., 2015 found that this perched water can persist for several months or longer, with water levels declining slowly over time. Chloride concentrations measured on cores obtained from beneath the perched water reveal that 25% of this water leaks through the low permeability sediments to recharge the deeper aquifer, and the remainder is used by the riparian vegetation or lost to evaporation (Villeneuve et al., 2015).

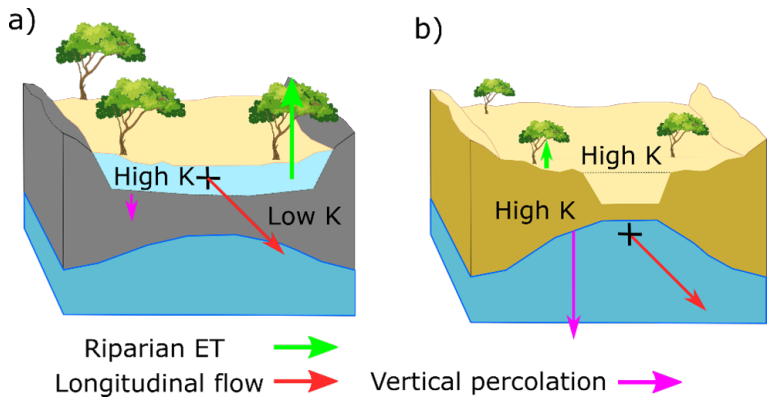

Fig. 4.3 Differences in water balance partitioning in a) high permeability contrasts b) low permeability contrasts IRES systems.

This perched groundwater provides a key source of plant available water to riparian ecosystems (Sabathier et al., 2021), and in areas of very high contrast, perched water may be entirely lost to riparian evapotranspiration. In the ephemeral streams of the Cuvelai-Etosha Basin, Namibia, high permeability contrasts cause perched aquifers to have negligible contributions to recharge in the catchment, as most shallow water in the perched aquifer becomes lost to evaporation (Hamutoko et al., 2019). Similarly, a study in the Shashe River Valley in Botswana concluded that permeability contrasts between bedrock and alluvium created perched water that was entirely consumed by riparian vegetation, with no evidence of recharge to regional groundwater (Bauer et al., 2006).

The formation of perched water at the layer interface can increase the likelihood and magnitude of longitudinal or lateral flow, particularly if the perched layer is sloped. In Chapter 3 I described how high permeability contrasts between streambed alluvium and the surrounding superficial geology controls water balance partitioning within the stream by creating an 'alluvial store' of perched water within the streambed sediments that is partitioned longitudinally downstream within the alluvium (Fig 4.3a, Fig 3.8). Longitudinal flow from alluvial volumes upstream manifests itself as streamflow and maintains the

saturation of alluvium downstream. This behaviour can also occur in mountain blocks, where local flow paths are developed over low permeability bedrock (Manning and Solomon, 2005), and in interfluve areas with superficial deposits underlain by lower conductivity geology where rainfall can lead to the formation of perched saturated zones that contribute to saturation excess runoff (Latron and Gallart, 2008, 2007).

This longitudinal supply of flow and surface water can create 'waterholes' within IRES, providing a hydrological refugia for aquatic species (Hamilton et al., 2005), and flow may further discharge downstream to sustain wetlands containing delicate ecological systems, often with unique biodiversity (Herrera et al., 2021). Due to the widespread occurrence of riparian vegetation along ephemeral river channels (Sandercock et al., 2007) it is possible that perched aquifer systems are widespread in similar ephemeral systems.

Longitudinal flow can redistribute this perched water to areas with low permeability contrasts or areas underlain by permeable pathways. In these areas, perched water formation is limited and vertical percolation to regional groundwater can occur. Due to this redistribution in the subsurface, the distribution of recharge to regional groundwater may differ considerably from the distribution of potential recharge from the surface, and in my framework, I term this redistributed delivery of recharge indirect delivery (see Fig 4.3b). This indirect delivery has been observed in studies within areas of highly fractured bedrock (Rusagara et al., 2022), porous karst (Modie et al., 2022), permeable sands and gravels (Herrera et al., 2021).

In addition, focused recharge to regional groundwater that bypasses the soil matrix and therefore precludes the formation of perched groundwater can also occur via indirect delivery through the activation of preferential flow paths such as faults (Beetle-Moorcroft et al., 2021; Flint et al., 2002; Zarate et al., 2021) (see Chapter 2).

If the permeability of the cover is instead lower than the underlying geology, than infiltration into the deeper aquifer will only occur once the field capacity of the overlying cover is exceeded, and this has been observed in sites with weathered saprolitic cover overlying fractured bedrock systems (Salve et al., 2012) or alluvial cover overlying karstified bedrock (Camarasa Belmonte and Segura Beltrán, 2001).

Volume of superficial store

The volume of this high permeability superficial cover, which I term here the volume of superficial store and its relationship with infiltrating runoff volumes plays a key role in controlling water balance partitioning in drylands. These relationships are explored in Figure 4.4.

These superficial deposits exist in a variety of configurations in the landscape, such as deposits lining the floors of topographic depressions in the landscape (Hamutoko et al., 2019; Shaw and Bryant, 2011), or saprolitic weathered cover overlying fractured bedrock in in steep slopes or mountain blocks (Manning and Solomon, 2005; Naves et al., 2021; Salve et al., 2012). The largest and most permeable of which occur as alluvial deposits within IRES or former 'paleo' channels. The significance of these deposits in controlling transmission losses in IRES was first observed by Telvari et al., 1998, who used the term alluvial store to describe such deposits, and I adopt the term in this thesis to denote the superficial deposits situated within IRES streambeds. In drylands, alluvial stores within streambeds are recharged episodically or perhaps seasonally by river transmission losses following heavy rainfall (Benito et al., 2010, Walker et al., 2019, Seddon et al., 2021). During an intensively monitored flow, Villeneuve et al., 2015 found that the downstream decrease in river discharge was approximately equal to the alluvial volume.

In cases of little to no superficial or alluvial stores, such as in areas with bedrock close to the surface and steep slopes such as mountain headwater streams, it is then the permeability of the underlying geology that controls recharge, and the principles and pathways discussed in Section 4.2.3 apply. For example, surface water infiltration directly through fractured bedrock has been observed to occur mountain block regions (Markovich et al., 2019).

Small volumes of alluvial stores (Fig 4.4 1a, b, c) can quickly become saturated in response to runoff events and in combination with high permeability contrasts, form perched groundwater that can contribute saturation excess runoff on hillslopes (Beven, 2002; Latron and Gallart, 2008, 2007), or manifest as streamflow downstream within IRES (see Permeability Contrast). This limited alluvial store can easily lead to bank-full streamflow that lead to overbank flooding, enabling groundwater recharge in overbank areas into permeable pathways (see Section 4.2.3) such as permeable surface geology (e.g. Lange, 2005; Meredith et al., 2015), fractures (e.g. Acworth et al., 2021) or faulted zones (see Chapter 2).

Within large volumes of alluvial store (Fig 4.4 3a,b,c) perched water is unable to form, and instead streamflow is partitioned vertically to a greater extent, recharging the water table within the alluvial store. However, large amounts of concentrated runoff are needed to exceed field capacity of the store and percolate deeper, and as such only the large events may contribute to direct delivery of focused recharge in these systems. These stores can occur in large stream systems or in systems where the permeability contrast is so low that the hydraulic properties of the superficial store are indiscernible from the surrounding geology (Fig 4.4 1c, 2c and 3c). In IRES that incise through large volumes of quaternary

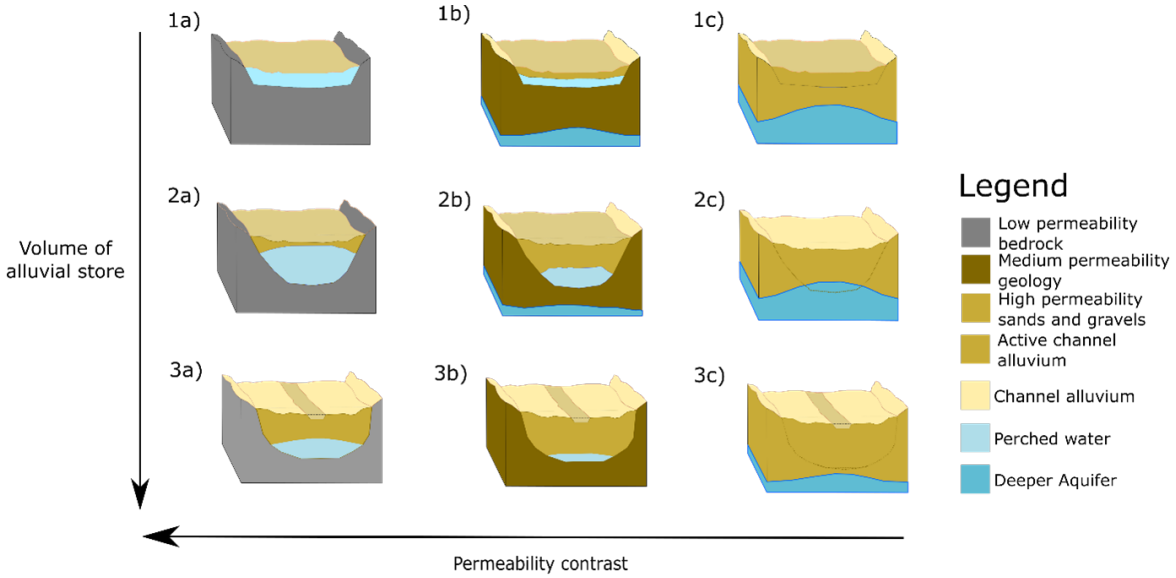

Fig. 4.4 The relationships between alluvial storage and permeability contrast exist on a continuum in a given dryland IRES and across the dryland landscape. Large alluvial stores with high permeability contrasts (3a) may act like smaller alluvial stores surrounded by indiscernible material (1c and 2c). Large alluvial stores (3a and 3c) may form the regional aquifer in the region, and perched recharge to this aquifer can be said to be aquifer recharge.

fill, the bedrock is so deep that it has no discernible effect on surface-groundwater dynamics within the store (Fig 4.4 3a,3b (Kristin L. Jaeger et al., 2017; Sutfin et al., 2014a).

The volume of alluvial store at a particular site, and upstream of it, will also vary depending on stream order and position within the catchment (Sutfin et al., 2014a; Tooth, 2012). As discussed in the previous section, high permeability contrasts between superficial stores and surrounding geology can cause restricted vertical infiltration into surrounding low conductivity materials and allows for perched water and preferential longitudinal flow within the superficial store. Thus, assuming a degree of connectivity between volumes of superficial store, longitudinal flow can keep stores downstream 'topped up' even when surface runoff has ceased. In superficial stores located upstream (Fig 4.5 1a,b,c), which drain a smaller area of catchment, there is not only a smaller superficial store, but also less contributions in longitudinal flow due to a smaller volume of superficial store upstream. In contrast, downstream reaches, which drain a greater extent of the catchment, receive a greater volume of potential alluvial water from upstream reaches (Fig 4.4 2a,2b,2c).

Large alluvial stores within IRES (Fig 4.5 3a,b,c) serve as important shallow aquifers that receive and store streamflow infiltration during hydrologic events, sustaining baseflow and riparian communities (Sabathier et al., 2021; Sargeant and Singer, 2016), animals (Bourke et al., 2020), and humans (MacDonald and Calow, 2009) that inhabit dryland

regions. For example, these stores are exploited in dryland environments by way of sand dams - small weirs constructed across IRES with high permeability contrasts, providing a readily accessible source of freshwater for domestic supplies, livestock, and small-scale irrigation (Eisma and Merwade, 2020; Xu et al., 2019). In addition, perched water within larger superficial stores situated within permeable unconsolidated sediments and in larger ephemeral or seasonal river systems (in the Limpopo, for example, Boroto and Gorgens, 2003) form some of the most productive aquifers in Africa (MacDonald et al., 2012).

Unsaturated zone characteristics

Once water percolates from the perched groundwater within the superficial store the unsaturated zone thickness of the underlying layer will act to lag and attenuate any direct or indirect delivery of recharge to the water table (Abdulrazzak et al., 1989; T. Huang et al., 2017).

If the unsaturated zone is too thick and dry due to evapotranspiration, and/or the volume of direct or indirect delivery of infiltrating water too small, there may not be much recharge to deeper regional groundwater (Cao et al., 2016; Izbicki et al., 2000; Jadoon et al., 2016), unless secondary permeable pathways exist that bypass this matrix. For example, as discussed in Section 4.2.3, fracture flow in underlying rocks or faults may provide conduits that may bypass the underlying soil or rock matrix to enable the indirect delivery of focused recharge to deeper aquifers, even if the upper superficial layer is not completely saturated (Beetle-Moorcroft et al., 2021; Salve et al., 2012; Zarate et al., 2021).

At the other extreme, the water table may sit within the superficial store, and no unsaturated zone conditions exist between the superficial store and regional groundwater. Hence the perched and regional groundwaters may be in hydraulic continuity with each other and in my framework, recharge would be directly delivered to regional groundwater. This importance of UZ soil moisture deficits in controlling surface to groundwater interactions partly explains why groundwater recharge in these regions favoured along topographic depressions and stream reaches, as the subsurface water contents of the stream beds are generally larger, and deeper water tables are closer to the surface, than on the nearby soils (Izbicki et al., 2000).

Perennial rivers and streams, for which there is a continuous saturated zone between the streambed and surrounding geology, forms the most extreme end member of my model, where no unsaturated zone exists in the second or first layers. Here it is expected that groundwater discharges would be the most dominant process (providing baseflow for the stream), however in periods of low flow recharge can occur (Herrera et al., 2021). Dryland regions with deep regional water tables and/or experiencing low potential recharge rates

can have lag times between infiltration and recharge that vary on timescales of decades to millennia (Flint et al., 2002; Izbicki et al., 2000; Jie et al., 2022; McMahon et al., 2006; Phillips, 1994). Thus, changes in potential recharge in response to changes in climate occurring within the 21st century (the period for which climate change projections are commonly made) may not affect groundwater resources within the same time frame, and actual groundwater recharge may remain the same (Cuthbert et al., 2019a; Rossman et al., 2014).

4.3 Catchment scale recharge variability

Within a given climatic and geological setting, I propose that the controls outlined in this framework can exhibit differing characteristics and exist in specific ranges depending on their longitudinal (i.e., upstream, or downstream) landscape position. For example, steep slopes with low-permeability bedrock overlain by a small volume of superficial store are more likely to exist in upland, mountainous areas. In contrast, lowland slopes consisting of high permeability quaternary sands existing as large superficial stores almost entirely occur in lowlands.

These longitudinal trends in geomorphology were outlined by Schumm (1977) who described three zones in relation to relative elevation and catchment position: production, transfer, and deposition. In recent years, Tooth and Nanson (2011) extended Schumm's conceptual model to dryland river systems, subdividing catchments into upland, piedmont and lowland settings (corresponding to Schumm's original zones) and adding a fourth, floodout, to describe the termination of the catchment into either an endorheic basin, as part of a larger catchment, or flowing to the coast.

In this section, I adopt the Tooth and Nanson (2011) model as a basis for creating a catchment scale geomorphic model that allows for the grouping of controls outlined in Section 4.2 based on their likelihood of occurrence within Tooths and Nanson's (2011) upland, piedmont, lowland and floodout zones. Characterising my framework in the context of these zones provides a logical, physically meaningful way of constraining my broad continuum of controls with respect to their longitudinal position within the catchment that allows me to explore the efficacy of this framework in explaining the observed variability of dryland recharge processes at the catchment scale.

Within my model, each zone is functionally related upslope and downslope of each other, with IRES and floodplains linking the uplands with the piedmont and subsequently to the lowlands and floodout, with the spatial extent and relative proportions of each zone varying depending on the geomorphology of the dryland catchment. Along this continuum

of zones are associated sequences of climate/aridity, landscape controls, vegetation, and subsurface characteristics. This is summarised in Figure 4.5, and discussed below.

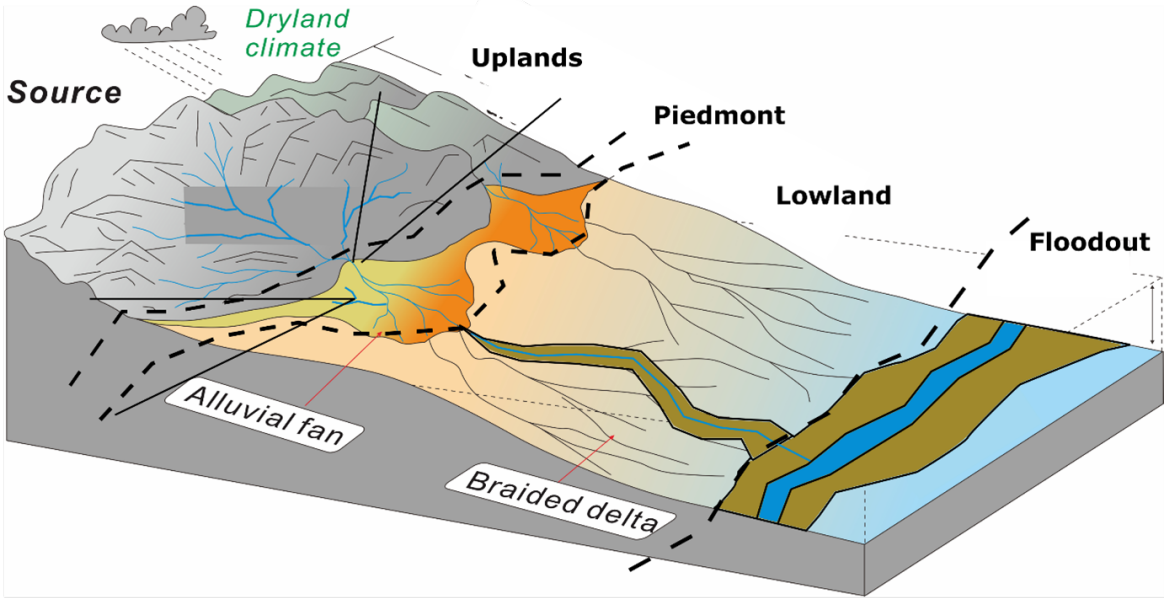

	Uplands	Piedmont	Lowlands	Floodout
Precipitation	Snowmelt, orographic rainfall	Frontal and convective storms	Local convective storms	
Aridity	Low →		High	
Slope	High ←		Low	Low/flat
Rainfall - runoff response	Rapid →		Low	Very low
Geomorphology	Erosive	Transfer	Deposition	
Alluvial stores	Low →		High	
Permeability contrasts	Bedrock with alluvium	Bedrock confined and incised alluvium	Incised alluvium	

Fig. 4.5 Conceptual model of dryland geomorphology with longitudinal zones adapted from Tooth and Nanson (2011). Process controls outlined in Section 4.2 exist as a continuum in the landscape and are summarised in the table

In this geomorphic model, there is a general decrease in rainfall and increase in aridity downstream, because of the common occurrence of orographic enhancement of rainfall in the uplands (Nicholson, 2011). Slopes decrease in gradient and IRES channels become wider downstream (Leopold and Miller, 1956; Miller et al., 1996; Youberg et al., 1998), with a corresponding change in the nature of drainage from connected, branching systems with distinct channels in the uplands, to disorganized and disintegrated networks with sparse, thin channels of flow in the lower regions (Goudie, 2011).

Surface permeability (a function of surface soils and geology) can span orders of magnitude in range and is dependent on the local geological and geomorphological characteristics of the catchment and in my geomorphic model I do not make any assumptions about changes in surface permeability. There are potential strong differences in vegetation type and

density across a catchment depending on this surface permeability, local geologic controls and geomorphology (Sabathier et al., 2021), however vegetation is typically concentrated at IRES, where runoff accumulates and or where the water table is close to the surface (Stromberg and Merritt, 2016). Thus when examining vegetation trends across the four zones, I primarily focus on changes in riparian vegetation and integrate the work of Shaw and Cooper, 2008, who defined riparian vegetation classifications within based on the area of catchment they drain, and map these classifications to similar landscape characteristics in myconceptual model.

Based on the literature, I propose that there is an increase in sediment supply relative to transport capacity downstream, resulting in longer sediment storage times allowing vertical and lateral accretion to form progressively thicker superficial and alluvial deposits up to the lowlands (Graf, 1987, 1983; Hupp, 1986). Thus, as the magnitude of channel networks and alluvial deposits increases downstream, I assume an increase in transmission losses. Combined with rainfall characteristics, these losses lead to an attenuation and decrease in rainfall-runoff responses downstream (Goodrich et al., 1997).

When examining changes in subsurface distribution between zones, I draw extensively upon the work of Sutfin et al., 2014, who created ephemeral stream classifications based on dryland mountainous geomorphology. I extend these conceptual models to the subsurface by incorporating changes in superficial storage and permeability contrasts between zones. These block models are shown with their location within the dryland catchment and geomorphic zones in Figure 4.6. Furthermore, as my framework for recharge emphasizes the concentration and channelling of surface water, my conceptual block models are subsequently centred around subsurface structures around IRES, as they represent the main conduits for water and sediment movement between my zones.

4.3.1 Uplands

The upland zone receives disproportionately large amounts of rainfall compared to zones downstream because of orographic forcing on rainfall (Carling et al., 2012; Morin et al., 2020; Nicholson, 2011). Upland zones at higher elevations, much of the precipitation in uplands is sourced from snowpack (Meixner et al., 2016) and meltwater maintains critical runoff and streamflow during warmer and drier months (Haiyan et al., 2018; Jódar et al., 2017).

These large precipitation inputs create significant opportunities for recharge in the upland zone. At higher elevations, infiltration of snowmelt and rainfall via discrete geological features in the mountain block such as fractures and faults has been found to be significant pathways for recharge (Phillips et al., 2004) and stored groundwater at high-elevations

supports shallow groundwater circulation (Jódar et al., 2017; Staudinger et al., 2017; Taucare et al., 2020) which feeds high-elevation springs and wetlands (López-Angulo et al., 2020).

The steep slopes and high gradient channels in this zone experience rapid runoff which is tightly coupled with local rainfall (Murphey et al., 1977), and high intensity storms can quickly generate flash floods capable of high rates of erosion, and deposition downstream (Michaelides and Martin, 2012; Lucía et al., 2013). This runoff can vary however, and some upland zones with deeper soils, lower gradients and those consisting mainly of fractured rock, will have higher infiltration capacities and lower amounts of overland flow (Blasch and Bryson, 2007).

At lower elevations, runoff and subsurface flow from higher elevation areas are concentrated into upland IRES. This increased runoff promotes more active erosion in this zone, preventing the accumulation of soils (Acosta et al. 2015) and as such streambeds in the upland zone consist of bedrock or bedrock covered by thin volumes of alluvium which are commonly restricted in width and longitudinal extent by outcropping bedrock (Sutfin et al., 2014).

Runoff in these IRES interact with discrete geological features in the mountain block such as steeply dipping fault zones or high permeability sedimentary rock units, which can provide permeable pathways for potential recharge occur (Coes and Pool, 2005; Markovich et al., 2019). Subsurface longitudinal flows within the bedrock zone have been shown to recharge downstream adjacent aquifers in the piedmont via interconnected fractures and oblique high-permeability fault systems (Wilson and Guan, 2004; Kebede et al., 2008; Taillefer et al., 2018; Walter et al., 2019), a process called mountain block recharge (Wilson and Guan, 2004).

IRES geology in this region consists of primarily bedrock channels (Fig 4.6 1a) or bedrock with small volumes of alluvium (Fig 4.6 2a). While the occurrence of relatively impermeable bedrock at shallow depths can promote shallow subsurface flow within these systems (Mansell and Hussey, 2005), the small volumes and discontinuity of the alluvium mean that only localised parts of the channel bed can support surface water in dry conditions (Jaeger and Olden, 2012; Godsey and Kirchner, 2014). For example, stream potholes that are eroded into bedrock outcrops during successive large floods can retain water for several months, providing critical aquatic and terrestrial habitats (Bogan et al., 2014).

The scarcity of alluvium within this zone limits plant establishment sites, and vegetation development is further constrained by disturbance from debris flows and flood scouring (Shaw and Cooper, 2008). In the semi-arid watersheds of the south-west united states, these upland zones are dominated by drought-deciduous subshrubs, whose rapid growth

rates allow them to colonize frequently disturbed sites, and foliage enables them to utilize brief moisture pulses and minimize water demand during drought periods (Shaw et al., 2018). At lower elevations, greater volumes of alluvial store allow channelised runoff to be stored as which can flow downstream to supply and top up alluvial stores within piedmont IRES.

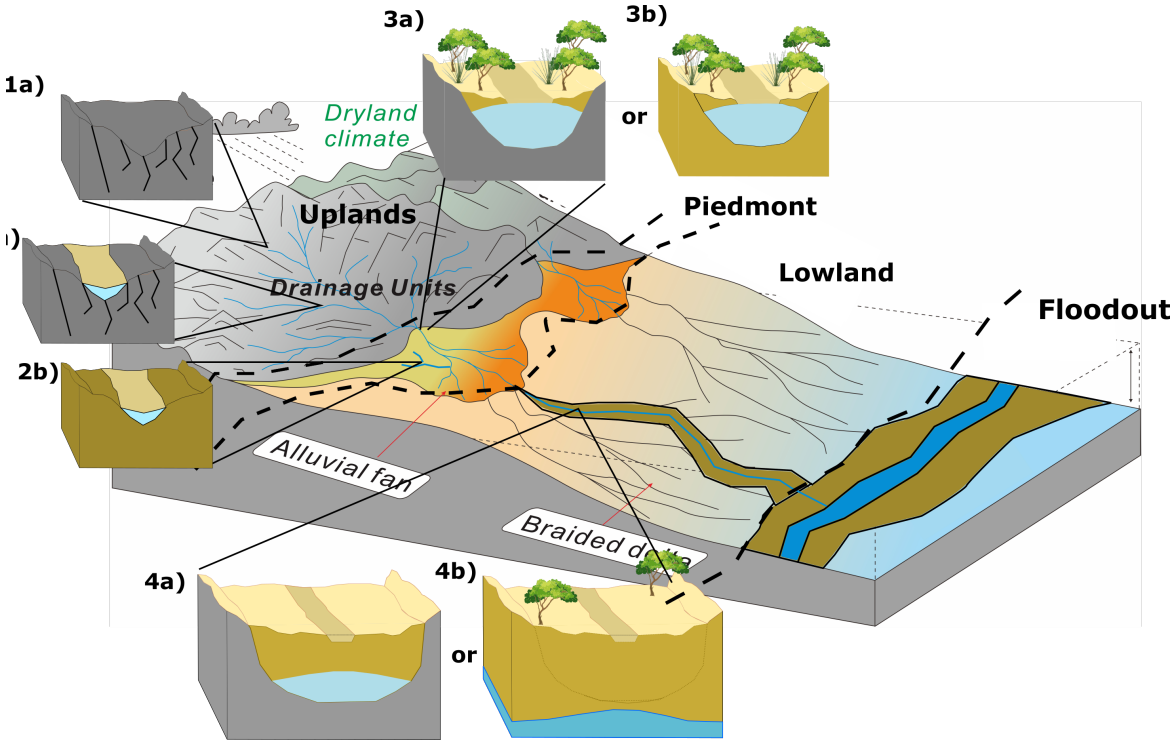

Fig. 4.6 Conceptual block models of IRES superficial geological structure (adapted from channel classifications defined by Sutfin et al., 2014) overlain on a conceptual model of dryland geomorphology. These classifications are as follows 1a) Bedrock (no alluvium) 2a) Bedrock with alluvium 2b) Piedmont headwater 3a) Bedrock confined alluvium 3b) Incised alluvium 4a) Braided bedrock 4b) Braided Channels.

4.3.2 Piedmonts

The piedmont zone represents a transition zone from steep mountain slopes of the uplands to the lower gradient slopes of the lowlands. This transition in slope is typically abrupt and well defined and coincident with geological structures where an active fault bounds the mountain front, or where more resistant geology is bounded by younger sedimentary rock (Parsons and Abrahams, 1994). Geomorphologically, its position in the catchment represents a transition from a zone of net erosion (uplands) to net deposition (lowlands).

While not as responsive as the upland zone, runoff remains sensitive to rainfall due to proximity of the upland zone (Yair and Kossovsky, 2002). As runoff from the upland zone and enters the piedmont, valley floors and IRES channel widths become wider and there is a subsequent increase in size of alluvial store. Alluvium within the channels represents permeable pathways for infiltration, and groundwater recharge via these pathways, also referred to as mountain front recharge has been highlighted in the literature to be significant (Manning and Solomon, 2003; Sakakibara et al., 2017) and in some studies, identified as the dominant source of recharge to lowland aquifers (Earman et al., 2006; Scanlon et al., 2006).

Once water has infiltrated the alluvium, potential recharge depends on the degree of channel confinement and nature of confining material (which in turn both depend on lithology and sediment supply from the uplands). In my conceptual model, runoff exiting the uplands flows into two channel types: Bedrock confined channels (Fig 4.6 3a) and channels that are incised into alluvial plain or fan sediments, which Sutfin et al., 2014 term incised alluvium (Fig 4.6 3b) channels. I assume that any remaining unconfined sheetflow is either concentrated in downstream depressions or infiltrates the interfluve regions of the piedmont dependent on the surface permeability of the zone.

In bedrock confined channels, bedrock may crop out locally in channel beds, but commonly channel beds are fully alluvial, with a range of sediment sizes up to boulders. The bedrock depends on the geology of the catchment, for example ranging from weathered crystalline bedrock (See Chapter 2) or sedimentary rock abutting the mountain block (e.g. Markovich et al., 2021). In addition, piedmont zones defined by uplift and tectonic, bedrock may have geological structures such as faults and fractures that provide pathways for recharge (Carling et al., 2012; Wilson and Guan, 2004). In incised alluvial channels, permeability contrasts are typically lower than bedrock confined channels, due to the nature of confining materials. Channels incise into and are surrounded by older alluvial plain colluvial deposits and overbank clays (For example at Maules Creek, Chapter 3).

Incised alluvial channel on alluvial fan systems are also a distinctive feature in many dryland piedmont zones. In this case, surrounding material may be inactive fan lobe deposits that are indiscernible from channel alluvium, or consist of lower permeability overbank clays and sheet flow deposits (Bonsor et al., 2017). Runoff within fan systems may become less confined and concentrated into a single channel, instead distributed through multiple channels across the fan or form broad sections of sheet flow (Parker et al 1998 from Goodrich). Such fan deposits may be extensive and overlap with older/deeper fan deposits and these interconnected deposits provide permeable pathways for IRES infiltration to recharge underlying aquifers (Houston, 2002). Fan deposits also form extensive alluvial

aquifers in drylands (Carling et al., 2012) that are readily utilized by local people (e.g. Xiao et al., 2021).

A third type of channel may exist in some dryland piedmont zones, where headwater channels may initiate on piedmont surfaces and partially consolidated alluvium, such as those on alluvial aprons of fans. These are accordingly termed piedmont headwater channels (Fig 4.6, 2b). Sutfin (citation) notes however that these lack persistent active alluvium on the channel bed and are typically surrounded by low permeability silts and clays such that these channels generate frequent runoff when rainfall falls directly onto the fan system, but recharge only occurs when runoff becomes overbank or becomes concentrated into lowland IRES.

Vegetation within bedrock with alluvium and incised alluvium channels are similar, reflecting their co-occurrence along the transition zone form uplands to lowland valleys (Shaw et al., 2018; Sutfin et al., 2014). Active alluvium in both channel types allows for stores of available water for plant use, and differences in permeability contrasts within channel types at and upstream may produce varying degrees of available perched water. However, lateral confinement of channel alluvium and subsurface water stores commonly limits riparian habitats in this zone to narrow floodplain benches subjected to periodic scour, which limits the development of plant establishment sites (Shaw and Cooper, 2008). Piedmont headwater channels contain small amounts of alluvial stores and hence store less plant available water than active alluvium (McAuliffe, 1994, 1999).

4.3.3 Lowlands

In the lowland zone sediment supply exceeds transport capacity, and IRES channels become even wider, exhibiting a wide range of channel morphologies, many of which strongly contrast perennial systems (Tooth, 2012), such as braided systems (Goudie, 2011; Tooth and Nanson, 2011). These braided systems form large alluvial stores and stream networks that provide expansive permeable pathways for infiltration into unconsolidated alluvium, leading to large transmission losses (e.g., 2.5m^3 s^{-1} km^{-1}, Doering et al., 2007) when runoff enters this zone, and downstream decreases in runoff volumes.

Thus, flows tend to be less frequent and runoff less closely coupled to rainfall than the upland and piedmont zones, and only large frontal storms or local convective storms generate enough runoff for streamflow in this zone (Beven, 2002; Kampf et al., 2016; Nicholson, 2011). Transmission losses can also be attributed to overbank flows in this zone, where permeable pathways exist in the form of overbank sediments (e.g. (Acworth et al., 2020; Dahan et al., 2007) or faults bounding the IRES zone (such as Makutapora, Chapter 2).

Channel-bed substrates in the lowland zone are strongly influenced by catchment lithology and sediment supply, and so can vary widely, ranging from variable mixtures of alluvium and bedrock (Heritage et al., 1999), through sand and gravel (Reid and Frostick, 1997) to silt and clay (e.g., Knighton and Nanson, 1997). Likewise, material surrounding the channel system can also differ, from alluvial plain deposits of clays to sands and gravels, or entrenched in bedrock (Dahan et al., 2008).

As discussed in Section 4.3.4, as alluvial stores in these zones become large, they may instead form the regional aquifers and perched recharge in this zone becomes recharge to main aquifer. Similarly, as permeability contrasts become similar, the line between active alluvium and surrounding material becomes blurred and it is hydrogeologically difficult to distinguish between active and surrounding alluvium (see Figure 3.6).

These large stores mean that in many lowland IRES, filling of alluvial stores and surface expression of groundwater is limited, although exceptions may occur in reaches where bedrock outcrop has resulted in local development of pools (Heritage et al., 1999) or where the confluence of anastomosing channels on extensive muddy floodplains leads to scour and the formation of permanent waterholes (e.g., Knighton and Nanson, 1994, 2000). Despite this, transmission losses within channels can recharge alluvial soil moisture and water availability to riparian trees that otherwise have limited access to soil moisture (Singer et al., 2014).Furthermore, the largest riparian tree species in dryland regions appear to limited to downstream lowland reaches, where flood frequency and sediment transport potential were the lowest, and riparian species are protective from erosive floods (Hughes, 1990).

4.3.4 Floodout

Drainage in dryland catchments generally converges to three main areas, which I term here floodout zones: as a sub-catchment joins a larger IRES or perennial system, at the sea or coastal zone, into endorheic basin settings (Goudie, 2011).

While transmission losses in the lowland zone may limit runoff contributions from dryland sub-catchments that are tributaries to large systems, groundwater recharge via these systems have been found to support perennial reaches downstream (Larned et al., 2008; Sabathier et al., 2021). For IRES flowing to the coast there tends to be a gradual transition from the lowland zone to an estuarine or deltaic zone. Across the globe, however, many IRES fail to reach a coastline, instead undergoing various forms of "breakdown" or "failure," and ultimately terminating in inland topographic basins on alluvial plains (Mabbutt, 1977; Tooth, 1999; Billi, 2007) or on the margins of pans or playas (Fisheret al., 2008; Donselaar et al., 2013).

In most floodout zones, limited or absent hillslope-channel and rainfall-runoff coupling means that flow and substrate characteristics are largely determined by the distance from the upland and piedmont sources of runoff and sediment. For example, in small dryland catchments, the floodout zone may be within a few tens of kilometres of the uplands, so flow events may occur semiregularly (e.g., after every local convective thunderstorm) and channel-bed sediment may include local cobbles and boulders (Billi, 2007; Craddock et al., 2012).

In larger IRES, however, the floodout zone may be located many tens or even hundreds of kilometres from the uplands and the characteristic downstream decreases in discharge described earlier mean that flow events may be very infrequent, perhaps only once every few years or decades (O Dochartaigh et al., 2010). In the ephemeral Kuiseb in Namibia, which terminates on the coast, less than 9% of flows from the uplands reach the coastal floodout zone due to large transmission losses in the lowlands (Morin et al., 2009).

4.4 Discussion

Contextualizing dryland recharge processes within the conceptual model outlined in Section 4.3 allows for a physically meaningful framework from which to explain and compare the predominance of diffuse or focused recharge between dryland catchments across a spectrum of aridity and a range of tectonic, lithological, and physiographic settings.

For example, in the dune covered Stampriet Basin in Namibia, the predominance of diffuse recharge can be explained in the context of my framework. Rainfall that exceeds PET (on various timescales throughout the high rainfall year) enables the concentration of rainfall in time. The low gradient topography and permeable soils create favourable land surface conditions that produces little overland flow and runoff (Fig 4.7a) and as such large proportion of these rainfall events may be delivered below the root zone and overcome soil moisture deficits to become potential diffuse recharge (Small, 2005; Yair and Kossovsky, 2002).

Conversely, in the Sahel, land use change and clearing has caused crusting of slopes, lowering their surface permeability. Before land clearing had commenced, rainfall events were unlikely to overcome the high ET and soil moisture deficits on slopes and deliver diffuse recharge. However, the creation of lower permeability soils by way of crusting has caused a great majority of precipitation to quickly cause infiltration excess overland flow (Fig 4.7b) to be concentrated into ephemeral depressions, and focused recharge mechanisms to occur.

The potential wider applicability of the framework is a product of the generalized and simplified nature of identified landscape controls. I acknowledge that the simplification of

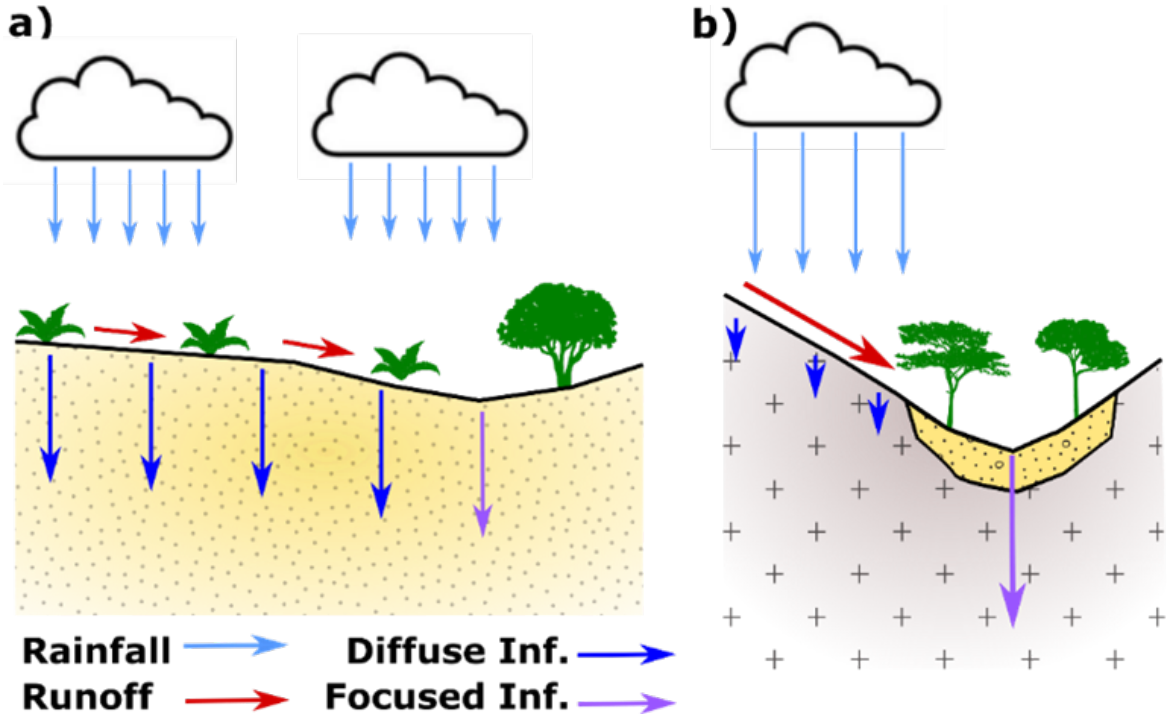

Fig. 4.7 Interactions between rainfall and land surface characteristics and their role in controlling the relative magnitude of diffuse vs focused recharge processes in the context of the conceptual model outlined in Section 4.3 A) The Stampriet Basin, Namibia where spatially distributed rainfall combined with permeable soils and low slopes mean high soil infiltration rates and less runoff, increasing the likelihood of diffuse recharge processes b) In the Sahel, intense, spatially heteregeneous rainfall combined with low permeability, steep slopes leads to low infiltration rates on slopes, but large amounts of runoff generated which increases the probability of focused recharge processes within topographical depressions.

these controls omits some detailed local nuances of each control that may play a role in the governing of subsequent highlighted hydrological processes at very small scales. For example, when determining surface permeability, the amount of organic matter and the aggregates can create different soils which change infiltration and storage of water, and which vary spatially and over depth. Greater infiltration rates have been observed to occur near semi-arid vegetation that have been attributed to soil properties under plants such as a lower bulk density (Belsky et al., 1993), a greater soil aggregate stability (Blackburn, 1975) and a greater density of macropores (Dunne et al., 1991,Bergkamp et al., 1996). Microtopography (vertical variations that are on the same order of magnitude as the flow depth during runoff events (i.e., mm to cm) and/or the horizontal variation of the microtopographic features are 2–3 orders of magnitude smaller than the hillslope length) can have an important effect on runoff at fine spatial scales (Yair and Lavee, 1976; Scoging, 1982; Wilcox et al., 1988; Dunne et al., 1991). Specific, local processes at such small

spatial scales as this were omitted from the framework in favour of providing a generalised larger scale overview of controls.

Setting controls within a catchment based on a generalised geomorphic model outlined in Section 4.3, allows for hypothetically generalised predictions of how recharge process may vary across a given dryland catchment. My framework predicts:

Uplands often receive higher precipitation amounts due to the orographic effect of rainfall and the contributions of snowmelt. High amounts and intensity of available rainfall in uplands provide favourable inputs for more diffuse processes (Flint and Flint, 2014), but this is dependent on the topography and surface permeability of the upland region. Where steep slopes and low permeability soils restrict the propensity for diffuse recharge, these characteristics allow upland zones to concentrate runoff more efficiently into topographical depressions. Potential recharge is then dependent on the existence of high permeability pathways underlying such depressions. Where the upland zone consists of uplifted and weathered bedrock, these pathways likely exist in the form of faults (pathway 5 in Fig 4.2) and fractures (pathway 4 in Fig 4.2). Typically, low volumes of stored superficial alluvium underlying IRES in uplands is likely to limit storage and water concentrated within depressions is likely partitioned as runoff given high permeability contrasts.

Piedmonts typically exhibit the coalescence of runoff within IRES which leads to a high concentration of infiltrating water that maximises focused recharge within IRES in such settings despite low amounts of direct precipitation falling onto these zones. This is consistent with observations of mountain front recharge within piedmont zones across the globe (Carling et al., 2012; Markovich et al., 2021). Increased stream width (or the development of alluvial fans) provides greater volumes of alluvial storage and potentially high permeability pathways for surface water to infiltrate. Incised alluvial fans increase potential for diffuse recharge due to high permeabilities of surrounding sediments and relative flat topography, however this requires large enough direct precipitation inputs to saturate the alluvial surface (Carling et al., 2012). Longitudinal subsurface flow from perched alluvial water from the upland zone also increases input of plant available water to alluvial stores in time, allowing for the development of extensive riparian corridors within this zone.

Lowlands: IRES exhibit decreased stream power and gradient lead to a preference towards depositional stream characteristics, leading to the development of large alluvial stores that often serve as the primary aquifers in the lowland zone. These large stores act as large permeability pathways that contribute to high transmission losses seen in

drylands worldwide (Shanafield and Cook, 2014) and the degree to which runoff flows into the floodout zone is dependent on the permeability of the alluvium and length of this zone.

Floodout: the presence of low permeability layers or topography cause deep groundwater to discharge in the floodout (Bourke et al., 2021; Goodrich et al., 2018). This deeper flow of recharged groundwater from upland and piedmont zones may sustain streamflow at low flows within perennial and intermittent streams in the floodout (Sabathier et al., 2021). Where floodouts consist of playas and endorheic basins, groundwater recharge depends on the permeability of the depression.

In the geomorphic model used to define the catchment I make broad assumptions that the connectivity of the catchment allows for high sediment delivery ratios (SDR, Walling, 1983) that allow for the transport of large volumes of alluvium downstream to form increasing volumes of alluvial stores (up to the lowland zone). Using a lower SDR when considering outputs of eroded sediment (and water) from the upland zone, the characteristics of alluvial stores in subsequent zones would be different. However, the goal of the model was not to make predictions about sediment delivery but was instead used as a tool to constrain controls and apply the framework to make predictions about the variations in recharge across a hypothetical dryland catchment. In cases of low SDR from the uplands, then the nature and flexibility of the framework allows for generalized predictions of water balance with decreasing alluvial stores.

Without direct observations or numerical simulations, one cannot quantify the relative magnitude or dominance of specific controls on the processes outlined in this chapter. However, my framework provides a first step by outlining dryland specific climate, landscape and geological controls which can be tested in a numerical model or mapped at a larger scale. In Section 3.4, I hypothesized that within a given dryland catchment, there may be 'goldilocks zones' by which certain components of the water balance may be maximised. This chapter builds upon this hypothesis by predicting that certain 'goldilocks values' of controls can interact with each other within the process hierarchy outlined in Section 4.3.

I address these hypotheses in Chapter 5 by conducting a series of numerical experiments within the context of a simplified ephemeral stream system to better understand the sensitivity of dryland near-stream water balance partitioning to changes in the controls outlined in this chapter, and to quantify the ranges and combinations of goldilocks values that may maximise groundwater recharge.

4.5 Conclusion

In this chapter I proposed a novel framework for understanding recharge in dryland catchments. This framework describes a set of processes that enable the conversion of rainfall to recharge given the challenges posed by near surface losses and dryland hydrological conditions. Each process is governed by a set of controls which have been explored in detail.

Climate controls water availability. Storm events that concentrate rainfall in time can increase potential for diffuse recharge, or increase runoff into topographical depressions that increases potential for focused recharge. Success of either scenarios depends on the delivery of water into the subsurface, which is controlled by the relationship between surface permeability or permeable pathways and vegetation. Potential recharge can be delivered directly to regional groundwater, or be redistributed laterally by superficial geological structures to be indirectly delivered.

I applied framework to catchment scale geomorphic model of a dryland catchment to make hypothetical generalized predictions of variations in water balance and recharge. These predictions are consistent with literature and demonstrates the flexibility of the framework to contexualise and understand predominant recharge processes within dryland catchments. The broad continuum nature of controls outlined within the framework allows for its transferability to explain the predominance of diffuse or focused recharge between dryland catchments by way of process controls.

Chapter 5

Quantifying geological controls on water balance partitioning in ephemeral stream systems using numerical modelling

5.1 Introduction

Within my framework for recharge in Chapter 4, I emphasize the concentration and channelling of surface water as a key process in increasing the potential for focused recharge in drylands. Since (1) they represent the main conduits for concentrated water in most dryland catchments and (2) are an understudied part of the dryland catchment. As such, I centred my generalized block models of superficial geological structures around IRES systems (see Section 4.2.3). Alluvial stores within these systems acts as a key permeable pathway for the direct and indirect delivery of channelised runoff as focused groundwater recharge to regional groundwater (Cuthbert et al., 2019; Cuthbert et al., 2016; Keppel and Renard, 1962a; Manna et al., 2019; Villeneuve et al., 2015)(Acworth et al., 2021; M O Cuthbert et al., 2016; Dahan et al., 2008a; Manna et al., 2019; Villeneuve et al., 2015) and these pathways are likely prevalent in dryland alluvial settings of large global extent where IRES comprise >80% of the dryland river network (Datry et al., 2014; Levick et al., 2008).

Despite its importance, the geological controls of focused recharge through the beds of these systems are much more poorly quantified than diffuse recharge. Furthermore, the storage and lateral redistribution of perched groundwater within these systems has knock -on effects for other components of the water balance, such as evapotranspiration (ET).

However, the sensitivity of these components to changes in superficial geological conditions, are also poorly understood and largely unquantified. Numerical modelling approaches that aim to quantify surface-water groundwater interactions in these systems typically assume that the system is geologically homogenous (Brunner et al., 2009; Noorduijn et al., 2014; Wang et al., 2017) and do not address the spatial-variation in surface water-groundwater interactions longitudinally along the channel (Quichimbo et al., 2020). To bring much needed quantification on the role of superficial geology in the context of IRES systems, a numerical model must capture both the geological heterogeneity of the subsurface and the storage (and subsequent lateral redistribution) of perched groundwater in the system.

In this chapter, I aim to quantify the sensitivity of focused recharge in dryland IRES to variations in superficial geology and to changes in environmental conditions by introducing a physically distributed model centred around a simplified, idealised ephemeral stream system with heterogeneous geology. I first outline the modelling approach and parameter choices before displaying the results of a series of experiments showing physical accuracy and validity of this model, comparing it to previous models of ephemeral stream dynamics. The controls outlined in Chapter 4 are then mapped to model parameters within this specific context, and series of numerical experiments were preformed to better understand the sensitivity of the near-stream water balance to changes in these parameters. Finally, using the catchment-scale geomorphic model proposed in Chapter 4, I explore how these water balance components vary within a typical dryland catchment and attempt to quantify the ranges and combinations of optimal or 'goldilocks' values that may maximise groundwater recharge.

5.2 Methods

5.2.1 Model choice

MODFLOW (McDonald and Harbaugh, 2003) was chosen for the modelling because it is a trusted, robust, industry standard code that enables me to capture the key processes from my conceptual model while still maintaining reasonably short run times and a moderate number of physically based parameters. This is in comparison to, for example, a fully integrated hydrological model like Parflow (Kuffour et al., 2020) or SHETRAN (Ewen et al., 2000), which are computationally much more expensive, have more unconstrained parameters to approximate, and numerically may struggle with key processes, such as the drying and re-wetting of stream or groundwater nodes that are a key component needed to

simulate the groundwater dynamics within superficial deposits of IRES, which is my focus in this chapter.

An additional motivation for choosing MODFLOW was the ability to use FloPy (Bakker et al., 2016), a python package that allows for the creation, running and post-processing of MODFLOW models. The ability to run MODFLOW via a Python script was of particular importance in this analysis, as it allowed for many MODFLOW models with different parameters to be created, run, and analysed within the same code, without the need to create and post-process each model laboriously individually, via a graphical user interface.

5.2.2 Model Geometry

The MODFLOW model was designed to resemble a typical ephemeral stream system, with geometries defined according to common values from ephemeral streams in dryland environments (S.-A. Chen et al., 2019; Singer and Michaelides, 2014; Sutfin et al., 2014). The model domain is a rectangular basin 4 km wide by 10 km long. (see Fig 5.1) chosen to reduce the influence of boundary conditions on the simulated processes, with a specified model width wide enough to support groundwater mounding beneath the stream because of stream infiltration. Physically, the model represents a series of parallel ephemeral streams spaced 4 km apart, a reasonable assumption in dryland settings (Martin S. Andersen and Acworth, 2009b; Hawlye and Kernodle, 2000; Morin et al., 2009).

Hydraulic head in the model is defined as the sum of elevation head and pressure head and is simply abbreviated to head in this chapter. When denoting dimensions of parameters, [L] denotes units of length (e.g. metres) and [T] denotes units of time (e.g. days).

The model is discretised horizontally in 41 (perpendicular to stream) x 200 (parallel to stream) rectangular elements. Grid elements vary in area but have the same length, 50 m, in the longitudinal direction parallel to the stream. A stream is located in the middle cell of the model along the longest dimension, and channel cross sections were defined as rectangular in shape and set to 3 m in depth, such that the streambed sits 3m below the elevation of the top of the model. Stream slope and surface slope were set the same at 1% for the base case.

For some time during and after an episodic streamflow event, I would expect a groundwater mound to rise and decay in the vicinity of the stream (Cuthbert et al., 2016). A groundwater mound is a localized rise in the groundwater table in response to focused recharge at a rate that exceeds the capacity of the aquifer or the soil to convey these amounts of water away from the recharge zone (Abotalib et al., 2021). Grid cells perpendicular to the stream were refined in orderly to properly capture the dissipation of a groundwater mound in the layers beneath the stream. For example, for a stream width of

25 m, cells on both sides of the stream have a width of 12.5 m. The remaining cells then increase in size with distance from the stream, increasing from 12.5 m to 58 m in the first 10 cells, then increasing to a maximum of 320 m in the outer cell.

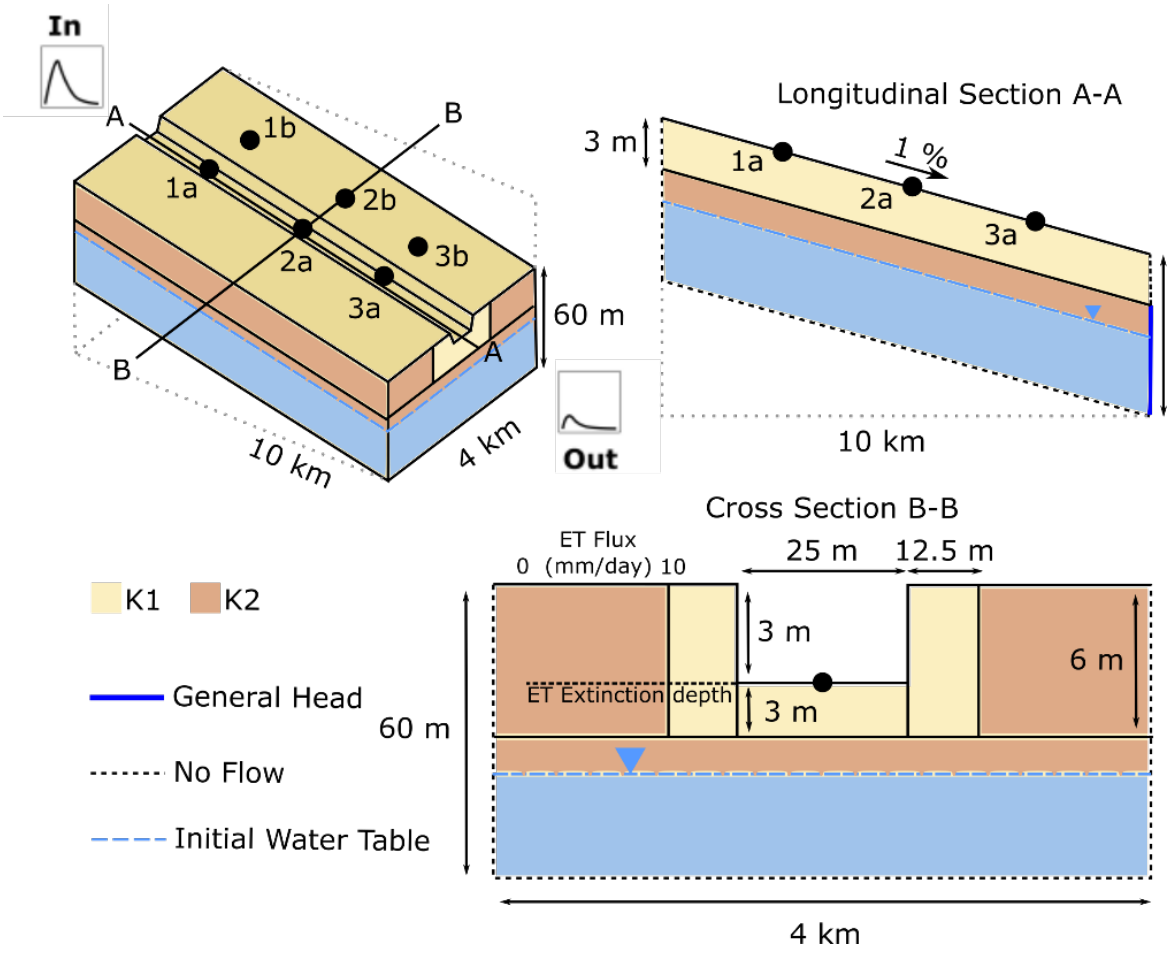

Fig. 5.1 Schematic of the model domain, geometry and boundary conditions used as base case in the numerical experiments. Points 1a,2a and 3a refer to head observation points within the middle cell (where the stream is located) at points 7500 m, 5000 m and 2500 m from the outflow respectively. Points 1b, 2b and 3b are head observation points located two cells away from the middle cell. High permeability alluvial deposits are defined in the middle cell and the cells either side. A schematic of how the EVT package is implemented is shown in green on Cross Section B-B, demonstrating the relationship between max ET flux and extinction depth.

Vertically, the model is discretised into 2 layers. The first layer measures 3m in thickness underneath the stream and represents a store of streambed alluvium. Outside of the stream cells, the upper layer measures 6 m in thickness. The total model depth was specified as 60

m, reasonable for representing a typical alluvial aquifer in arid and semi-arid regions (Coes and Pool, 2005; Lerner et al., 1990).

5.2.3 Boundary Conditions

No-flow boundary conditions were set on the lateral boundaries of the model, representative of a groundwater divide. The model is bounded at one (upstream) end by a no- flow boundary, representative of the edge of an alluvial aquifer abutting a mountain front, for example, typical in headwater ephemeral stream settings (Pool, 2005; Simmers, 1997), but with no groundwater inflow (or mountain block recharge) from the mountain front.

A head-dependent flux boundary in the form of MODFLOW's General Head Boundary (GHB) condition was specified at the other (downstream) end of the model. At this boundary, flow to and from a cell depends on the difference between head in the cell and an assigned reference head 10 m below the model top, and a constant of proportionality called Conductance [L^2/T]. This value is taken as:

$$Conductance = K * W * \frac{L}{D} \tag{5.1}$$

Where K is the hydraulic conductivity of the layer, W is the width of the cell (perpendicular to flow direction), L is the length of the cell (parallel to flow direction) and D is a scaling factor that conceptually represents the distance to a constant head boundary, such as a large surface body with known elevation, situated far away from the model domain. Using this boundary condition (as opposed to a constant head boundary) avoids the need to unnecessarily extend the model domain outward so that the boundary does not influence the head in the model. In my model, this distance $D = 1000$ m, representing a fixed head at the surface 1 km away (which conceptually represents a perennial body of surface water 1 km downstream).

The initial water table elevation was set 10 m below, and parallel to, the ground surface of the model. This was set so that the water table depth sits below the first layer of the model, and perching conditions in the first layer can be simulated given a permeability contrast between the two layers of the model.

Streamflow input

In real systems, ephemeral streamflow events may show a huge variation in hydrograph shape, return period and duration. In ephemeral streams, hydrograph shape is characterised by a rapid increase and decrease of the stream stage (Costigan et al., 2017; Malmon et al.,

2004). Streamflow durations can vary from several hours up to several days (Cataldo et al., 2004; Constantz and Thomas, 1997; Knighton and Nanson, 1994; Wheater, 2008) or even weeks (Chapter 3). To simulate an event with such characteristics, a linear reservoir model was used to create synthetic hydrographs which was passed in to the model to the first (upstream) stream cell of the model domain to simulate streamflow.

A linear reservoir model (Beven, 2011), assumes that water discharged from the reservoir Q [L^3/T] is proportional to its storage S [L^3]:

$$Q = kS \tag{5.2}$$

where k is rate constant [1/T]. By applying a mass balance for the reservoir:

$$\Delta S = I - Q \tag{5.3}$$

Where I is the input [L^3/T] into the reservoir and is akin to the resulting concentration of precipitation into the runoff in upstream tributaries in my framework (Chapter 4). By combining Eq. (5.2) and Eq. (5.3), and using a finite difference approach, the linear reservoir may be discretised over time as follows:

$$Q_t = (1 - k)Q_{t-\Delta t} + kI_t \tag{5.4}$$

Parameter k of the above represents the inverse of the decay constant of the reservoir T_r (and is subsequently used as a parameter in this chapter).

The hydrograph obtained from Eq 5.4 for a rectangular pulse event results in a hydrograph with a sharp rise at the beginning of the event, followed by an exponential decay of flow rate.

5.2.4 Implementation of MODFLOW Packages

Flopy

The FloPy package was used to create, run and post-process the MODFLOW models in this Chapter. The FloPy package consists of a set of Python scripts to run MODFLOW and MODFLOW packages within the Python environment. This allows for the coding of numerous scripts to be run on loop with ease, without having to manually create each model run. FloPy is open-source, and more information can be found in (https://github.com/flipmanny/Zarate-Thesis-Flopy-Codes).

MODFLOW-NWT

The USGS MODFLOW-NWT solver (Niswonger et al., 2011) is a Newton-Raphson formulation for MODFLOW-2005 to improve solution of unconfined groundwater-flow problems. It was chosen for its accuracy in solving problems involving drying and rewetting nonlinearities of the unconfined groundwater-flow equation. These nonlinearities are particularly prominent in my model, where the initial water table starts below the bottom of elevation of layer 1. As such, recharge to the water table in layer 2 involves the rewetting of the uppermost layer. MODFLOW-NWT solves this rewetting problem by always setting cells without head (also called dry cells) as active, such that conductance calculations can still be performed between this and surrounding cells. The solver parameters used throughout the model runs are summarised in the table below (Table 5.1) and were chosen to ensure convergence and negligible mass balance errors in the model runs (see Fig A27 for an example). This is indicated within the OPTIONS settings, and complex indicates that default solver input values will be defined that work well for highly nonlinear models that consist of one or more unconfined layers representing complex geology and surface water - groundwater interaction, as anticipated in my model.

Parameter	**HEADTOL**	**FLUXTOL**	**MAXITEROUT**	**THICKFACT**	**LINMETH**	**OPTIONS**
Value	0.0001	0.1	500	0.00001	χMD	Complex

Table 5.1 MODFLOW-NWT solver parameters to ensure convergence and minimal mass balance errors

HEADTOL (L) is the maximum head change between outer iterations for solution of the nonlinear problem. FLUXTOL [L^3/T] is the maximum root-mean-squared flux difference between outer iterations for solution of the nonlinear problem. MAXITEROUT is the maximum number of iterations to be allowed for solution of the outer (nonlinear) problem (integer). THICKFACT is the portion of the cell thickness (length) used for smoothly adjusting storage and conductance coefficients to zero. LINMETH is a flag that determines which matrix solver will be used and in the case of the model the χMD solver is used (see Niswonger et al., 2011 for more details).

The model solver time step was specified at 30-minute intervals, with total simulation time up to a maximum of 100 days. This time step was chosen as the maximum interval that provides negligible mass balance errors, minimal run times and realistic streamflow routing. Model inputs (flow) and outputs were also reported at this time step, and Python scripts were used to post-process the MODFLOW output files.

MODFLOW SFR2 Stream Package

To simulate the ephemeral stream at the surface of the model domain, the SFR2 package (Niswonger and Prudic, 2010) was used. The SFR2 package was developed as a package for MODFLOW to simulate stream and aquifer interactions by routing flow through a network of surface water channels. Input flow to the stream was assigned at the most upstream SFR2 cell (see Fig 5.1) and shape and magnitude were defined by the flow output of a linear reservoir model as described in 5.2.3. This package also permits discharge of excess streamflow due to high water tables or high input flows.

MODFLOW EVT Evapotranspiration Package

ET was simulated using the EVT package (Harbaugh et al., 2000) which simulates the effect of plant transpiration and direct evaporation by removing water from cells in the upper layer in and around the stream during a simulation. This simulation is a head dependent flux function that uses a maximum elevation, in this case defined at the model surface, at which maximum evapotranspiration (ET) flux will occur if the head is at or above that elevation. This maximum ET flux was defined as 10 mm/day in the model, typical of potential evapotranspiration values from riparian zones in dryland regions (Lautz, 2008; Serrat-Capdevila et al., 2011; Singer et al., 2021). A minimum elevation, termed the extinction depth, is also defined for which ET flux is zero when the head is at or below this elevation. This extinction depth is defined as 3 m and set the same as the thickness of my alluvial store. Conceptually, this means riparian vegetation in my model can only use water stored within the superficial deposits at the top few metres of the model, and again is not an unreasonable assumption in dryland environments where flow in the alluvium is not limiting and provides enough water for riparian vegetation (Sabathier et al., 2021). The relationship between extinction depth and top of model is shown in Figure 5.1.

5.2.5 Experimental setup

Base Case Homogeneous Model

Before exploring the full parameter space of controls, I first demonstrate that the model results are physically plausible by running a simulation using a base case, homogeneous model with one flow event. I then compare the outputs of this model with previous numerical models of homogeneous ephemeral stream systems, such as that of Cuthbert et al., 2016 and Quichimbo et al., 2020.

The base case homogeneous model was defined with a K_{sat} of 3.5 m/day in both layers, which corresponds to coarse loamy sand or medium sand sediments (Carsel and Parrish, 1988) that is consistent with the permeability of sandy streambed typical of ephemeral streams. For example this would be representative of a large alluvial aquifer beneath larger ephemeral river systems (in the Limpopo, for example, Boroto and Gorgens, 2003) that form some of the most productive aquifers in Africa (A M MacDonald et al., 2012). Channel hydraulic properties were specified using a Mannings roughness of 0.035 [-] (Strickler coefficient, M = 20), which corresponds to coarse sandy material within a regular cross section (Phillips and Tadayon, 2006). A specific yield of 0.35 [-] and specific storage of 3x10-6 [m^{-1}] were used for all K_{sat}used in the model simulations. A stream width of 25 m was used, with a stream and land surface gradient of 1%, typical of ephemeral stream systems situated at piedmont or intermediate zones of transfer in the dryland catchment (Sutfin et al., 2014). These base parameters are summarised in Table 5.2 below. Using

K_{sat}	Specific Yield [-]	Specific storage (m^{-1})	Permeability contrast	Gradient (%)	Stream width (m)	Mannings roughness [-]
3.5	0.35	0.00001	1	1	25	0.035

Table 5.2 Base model used in simulations. Permeability contrast denotes difference in K_{sat} between layers 1 and 2 (which in this base, homogeneous case, is none).

these parameters, the model was first run at a steady-state for 100 days with no-flow, to establish initial conditions. Then, a transient model was run and, using Eq 5.4, streamflow was generated considering a peak pulse event of 12 m^3/s with a time constant of two days. Integrated over time, this corresponds to a fixed total input flow volume of 1036768 m^3, and is equivalent to 4 mm of excess precipitation falling across a 25km^2 catchment, over a 10 day period.

The parameters of base case model were chosen to broadly emulates the situation described conceptually in Chapter 3 for the Middle Creek reach of the Maules Creek ephemeral stream system in NSW, Australia. However, the focus here is not to produce a calibrated model of that field study, but rather to develop a general understanding of the water balance partitioning of a wide range of typical ephemeral stream systems.

Heterogeneous Geology Scenarios

After illustrating the results of the homogeneous model, the model parameters were altered to simulate how water balance components change due to a range of heterogeneous geological scenarios. Keeping K_{sat} of only the stream cell and adjacent surrounding cells

at the base case value of K_{sat} = 3.5 m/day. Henceforth, I refer to the K_{sat} of the stream cell and adjacent surrounding cells as K_1 (see Figure 5.1). The rest of the model domain has a K_{sat} of 0.0035 m/day, which corresponds to loamy or poorly structured clay, and represents a permeability contrast (PC) of 1000, and I refer the K_{sat} of this zone herein as K_2. The same input flow (a peak input flow of 12 m^3/s with a residence time of two days) was generated for this model, and the results compared with the base case.

Next, the effects of variations in K_1, permeability contrast, flow volume and flow duration on the water balance of the model were explored. The parameter ranges used in these experiments are shown in Table 5.3. These variations map to different controls outlined in the conceptual model as follows: K_1 maps to surface permeability (section 4.2.2). Permeability contrast maps to permeability contrast between layers in the close vicinity of IRES (section 4.2.3). Flow volume is a proxy for rainfall amounts (for a given time frame), and thus my model assumed a given rainfall event can be concentrated as runoff and delivered as flow to the IRES system. Flow duration acts as a proxy for rainfall intensity in my model, of which the underlying control in Chapter 4 is rainfall characteristics. However, I acknowledge that the characteristics of runoff generation and partitioning in the subsurface due to geological heterogeneities (Chapter 3) may cause the storage and release of water long after rainfall events. These implications are discussions in Section 5.4.

Parameter	**PC (K1/K2)**	**K1**	**Ratio of total flow/volume of store**	**Time constant**
Range of variation	1 to 2500	1.67, 3.5, 10	0.66, 2 , 4	1 to 14

Table 5.3 Parameters and range of parameter variation explored in numerical experiments with heterogeneous model geology.

First, a parameter space representing 15 values of permeability contrast (PC between 1 and 2500 are explored in combination with three different values of K_1: 1.67, 3.5 (base case) and 10 m/day, which correspond to streambeds composed of sandy loam, medium sand, and coarse sands respectively. Finally, using a value of 10 m/day for the $K_{sat}$of the alluvium, the effects of varying input flow volumes were explored. The volume of these flow sizes was chosen to be 0.66, 2 and 4 times the size of the volume of the alluvial store in these numerical experiments (in both the homogeneous and the base case is 525000 m^3). Variations in flow duration, range from 1 day residence time (representing short duration, intense storms) to 14 days (representing multiple small rainfall events clustered in a short time period) were explored with three values of permeability contrast (1,100,1000) and the three values of flow volume.

Catchment setting scenarios

A series of numerical experiments were conducted to explore how water balances vary within a hypothetical dryland catchment, using parameter ranges defined in my geomorphic model from Chapter 4.

Values of gradient (which maps to topography) and width (which is a proxy for volume of superficial store, as thickness is fixed) were defined for three geomorphic zones: Upland, Piedmont, and Lowland. The parameters chosen for these zones are summarized in Table 5.4 and described in turn.

	Upland	**Piedmont**	**Lowland**
Gradient (%)	2.5	1	0.05
Width (m)	10	25	100

Table 5.4 Representative values of gradient and width chosen for each of the geomorphic zones simulated in the numerical experiments

Three values of stream and land surface gradient were chosen to represent the variation in geomorphological zone defined in Chapter 4. Steep gradients of 2.5% are representative of mountain streams in the upland zone, intermediate gradients of 1% representative of ephemeral streams situated in the mountain front or transfer zone, and gradients of 0.05% representative of lowland ephemeral streams.

To control the variations in alluvial store volume, the thickness was assumed constant, but the width varies. This is a reasonable assumption, as discussed in Chapter 4, sediment loads and volumes are known to increase downstream as the transport capacity of flows decrease and sediments are deposited. With respect to the different geomorphological zones, streams 10 m in width are assumed to be representative of narrow mountain headwater streams in the upland zone, 25 m to streams in the intermediate zone, and 100 m to large, braided ephemeral stream systems found in the lowlands (Sutfin et al 2014).

Combinations of variations of permeability contrast (10, 100, 1000) and flow residence time (1 to 14 days) were simulated in combination using an event the streamflow characteristics as used in the base case model (A peak flow volume of 12 m^3 with a two-day decay constant), and corresponds to a fixed total input flow volume of 1036768 m^3. This value of flow was specifically chosen to simulate the differences in filling of volume of alluvial store within the three model domains, with this value of flow being 2.67 more than the alluvial store in the Upland zone, 1.06 times the volume of the alluvial store in the piedmont zone, and 0.267 times the volume of the alluvial store in the lowland.

Calculating catchment water balance

Measured components of the volumetric water balance shown in Section 5.3 were calculated as follows:

Outflow: Cumulative volumetric runoff at the downstream end of the stream channel throughout the duration of the simulation

Stream Infiltration: Cumulative volume of streamflow input that infiltrates into Layer 1 throughout the whole length of the stream and duration of simulation.

ET Cumulative volumetric evapotranspiration (defined in Section 5.2.4, evapotranspiration) taken from the stream cell and adjacent cells (cells in which K_1 is defined) throughout the duration of the simulation

Recharge Cumulative volume of water leaving layer 1 throughout the whole model, and entering Layer 2, throughout the duration of the simulation

5.3 Results

5.3.1 Base case model

The base case results (Figures 5.2 & 5.3) demonstrate large streambed transmission losses typical of ephemeral stream systems, with flow responses diminishing between points 1 and 2 (see Figure 5.1), and ceasing just after point 2, at 4800 m from the outlet. Groundwater levels respond in turn to the changes in downstream flow transmission losses. Greater head increases occur upstream than at the downstream end as can be seen, for example, in the sloping nature of the peak groundwater response at 2 days (Figure 5.3b).

There are two peaks in the streamflow hydrograph at point 1 (see Fig 5.2). The streamflow peaks in response to peak input streamflow at 1 day, and then recedes. There is then a second rise and peak at 3 days. This second rise corresponds to when groundwater upstream of point 1 (between 10000 and 7500 m from the outflow) has reached the streambed elevation, causing the vertical hydraulic gradient between the streambed and groundwater to decrease, and thus the transmission losses to substantially reduce. Hence the flow volume at points downstream increases briefly. Recession in groundwater heads occur after streamflow recedes.

Perpendicular to the direction of streamflow, a groundwater mound can be seen rising in response to streamflow transmission losses, showing a sharp peak before dissipating and spreading out, transversely towards the lateral boundaries (Figure 5.3 c-e). The size of this

mound, and the subsequent lateral extent of mounding is greater upstream than at the downstream end, as a response to decreasing flow volumes due to transmission losses along the reach in the downstream direction.

Perching or groundwater in Layer 1 (Figures 5.2 and 5.3) occurs as a result of large streamflow losses during the first two days of streamflow, creating a downwards vertical hydraulic gradient between layers 1 and 2. When compared with a one layer homogeneous model with identical parameters, the two layer homogeneous model showed a R2 = 0.99 correlation in water balance components. Furthermore, the total volumetric water balance in the two-layer model contains a percent discrepancy of 0.001%. Finally, the results in this section are consistent with the behavior from other models reported for example by Cuthbert et al., 2016 and Quichimbo et al., 2020. The two-layer MODFLOW set-up developed here therefore seems robust for the stated purpose of exploring the impact of geological heterogeneity on the water balance partitioning.

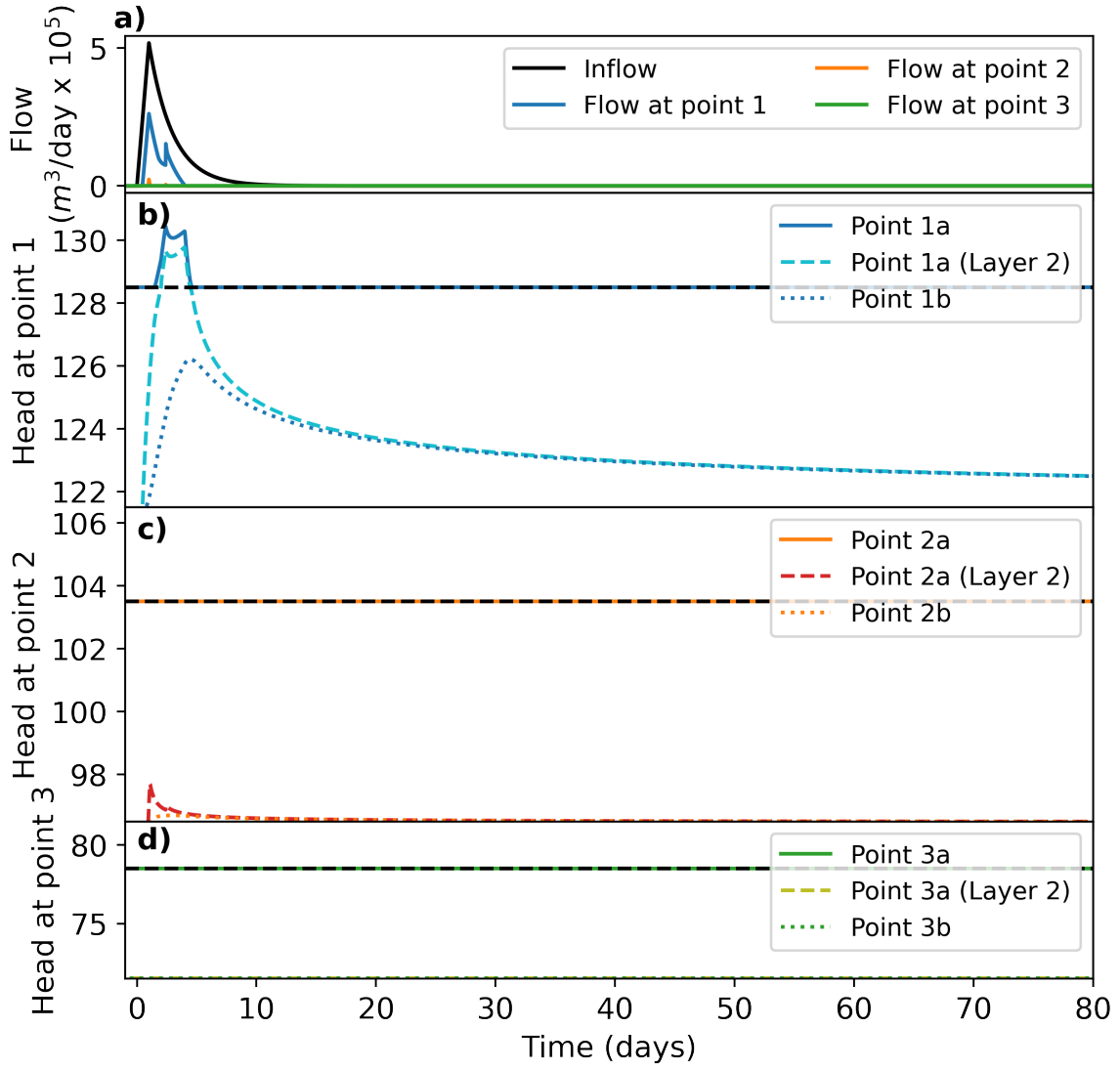

Fig. 5.2 Stream flow and groundwater hydrographs for the base case homogenous model. Points 1,2 and 3 correspond to points shown in Figures 5.1 at 7500, 5000 and 2500 m from the outflow respectively.

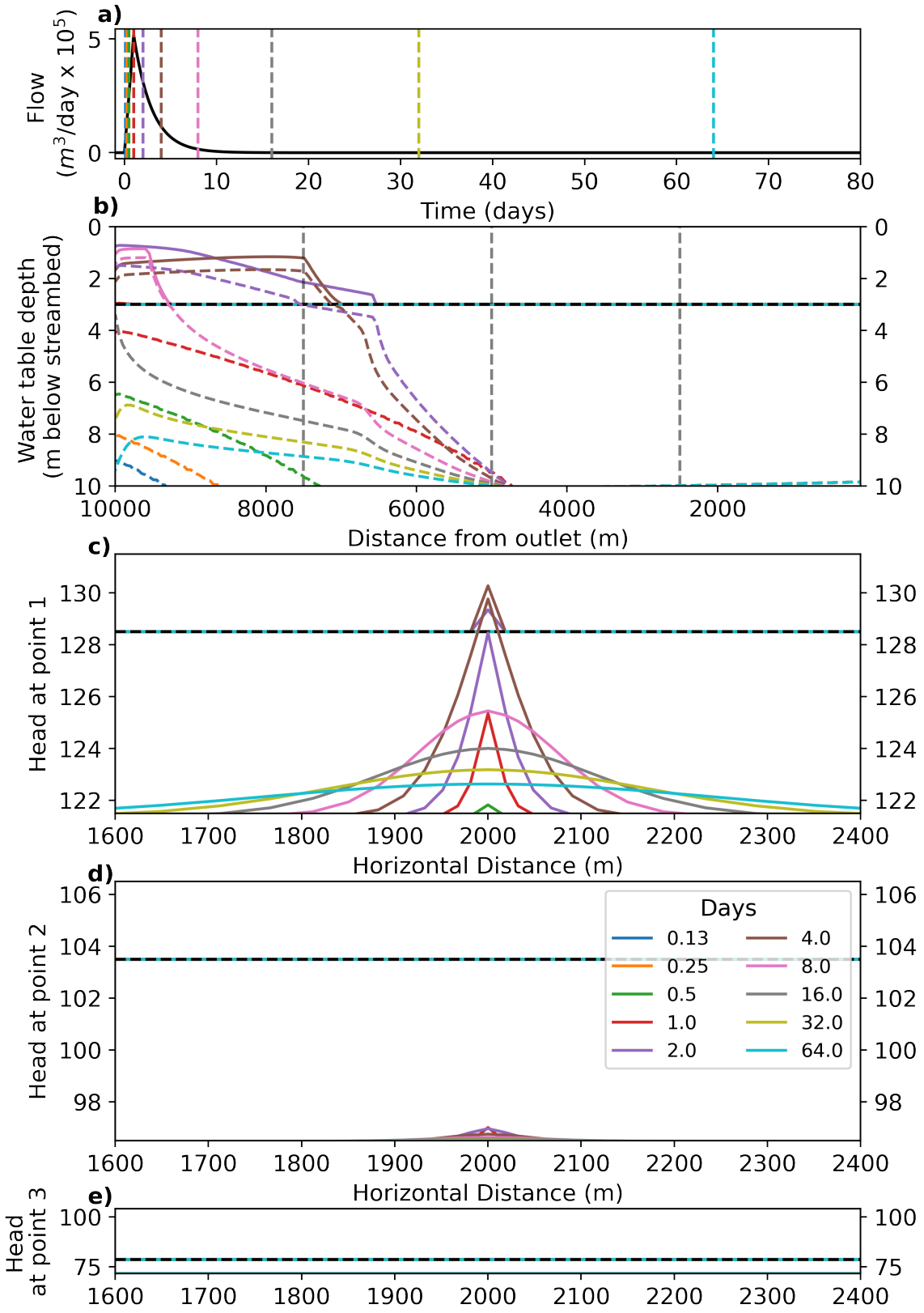

Fig. 5.3 Longitudinal and lateral variations in groundwater heads in the homogeneous model. Time slices denoted by coloured lines on the top streamflow hydrograph correspond to coloured lines in plots. Dashed lines in longitudinal section (second from top) indicate heads from layer 2 (with solid lines in this plot exclusively heads in layer 1). Vertical grey lines in longitudinal section correspond to locations of three model cross sections at Points 1, 2 and 3. Horizontal dashed line in each plot denotes bottom elevation of layer 1.

5.3.2 Numerical simulations with Heterogeneous geology

Comparison with the base case homogeneous model

Results of a heterogeneous geology model are shown in Figures 5.4 and 5.5. This model has the same parameters and input flow as base case, but with a permeability contrast of 1000 between streambed alluvium and surrounding geology (i.e. $K_1/K_2 = 1000$, see Figure 5.1 for schematic of how conductivities are distributed).

As seen in Figure 5.5, heads within the alluvium in the heterogeneous model almost all reach streambed elevation at 1 day, decreasing the hydraulic gradient between the streambed and underlying geology, and leading to decreased transmission losses in comparison to the base case homogenous scenario.

The alluvial store stays 'full' during the entire time period where there is flow within the stream, before slowly receding once streamflow ceases. Heads in the alluvium recede and persist for up to 40 days at point 1. These dynamics show clear similarities to the groundwater dynamics seen at the East Lynne site on Middle Creek described in Chapter 3. There, streamflow (hypothesized to be derived from longitudinal flow within alluvial storage) persists for 44 $\pm$ 3 days throughout the entire monitoring period. In a similar vein, the persistence of heads in the alluvium decreases from 40 days to 35 days at point 3, similar to dynamics seen from East Lynne to Middle Creek Farm. This occurs because permeability contrasts between K_1 and K_2 limit vertical percolation of water between layers, causing perched water within layer 1 to be preferentially distributed laterally downstream (see Section 3.4).

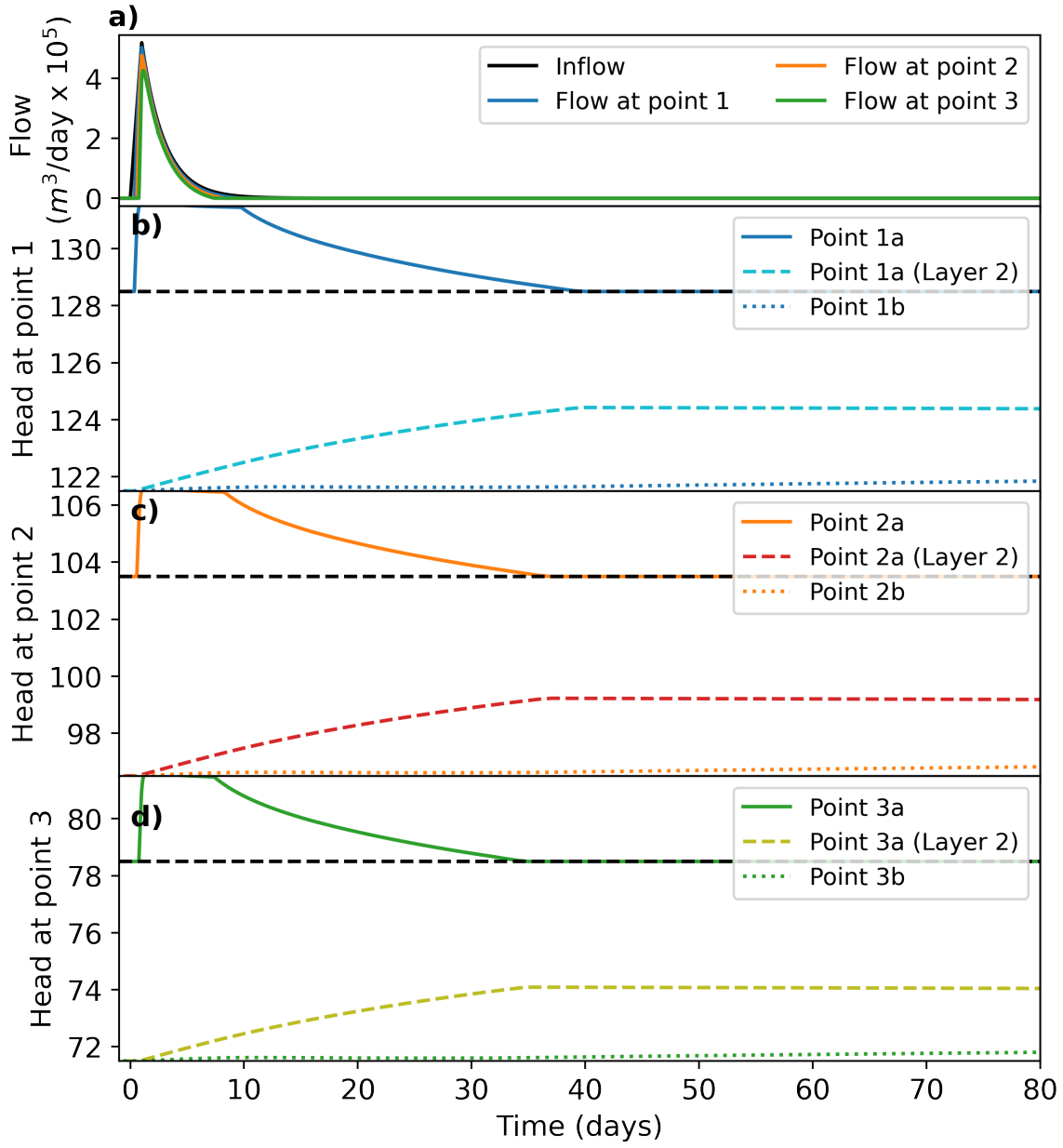

Fig. 5.4 Stream flow and groundwater hydrographs for a model with heteregeneous geology. Streambed alluvium has a Ksat of 3.5, with the surround geology a Ksat of 0.0035, corresponding to a permeability contrast of 1000. Points 1,2 and 3 correspond to points shown in Figures 5.1 at 7500, 5000 and 2500 m uupstream of the outflow respectively.

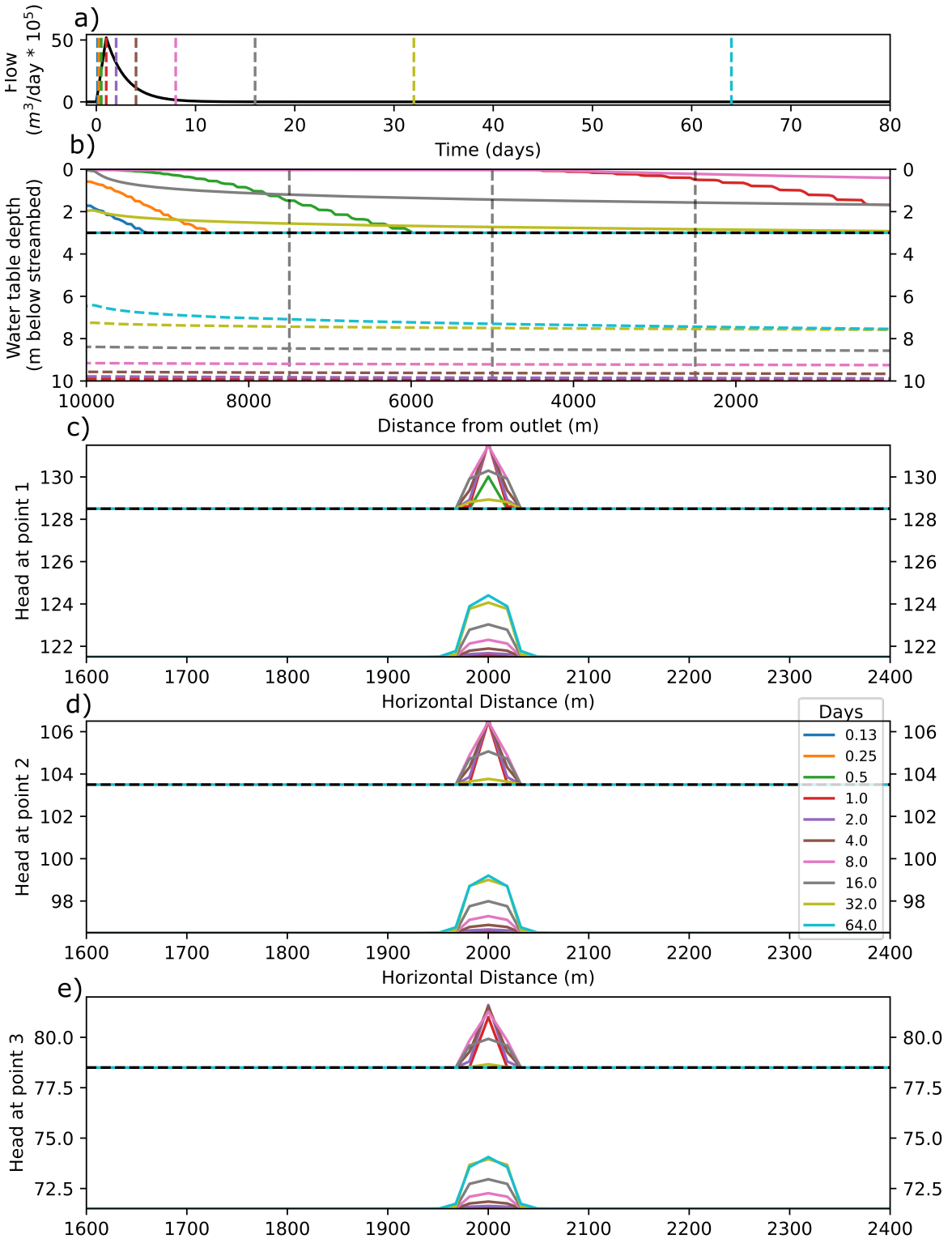

Fig. 5.5 Longitudinal and lateral variations in groundwater heads in a heterogeneous model with a $PC = 1000$. Time slices denoted by coloured lines on the top streamflow hydrograph correspond to coloured lines in plots. Dashed lines in longitudinal section (second from top) indicate heads from layer 2 (with solid lines in this plot exclusively heads in layer 1). Vertical grey lines in longitudinal section correspond to locations of three model cross sections at Points 1, 2 and 3. Horizontal dashed line in each plot denotes bottom elevation of layer 1.

Heads in Layer 2 rise at a much slower rate but continue rising while there is water within the alluvial store, before tending to a maximum value. These dynamics again show strong similarities to head responses observed at East Lynne (e.g., Figure 3.3). The formation of a groundwater mound can also be seen in Figure 5.3 and 5.4, however its lateral distribution is restricted to within the alluvial sediments in layer 1, and directly below them in layer 2.

Hence, while the intention here was not to provide a calibrated model of Middle Creek, these results illustrate that the model can provide realistic hydrological responses. This provides additional confidence that the parameter sensitivity explored below yields robust quantification of the range of water balance partitioning effects of various arrangements of superficial geology in combination with changes in the flow inputs from upstream.

Quantifying the effects of alluvial conductivity, permeability contrast, flow volume and flow duration on water balance partitioning

Simulations which combine permeability contrast (PC) from 1 to 2500 and K_1 of a) 1.67 b) 3.5 and c) 10m/day are shown in Figure 5.6.

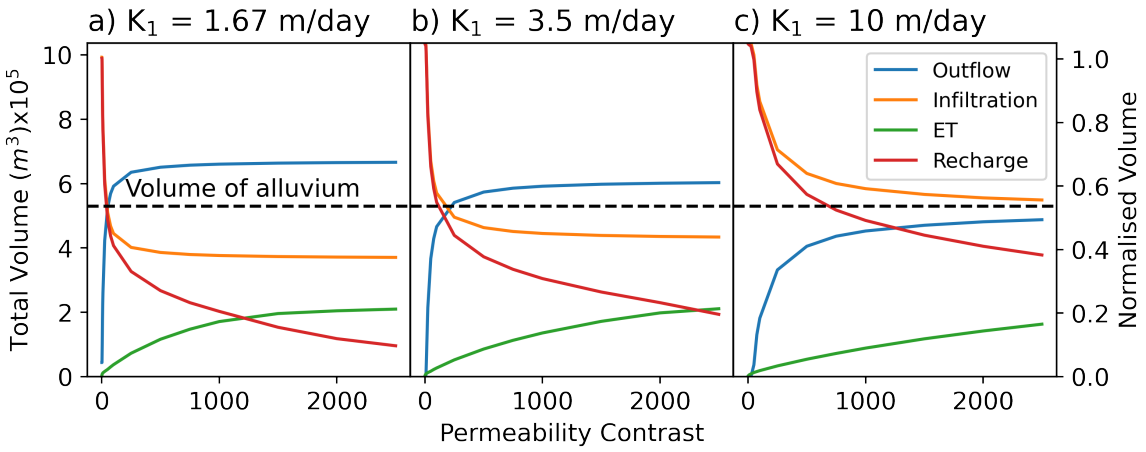

Fig. 5.6 Changes in water balance with changes in permeability contrast, for different values of K_1. Note that the Normalised volume indicates water balance component divided by the total input flow volume. Black dashed line indicates the volume of alluvial store.

At low flows (Figure 5.6 a), no outflow is produced, and all the input flow infiltrates into the alluvial store, regardless of permeability contrast, but does not fill it. The resulting recharge is subsequently a function of ET, which increases with increasing PC. I can therefore conclude that for flow volumes less than the size of the alluvial store, it is the flow volume that controls the volume of stream infiltration and hence recharge into layer 2 if the alluvial K is not a limiting factor. At flow volumes greater than the alluvial store and at PC

< 100, (Figure 5.6 b & c) the volume of flow is also a key control on streamflow infiltration and recharge. However, as PC increases, the differences in streamflow infiltration and recharge volumes between the two models begin to decrease, and at very high PC they are nearly identical. Therefore, when the flow volume exceeds the volume of the alluvial store, it is the volume of the alluvial store that becomes the limiting factor on recharge if K_1 is not itself a limiting factor.

Recharge into layer 2 can obviously only occur when there is water in the alluvial store. Thus, I hypothesize that flows that maximize the duration of water within the store also maximize recharge to layer 2 at high PC. To test this hypothesis, I conducted a series of numerical experiments exploring changing flow volume and flow duration (by changing the residence time factor, see Eq 5.3) for three different permeability contrasts of 1, 100 and 1000. The results are shown in Figure 5.7 and discussed below.

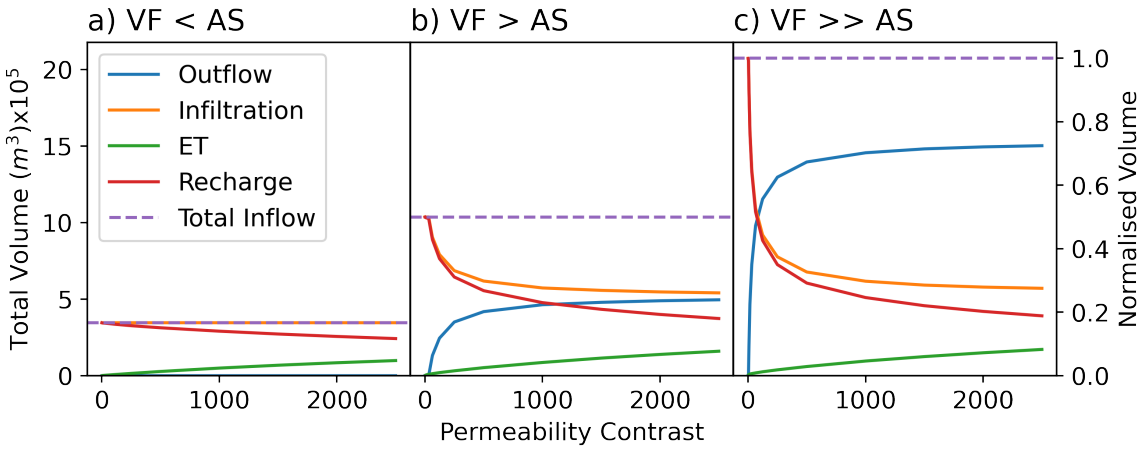

Fig. 5.7 Changes in water balance with changes in PC, for differing flow volumes. $K_1 =$ 10 m/day. Normalised volume indicates a water balance component divided by the total input flow volume of the largest flow event. VF and AS are abbreviations of Volume of flow and Volume of alluvial store respectively.

At low flows (Figure 5.7 a), no outflow is produced, and all the input flow infiltrates into the alluvial store, regardless of permeability contrast, but does not fill it. The resulting recharge is subsequently a function of ET, which increases with increasing PC. I can therefore conclude that for flow volumes less than the size of the alluvial store, it is the flow volume that controls the volume of stream infiltration and hence recharge into layer 2 if the alluvial K is not a limiting factor.

At flow volumes greater than the alluvial store and at PC < 100, (Figure 5.7 b & c) the volume of flow is also a key control on streamflow infiltration and recharge. However, as PC increases, the differences in streamflow infiltration and recharge volumes between

the two models begin to decrease, and at very high PC they are nearly identical. Therefore, when the flow volume exceeds the volume of the alluvial store, it is the volume of the alluvial store that becomes the limiting factor on recharge if K_1 is not itself a limiting factor.

Recharge into layer 2 can obviously only occur when there is water in the alluvial store. Thus, I hypothesize that flows that maximize the duration of water within the store also maximize recharge to layer 2 at high PC. To test this hypothesis, I conducted a series of numerical experiments exploring changing flow volume and flow duration (by changing the residence time factor, see Eq 5.3) for three different permeability contrasts of 1, 100 and 1000. The results are shown in Figure 5.8 and discussed below.

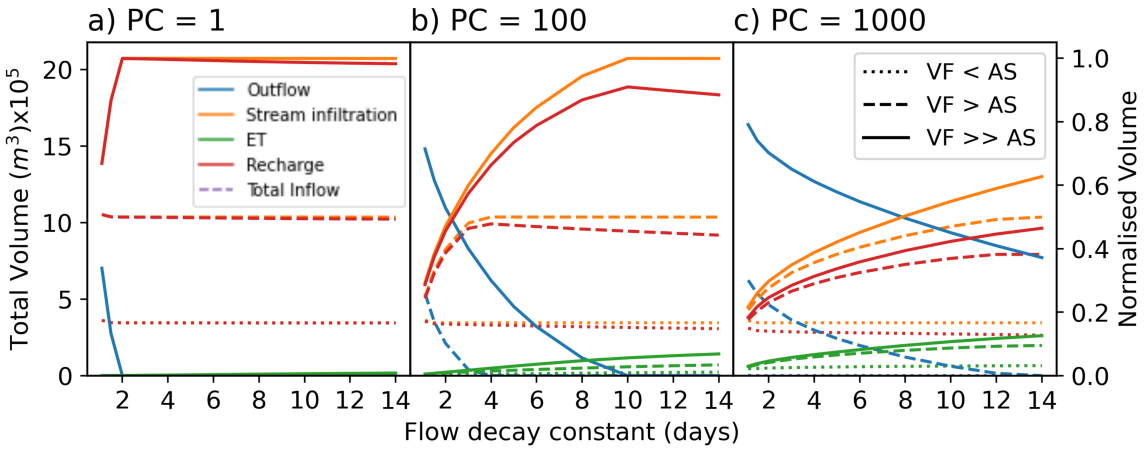

Fig. 5.8 Changes in water balance with changes in flow decay constant, for three different permeability contrasts and three different flow volumes. K_1 = 10m/day. Note that Normalised volume indicates water balance component divided by total input flow volume of the largest flow event. VF and AS are abbreviations of Volume of flow and Volume of alluvial store respectively.

For $PC = 1$ and high flow volumes (Fig 5.8a), streamflow infiltration and recharge are maximised at a residence time of 3 days, as high peak flows at lower residence times exceed the infiltration capacity of the alluvium. After this point, streamflow infiltration remains the same, however the effect of ET on recharge means that recharge begins to decrease at long flow durations.

At $PC = 100$ (Fig 5.8b), the peak in streamflow infiltration is dependent on the size of the event, an effect which is again related to the infiltration capacity of the alluvium. For very large events, streamflow infiltration peaks at 10 days before plateauing, while at medium flows this peak occurs at 4 days. These peaks in streamflow infiltration coincide

with peaks in recharge volumes, however after the peak, recharge volumes subsequently decrease because of increasing ET with flow duration.

At $PC = 1000$ (Fig 5.8c), there is an overall increase in streamflow infiltration for flow volumes greater than the alluvial store, although streamflow infiltration and subsequent recharge appears to be beginning to plateau at moderate flow volumes. For very large flow volumes, it is assumed that both streamflow infiltration and recharge will peak at a residence time outside of the parameter space explored here.

These numerical experiments demonstrate that, for a given flow volume and PC, there is an optimal flow duration that maximises streamflow infiltration but minimises the role of ET on recharge. This optimum flow duration increases with increasing flow volume and PC.

Variation of water balance within the catchment setting

Finally, numerical experiments were run to explore the variation in water balance in a hypothetical dryland catchment based on ranges of controls defined in geomorphic zones from Chapter 4. The resulting water balances for each geomorphic zone are shown in Figure 5.9.

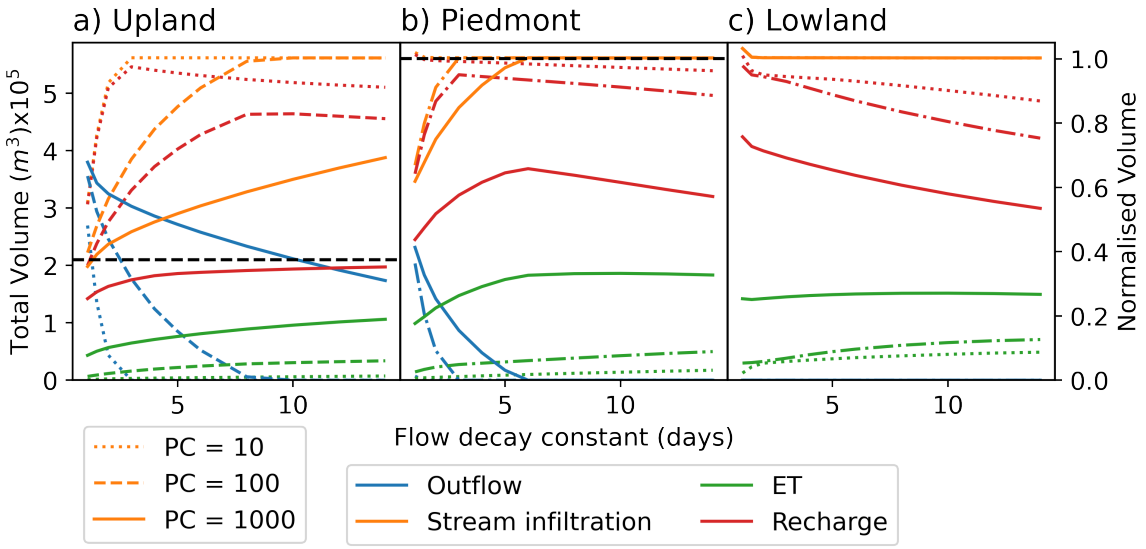

Fig. 5.9 Changes in water balance across hypothetical dryland catchment zones(see section 4.3) for varying decay constants, and for three different PC (denoted by changes in linestyle). Black dashed line indicates volume of alluvial store, which changes in size across the three zones. Note that the volume of the alluvial store in the lowlands is very large (700000 m^3) and is outside of the axis range.

The volume of the alluvial store changes and increases downstream across each geomorphic setting. Combined with equal input flow volumes this therefore leads to differing relationships between the alluvial store and flow volume across the landscape. Recharge across the three zones increases with decreasing PC, however there are interesting differences in recharge when examining recharge for given flow durations.

For example, for residence times of 6 days, recharge is maximised in the piedmont zone at $PC = 1000$. When comparing across zones, this is higher than the lowland zone and much greater than the upland zone at the same PC. Furthermore, this recharge is only slightly less than recharge at $PC = 100$ in the uplands. This effect occurs as a direct result of the partitioning of streamflow into ET and recharge. At a residence time of 6 days, streamflow infiltration is maximised in the piedmont, and does not increase when increasing duration further at this PC. However, ET increases as residence time of flows increase the duration of water within the alluvial store. This increased duration, at high PC, is readily utilized by simulated ET in my model (which can only take water from the alluvial store) and thus ET increases.

These effects are consistent with those in observed in literature, as discussed in Section 4.3.4 (permeability contrasts), where, in the ephemeral streams of the Cuvelai-Etosha Basin, Namibia, high permeability contrasts cause perched aquifers to have negligible contributions to recharge in the catchment, as most shallow water in the perched aquifer becomes lost to evaporation (Hamutoko et al., 2019). Similarly, a study in the Shashe River Valley in Botswana concluded that permeability contrasts between bedrock and alluvium created perched water that was entirely consumed by riparian vegetation, with no evidence of recharge to regional groundwater (Bauer et al., 2006).

In the lowland zone, there is an inverse relationship between flow duration and recharge at all PC, due to large volumes of alluvial store in this zone. This effect is equivalent to partitioning seen in Figure 5.7, when flow volumes < volume of alluvial store. The difference being that even at high flow volumes in this model, no outflow is generated, and is likely due to the contributions of increased stream width in this model in generating increased streambed infiltration.

5.4 Discussion

The finding that recharge is dependent on streamflow volumes (where streamflow volume < volume of alluvial store) is intuitive and consistent with my framework outlined in Chapter 4, that rainfall is a first order control on recharge volume. However, what was not considered when generalising the role of superficial geology was the conductivity of the overlying

alluvium, which was always assumed to be highly conductive. My results demonstrate that the conductivity of the alluvium is a second order control on recharge processes, and accounts for the delivery processes outlined in Chapter 4 (neglecting concentration, which was not simulated in these experiments).

These results further elucidate the role of not just the volume of alluvial store, but its relationship to event size (or in this case, volume of flow) and permeability contrast. At flow volumes < volume of alluvial store, then the volume of flow and K_1 (permeability of streambed) are the key controls on groundwater recharge. This has implications for regions with projected increases in rainfall intensification and large alluvial stores.

At low contrasts, high vertical flows between the layers limits the formation of perched groundwater allows for the direct delivery of potential recharge to deeper aquifers. At permeability contrasts greater than 100, there are stark similarities in water balance partitioning between high and very high flow volumes. At these values, the volume of the store becomes a limiting factor as the formation perched groundwaters quickly fills the alluvial store, and streamflow remains on the surface. A permeability contrast of 100 is typical of a coarse gravel overlaying finer sands or loamy sands. As such, even at minimal permeability contrasts, the volume of alluvial store begins to play a key role.

This interaction between available surface water and subsurface geology is outlined in my framework in Chapter 4 and observed in Chapter 3. Large rainfall events that generate large amounts of concentrated runoff, and activate permeable pathways (in this context, the permeable alluvium of IRES systems) may still not become recharge, but instead exists as potential recharge that can recharge perched aquifers and my results highlight the need for this distinction between perched and regional groundwater recharge as large streamflow volumes are mitigated by the volume of the store and its relationship with permeability contrast.

Furthermore, Fig 5.8 shows that by maximising the duration of streamflow, the duration of water within the store is maximised in time (see Section 4.3.4, and Section 3.4), allowing for more perched water to percolate to deeper groundwaters. When comparing to Chapter 3 and 4, however, I acknowledge that in this case, streamflow duration is used as a proxy for rainfall durations. In the context of my framework, this increased streamflow duration could also be seen as an increase in contributing alluvial store in time (section 4.3.4, volume of alluvial store). For a given location within an IRES at a dryland catchment, recharge is maximised by both event duration (or through the compounding of multiple rainfall events) or through the storage of a rainfall event in upstream stores that can contribute to later subsurface distribution to downstream stores.

In the final run of numerical experiments, I set ranges of values to account for variations in slope, volume of alluvial store, and streamflow volume within three geomorphological zones defined in Chapter 4. These experiments show how certain values of permeability contrast and flow duration can maximise certain components of the water balance within an idealised Upland, Piedmont, and Lowland zone, and confirms the hypothesis outlined in Chapter 4.

However this analysis assumes that the same streamflow occurs across the same three zones, and this may be unrealistic given the prevalence of transmission losses in dryland catchments that diminish flow volumes downstream (Shanafield and Cook, 2014; Tooth and Nanson, 2011). However, to fully consider the variations in flow downstream one must also consider the spatial heterogeneity in rainfall, which can cover discontinuous parts of the catchment and activate differing tributaries that lead to differences in contributing downstream flow depending on the rainfall coverage.

The heterogeneous models described in this section provide a first step in understanding the relative fluxes and relationships between controls within the specific IRES setting that, while prevalent through out dryland settings (see Chapter 4) is limited in its incorporation of a number of key processes. First, while the results of the base case scenario are consistent with the behavior of models that incorporate variable saturation (e.g. Quichimbo et al., 2020), it is unknown how variable saturation would effect the development of perched groundwater and subsequent interactions seen in this chapter. In addition, my models do not consider or simulate processes such as rainfall and overland flow, which play a key role in the framework in Chapter 4, and instead focuses on IRES systems, using streamflow as a proxy for concentrated rainfall accumulated from upstream. Future work should extend this model by adding it's conceptual set-up to a more distributed model of dryland water balance partitioning, such as DRYP (Quichimbo et al., 2021), including variable saturated flow, and perhaps also by incorporating the simulation of more discrete sources of focused recharge such as faults (as discussed in Chapters 2 and 4).

5.5 Conclusion

In this chapter, I quantified the role of changing geological parameters, such as the alluvial conductivity and the permeability contrast between the alluvium and surrounding geology, with those of changing climatological components in the form of streamflow characteristics, by conducting a series of numerical experiments using MODFLOW and Flopy. Based on these experiments, the following key insights were gained:

1. The conductivity of the streambed is a limiting factor in recharge and ET by controlling the infiltration into the alluvial store.

2. For inflow volumes < volume of alluvial store, the inflow volume is the main control on streamflow infiltration and recharge. At these volumes of flow, recharge decreases with increasing permeability contrast because of riparian ET on water within the alluvial store.

3. At flow volumes > volume of alluvial store, the volume of the alluvial store plays a key role in mediating the amount of recharge to underlying geology at high permeability contrasts, regardless of the volume of flow.

4. Increasing flow duration leads to increasing streamflow infiltration before streamflow infiltration is maximised. Recharge subsequently follows this streamflow infiltration peak, however due to the increasing ET fluxes at longer flow durations, it begins to recede after the streamflow infiltration peak.

5. For a given combination of flow volume and permeability contrast, there is an optimal value or 'goldilocks zone' of streamflow duration that maximises recharge. This value of streamflow duration increases with the volume of flow event, and with the permeability contrast of the model.

6. For a given combination of flow volume and permeability contrast, there is an optimal value or 'goldilocks zone' of streamflow duration that maximises recharge. This value of streamflow duration increases with the volume of flow event, and with the permeability contrast of the model.

7. This concept can be applied to the catchment scale, where for given flow characteristics (volume and duration) there are various combinations of landscape components that can maximise various components of the water balance.

This chapter presents a first step in modelling and understanding surface water – groundwater interactions in dryland catchments with varying alluvial stores, and surrounding geology (in the vicinity of IRES systems). In the next chapter, I discuss the implications of these findings in relation to those of the rest of the thesis, as well as the next steps in future research.

Chapter 6

Conclusions and future outlooks

6.1 Introduction

The aim of this thesis is to address a key knowledge gap on the role of superficial geology in governing the timing, magnitude, and spatial distribution of groundwater recharge in drylands. To this end, a series of objectives were outlined in Chapter 1, and a combination of analysis and interpretation of field data, a synthesis of literature and numerical simulations were performed to address them.

First, the results of a series of geophysical surveys using Electrical Resistivity Tomography (ERT) to delineate shallow subsurface stratigraphy in the Makutapora wellfield, central Tanzania, were presented in Chapter 2. Based on these results, a series of local-scale conceptual hydrogeological models were produced and collated to generate a 3-D conceptual model of groundwater recharge to the wellfield.

Second, a new and unusually rich set of streamflow and groundwater observations from the Maules Creek Catchment, semi-arid Australia, were presented in Chapter 3, alongside targeted geophysical characterisation of the subsurface. Based on these data, a conceptual model of water balance partitioning within this catchment was developed, and then broadened to be applicable to a wide range of dryland settings and IRES systems.

The findings of Chapters 2 and 3 were then combined in Chapter 4, with a synthesis of current literature to propose a new framework that groups recharge controls into a hierarchy of processes that encapsulate their role in converting rainfall to recharge. This framework is then explored at the catchment scale, using geomorphological model to examine the spatial variability of recharge within a given catchment.

Finally, a series of 3-D numerical simulations using a physically based distributed model were presented in Chapter 5, to better quantify the sensitivity of IRES water balance partitioning to changes in geological controls and climate forcing. Based on the main

objectives presented in Chapter 1, a summary of the novel and significant contributions of this thesis to the existing body of literature are presented in this chapter.

6.2 Conclusions

Objective 1: To make quantitative detailed observations of superficial geological structure in drylands to better understand the likely flowpaths and processes controlling groundwater recharge.

Few studies have made detailed observations of superficial geological structure in dryland regions. The series of geophysical investigations presented in Chapter 2 reveal the role of superficial deposits in providing multiple potential pathways for focused groundwater recharge in the catchments surrounding the Makutapora wellfield in Tanzania. These can be summarized as follows:

1. Superficial sand deposits act as collectors and stores that slowly feed recharge into zones of active faulting.
2. These fault zones provide permeable pathways enabling greater recharge to occur and rapid redistribution of recharge
3. Windows within layers of smectitic clay underlying ephemeral streams may provide pathways for focused recharge via transmission losses.
4. Overbank flooding during high intensity precipitation events that inundate a greater area of the catchment, increases the probability of activating such permeable pathways.

These pathways are consistent with previous studies where residence time indicators have suggested local recharge at Makutapora has a strong component of preferential flow during high intensity rainfall events, and that recharge at Makutapora occurs episodically following intensive precipitation.

Objective 2: To elucidate how configurations of superficial geology control the variability of water balance partitioning in dryland IRES.

A rich hydro(geo)logical dataset was collated for Middle Creek (NSW, Australia) and presented in Chapter 3. This indicates several novel characteristics which have enabled this objective to be met by developing new conceptual understandings of recharge controls in an ephemeral stream system as follows:

- Spatially resolved responses to a single runoff event reveal that periods of highly stable stream-stage (following streamflow peaks) increase downstream to a maximum, before reducing abruptly further downstream. Long term hydrometric monitoring indicates that streamflow lasts 44±3 days after each streamflow peak and is independent of the size of the preceding streamflow peak. Geophysical investigations at different sites along Middle Creek reveal regional sediments surrounding the streambed alluvium transition from low permeability clay dominated sediments to higher permeability sands and gravels downstream.

- Based on this evidence, I hypothesised that two dominant controls on water balance partitioning exist in such systems, which are likely present in, and widely transferable to, other dryland catchments:

    1. The permeability contrast between recent streambed alluvium and surrounding geology
    2. The volume of recent alluvium at and upstream at a given location within the catchment

Groundwater recharge is limited by streamflow duration which, in turn, is independent of the size of rainfall and subsequent runoff event. Since streamflow length is mediated by geological controls to an almost constant value, the largest recharge events in the catchment occur when multiple streamflow events are compounded, generating flow in the stream for much longer than 47-days. Although general climate projections for the region show that the mean annual rainfall will remain the same even though it is likely to arrive in more intense events (Taylor et al., 2013a). In Middle Creek, it may be the frequency of events that lead to more recharge and not the intensity of rainfall.

Objective 3: To produce a conceptual model, applicable to a wide range of dryland settings, that illustrates how superficial geology controls groundwater recharge between and within dryland catchments.

In Chapter 4 I propose a new framework for understanding recharge in drylands, based on a combination of existing literature and the insights gained from my two field studies presented in Chapters 2 and 3. The key elements are as follows:

Climate: Rainfall is a first order control on available water for recharge and generating runoff. Aridity greatly impacts the partitioning of available water for recharge & dominant processes.

Concentration: Land surface characteristics interact with rainfall characteristics to enable the potential for diffuse recharge by focussing infiltration in time, or produce and concentrate runoff into topographical depressions, increasing the potential for focused recharge by concentrating water in space.

Delivery: Permeable pathways deliver this concentrated infiltration to perched or regional water tables. Vegetation controls partitioning of this infiltration into evapotranspiration or potential recharge. Potential recharge can be delivered via:

1. Direct delivery to perched or deeper water tables via permeable pathways.
2. Indirect delivery via lateral re-distribution of perched water within certain configurations of superficial geology or permeable pathways in the subsurface.

Contextualizing dryland recharge processes within this process hierarchy allows for a physically meaningful framework from which to explain and compare the predominance of diffuse or focused recharge between dryland catchments across a spectrum of aridity and a range of tectonic, lithological, and physiographic settings.

I propose that the controls outlined in this framework can exhibit differing characteristics and exist in specific ranges depending on their longitudinal (i.e., upstream, or downstream) landscape position. Hence, I grouped these controls based on their likelihood of occurrence with respect to their position within a catchment-scale geomorphic model. This allows for hypothetically generalised predictions of variations of dominant recharge processes within, and between, dryland catchment settings to be proposed as follows:

Uplands often receive higher rainfall amounts and can concentrate runoff more efficiently due to steep slopes. Recharge is then dependent on the existence of high permeability pathways underlying topographic depressions such as upland IRES to route infiltration to the water table. Typically low volumes of stored superficial alluvium underlying IRES in uplands is likely to limit storage and water concentrated within depressions is likely partitioned as runoff given high permeability contrasts.

Piedmonts typically exhibit the coalescence of runoff within IRES which leads to a high concentration of infiltrating water from uplands that maximises focused recharge within IRES in such settings. Increased stream width (or the development of alluvial fans) provides greater volumes of alluvial storage and potentially high permeability pathways for surface water to infiltrate. Water stored within these stores is greater in space and time than the upland zone, allowing for the development of extensive riparian zones.

Lowlands contain large alluvial stores that serve as primary aquifers in these zones, and lead to high transmission losses seen in drylands worldwide.

Objective 4: To quantify the sensitivity of focused recharge in dryland IRES to variations in superficial geology and to changes in environmental conditions.

In Chapter 5, a series of 3-D numerical simulations using a physically based distributed model of an idealised IRES system were presented, to better understand the sensitivity of IRES water balance partitioning to changes in geological controls and climate forcing. The key conclusions from the modelling are as follows:

- Within IRES systems, streambed hydraulic conductivity limits the rate of infiltrating streamflow.
- Once infiltrated:
  - At inflow volumes < volume of alluvial store, the inflow volume is the main control on streamflow infiltration and recharge. Recharge decreases with increasing permeability contrast due riparian ET on water within the alluvial store.
  - At flow volumes > volume of alluvial store, the volume of the alluvial store plays a key role in mediating the amount of recharge to underlying geology at high permeability contrasts, regardless of the volume of flow.
- Increasing flow duration leads to increasing streamflow infiltration before streamflow infiltration is maximised. Recharge subsequently follows this trend, however, due to the increasing ET fluxes at longer flow durations, it recedes after the streamflow infiltration peak.
- For a given combination of flow volume and permeability contrast, there is an optimal 'goldilocks' value of streamflow duration that maximises recharge.

My research thus opens a series of possible future research directions which I outline below.

6.3 Directions for future research

6.3.1 Groundwater recharge under changing climate

Highly uncertain projections of dryland climate have indicated that precipitation changes in drylands may manifest in drier conditions seasonally or annually, but storm events will

manifest themselves with greater intensity (Caretta et al., 2022). The findings of the thesis show, in the context of IRES systems, that superficial geological structures can act in two key ways, and help reduce uncertainty in the likely recharge response to high intensity precipitation events. 1) The results of Chapter 2 highlight the importance of large rainfall events in generating overbank flows that activate permeable pathways in adjacent areas and 2) observed stream stage and groundwater dynamics in Chapter 3 and modelled water balance partitioning in Chapter 5 serve to highlight the importance of the volume of superficial store, the permeability contrast, or some combination of these controls acting as limiting factors on groundwater recharge.

These superficial geological controls highlight the importance of permeable pathways in delivering surface water to groundwater systems during large, overbank flow generating rainfall events. Where these pathways are not present, such as in Fowlers Gap, Australia, overbank flows are mostly lost to ET (Acworth et al., 2020). Under these conditions, it may then be the more frequent, smaller events that keep superficial stores filled for longer durations, that lead to more focused recharge in IRES systems. This hypothesis should be tested in detail in further studies as it has implications for groundwater recharge and ecosystem functioning under changing climate and hydrological conditions in the future.

6.3.2 Managed Aquifer Recharge

Recent studies on Managed Aquifer Recharge (MAR) have noted the importance of geological structures in determining their (Peipeng et al., 2021; Perzan et al., 2023). My conceptual framework in Chapter 4 provides a useful tool for contextualising and comparing findings from MAR studies, and furthermore can be used as a basis for the further implementation of MAR in future studies by allowing for generalised predictions about MAR best practises. For example, interconnected permeable sands have been shown to improve efficiency of MAR in a highly heterogeneous, semi-confined aquifer system (Maples et al., 2019), showing the importance of permeable pathways in delivery of surface waters as recharge. Permeability contrasts between the top two geological layers has been shown to control the performance of MAR systems in laboratory (Peipeng et al., 2021) and observed settings (Nicolas et al., 2019).

In the context of my framework, the efficacy of MAR systems depends on configurations of superficial geological structure that allow of the direct or indirect delivery of potential recharge to actual recharge. Therefore, MAR practises that bypass the permeability contrast by allowing for the direct delivery of surface waters to regional groundwater should be considered. Furthermore, the results of numerical experiments from Chapter 5 highlight that water stored within superficial stores can be susceptible to ET if vegetation rooting

depth is deep enough to access this water. To mitigate these losses, MAR systems that utilise the subsurface redistribution and indirect delivery pathways should seek large volumes of superficial stores that enable the indirect delivery of subsurface water to deep perched water tables, as in the case of sand dams (Love et al., 2011).

Future work needs to focus on the transferability of my framework (Chapter 4) to other dryland catchments which have sufficient groundwater level data available, to further test and refine the general nature of my conclusions in other settings. In addition, focused recharge processes and superficial geological structure are not limited to drylands, but instead exist on spectrum of aridity, and there are numerous examples of key focused recharge playing a key role in humid catchments (Hartmann et al., 2021, 2017). Therefore, future work could also include the transferability of my framework to humid catchments to create a holistic, generalised framework for groundwater recharge that can be applied and modified to inform conceptual models for catchments worldwide.

6.3.3 Upscaling of framework

Eventually my key aspiration for research in this area is to develop a rigorous and general enough process understanding of water balance partitioning applicable to a spectrum of climates that can be upscaled over broad areas and ungauged catchments through, for example, a novel mapping or screening tool. Indeed, there are many studies that attempt to map recharge potential at a catchment scale in drylands, using remote sensing derived landscape attributes (Shaban et al., 2006; Souissi et al., 2018; Yeh et al., 2009). These studies have generally followed similar methodologies as each other, with the establishment of several factors thought to influence groundwater recharge in these regions, and weighting these based on the characteristics of the study area. These methodologies, however, lack the incorporation of key hydrological processes, such as focused recharge, that have been highlighted in this chapter.

The controls in my framework can potentially be mapped by integrating remote sensing and climate data. By highlighting dryland specific hydrological controls, such an approach could provide an improved basis for adequately mapping potential recharge in drylands. For example, precipitation and aridity controls can be mapped based on widely available and spatially resolved hourly rainfall (Sun et al., 2018) and PET data (Singer et al., 2021). There is also a plethora of DEM datasets by which to derive landscape attributes such as slope (Deilami and Hashim, 2011). However, other necessary characteristics in the framework may prove more challenging to map. For example, while publicly available maps of regional geology can be useful for identifying heterogeneity in surface lithologies, these generally provide little information on subsurface structures. For instance, the

hydrogeological structures and processes identified in Chapters 2 and 3 were not evident from regional scale geological maps and were only able to be elucidated by combining geophysical surveys with ground-truthing data on lithologies (in the case of this thesis, from borehole logs). Currently, to model the complexity in sub-surface flow processes outlined at the scale of my conceptual model, geophysical surveys must be combined with regional scale geological maps to accurately delineate structures around IRES systems. This problem therefore becomes a problem of scale, and the degree to which mappable superficial geological structures become important. This is an important research gap to be met in future research, as incorporating insights on superficial geology may allow for the extrapolation of potential recharge to actual recharge.

In addition, the importance of superficial alluvial stores has been highlighted throughout the thesis. The connectivity and widths of alluvial stores in drylands have already been mapped from remote sensing imagery in the context of recharge estimation (Coelho et al., 2017), and great strides have been made in mapping soil thicknesses on hillslopes by determining curvature (Patton et al., 2018). I hypothesise that there is a link between width, catchment position, slope and climate variables that can be utilised to determine depth of alluvial stores based on remote sensing outputs and identify the determination of this depth to be a key research gap to be met for the upscaling and transferability of my framework.

Globally, water scarcity already affects between 1 and 2 billion people, the vast majority of whom live in drylands, where the gap between the demand for and supply of water is the highest in the world (Stringer et al., 2021). This challenge means that the impacts of climate change, combined with water management decisions, will have profound impacts on drylands and their inhabitants into the future. Projected climate changes indicate that, in a matter of just a few decades, millions more people (approximately half the world's population in total) will be living under conditions of high water stress (Byers et al., 2018).

Proactive strategies are needed to plan for a water-secure future in drylands. Improved understanding and quantification of groundwater recharge in dryland areas is a growing research and management priority (Gleeson et al., 2020; Keshavarzi et al., 2017; Meixner et al., 2016). Accurate quantification of recharge in dryland settings remains elusive, with no widely applicable method currently available that can directly and accurately quantify the volume of rainwater that reaches the water table (Healy and Scanlon, 2010; Scanlon et al., 2002; Shanafield and Cook, 2014).

This thesis helps address one uncertainty: the role of superficial geology in controlling the spatiotemporal complexity in groundwater recharge processes, and the sensitivity of these processes to environmental and anthropogenic change in drylands with varying geology.

With further sustained work in this area it may be possible to one day accurately map, quantify, and forecast groundwater recharge in drylands.

References

Abdulrazzak, M.J., Sorman, A.U., Alhames, A.S., 1989. Water balance approach under extreme arid conditions — A case study of Tabalah Basin, Saudi Arabia. Hydrol. Process. 3, 107–122. https://doi.org/10.1002/hyp.3360030202

Abel, C., Horion, S., Tagesson, T., De Keersmaecker, W., Seddon, A.W.R., Abdi, A.M., Fensholt, R., 2020. The human–environment nexus and vegetation–rainfall sensitivity in tropical drylands. Nat. Sustain. https://doi.org/10.1038/s41893-020-00597-z

Abotalib, A.Z., Heggy, E., El Bastawesy, M., Ismail, E., Gad, A., Attwa, M., 2021. Groundwater mounding: A diagnostic feature for mapping aquifer connectivity in hyper-arid deserts. Sci. Total Environ. 801, 149760.

Acuña, V., Hunter, M., Ruhí, A., 2017. Managing temporary streams and rivers as unique rather than second-class ecosystems. Biol. Conserv. 211, 12–19.

Acworth, R.I., Rau, G.C., Cuthbert, M.O., Jensen, E., Leggett, K., 2016a. Long-term spatio-temporal precipitation variability in arid-zone Australia and implications for groundwater recharge. Hydrogeol. J. 24, 905–921. https://doi.org/10.1007/s10040-015-1358-7

Acworth, R.I., Rau, G.C., Cuthbert, M.O., Jensen, E., Leggett, K., 2016b. Long-term spatio-temporal precipitation variability in arid-zone Australia and implications for groundwater recharge. Hydrogeol. J. https://doi.org/10.1007/s10040-015-1358-7

Acworth, R.I., Rau, G.C., Cuthbert, M.O., Leggett, K., Andersen, M.S., 2021. Runoff and focused groundwater-recharge response to flooding rains in the arid zone of Australia. Hydrogeol. J. 29, 737–764.

Acworth, R.I., Rau, G.C., Cuthbert, M.O., Leggett, K., Andersen, M.S., 2020. Runoff and focused groundwater-recharge response to flooding rains in the arid zone of Australia. Hydrogeol. J. 1–28.

Acworth, R.I., Timms, W.A., 2003. Hydrogeological investigation of mud-mound springs developed over a weathered basalt aquifer on the Liverpool Plains, New South Wales, Australia. Hydrogeol. J. 11, 659–672.

Aizebeokhai, A.P., Singh, V.S., 2013. Field evaluation of 3D geo-electrical resistivity imaging for environmental and engineering studies using parallel 2D profiles. Curr. Sci.

504–512.

Ajami, H., Troch, P.A., Maddock III, T., Meixner, T., Eastoe, C., 2011. Quantifying mountain block recharge by means of catchment-scale storage-discharge relationships. Water Resour. Res. 47.

Alan Yeakley, J., Ervin, D., Chang, H., Granek, E.F., Dujon, V., Shandas, V., Brown, D., 2016. Ecosystem services of streams and rivers. River Sci. Res. Manag. 21st century 335–352.

Alazard, M., Boisson, A., Maréchal, J.-C., Perrin, J., Dewandel, B., Schwarz, T., Pettenati, M., Picot-Colbeaux, G., Kloppman, W., Ahmed, S., 2016. Investigation of recharge dynamics and flow paths in a fractured crystalline aquifer in semi-arid India using borehole logs: implications for managed aquifer recharge. Hydrogeol. J. 24, 35–57.

Allison, G.B., Gee, G.W., Tyler, S.W., 1994. Vadose-zone techniques for estimating groundwater recharge in arid and semiarid regions. Soil Sci. Soc. Am. J. 58, 6–14.

Andersen, Martin S., Acworth, R.I., 2009a. Stream-aquifer interactions in the Maules Creek catchment, Namoi Valley, New South Wales, Australia. Hydrogeol. J. 17, 2005–2021. https://doi.org/10.1007/s10040-009-0500-9

Andersen, M S, Acworth, R.I., 2009. Stream-aquifer interactions in the Maules Creek catchment, Namoi Valley, New South Wales, Australia. Hydrogeol. J. 17, 2005–2021. https://doi.org/10.1007/s10040-009-0500-9

Andersen, Martin S., Acworth, R.I., 2009b. Stream-aquifer interactions in the Maules Creek catchment, Namoi Valley, New South Wales, Australia. Hydrogeol. J. 17, 2005–2021. https://doi.org/10.1007/s10040-009-0500-9

Anudu, G.K., Essien, B.I., Obrike, S.E., 2014. Hydrogeophysical investigation and estimation of groundwater potentials of the Lower Palaeozoic to Precambrian crystalline basement rocks in Keffi area, north-central Nigeria, using resistivity methods. Arab. J. Geosci. 7, 311–322.

Aryal, S.K., Silberstein, R.P., Fu, G., Hodgson, G., Charles, S.P., McFarlane, D., 2020. Understanding spatio-temporal rainfall-runoff changes in a semi-arid region. Hydrol. Process. 34, 2510–2530.

Attandoh, N., Yidana, S.M., Abdul-Samed, A., Sakyi, P.A., Banoeng-Yakubo, B., Nude, P.M., 2013. Conceptualization of the hydrogeological system of some sedimentary aquifers in Savelugu-Nanton and surrounding areas, Northern Ghana. Hydrol. Process. 27, 1664–1676. https://doi.org/10.1002/hyp.9308

Baguma, A., Bizoza, A., Carter, R., Cavill, S., Foster, S., Foster, T., Jobbins, G., Hope, R., Katuva, J., Koehler, J., 2017. Groundwater and poverty in sub-Saharan Africa. UPGro Work. Pap.

Bakker, M., Post, V., Langevin, C.D., Hughes, J.D., White, J.T., Starn, J.J., Fienen, M.N., 2016. Scripting MODFLOW model development using Python and FloPy. Groundwater 54, 733–739.

Banks, E.W., Cook, P.G., Owor, M., Okullo, J., Kebede, S., Nedaw, D., Mleta, P., Fallas, H., Gooddy, D., MacAllister, D.J., others, 2020. Environmental tracers to evaluate groundwater residence times and water quality risk in shallow unconfined aquifers in sub Saharan Africa. J. Hydrol. 125753.

Bargués-Tobella, A., Hasselquist, N.J., Bazié, H.R., Bayala, J., Laudon, H., Ilstedt, U., 2020. Trees in African drylands can promote deep soil and groundwater recharge in a future climate with more intense rainfall. L. Degrad. Dev. 31, 81–95.

Barongo, J.O., Palacky, G.J., 1991. Investigations of electrical properties of weathered layers in the Yala area, western Kenya, using resistivity soundings. Geophysics 56, 133–138.

Batlle-Aguilar, J., Banks, E.W., Batelaan, O., Kipfer, R., Brennwald, M.S., Cook, P.G., 2017. Groundwater residence time and aquifer recharge in multilayered, semi-confined and faulted aquifer systems using environmental tracers. J. Hydrol. 546, 150–165. https://doi.org/https://doi.org/10.1016/j.jhydrol.2016.12.036

Bauer, P., Held, R.J., Zimmermann, S., Linn, F., Kinzelbach, W., 2006. Coupled flow and salinity transport modelling in semi-arid environments: The Shashe River Valley, Botswana. J. Hydrol. 316, 163–183.

Beauvais, A., Ritz, M., Parisot, J.-C., Dukhan, M., Bantsimba, C., 1999. Analysis of poorly stratified lateritic terrains overlying a granitic bedrock in West Africa, using 2-D electrical resistivity tomography. Earth Planet. Sci. Lett. 173, 413–424.

Beetle-Moorcroft, F., Shanafield, M., Singha, K., 2021. Exploring conceptual models of infiltration and groundwater recharge on an intermittent river: The role of geologic controls. J. Hydrol. Reg. Stud. 35, 100814.

Belle, P., Lachassagne, P., Mathieu, F., Barbet, C., Brisset, N., Gourry, J.-C., 2019. Characterization and location of the laminated layer within hard rock weathering profiles from electrical resistivity tomography: implications for water well siting. Geol. Soc. London, Spec. Publ. 479, 187–205.

Bense, V.F., Gleeson, T., Loveless, S.E., Bour, O., Scibek, J., 2013. Fault zone hydrogeology. Earth-Science Rev. 127, 171–192.

Berdugo, M., Delgado-Baquerizo, M., Soliveres, S., Hernández-Clemente, R., Zhao, Y., Gaitán, J.J., Gross, N., Saiz, H., Maire, V., Lehman, A., Rillig, M.C., Solé, R. V, Maestre, F.T., 2020. Global ecosystem thresholds driven by aridity. Science (80-.). 367, 787–790. https://doi.org/10.1126/science.aay5958

Bergkamp, G., 1998. A hierarchical view of the interactions of runoff and infiltration with vegetation and microtopography in semiarid shrublands. Catena 33, 201–220.

Beven, K., 2012. Rainfall-Runoff Modelling. John Wiley & Sons, Ltd, Chichester, UK. https://doi.org/10.1002/9781119951001

Beven, K., 2002. Runoff generation in semi-arid areas. Dryl. Rivers Hydrol. Geomorphol. Semi-Arid Channels 57–105.

Beven, K., Germann, P., 1982. Macropores and water flow in soils. Water Resour. Res. 18, 1311–1325. https://doi.org/10.1029/WR018i005p01311

Beven, K.J., 2011. Rainfall-runoff modelling: the primer. John Wiley & Sons.

Bianchi, M., MacDonald, A.M., Macdonald, D.M.J., Asare, E.B., 2020. Investigating the productivity and sustainability of weathered basement aquifers in tropical Africa using numerical simulation and global sensitivity analysis. Water Resour. Res. 56, e2020WR027746.

Bianconi, F., Borshoff, J., 1984. Surficial uranium occurrences in the United Republic of Tanzania.

Binley, A., Hubbard, S.S., Huisman, J.A., Revil, A., Robinson, D.A., Singha, K., Slater, L.D., 2015. The emergence of hydrogeophysics for improved understanding of subsurface processes over multiple scales. Water Resour. Res. 51, 3837–3866. https://doi.org/10.1002/2015WR017016

Blasch, K.W., Bryson, J.R., 2007. Distinguishing sources of ground water recharge by delta2H and delta18O. Ground Water 45, 294–308. https://doi.org/10.1111/j.1745-6584.2006.00289.x

Boas, T., Mallants, D., 2022. Episodic extreme rainfall events drive groundwater recharge in arid zone environments of central Australia. J. Hydrol. Reg. Stud. 40, 101005.

Bonsor, H.C., MacDonald, A.M., Ahmed, K.M., Burgess, W.G., Basharat, M., Calow, R.C., Dixit, A., Foster, S.S.D., Gopal, K., Lapworth, D.J., 2017. Hydrogeological typologies of the Indo-Gangetic basin alluvial aquifer, South Asia. Hydrogeol. J. 25, 1377.

Bonsor, H.C., Macdonald, A.M., Davies, J., 2014. Evidence for extreme variations in the permeability of laterite from a detailed analysis of well behaviour in Nigeria. Hydrol. Process. 28, 3563–3573. https://doi.org/10.1002/hyp.9871

Boroto, R.A.J., Gorgens, A.H.M., 2003. Estimating transmission losses along the Limpopo River: an overview of alternative methods. IAHS Publ. 278, 138–143.

Bourke, S.A., Degens, B., Searle, J., de Castro Tayer, T., Rothery, J., 2021. Geological permeability controls streamflow generation in a remote, ungauged, semi-arid drainage system. J. Hydrol. Reg. Stud. 38, 100956.

Bourke, S.A., Shanafield, M., Hedley, P., Dogramaci, S., 2020. A hydrological framework for persistent river pools in semi-arid environments. Hydrol. Earth Syst. Sci. Discuss. 1–18.

Braune, E., Xu, Y., 2010. The role of ground water in sub-Saharan Africa. Ground Water 48, 229–238. https://doi.org/10.1111/j.1745-6584.2009.00557.x

Bredehoeft, J.D., 2002. The water budget myth revisited: Why hydrogeologists model. Ground Water 40, 340–345. https://doi.org/10.1111/j.1745-6584.2002.tb02511.x

Bromley, J., Brouwer, J., Barker, A.P., Gaze, S.R., Valentine, C., 1997a. The role of surface water redistribution in an area of patterned vegetation in a semi-arid environment, south-west Niger. J. Hydrol. 198, 1–29.

Bromley, J., Edmunds, W.M., Fellman, E., Brouwer, J., Gaze, S.R., Sudlow, J., Taupin, J.-D., 1997b. Estimation of rainfall inputs and direct recharge to the deep unsaturated zone of southern Niger using the chloride profile method. J. Hydrol. 188–189, 139–154. https://doi.org/10.1016/S0022-1694(96)03157-5

Brunet, P., Clément, R., Bouvier, C., 2010. Monitoring soil water content and deficit using Electrical Resistivity Tomography (ERT) – A case study in the Cevennes area, France. J. Hydrol. 380, 146–153. https://doi.org/10.1016/J.JHYDROL.2009.10.032

Brunner, P., Cook, P.G., Simmons, C.T., 2011. Disconnected Surface Water and Groundwater: From Theory to Practice. Ground Water 49, 460–467. https://doi.org/10.1111/j.1745-6584.2010.00752.x

Brunner, P., Cook, P.G., Simmons, C.T., 2009. Hydrogeologic controls on disconnection between surface water and groundwater. Water Resour. Res. 45.
https://doi.org/10.1029/2008WR006953

Brutsaert, W., Stricker, H., 1979. An advection-aridity approach to estimate actual regional evapotranspiration. Water Resour. Res. 15, 443–450.

Bull, L.J., Kirkby, M.J., 2002. Dryland river characteristics and concepts. Dryl. Rivers Hydrol. Geomorphol. Semi-Arid Channels 3–15.

Burch, G.J., Bath, R.K., Moore, I.D., O'loughlin, E.M., 1987. Comparative hydrological behaviour of forested and cleared catchments in southeastern Australia. J. Hydrol. 90, 19–42.

Byers, E., Gidden, M., Leclère, D., Balkovic, J., Burek, P., Ebi, K., Greve, P., Grey, D., Havlik, P., Hillers, A., 2018. Global exposure and vulnerability to multi-sector development and climate change hotspots. Environ. Res. Lett. 13, 55012.

Callegary, J.B., Leenhouts, J.M., Paretti, N. V, Jones, C.A., 2007. Rapid estimation of recharge potential in ephemeral-stream channels using electromagnetic methods, and measurements of channel and vegetation characteristics. J. Hydrol. 344, 17–31.

https://doi.org/10.1016/j.jhydrol.2007.06.028

Camarasa Belmonte, A.M., Segura Beltrán, F., 2001. Flood events in Mediterranean ephemeral streams (ramblas) in Valencia region, Spain. Catena 45, 229–249. https://doi.org/10.1016/S0341-8162(01)00146-1

Canadell, J., Jackson, R.B., Ehleringer, J.B., Mooney, H.A., Sala, O.E., Schulze, E.-D., 1996. Maximum rooting depth of vegetation types at the global scale. Oecologia 108, 583–595.

Cao, G., Scanlon, B.R., Han, D., Zheng, C., 2016. Impacts of thickening unsaturated zone on groundwater recharge in the North China Plain. J. Hydrol. https://doi.org/10.1016/j.jhydrol.2016.0

Caretta, A.M.M.A., Arfanuzzaman, R.A.B.M., Morgan, S.M.R., Kumar, M., 2022. Water. In: Climate Change 2022: Impacts, Adaptation, and Vulnerability. Contribution of Working Group II to the Sixth Assessment Report of the Intergovernmental Panel on Climate Change.

Carling, G.T., Mayo, A.L., Tingey, D., Bruthans, J., 2012. Mechanisms, timing, and rates of arid region mountain front recharge. J. Hydrol. 428–429, 15–31.
https://doi.org/10.1016/j.jhydrol.2011.12.043

Carsel, R.F., Parrish, R.S., 1988. Developing joint probability distributions of soil water retention characteristics. Water Resour. Res. 24, 755–769.
https://doi.org/10.1029/WR024i005p00755

Cataldo, J., Behr, C., Montalto, F., Pierce, R., 2004. A summary of published reports of transmission losses in ephemeral streams in the U.S. Natl. Cent. Hous. Environ. 28–29.

Chen, C., Park, T., Wang, X., Piao, S., Xu, B., Chaturvedi, R.K., Fuchs, R., Brovkin, V., Ciais, P., Fensholt, R., Tømmervik, H., Bala, G., Zhu, Z., Nemani, R.R., Myneni, R.B., 2019. China and India lead in greening of the world through land-use management. Nat. Sustain. 2, 122–129. https://doi.org/10.1038/s41893-019-0220-7

Chen, S.-A., Michaelides, K., Grieve, S.W.D., Singer, M.B., 2019. Aridity is expressed in river topography globally. Nature 573, 573–577. https://doi.org/10.1038/s41586-019-1558-8

Cheng, L., Si, B., Wang, Y., Liu, W., 2021. Groundwater recharge mechanisms on the Loess Plateau of China: New evidence for the significance of village ponds. Agric. Water Manag. 257, 107148.

Cherlet, M., Hutchinson, C., Reynolds, J., Hill, J., Sommer, S., von Maltitz, G., 2018. World Atlas of Desertification. World Atlas Desertif.

Clifford, J., Binley, A., 2010. Geophysical characterization of riverbed hydrostratigraphy using electrical resistance tomography. Near Surf. Geophys. 8, 493–501.

Cobbing, J., Hiller, B., 2019. Waking a sleeping giant: Realizing the potential of groundwater in Sub-Saharan Africa. World Dev. 122, 597–613.

Coelho, V.H.R., Montenegro, S., Almeida, C.N., Silva, B.B., Oliveira, L.M., Gusmao, A.C. V, Freitas, E.S., Montenegro, A.A.A., 2017. Alluvial groundwater recharge estimation in semi-arid environment using remotely sensed data. J. Hydrol. 548, 1–15.

Coes, A., Pool, D., 2005. Ephemeral-stream channel and basin-floor infiltration and recharge in the Sierra Vista subwatershed of the Upper San Pedro Basin, southeastern Arizona. USGS Prof. Pap. 1703.

Constantz, J., Thomas, C.L., 1997. Stream bed temperature profiles as indicators of percolation characteristics beneath arroyos in the Middle Rio Grande Basin, USA. Hydrol. Process. 11, 1621–1634. https://doi.org/10.1002/(SICI)1099-1085(19971015)11:12<1621::AID-HYP493>3.0.CO;2-X

Cook, P.G., Kilty, S., 1992. A helicopter-borne electromagnetic survey to delineate groundwater recharge rates. Water Resour. Res. 28, 2953–2961.

Cook, P.G., O'Grady, A.P., Wischusen, J.D.H., Duguid, A., Fass, T., Eamus, D., 2008. Ecohydrology of sand plain woodlands in central Australia.

Cook, P.G., Walker, G.R., Jolly, I.D., 1989. Spatial variability of groundwater recharge in a semiarid region. J. Hydrol. 111, 195–212. https://doi.org/10.1016/0022-1694(89)90260-6

Cordery, I., 2004. Arid zone surface runoff - A significant resource in australia. Aust. J. Water Resour. 8, 37–43.

Costa, A.C., Foerster, S., de Araújo, J.C., Bronstert, A., 2013. Analysis of channel transmission losses in a dryland river reach in north-eastern Brazil using streamflow series, groundwater level series and multi-temporal satellite data. Hydrol. Process. 27, 1046–1060. https://doi.org/10.1002/hyp.9243

Costigan, K.H., Jaeger, K.L., Goss, C.W., Fritz, K.M., Goebel, P.C., 2016. Understanding controls on flow permanence in intermittent rivers to aid ecological research: integrating meteorology, geology and land cover. Ecohydrology 9, 1141–1153. https://doi.org/10.1002/eco.1712

Costigan, K.H., Kennard, M.J., Leigh, C., Sauquet, E., Datry, T., Boulton, A.J., 2017. Flow Regimes in Intermittent Rivers and Ephemeral Streams. U.S. Geological Survey Scientific Investigations Report 2005-519., Intermittent Rivers and Ephemeral Streams: Ecology and Management. https://doi.org/10.1016/B978-0-12-803835-2.00003-6

Crane, R.A., Cuthbert, M.O., Timms, W., 2015. The use of an interrupted-flow centrifugation method to characterise preferential flow in low permeability media. Hydrol. earth Syst. Sci. 19, 3991–4000.

Crosbie, R.S., McCallum, J.L., Walker, G.R., Chiew, F.H.S., 2012. Episodic recharge and climate change in the Murray-Darling Basin, Australia. Hydrogeol. J. 20, 245–261. https://doi.org/10.1007/s10040-011-0804-4

Cuthbert, M. O., Acworth, R.I., Andersen, M.S., Larsen, J.R., McCallum, A.M., Rau, G.C., Tellam, J.H., 2016. Understanding and quantifying focused, indirect groundwater recharge from ephemeral streams using water table fluctuations. Water Resour. Res. 52, 827–840. https://doi.org/10.1002/2015WR017503

Cuthbert, M O, Acworth, R.I., Andersen, M.S., Larsen, J.R., McCallum, A.M., Rau, G.C., Tellam, J.H., 2016. Understanding and quantifying focused, indirect groundwater recharge from ephemeral streams using water table fluctuations. Water Resour. Res. 52, 827–840. https://doi.org/10.1002/2015WR017503

Cuthbert, M.O., Gleeson, T., Moosdorf, N., Befus, K.M., Schneider, A., Hartmann, J., Lehner, B., 2019a. Global patterns and dynamics of climate–groundwater interactions. Nat. Clim. Chang. 9, 137–141. https://doi.org/10.1038/s41558-018-0386-4

Cuthbert, M.O., Gleeson, T., Reynolds, S.C., Bennett, M.R., Newton, A.C., McCormack, C.J., Ashley, G.M., 2017. Modelling the role of groundwater hydro-refugia in East African hominin evolution and dispersal. Nat. Commun. 8, 1–11.

Cuthbert, M.O., Mackay, R., Tellam, J.H., Barker, R.D., 2009. The use of electrical resistivity tomography in deriving local-scale models of recharge through superficial deposits. Q. J. Eng. Geol. Hydrogeol. 42, 199–209. https://doi.org/10.1144/1470-9236/08-023

Cuthbert, M.O., Taylor, R.G., Favreau, G., Todd, M.C., Shamsudduha, M., Villholth, K.G., MacDonald, A.M., Scanlon, B.R., Kotchoni, D.O. V, Vouillamoz, J.-M., Lawson, F.M.A., Adjomayi, P.A., Kashaigili, J., Seddon, D., Sorensen, J.P.R., Ebrahim, G.Y., Owor, M., Nyenje, P.M., Nazoumou, Y., Goni, I., Ousmane, B.I., Sibanda, T., Ascott, M.J., Macdonald, D.M.J., Agyekum, W., Koussoubé, Y., Wanke, H., Kim, H., Wada, Y., Lo, M.-H., Oki, T., Kukuric, N., 2019b. Observed controls on resilience of groundwater to climate variability in sub-Saharan Africa. Nature 572, 230–234. https://doi.org/10.1038/s41586-019-1441-7

Cuthbert, M.O., Tindimugaya, C., 2010. The importance of preferential flow in controlling groundwater recharge in tropical Africa and implications for modelling the impact of climate change on groundwater resources. J. Water Clim. Chang. 1, 234–245. https://doi.org/10.2166/wcc.2010.040

Dahan, O., Shani, Y., Enzel, Y., Yechieli, Y., Yakirevich, A., 2007. Direct measurements of floodwater infiltration into shallow alluvial aquifers. J. Hydrol. 344, 157–170. https://doi.org/10.1016/j.jhydrol.2007.06.033

Dahan, O., Tatarsky, B., Enzel, Y., Kulls, C., Seely, M., Benito, G., 2008a. Dynamics of Flood Water Infiltration and Ground Water Recharge in Hyperarid Desert. Ground Water 46, 450–461. https://doi.org/10.1111/j.1745-6584.2007.00414.x

Dahan, O., Tatarsky, B., Enzel, Y., Kulls, C., Seely, M., Benito, G., 2008b. Dynamics of Flood Water Infiltration and Ground Water Recharge in Hyperarid Desert. Ground Water 46, 450–461. https://doi.org/10.1111/j.1745-6584.2007.00414.x

Dahlin, T., Owen, R., 1998. Geophysical investigations of alluvial aquifers in Zimbabwe. Proc. IV Meet. Environ. Eng. Geophys. Soc. (European Sect. 151–154.

Dahlin, T., Wisén, R., Zhang, D., 2007. 3D effects on 2D resistivity imaging--modelling and field surveying results, in: Near Surface 2007-13th EAGE European Meeting of Environmental and Engineering Geophysics. p. cp--30.

Dai, A., 2013. Increasing drought under global warming in observations and models. Nat. Clim. Chang. 3, 52–58. https://doi.org/10.1038/nclimate1633

Datry, T., Arscott, D.B., Sabater, S., 2011. Recent perspectives on temporary river ecology. Aquat. Sci. 73, 453–457. https://doi.org/10.1007/s00027-011-0236-1

Datry, T., Bonada, N., Boulton, A., 2017. Intermittent rivers and ephemeral streams: Ecology and management. Hrvat. vode 25, 102.

Datry, Thibault, Fritz, K., Leigh, C., 2016. Challenges, developments and perspectives in intermittent river ecology. Freshw. Biol. 61, 1171–1180. https://doi.org/10.1111/fwb.12789

Datry, T., Larned, S.T., Tockner, K., 2014. Intermittent rivers: A challenge for freshwater ecology. Bioscience 64, 229–235. https://doi.org/10.1093/biosci/bit027

Datry, T, Pella, H., Leigh, C., Bonada, N., Hugueny, B., 2016. A landscape approach to advance intermittent river ecology. Freshw. Biol. 61, 1200–1213.
https://doi.org/10.1111/fwb.12645

Dawes, W., Ali, R., Varma, S., Emelyanova, I., Hodgson, G., McFarlane, D., 2012. Modelling the effects of climate and land cover change on groundwater recharge in southwest Western Australia. Hydrol. Earth Syst. Sci. 16, 2709–2722.

Dawson, J.B., 2008. The Gregory rift valley and Neogene-recent volcanoes of northern Tanzania.

De Pauw, E.F., Magoggo, J.P., Niemeyer, W., 1983. Soil survey report of Dodoma Capital City district.

De Vries, J.J., Selaolo, E.T., Beekman, H.E., 2000. Groundwater recharge in the Kalahari, with reference to paleo-hydrologic conditions. J. Hydrol. 238, 110–123.
https://doi.org/10.1016/S0022-1694(00)00325-5

de Vries, J J, Simmers, I., 2002. Groundwater recharge: An overview of process and challenges. Hydrogeol. J. 10, 5–17. https://doi.org/10.1007/s10040-001-0171-7

de Vries, Jacobus J., Simmers, I., 2002. Groundwater recharge: an overview of processes and challenges. Hydrogeol. J. 10, 5–17. https://doi.org/10.1007/s10040-001-0171-7

Deilami, K., Hashim, M., 2011. Very high resolution optical satellites for DEM generation: a review. Eur. J. Sci. Res. 49, 542–554.

Dennis, P.G., Hirsch, P.R., Smith, S.J., Taylor, R.G., Valsami-Jones, E., Miller, A.J., 2009. Linking rhizoplane pH and bacterial density at the microhabitat scale. J. Microbiol. Methods 76, 101–104.

DESA, U.N., 2017. World population prospects, the 2017 Revision, Volume I: comprehensive tables. New York United Nations Dep. Econ. Soc. Aff.

Dewandel, B., Lachassagne, P., Wyns, R., Maréchal, J.C., Krishnamurthy, N.S., 2006. A generalized 3-D geological and hydrogeological conceptual model of granite aquifers controlled by single or multiphase weathering. J. Hydrol. https://doi.org/10.1016/j.jhydrol.2006.03.026

Díaz-Alcaide, S., Martínez-Santos, P., 2019. Advances in groundwater potential mapping. Hydrogeol. J. 27, 2307–2324.

Dillon, P., Stuyfzand, P., Grischek, T., Lluria, M., Pyne, R.D.G., Jain, R.C., Bear, J., Schwarz, J., Wang, W., Fernandez, E., others, 2019. Sixty years of global progress in managed aquifer recharge. Hydrogeol. J. 27, 1–30.

Döll, P., Fiedler, K., 2008. Global-scale modeling of groundwater recharge. Hydrol. Earth Syst. Sci. 12, 863–885. https://doi.org/10.5194/hess-12-863-2008

Döll, P, Fiedler, K., 2008. Global-scale modeling of groundwater recharge. Hydrol. Earth Syst. Sci. 12, 863–885. https://doi.org/10.5194/hess-12-863-2008

Dunkerley, D., 2012. Effects of rainfall intensity fluctuations on infiltration and runoff: rainfall simulation on dryland soils, Fowlers Gap, Australia. Hydrol. Process. 26, 2211–2224. https://doi.org/10.1002/hyp.8317

DUWASA, 2017. Needs, Production and Water Supply.

Dvory, N.Z., Livshitz, Y., Kuznetsov, M., Adar, E., Yakirevich, A., 2016. The effect of hydrogeological conditions on variability and dynamic of groundwater recharge in a carbonate aquifer at local scale. J. Hydrol. https://doi.org/10.1016/j.jhydrol.2016.02.011

Earman, S., Campbell, A.R., Phillips, F.M., Newman, B.D., 2006. Isotopic exchange between snow and atmospheric water vapor: Estimation of the snowmelt component of groundwater recharge in the southwestern United States. J. Geophys. Res. Atmos. 111.

Edmunds, W.M., Darling, W.G., Kinniburgh, D.G., Kotoub, S., Mahgoub, S., 1992. Sources of recharge at Abu Delaig, Sudan. J. Hydrol. 131, 1–24. https://doi.org/10.1016/0022-1694(92)90211-D

Edmunds, W.M., Gaye, C.B., 1994. Estimating the spatial variability of groundwater recharge in the Sahel using chloride. J. Hydrol. 156, 47–59. https://doi.org/10.1016/0022-1694(94)90070-1

Edwards, L.S., 1977. A modified pseudosection for resistivity and IP. Geophysics 42, 1020–1036.

Eilers, V.H.M., Carter, R.C., Rushton, K.R., 2007. A single layer soil water balance model for estimating deep drainage (potential recharge): An application to cropped land in semi-arid North-east Nigeria. Geoderma 140, 119–131. https://doi.org/10.1016/j.geoderma.2007.03.011

Eisma, J.A., Merwade, V.M., 2020. Investigating the environmental response to water harvesting structures: a field study in Tanzania. Hydrol. Earth Syst. Sci. 24, 1891–1906.

El Khalki, E.M., Tramblay, Y., Massari, C., Brocca, L., Simonneaux, V., Gascoin, S., Saidi, M.E.M., 2020. Challenges in flood modeling over data-scarce regions: how to exploit globally available soil moisture products to estimate antecedent soil wetness conditions in Morocco. Nat. Hazards Earth Syst. Sci. 20, 2591–2607.

Ewen, J., Parkin, G., O'Connell, P.E., 2000. SHETRAN: distributed river basin flow and transport modeling system. J. Hydrol. Eng. 5, 250–258.

Fan, Y., Li, H., Miguez-Macho, G., 2013. Global patterns of groundwater table depth. Science (80-.). 339, 940–943. https://doi.org/10.1126/science.1229881

Farid, I., Zouari, K., Trabelsi, R., Kallali, A.R., 2014. Application of environmental tracers to study groundwater recharge in a semi-arid area of Central Tunisia [Application des traceurs environnementaux à l'étude de la recharge des eaux souterraines dans une région semi-aride en Tunisie centrale]. Hydrol. Sci. J. 59, 2072–2085.
https://doi.org/10.1080/02626667.2013.863424

Favreau, G., Cappelaere, B., Massuel, S., Leblanc, M., Boucher, M., Boulain, N., Leduc, C., 2009. Land clearing, climate variability, and water resources increase in semiarid southwest Niger: A review. Water Resour. Res. 45. https://doi.org/10.1029/2007WR006785

Fawley, A.P., 1958. Evaporation rate at Dodoma, Tanganyika.

Feng, S., Fu, Q., 2013. Expansion of global drylands under a warming climate. Atmos. Chem. Phys. 13, 10081–10094. https://doi.org/10.5194/acp-13-10081-2013

Flinchum, B.A., Banks, E., Hatch, M., Batelaan, O., Peeters, L.J.M., Pasquet, S., 2020. Identifying recharge under subtle ephemeral features in a flat-lying semi-arid region using a combined geophysical approach. Hydrol. Earth Syst. Sci. 24, 4353–4368.

Flint, A.L., Flint, L.E., Kwicklis, E.M., Fabryka-Martin, J.T., Bodvarsson, G.S., 2002. Estimating recharge at Yucca Mountain, Nevada, USA: Comparison of methods. Hydrogeol. J. https://doi.org/10.1007/s10040-001-0169-1

Flint, L.E., Flint, A.L., 2014. California basin characterization model: a dataset of historical and future hydrologic response to climate change. US Geol. Surv. Dataset Release. doi 10, F76T0JPB.

Fookes, P.G., 1997. Tropical residual soils: A Geological Society Engineering Group working party revised report.

French, R.H., Jacobson, R.L., Lyles, B.F., 1996. Threshold precipitation events and potential ground-water recharge. J. Hydraul. Eng. 122, 573–578.

Gates, J.B., Edmunds, W.M., Ma, J., Sheppard, P.R., 2008. A 700-year history of groundwater recharge in the drylands of NW China. The Holocene 18, 1045–1054.

Gates, J.B., Scanlon, B.R., Mu, X., Zhang, L., 2011. Impacts of soil conservation on groundwater recharge in the semi-arid Loess Plateau, China. Hydrogeol. J. 19, 865–875. https://doi.org/10.1007/s10040-011-0716-3

Gaye, C.B., Tindimugaya, C., 2019. Challenges and opportunities for sustainable groundwater management in Africa. Hydrogeol. J. 27, 1099–1110.

Gee, G.W., Fayer, M.J., Rockhold, M.L., Wierenga, P.J., Young, M.H., Andraski, B.J., 1994. Variations in Water Balance and Recharge Potential at Three Western Desert Sites. Soil Sci. Soc. Am. J. 58, 63. https://doi.org/10.2136/sssaj1994.03615995005800010009x

Gee, G.W., Hillel, D., 1988. Groundwater recharge in arid regions: Review and critique of estimation methods. Hydrol. Process. 2, 255–266. https://doi.org/10.1002/hyp.3360020306

George, R.J., Nulsen, R.A., Ferdowsian, R., Raper, G.P., 1999. Interactions between trees and groundwaters in recharge and discharge areas–A survey of Western Australian sites. Agric. water Manag. 39, 91–113.

Gleeson, T., Alley, W.M., Allen, D.M., Sophocleous, M.A., Zhou, Y., Taniguchi, M., VanderSteen, J., 2012. Towards Sustainable Groundwater Use: Setting Long-Term Goals, Backcasting, and Managing Adaptively. Ground Water 50, 19–26. https://doi.org/10.1111/j.1745-6584.2011.00825.x

Gleeson, T., Befus, K.M., Jasechko, S., Luijendijk, E., Cardenas, M.B., 2016. The global volume and distribution of modern groundwater. Nat. Geosci. 9, 161–164. https://doi.org/10.1038/ngeo2590

Gleeson, T., Cuthbert, M., Ferguson, G., Perrone, D., 2020. Global Groundwater Sustainability, Resources, and Systems in the Anthropocene. Annu. Rev. Earth Planet. Sci. 48, 431–463. https://doi.org/10.1146/annurev-earth-071719-055251

Godsey, S.E., Kirchner, J.W., 2014. Dynamic, discontinuous stream networks: Hydrologically driven variations in active drainage density, flowing channels and stream order. Hydrol. Process. 28, 5791–5803. https://doi.org/10.1002/hyp.10310

Goni, I.B., Taylor, R.G., Favreau, G., Shamsudduha, M., Nazoumou, Y., Ngounou Ngatcha, B., 2021. Groundwater recharge from heavy rainfall in the southwestern Lake Chad Basin: evidence from isotopic observations. Hydrol. Sci. J. 66, 1359–1371.

Good, S.P., Noone, D., Bowen, G., 2015. Hydrologic connectivity constrains partitioning of global terrestrial water fluxes. Science (80-.). 349, 175–177. https://doi.org/10.1126/science.aaa5931

Goodrich, D.C., Kepner, W.G., Levick, L.R., Wigington, P.J., 2018. Southwestern Intermittent and Ephemeral Stream Connectivity. J. Am. Water Resour. Assoc. https://doi.org/10.1111/1752-1688.12636

Goodrich, D.C., Lane, L.J., Shillito, R.M., Miller, S.N., Syed, K.H., Woolhiser, D.A., 1997. Linearity of basin response as a function of scale in a semiarid watershed. Water Resour. Res. 33, 2951–2965. https://doi.org/10.1029/97WR01422

Goodrich, D.C., Williams, D.G., Unkrich, C.L., Hogan, J.F., Scott, R.L., Hultine, K.R., Pool, D., Goes, A.L., Miller, S., 2004. Comparison of methods to estimate ephemeral channel recharge, Walnut Gulch, San Pedro River Basin, Arizona. pp. 77–99. https://doi.org/10.1029/009WSA06

Gordon, L.J., Steffen, W., Jönsson, B.F., Folke, C., Falkenmark, M., Johannessen, Å., 2005. Human modification of global water vapor flows from the land surface. Proc. Natl. Acad. Sci. U. S. A. 102, 7612–7617. https://doi.org/10.1073/pnas.0500208102

Goudie, A.S., 2011. Arid and semi-arid geomorphology, Arid and Semi-Arid Geomorphology. https://doi.org/10.1017/CBO9780511794261

Gourdol, L., Clément, R., Juilleret, J., Pfister, L., Hissler, C., 2018. Large-scale ERT surveys for investigating shallow regolith properties and architecture. Hydrol. Earth Syst. Sci. Discuss. 1–39. https://doi.org/10.5194/hess-2018-519

Gourry, J.-C., Vermeersch, F., Garcin, M., Giot, D., 2003. Contribution of geophysics to the study of alluvial deposits: a case study in the Val d'Avaray area of the River Loire, France. J. Appl. Geophys. 54, 35–49.

Govers, G., Takken, I., Helming, K., 2000. Soil roughness and overland flow. Agronomie 20, 131–146.

Graf, W.L., 1987. Late Holocene sediment storage in canyons of the Colorado Plateau. Geol. Soc. Am. Bull. 99, 261–271.

Graf, W.L., 1983. Variability of sediment removal in a semiarid watershed. Water Resour. Res. 19, 643–652.

Green, T.R., Taniguchi, M., Kooi, H., Gurdak, J.J., Allen, D.M., Hiscock, K.M., Treidel, H., Aureli, A., 2011. Beneath the surface of global change: Impacts of climate change on groundwater. J. Hydrol. 405, 532–560.

Griffiths, K.J., MacDonald, A.M., Robins, N.S., Merritt, J., Booth, S.J., Johnson, D., McConvey, P.J., 2011. Improving the characterization of Quaternary deposits for groundwater vulnerability assessments using maps of recharge and attenuation potential. Q. J. Eng. Geol. Hydrogeol. 44, 49–61.

Gurdak, J.J., Roe, C.D., 2010. Recharge rates and chemistry beneath playas of the High Plains aquifer, USA. Hydrogeol. J. 18, 1747–1772.

Gutiérrez-Jurado, K.Y., Partington, D., Batelaan, O., Cook, P., Shanafield, M., 2019. What triggers streamflow for intermittent rivers and ephemeral streams in low-gradient catchments in Mediterranean climates. Water Resour. Res. 55, 9926–9946.

Haiyan, C., Yaning, C., Weihong, L., Xinming, H., Yupeng, L., Qifei, Z., 2018. Identifying evaporation fractionation and streamflow components based on stable isotopes in the Kaidu River Basin with mountain–oasis system in north-west China. Hydrol. Process. 32, 2423–2434.

Hamilton, S.K., Bunn, S.E., Thoms, M.C., Marshall, J.C., 2005. Persistence of aquatic refugia between flow pulses in a dryland river system (Cooper Creek, Australia). Limnol. Oceanogr. 50, 743–754. https://doi.org/10.4319/lo.2005.50.3.0743

Hamutoko, J.T., Post, V.E.A., Wanke, H., Beyer, M., Houben, G., Mapani, B., 2019. The role of local perched aquifers in regional groundwater recharge in semi-arid environments: evidence from the Cuvelai-Etosha Basin, Namibia. Hydrogeol. J. 27, 2399–2413.

Hamza, M.A., Anderson, W.K., 2005. Soil compaction in cropping systems: A review of the nature, causes and possible solutions. Soil Tillage Res. 82, 121–145. https://doi.org/10.1016/j.still.2004.08.009

Harbaugh, A.W., Banta, E.R., Hill, M.C., McDonald, M.G., 2000. MODFLOW-2000, The U.S. Geological Survey modular ground-water model: User guide to modularization concepts and the ground-water flow process, Open-File Report. https://doi.org/10.3133/ofr200092

Hartmann, A., Gleeson, T., Wada, Y., Wagener, T., 2017. Enhanced groundwater recharge rates and altered recharge sensitivity to climate variability through subsurface heterogeneity. Proc. Natl. Acad. Sci. 114, 2842–2847.

Hartmann, A., Jasechko, S., Gleeson, T., Wada, Y., Andreo, B., Barberá, J.A., Brielmann, H., Bouchaou, L., Charlier, J.-B., Darling, W.G., 2021. Risk of groundwater contamination widely underestimated because of fast flow into aquifers. Proc. Natl. Acad. Sci. 118, e2024492118.

Hawlye, J., Kernodle, M., 2000. Overview of the hydrogeology and geohydrology of the northern Rio Grande Basin- Colorado, New Mexico, and Texas. Rio Gd. Compact It's Law, New Mex. Water Resour. Res. Institute, New Mex. State Univ. Las Cruces NM 88003 USA, 79–102.

Hayashi, M., & Chiba, H., 1994. Identification of groundwater components by Cl" and stable isotope signatures: a case study in a semi-arid basin in Tanzania. Jap. Groundw. Hydrol. 36, 259–275.

Healy, R.W., Scanlon, B.R., 2010. Estimating Groundwater Recharge. Cambridge University Press, Cambridge. https://doi.org/10.1017/CBO9780511780745

Herrera, C., Godfrey, L., Urrutia, J., Custodio, E., Jordan, T., Jódar, J., Delgado, K., Barrenechea, F., 2021. Recharge and residence times of groundwater in hyper arid areas: The confined aquifer of Calama, Loa River Basin, Atacama Desert, Chile. Sci. Total Environ. 752, 141847.

Holman, I.P., Rivas-Casado, M., Howden, N.J.K., Bloomfield, J.P., Williams, A.T., 2009. Linking North Atlantic ocean-atmosphere teleconnection patterns and hydrogeological responses in temperate groundwater systems. Hydrol. Process. 23, 3123–3126.

Houston, J., 2002. Groundwater recharge through an alluvial fan in the Atacama Desert, northern Chile: Mechanisms, magnitudes and causes. Hydrol. Process. 16, 3019–3035. https://doi.org/10.1002/hyp.1086

Hu, W., Wang, Y.Q., Li, H.J., Huang, M.B., Hou, M.T., Li, Z., She, D.L., Si, B.C., 2019. Dominant role of climate in determining spatio-temporal distribution of potential groundwater recharge at a regional scale. J. Hydrol. 578, 124042.

Huang, J., Li, Y., Fu, C., Chen, F., Fu, Q., Dai, A., Shinoda, M., Ma, Z., Guo, W., Li, Z., Zhang, L., Liu, Y., Yu, H., He, Y., Xie, Y., Guan, X., Ji, M., Lin, L., Wang, S., Yan, H., Wang, G., 2017. Dryland climate change: Recent progress and challenges. Rev. Geophys. 55, 719–778. https://doi.org/10.1002/2016RG000550

Huang, J., Yu, H., Guan, X., Wang, G., Guo, R., 2016. Accelerated dryland expansion under climate change. Nat. Clim. Chang. 6, 166–171. https://doi.org/10.1038/nclimate2837

Huang, T., Pang, Z., Liu, J., Yin, L., Edmunds, W.M., 2017. Groundwater recharge in an arid grassland as indicated by soil chloride profile and multiple tracers. Hydrol. Process. 31, 1047–1057. https://doi.org/10.1002/hyp.11089

Hughes, D.A., 2008. Modelling semi-arid and arid hydrology and water resources: The southern Africa experience. Hydrol. Model. Arid Semi-Arid Areas 1–20.

Huntington, J.L., Niswonger, R.G., 2012. Role of surface-water and groundwater interactions on projected summertime streamflow in snow dominated regions: An integrated modeling approach. Water Resour. Res. 48.

Hupp, C.R., 1986. The headward extent of fluvial landforms and associated vegetation on Massanutten Mountain, Virginia. Earth Surf. Process. Landforms 11, 545–555.

Hussey, S.W., 1997. Small-scale sand abstraction systems, in: 1997 23rd WEDC International Conference: Water and Sanitation for All - Partnerships and Innovations.

Water Workshop Programme, Zimbabwe, pp. 283–285.

Hvorslev, M.J., 1951. Time lag and soil permeability in ground-water observations. Waterways Experiment Station, Corps of Engineers, US Army.

Issa, O.M., Valentin, C., Rajot, J.-L., Cerdan, O., Desprats, J.-F., Bouchet, T., 2011. Runoff generation fostered by physical and biological crusts in semi-arid sandy soils. Geoderma 167, 22–29.

Izbicki, J.., Radyk, J., Michel, R.., 2000. Water movement through a thick unsaturated zone underlying an intermittent stream in the western Mojave Desert, southern California, USA. J. Hydrol. 238, 194–217. https://doi.org/10.1016/S0022-1694(00)00331-0

Jacks, G., Traoré, M.S., 2014. Mechanisms and rates of groundwater recharge at Timbuktu, Republic of Mali. J. Hydrol. Eng. 19, 422–427.

Jadoon, K.Z., Al-Mashharawi, S., Hanafy, S.M., Schuster, G.T., Missimer, T.M., 2016. Anthropogenic-induced changes in the mechanism of drylands ephemeral stream recharge, Western Saudi Arabia. Water (Switzerland). https://doi.org/10.3390/w8040136

Jaeger, K L, Sutfin, N.A., Tooth, S., Michaelides, K., Singer, M., 2017. Geomorphology and Sediment Regimes of Intermittent Rivers and Ephemeral Streams. U.S. geological survey information technology report, 2002-0010., Intermittent Rivers and Ephemeral Streams: Ecology and Management. https://doi.org/10.1016/B978-0-12-803835-2.00002-4

Jaeger, Kristin L., Sutfin, N.A., Tooth, S., Michaelides, K., Singer, M., 2017. Geomorphology and Sediment Regimes of Intermittent Rivers and Ephemeral Streams, in: Intermittent Rivers and Ephemeral Streams. https://doi.org/10.1016/b978-0-12-803835-2.00002-4

Jasechko, S., Taylor, R.G., 2015. Intensive rainfall recharges tropical groundwaters. Environ. Res. Lett. 10. https://doi.org/10.1088/1748-9326/10/12/124015

Jie, F., Fei, L., Li, S., Hao, K., Liu, L., Li, J., Liu, N., 2022. Quantitative effects of vadose zone thickness on delayed recharge of groundwater for an irrigation district in an arid area of Northwest China. J. Hydrol. Reg. Stud. 40, 101022.

Jiménez Cisneros, B.E., Oki, T., Arnell, N.W., Benito, G., Cogley, J.G., Döll, P., Jiang, T., Mwakalila, S.S., Kundzewicz, Z., Nishijima, A., 2014. Freshwater resources, in: Climate Change 2014 Impacts, Adaptation and Vulnerability: Part A: Global and Sectoral Aspects. pp. 229–270. https://doi.org/10.1017/CBO9781107415379.008

Jódar, J., Cabrera, J.A., Martos-Rosillo, S., Ruiz-Constán, A., González-Ramón, A., Lambán, L.J., Herrera, C., Custodio, E., 2017. Groundwater discharge in high-mountain watersheds: A valuable resource for downstream semi-arid zones. The case of the Bérchules River in Sierra Nevada (Southern Spain). Sci. Total Environ. 593, 760–772.

Julian, W., Lounsberry, W., Tamura, A., Van Loenen, R., Wright, M.P., 1963. Brief explanation of the geology, Quarter Degree Sheet 134.

Kabete, J.M., Groves, D.I., McNaughton, N.J., Mruma, A.H., 2012. A new tectonic and temporal framework for the Tanzanian Shield: implications for gold metallogeny and undiscovered endowment. Ore Geol. Rev. 48, 88–124.

Kampf, S.K., Faulconer, J., Shaw, J.R., Sutfin, N.A., Cooper, D.J., 2016. Rain and channel flow supplements to subsurface water beneath hyper-arid ephemeral stream channels. J. Hydrol. 536, 524–533. https://doi.org/10.1016/j.jhydrol.2016.03.016

Kashaigili, J.J., 2010. Assessment of groundwater availability and its current and potential use and impacts in Tanzania. Morogoro, Tanzania.

Kashaigili, J.J., Mashauri, D.A., Abdo, G., 2003. Groundwater management by using mathematical modeling: case of the Makutupora groundwater basin in dodoma Tanzania. Botswana J. Technol. 12. https://doi.org/10.4314/bjt.v12i1.15342

Katz, G.L., Denslow, M.W., Stromberg, J.C., 2012. The Goldilocks effect: intermittent streams sustain more plant species than those with perennial or ephemeral flow. Freshw. Biol. 57, 467–480.

Keese, K.E., Scanlon, B.R., Reedy, R.C., 2005. Assessing controls on diffuse groundwater recharge using unsaturated flow modeling. Water Resour. Res. 41.

Keppel, R. V, Renard, K.G., 1962a. Transmission losses in ephemeral stream beds. J. Hydraul. Div. Am. Soc. Civ. Eng 88, 59–68.

Keppel, R. V, Renard, K.G., 1962b. Transmission losses in ephemeral stream beds. J. Hydraul. Div. Am. Soc. Civ. Eng 88, 59–68.

Keshavarzi, M., Baker, A., Kelly, B.F.J., Andersen, M.S., 2017. River–groundwater connectivity in a karst system, Wellington, New South Wales, Australia. Hydrogeol. J. 25, 557–574.

Kim, J.H., Jackson, R.B., 2012. A global analysis of groundwater recharge for vegetation, climate, and soils. Vadose Zo. J. 11.

Knighton, A.D., Nanson, G.C., 2000. Waterhole form and process in the anastomosing channel system of Cooper Creek, Australia. Geomorphology 35, 101–117. https://doi.org/10.1016/S0169-555X(00)00026-X

Knighton, A.D., Nanson, G.C., 1994. Waterholes and their significance in the anastomosing channel system of Cooper Creek, Australia. Geomorphology 9, 311–324.
https://doi.org/10.1016/0169-555X(94)90052-3

Kolusu, S.R., Shamsudduha, M., Todd, M.C., Taylor, R.G., Seddon, D., Kashaigili, J.J., Ebrahim, G.Y., Cuthbert, M.O., Sorensen, J.P.R., Villholth, K.G., others, 2019. The El

Niño event of 2015--2016: climate anomalies and their impact on groundwater resources in East and Southern Africa. Hydrol. Earth Syst. Sci. 23, 1751–1762.

Kuffour, B.N.O., Engdahl, N.B., Woodward, C.S., Condon, L.E., Kollet, S., Maxwell, R.M., 2020. Simulating coupled surface–subsurface flows with ParFlow v3. 5.0: capabilities, applications, and ongoing development of an open-source, massively parallel, integrated hydrologic model. Geosci. Model Dev. 13, 1373–1397.

Kuss, A.J.M., Gurdak, J.J., 2014. Groundwater level response in US principal aquifers to ENSO, NAO, PDO, and AMO. J. Hydrol. 519, 1939–1952.

Labbe, T.R., Fausch, K.D., 2000. Dynamics of intermittent stream habitat regulate persistence of a threatened fish at multiple scales. Ecol. Appl. 10, 1774–1791.

LaBrecque, D.J., Miletto, M., Daily, W., Ramirez, A., Owen, E., 1996. The effects of noise on Occam's inversion of resistivity tomography data. Geophysics 61, 538–548.

Lange, J., 2005. Dynamics of transmission losses in a large arid stream channel. J. Hydrol. 306, 112–126. https://doi.org/10.1016/j.jhydrol.2004.09.016

Lange, J., Leibundgut, C., Grodek, T., Lekach, J., Schick, A., 1998. Using artificial tracers to study water losses of ephemeral floods in small arid streams. IAHS-AISH Publ. 247, 31–40.

Lapworth, D.J., Nkhuwa, D.C.W., Okotto-Okotto, J., Pedley, S., Stuart, M.E., Tijani, M.N., Wright, J., 2017. Urban groundwater quality in sub-Saharan Africa: current status and implications for water security and public health. Hydrogeol. J. 25, 1093.

Larned, S.T., Hicks, D.M., Schmidt, J., Davey, A.J.H., Dey, K., Scarsbrook, M., Arscott, D.B., Woods, R.A., 2008. The Selwyn River of New Zealand: A benchmark system for alluvial plain rivers. River Res. Appl. 24, 1–21. https://doi.org/10.1002/rra.1054

Latron, J., Gallart, F., 2008. Runoff generation processes in a small Mediterranean research catchment (Vallcebre, Eastern Pyrenees). J. Hydrol. 358, 206–220.

Latron, J., Gallart, F., 2007. Seasonal dynamics of runoff-contributing areas in a small mediterranean research catchment (Vallcebre, Eastern Pyrenees). J. Hydrol. 335, 194–206.

Lautz, L.K., 2008. Estimating groundwater evapotranspiration rates using diurnal water-table fluctuations in a semi-arid riparian zone. Hydrogeol. J. 16, 483–497.

Leblanc, M.J., Favreau, G., Massuel, S., Tweed, S.O., Loireau, M., Cappelaere, B., 2008. Land clearance and hydrological change in the Sahel: SW Niger. Glob. Planet. Change 61, 135–150.

Leketa, K., Abiye, T., Zondi, S., Butler, M., 2019. Assessing groundwater recharge in crystalline and karstic aquifers of the Upper Crocodile River Basin, Johannesburg, South

Africa. Groundw. Sustain. Dev. 8, 31–40.

Leopold, L.B., Miller, J.P., 1956. Ephemeral streams - hydraulic factors and their relation to the drainage net. Ephemer. Streams Hydraul. Factors Their Relat. to Drain. Net.

Lerner, D.N., Issar, A., Simmers, I. (Ian), International Association of Hydrogeologists., 1990. Groundwater recharge : a guide to understanding and estimating natural recharge.

Levick, L.R., Goodrich, D.C., Hernandez, M., Fonseca, J., Semmens, D.J., Stromberg, J., Tluczek, M., Leidy, R.A., Scianni, M., Guertin, D.P., 2008. The Ecological and Hydrological Significance of Ephemeral and Intermittent Streams in the Arid and Semi-arid American Southwest.

Liu, Q.Q., Singh, V.P., 2004. Effect of microtopography, slope length and gradient, and vegetative cover on overland flow through simulation. J. Hydrol. Eng. 9, 375–382.

Lloyd, J.W., 1986. A review of aridity and groundwater. Hydrol. Process. 1, 63–78. https://doi.org/10.1002/hyp.3360010107

Loke, M.H., 2006. RES2DINV ver. 3.55, Rapid 2-D resistivity & IP inversion using the least-squares method. Softw. Man. 139.

Loke, M.H., 2002. RES2DMOD ver. 3.01. Rapid 2D Resist. Forw. Model. using finite-difference finite-elements method. Geotomo Software. Man.

Loke, M.H., 2001. RES1D ver. 1.0. 1-D Resistivity, IP & SIP Inversion and Forward Modeling. Wenner and Schlumberger arrays, User's Manual.

Loke, M.H., Acworth, I., Dahlin, T., 2003. A comparison of smooth and blocky inversion methods in 2D electrical imaging surveys. Explor. Geophys. 34, 182–187. https://doi.org/10.1071/EG03182

Lorentz, S., Riddell, E.S., Nel, J., Van Tol, J., Fundisi, D., Jumbi, F., van Niekerk, A., 2020. Groundwater-surface water interactions in an ephemeral savanna catchment, Kruger National Park. Koedoe African Prot. Area Conserv. Sci. 62, 1–14.

Love, D., van der Zaag, P., Uhlenbrook, S., Owen, R.J.S., 2011. A water balance modelling approach to optimising the use of water resources in ephemeral sand rivers. River Res. Appl. 27, 908–925. https://doi.org/10.1002/rra.1408

Love, D., van der Zaag, P., Uhlenbrook, S., Owen, R.J.S., 2010. A water balance modelling approach to optimising the use of water resources in ephemeral sand rivers. River Res. Appl. n/a-n/a. https://doi.org/10.1002/rra.1408

MacDonald, A M, Bonsor, H.C., Dochartaigh, B.É.Ó., Taylor, R.G., 2012. Quantitative maps of groundwater resources in Africa. Environ. Res. Lett. 7, 024009.

https://doi.org/10.1088/1748-9326/7/2/024009

MacDonald, A.M., Calow, R.C., 2009. Developing groundwater for secure rural water supplies in Africa. Desalination 248, 546–556. https://doi.org/10.1016/j.desal.2008.05.100

Macdonald, A.M., Davies, J., Calow, R.C., 2008. African hydrogeology and rural water supply, in: Applied Groundwater Studies in Africa. pp. 127–148.

MacDonald, A.M., Lark, R.M., Taylor, R.G., Abiye, T., Fallas, H.C., Favreau, G., Goni, I.B., Kebede, S., Scanlon, B., Sorensen, J.P.R., 2021. Mapping groundwater recharge in Africa from ground observations and implications for water security. Environ. Res. Lett. 16, 34012.

MacDonald, Alan M, Taylor, R.G., Bonsor, H.C., 2012. Groundwater in Africa: Is there sufficient water to support the intensification of agriculture from 'land grabs'?, in: Handbook of Land and Water Grabs in Africa. Routledge, pp. 376–383.

Macheyeki, A.S., Delvaux, D., De Batist, M., Mruma, A., 2008. Fault kinematics and tectonic stress in the seismically active Manyara--Dodoma Rift segment in Central Tanzania--Implications for the East African Rift. J. African Earth Sci. 51, 163–188.

Mádl-Szőnyi, J., Batelaan, O., Molson, J., Verweij, H., Jiang, X.-W., Carrillo-Rivera, J.J., Tóth, Á., 2022. Regional groundwater flow and the future of Hydrogeology: evolving concepts and communication. Hydrogeol. J. 1–4.

Malmon, D. V, Reneau, S.L., Dunne, T., 2004. Sediment sorting and transport by flash floods. J. Geophys. Res. Surf. 109.

Manna, F., Murray, S., Abbey, D., Martin, P., Cherry, J., Parker, B., 2019. Spatial and temporal variability of groundwater recharge in a sandstone aquifer in a semiarid region. Hydrol. Earth Syst. Sci. 23, 2187–2205.

Manning, A.H., Solomon, D.K., 2005. An integrated environmental tracer approach to characterizing groundwater circulation in a mountain block. Water Resour. Res. 41.

Manning, A.H., Solomon, D.K., 2003. Using noble gases to investigate mountain-front recharge. J. Hydrol. 275, 194–207. https://doi.org/10.1016/S0022-1694(03)00043-X

Mansell, M.G., Hussey, S.W., 2005. An investigation of flows and losses within the alluvial sands of ephemeral rivers in Zimbabwe. J. Hydrol. 314, 192–203.
https://doi.org/10.1016/j.jhydrol.2005.03.015

Maples, S.R., Fogg, G.E., Maxwell, R.M., 2019. Modeling managed aquifer recharge processes in a highly heterogeneous, semi-confined aquifer system. Hydrogeol. J. 27, 2869–2888.

Markovich, K.H., Condon, L.E., Carroll, K.C., Purtschert, R., McIntosh, J.C., 2021. A Mountain-Front Recharge Component Characterization Approach Combining Groundwater

Age Distributions, Noble Gas Thermometry, and Fluid and Energy Transport Modeling. Water Resour. Res. 57, e2020WR027743.

Markovich, K.H., Manning, A.H., Condon, L.E., McIntosh, J.C., 2019. Mountain-block recharge: A review of current understanding. Water Resour. Res. 55, 8278–8304.

Maurice, L., Taylor, R.G., Tindimugaya, C., MacDonald, A.M., Johnson, P., Kaponda, A., Owor, M., Sanga, H., Bonsor, H.C., Darling, W.G., others, 2019. Characteristics of high-intensity groundwater abstractions from weathered crystalline bedrock aquifers in East Africa. Hydrogeol. J. 27, 459–474.

Maxwell, R.M., Kollet, S.J., 2008. Quantifying the effects of three-dimensional subsurface heterogeneity on Hortonian runoff processes using a coupled numerical, stochastic approach. Adv. Water Resour. 31, 807–817.

Mccallum, A.M., Andersen, M.S., Giambastiani, B.M.S., Kelly, B.F.J., Ian Acworth, R., 2013. River-aquifer interactions in a semi-arid environment stressed by groundwater abstraction. Hydrol. Process. 27, 1072–1085. https://doi.org/10.1002/hyp.9229

McCallum, A.M., Andersen, M.S., Rau, G.C., Larsen, J.R., Acworth, R.I., 2014. River-aquifer interactions in a semiarid environment investigated using point and reach measurements. Water Resour. Res. 50, 2815–2829. https://doi.org/10.1002/2012WR012922

McDonald, M.G., Harbaugh, A.W., 2003. The history of MODFLOW. Ground Water 41, 280.

McKenna, O.P., Sala, O.E., 2018. Groundwater recharge in desert playas: current rates and future effects of climate change. Environ. Res. Lett. 13, 14025.

McMahon, P.B., Dennehy, K.F., Bruce, B.W., Böhlke, J.K., Michel, R.L., Gurdak, J.J., Hurlbut, D.B., 2006. Storage and transit time of chemicals in thick unsaturated zones under rangeland and irrigated cropland, High Plains, United States. Water Resour. Res. 42.

Meixner, T., Manning, A.H., Stonestrom, D.A., Allen, D.M., Ajami, H., Blasch, K.W., Brookfield, A.E., Castro, C.L., Clark, J.F., Gochis, D.J., Flint, A.L., Neff, K.L., Niraula, R., Rodell, M., Scanlon, B.R., Singha, K., Walvoord, M.A., 2016. Implications of projected climate change for groundwater recharge in the western United States. J. Hydrol. 534, 124–138. https://doi.org/10.1016/j.jhydrol.2015.12.027

Meredith, K.T., Hollins, S.E., Hughes, C.E., Cendón, D.I., Chisari, R., Griffiths, A., Crawford, J., 2015. Evaporation and concentration gradients created by episodic river recharge in a semi-arid zone aquifer: Insights from Cl, delta18O, delta2H, and 3H. J. Hydrol. 529, 1070–1078.

Messager, M.L., Lehner, B., Cockburn, C., Lamouroux, N., Pella, H., Snelder, T., Tockner, K., Trautmann, T., Watt, C., Datry, T., 2021. Global prevalence of non-perennial

rivers and streams. Nature 594, 391–397.

Miller, D.E., Gardner, W.H., 1962. Water infiltration into stratified soil. Soil Sci. Soc. Am. J. 26, 115–119.

Miller, S.N., Guertin, D.P., Goodrich, D.C., 1996. Investigating stream channel morphology using a geographic information system, in: Proc. ESRI User Conf., Palm Springs, CA.

Ministry of Water, E. and M., 1976. Report on hydrological investigation of Makutapora Basin for Dodoma Capital water supply. Dodoma.

Misstear, B.D.R., Brown, L., Daly, D., 2009. A methodology for making initial estimates of groundwater recharge from groundwater vulnerability mapping. Hydrogeol. J. 17, 275–285.

Modie, L.T., Kenabatho, P.K., Stephens, M., Mosekiemang, T., 2022. Investigating groundwater and surface water interactions using stable isotopes and hydrochemistry in the Notwane River Catchment, South East Botswana. J. Hydrol. Reg. Stud. 40, 101014.

Moeck, C., Grech-Cumbo, N., Podgorski, J., Bretzler, A., Gurdak, J.J., Berg, M., Schirmer, M., 2020. A global-scale dataset of direct natural groundwater recharge rates: A review of variables, processes and relationships. Sci. Total Environ. 717, 137042.

Mohan, C., Western, A.W., Wei, Y., Saft, M., 2018. Predicting groundwater recharge for varying land cover and climate conditions–a global meta-study. Hydrol. Earth Syst. Sci. 22, 2689–2703.

Morin, E., Grodek, T., Dahan, O., Benito, G., Kulls, C., Jacoby, Y., Langenhove, G. Van, Seely, M., Enzel, Y., 2009. Flood routing and alluvial aquifer recharge along the ephemeral arid Kuiseb River, Namibia. J. Hydrol. 368, 262–275. https://doi.org/10.1016/j.jhydrol.2009.02.015

Morin, E., Marra, F., Armon, M., 2020. Dryland precipitation climatology from satellite observations. Satell. Precip. Meas. Vol. 2 843–859.

Moulahoum, A.W., 2018. Using field assessment and numerical modelling tools to optimize a water abstraction system in the Shashane Sand River aquifer (Zimbabwe).

NASA, METI, AIST, Japan Spacesystems, US/Japan ASTER Science Team, 2019. ASTER Global Digital Elevation Model V003.
https://doi.org/https://doi.org/10.5067/ASTER/ASTGTM.003

Nash, D.J., Shaw, P.A., Thomas, D.S.G., 1994. Duricrust development and valley evolution: process–landform links in the Kalahari. Earth Surf. Process. Landforms 19, 299–317.

Naves, A., Samper, J., Pisani, B., Mon, A., Dafonte, J., Montenegro, L., García-Tomillo, A., 2021. Hydrogeology and groundwater management in a coastal granitic area with steep

slopes in Galicia (Spain). Hydrogeol. J. 29, 2655–2669.

Newman, B.D., Vivoni, E.R., Groffman, A.R., 2006. Surface water–groundwater interactions in semiarid drainages of the American southwest. Hydrol. Process. An Int. J. 20, 3371–3394.

Nicholson, S.E., 2011. Dryland climatology, Dryland Climatology. Cambridge University Press, Florida State University, United States. https://doi.org/10.1017/CBO9780511973840

Nicolas, M., Bour, O., Selles, A., Dewandel, B., Bailly-Comte, V., Chandra, S., Ahmed, S., Maréchal, J.-C., 2019. Managed Aquifer Recharge in fractured crystalline rock aquifers: Impact of horizontal preferential flow on recharge dynamics. J. Hydrol. 573, 717–732.

Nimmo, J.R., Creasey, K.M., Perkins, K.S., Mirus, B.B., 2017. Preferential flow, diffuse flow, and perching in an interbedded fractured-rock unsaturated zone. Hydrogeol. J. 25, 421–444.

Nimmo, J.R., Perkins, K.S., Rose, P.E., Rousseau, J.P., Orr, B.R., Twining, B. V, Anderson, S.R., 2002. Kilometer-scale rapid transport of naphthalene sulfonate tracer in the unsaturated zone at the Idaho National Engineering and Environmental Laboratory. Vadose Zo. J. 1, 89–101.

Niswonger, R.G., Panday, S., Ibaraki, M., 2011. MODFLOW-NWT, a Newton formulation for MODFLOW-2005. US Geol. Surv. Tech. Methods 6, 44.

Nkotagu, H., 1996. Origins of high nitrate in groundwater in Tanzania. J. African Earth Sci. 22, 471–478. https://doi.org/10.1016/0899-5362(96)00021-8

Noorduijn, S.L., Shanafield, M., Trigg, M.A., Harrington, G.A., Cook, P.G., Peeters, L., 2014. Estimating seepage flux from ephemeral stream channels using surface water and groundwater level data. Water Resour. Res. https://doi.org/10.1002/2012WR013424

Nord, M., 1985. Sand Rivers of Botswana, Results from phase 2 of the Sand Rivers Project. Unpubl. report, Dep. Water Aff. Gov. Botswana, Gaborone.

O Dochartaigh, B.E., MacDonald, A.M., Darling, W.G., Hughes, A.G., Li, J.X., Shi, L.A., 2010. Determining groundwater degradation from irrigation in desert-marginal northern China. Hydrogeol. J. 18, 1939–1952.

Oakes, H., Thorp, J., 1951. Dark-clay Soils of Warm Regions Variously Called Rendzina, Black Cotton Soils, Regur, and Tirs 1. Soil Sci. Soc. Am. J. 15, 347–354.

Onodera, S., Kitaoka, K., Shindo, S., 1995. Stable isotopic compositions of deep groundwater caused by partial infiltration into the restricted recharge area of a semiarid basin in tanzania. Model. Assess. Monit. Groundw. Qual. 75–83.

Owen, R., Dahlin, T., 2005. Alluvial aquifers at geological boundaries : Geophysical investigations and groundwater resources, in: Groundwater and Human Development:

International Association of Hydrogeologists Selected Papers on Hydrogeology Volume 6. pp. 233–246.

Owor, M., Taylor, R.G., Tindimugaya, C., Mwesigwa, D., 2009. Rainfall intensity and groundwater recharge: empirical evidence from the Upper Nile Basin. Environ. Res. Lett. 4, 035009. https://doi.org/10.1088/1748-9326/4/3/035009

Owuor, S.O., Butterbach-Bahl, K., Guzha, A.C., Rufino, M.C., Pelster, D.E., Díaz-Pinés, E., Breuer, L., 2016. Groundwater recharge rates and surface runoff response to land use and land cover changes in semi-arid environments. Ecol. Process. 5, 1–21.

Oyarzún, J., Núñez, J., Fairley, J.P., Tapia, S., Alvarez, D., Maturana, H., Arumí, J.L., Aguirre, E., Carvajal, A., Oyarzún, R., 2019. Groundwater Recharge Assessment in an Arid, Coastal, Middle Mountain Copper Mining District, Coquimbo Region, North-central Chile. Mine Water Environ. 38, 226–242.

Pal, D.K., Deshpande, S.B., Venugopal, K.R., Kalbande, A.R., 1989. Formation of di-and trioctahedral smectite as evidence for paleoclimatic changes in southern and central Peninsular India. Geoderma 45, 175–184.

Parsekian, A.D., Singha, K., Minsley, B.J., Holbrook, W.S., Slater, L., 2015. Multiscale geophysical imaging of the critical zone. Rev. Geophys. 53, 1–26.
https://doi.org/10.1002/2014RG000465

Parsons, A.J., Abrahams, A.D., 1994. Geomorphology of desert environments. Springer.

Patton, N.R., Lohse, K.A., Godsey, S.E., Crosby, B.T., Seyfried, M.S., 2018. Predicting soil thickness on soil mantled hillslopes. Nat. Commun. 9, 3329.

Peipeng, W., Longcang, S., Jean-Christophe, C., Qiting, Z., Wang, M., Li, F., Chen, H., 2021. The effect of typical geological heterogeneities on the performance of managed aquifer recharge: physical experiments and numerical simulations. Hydrogeol. J. 29, 2107–2125.

Perzan, Z., Osterman, G., Maher, K., 2023. Controls on flood managed aquifer recharge through a heterogeneous vadose zone: hydrologic modeling at a site characterized with surface geophysics. Hydrol. Earth Syst. Sci. 27, 969–990.

Phillips, F.M., 1994. Environmental tracers for water movement in desert soils of the American Southwest. Soil Sci. Soc. Am. J. 58, 15–24.

Phillips, J. V, Tadayon, S., 2006. Selection of Manning's roughness coefficient for natural and constructed vegetated and non-vegetated channels, and vegetation maintenance plan guidelines for vegetated channels in Central Arizona. US Geological Survey.

Pilgrim, D.H., Chapman, T.G., Doran, D.G., 1988. Problems of rainfall-runoff modelling in arid and semiarid regions. Hydrol. Sci. J. https://doi.org/10.1080/02626668809491261

Pockman, W.T., Sperry, J.S., 2000. Vulnerability to xylem cavitation and the distribution of Sonoran desert vegetation. Am. J. Bot. 87, 1287–1299.

Pool, D.R., 2005. Variations in climate and ephemeral channel recharge in southeastern Arizona, United States. Water Resour. Res. 41. https://doi.org/10.1029/2004WR003255

Pörtner, H.-O., Roberts, D.C., Adams, H., Adler, C., Aldunce, P., Ali, E., Begum, R.A., Betts, R., Kerr, R.B., Biesbroek, R., 2022. Climate change 2022: Impacts, adaptation and vulnerability. IPCC Geneva, Switzerland:

Prasad, R.K., Mondal, N.C., Banerjee, P., Nandakumar, M. V, Singh, V.S., 2008. Deciphering potential groundwater zone in hard rock through the application of GIS. Environ. Geol. 55, 467–475.

Prăvălie, R., 2016. Drylands extent and environmental issues. A global approach. Earth-Science Rev. 161, 259–278. https://doi.org/10.1016/j.earscirev.2016.08.003

Quichimbo, E.A., Singer, M.B., Cuthbert, M.O., 2020. Characterising groundwater–surface water interactions in idealised ephemeral stream systems. Hydrol. Process. 34, 3792–3806. https://doi.org/10.1002/hyp.13847

Quichimbo, E.A., Singer, M.B., Michaelides, K., Hobley, D.E.J., Rosolem, R., Cuthbert, M.O., 2021. DRYP 1.0: a parsimonious hydrological model of DRYland Partitioning of the water balance. Geosci. Model Dev. 14, 6893–6917.

Rassam, D.W., Fellows, C.S., De Hayr, R., Hunter, H., Bloesch, P., 2006. The hydrology of riparian buffer zones; two case studies in an ephemeral and a perennial stream. J. Hydrol. 325, 308–324.

Rau, G.C., Halloran, L.J.S., Cuthbert, M.O., Andersen, M.S., Acworth, R.I., Tellam, J.H., 2017. Characterising the dynamics of surface water-groundwater interactions in intermittent and ephemeral streams using streambed thermal signatures. Adv. Water Resour. 107, 354–369. https://doi.org/10.1016/j.advwatres.2017.07.005

Ren, X., Zhu, B., Liu, M., Zhang, Y., He, Z., Rioual, P., 2019. Mechanism of groundwater recharge in the middle-latitude desert of eastern Hunshandake, China: diffuse or focused recharge? Hydrogeol. J. 27, 761–783.

Richardson, C.M., Zimmer, M.A., Fackrell, J.K., Paytan, A., 2020. Geologic controls on source water drive baseflow generation and carbon geochemistry: Evidence of nonstationary baseflow sources across multiple subwatersheds. Water Resour. Res. 56, e2019WR026577.

Ritz, M., Parisot, J.-C., Diouf, S., Beauvais, A., Dione, F., Niang, M., 1999. Electrical imaging of lateritic weathering mantles over granitic and metamorphic basement of eastern Senegal, West Africa. J. Appl. Geophys. 41, 335–344.

Robineau, B., Join, J.-L., Beauvais, A., Parisot, J.-C., Savin, C., 2007. Geoelectrical imaging of a thick regolith developed on ultramafic rocks: groundwater influence. Aust. J.

Earth Sci. 54, 773–781.

Rossman, N.R., Zlotnik, V.A., Rowe, C.M., Szilagyi, J., 2014. Vadose zone lag time and potential 21st century climate change effects on spatially distributed groundwater recharge in the semi-arid Nebraska Sand Hills. J. Hydrol. 519, 656–669.

Rubin, Y., Hubbard, S.S., 2006. Hydrogeophysics. Springer Science & Business Media.

Rusagara, R., Koïta, M., Plagnes, V., Jost, A., 2022. Groundwater recharge pathways to a weathered-rock aquifer system in a dryland catchment in Burkina Faso. Hydrogeol. J. 30, 1489–1512.

Rwebugisa, R.A., 2008. Groundwater re-charge assessment in the Makutupora Basin, Dodoma, Tanzania. Msc Thesis. International Institute for Geo-Information Science and Earth Observation, Enschede, The Netherlands.

Sabathier, R., Singer, M.B., Stella, J.C., Roberts, D.A., Caylor, K.K., 2021. Vegetation responses to climatic and geologic controls on water availability in southeastern Arizona. Environ. Res. Lett. 16, 64029.

Saccò, M., Blyth, A.J., Humphreys, W.F., Cooper, S.J.B., White, N.E., Campbell, M., Mousavi-Derazmahalleh, M., Hua, Q., Mazumder, D., Smith, C., 2021. Rainfall as a trigger of ecological cascade effects in an Australian groundwater ecosystem. Sci. Rep. 11, 1–15.

Saghir, J., Santoro, J., 2018. Urbanization in Sub-Saharan Africa, in: Meeting Challenges by Bridging Stakeholders. Washington, DC, USA: Center for Strategic & International Studies. JSTOR.

Sakakibara, K., Tsujimura, M., Song, X., Zhang, J., 2017. Spatiotemporal variation of the surface water effect on the groundwater recharge in a low-precipitation region: Application of the multi-tracer approach to the Taihang Mountains, North China. J. Hydrol. 545, 132–144.

Salve, R., Rempe, D.M., Dietrich, W.E., 2012. Rain, rock moisture dynamics, and the rapid response of perched groundwater in weathered, fractured argillite underlying a steep hillslope. Water Resour. Res. 48.

Sandercock, P.J., Hooke, J.M., Mant, J.M., 2007. Vegetation in dryland river channels and its interaction with fluvial processes. Prog. Phys. Geogr. 31, 107–129. https://doi.org/10.1177/0309133307076106

Sapriza-Azuri, G., Jódar, J., Navarro, V., Slooten, L.J., Carrera, J., Gupta, H. V, 2015. Impacts of rainfall spatial variability on hydrogeological response. Water Resour. Res. 51, 1300–1314.

Sargeant, C.I., Singer, M.B., 2016. Sub-annual variability in historical water source use by Mediterranean riparian trees. Ecohydrology 9, 1328–1345. https://doi.org/10.1002/eco.1730

Scanlon, B.R., 1994. Water and heat fluxes in desert soils: 1. Field studies. Water Resour. Res. 30, 709–719. https://doi.org/10.1029/93WR03251

Scanlon, B.R., Healy, R.W., Cook, P.G., 2002. Choosing appropriate techniques for quantifying groundwater recharge. Hydrogeol. J. 10, 18–39. https://doi.org/10.1007/s10040-001-0176-2

Scanlon, B.R., Keese, K.E., Flint, A.L., Flint, L.E., Gaye, C.B., Edmunds, W.M., Simmers, I., 2006. Global synthesis of groundwater recharge in semiarid and arid regions. Hydrol. Process. 20, 3335–3370. https://doi.org/10.1002/hyp.6335

Scanlon, B.R., Reedy, R.C., Stonestrom, D.A., Prudic, D.E., Dennehy, K.F., 2005. Impact of land use and land cover change on groundwater recharge and quality in the southwestern US. Glob. Chang. Biol. 11, 1577–1593.

Scanlon, B.R., Zhang, Z., Save, H., Sun, A.Y., Müller Schmied, H., Van Beek, L.P.H., Wiese, D.N., Wada, Y., Long, D., Reedy, R.C., 2018. such that the distribution of recharge to the unsaturated zone may differ considerably from the distribution of surface infiltration. Proc. Natl. Acad. Sci. 115, E1080–E1089.

Schenk, H.J., Jackson, R.B., 2002. THE GLOBAL BIOGEOGRAPHY OF ROOTS. Ecol. Monogr. 72, 311–328. https://doi.org/10.1890/0012-9615(2002)072[0311:TGBOR]2.0.CO;2

Schlesinger, W.H., Jasechko, S., 2014. Transpiration in the global water cycle. Agric. For. Meteorol. 189, 115–117.

Schreiner-McGraw, A.P., Ajami, H., Vivoni, E.R., 2019. Extreme weather events and transmission losses in arid streams. Environ. Res. Lett. 14, 84002.

Schumm, S.A., 1977. The fluvial system.

Seddon, D., 2019. The Climate Controls and Process of Groundwater Recharge in a Semi-Arid Tropical Environment: Evidence from the Makutapora Basin, Tanzania. UCL (University College London).

Seddon, D., Kashaigili, J.J., Taylor, R.G., Cuthbert, M.O., Mihale, L., Mwimbo, C., MacDonald, A.M., 2021a. Groundwater recharge in a dryland environment: evidence from the Makutapora Basin of Tanzania. J. Hydrol. Reg. Stud.

Seddon, D., Kashaigili, J.J., Taylor, R.G., Cuthbert, M.O., Mwihumbo, C., MacDonald, A.M., 2021b. Focused groundwater recharge in a tropical dryland: Empirical evidence from central, semi-arid Tanzania. J. Hydrol. Reg. Stud. 37, 100919.

Séguis, L., Kamagaté, B., Favreau, G., Descloitres, M., Seidel, J.-L., Galle, S., Peugeot, C., Gosset, M., Le Barbé, L., Malinur, F., 2011. Origins of streamflow in a crystalline basement catchment in a sub-humid Sudanian zone: The Donga basin (Benin, West Africa): Inter-annual variability of water budget. J. Hydrol. 402, 1–13.

Senguji, F.H., 1999. Importance of isotope hydrology techniques in water resources management: A case study of the Makutupora basin in Tanzania. Proc. Int. Symp. Isot. Tech. Water Resour. Dev. Manag.

Serrano-Notivoli, R., Martínez-Salvador, A., García-Lorenzo, R., Espín-Sánchez, D., Conesa-García, C., 2022. Rainfall–runoff relationships at event scale in western Mediterranean ephemeral streams. Hydrol. Earth Syst. Sci. 26, 1243–1260.

Serrat-Capdevila, A., Scott, R.L., Shuttleworth, W.J., Valdés, J.B., 2011. Estimating evapotranspiration under warmer climates: Insights from a semi-arid riparian system. J. Hydrol. 399, 1–11.

Shaban, A., Khawlie, M., Abdallah, C., 2006. Use of remote sensing and GIS to determine recharge potential zones: the case of Occidental Lebanon. Hydrogeol. J. 14, 433–443.

Shanafield, M., Bourke, S.A., Zimmer, M.A., Costigan, K.H., 2021. An overview of the hydrology of non-perennial rivers and streams. Wiley Interdiscip. Rev. Water 8, e1504.

Shanafield, M., Cook, P.G., 2014. Transmission losses, infiltration and groundwater recharge through ephemeral and intermittent streambeds: A review of applied methods. J. Hydrol. 511, 518–529. https://doi.org/10.1016/j.jhydrol.2014.01.068

Shanafield, M., Gutiérrez-Jurado, K., White, N., Hatch, M., Keane, R., 2020. Catchment-Scale Characterization of Intermittent Stream Infiltration; a Geophysics Approach. J. Geophys. Res. Earth Surf. 125, e2019JF005330.

Sharon, D., 1972. The spottiness of rainfall in a desert area. J. Hydrol. 17, 161–175.

Shaw, J.R., Cooper, D.J., 2008. Linkages among watersheds, stream reaches, and riparian vegetation in dryland ephemeral stream networks. J. Hydrol. 350, 68–82. https://doi.org/10.1016/J.JHYDROL.2007.11.030

Shaw, J.R., Cooper, D.J., Sutfin, N.A., 2018. Applying a hydrogeomorphic channel classification to understand spatial patterns in riparian vegetation. J. Veg. Sci. 29, 550–559. https://doi.org/10.1111/jvs.12629

Shaw, P.A., Bryant, R.G., 2011. Pans, Playas and Salt Lakes, in: Arid Zone Geomorphology: Process, Form and Change in Drylands. Wiley Blackwell, Faculty of Science and Agriculture, University of the West Indies, St Augustine, Trinidad and Tobago, pp. 373–401. https://doi.org/10.1002/9780470710777.ch15

Shindo, S., 1990. Members of Japan-Tanzania Joint Research Project (1990) and (1994) Study on the recharge mechanism and development of groundwater in the inland area of Tanzania. Prog. Rep. Japan-Tanzania Jt. Res.

Shindo, S., 1989. Study on the recharge mechanism and development of groundwater in the inland area of Tanzania: Interim report of Japan-Tanzania Joint Research, 92p. Unpubl.

Rep.

Simmers, I., 2003. Understanding Water in a Dry Environment: Hydrological Processes in Arid and Semi-arid Zones, International Contributions to Hydrogeology: IAH International Association of Hydrogeologists. Underst. Water a Dry Environ. Hydrol. Process. Arid Semi-Arid Zo.

Simmers, I., 1997. Recharge of Phreatic Aquifers in (Semi-) Arid Areas. Recharg. Phreatic Aquifers Arid Areas.

Singer, M.B., Asfaw, D.T., Rosolem, R., Cuthbert, M.O., Miralles, D.G., MacLeod, D., Quichimbo, E.A., Michaelides, K., 2021. Hourly potential evapotranspiration at 0.1 resolution for the global land surface from 1981-present. Sci. Data 8, 224.

Singer, M.B., Michaelides, K., 2017. Deciphering the expression of climate change within the Lower Colorado River basin by stochastic simulation of convective rainfall. Environ. Res. Lett. 12. https://doi.org/10.1088/1748-9326/aa8e50

Singer, M.B., Michaelides, K., 2014. How is topographic simplicity maintained in ephemeral dryland channels? Geology. https://doi.org/10.1130/G36267.1

Singha, K., 2017. Geophysics Is Not a Silver Bullet, but Worth a Shot. Groundwater 55, 149–149. https://doi.org/10.1111/gwat.12495

Small, E.E., 2005a. Climatic controls on diffuse groundwater recharge in semiarid environments of the southwestern United States. Water Resour. Res. 41.
https://doi.org/10.1029/2004WR003193

Small, E.E., 2005b. Climatic controls on diffuse groundwater recharge in semiarid environments of the southwestern United States. Water Resour. Res. 41.
https://doi.org/10.1029/2004WR003193

Smerdon, B.D., Allen, D.M., Grasby, S.E., Berg, M.A., 2009. An approach for predicting groundwater recharge in mountainous watersheds. J. Hydrol. 365, 156–172.

Somaratne, N., Smettem, K.R.J., 2014. Theory of the generalized chloride mass balance method for recharge estimation in groundwater basins characterised by point and diffuse recharge. Hydrol. Earth Syst. Sci. Discuss. 11, 307–332.

Souissi, D., Msaddek, M.H., Zouhri, L., Chenini, I., El May, M., Dlala, M., 2018. Mapping groundwater recharge potential zones in arid region using GIS and Landsat approaches, southeast Tunisia. Hydrol. Sci. J. 63, 251–268.

Staudinger, M., Stoelzle, M., Seeger, S., Seibert, J., Weiler, M., Stahl, K., 2017. Catchment water storage variation with elevation. Hydrol. Process. 31, 2000–2015.

Stone, A.E.C., Edmunds, W.M., 2012. Sand, salt and water in the Stampriet Basin, Namibia: Calculating unsaturated zone (Kalahari dunefield) recharge using the chloride

mass balance approach. Water SA 38, 367–378.

Stonestrom, D.A., Harrill, J.R., 2007. Ground-water recharge in the arid and semiarid southwestern United States: climatic and geologic framework. US Geological Survey.

Stoops, G., Marcelino, V., Mees, F., 2018. Interpretation of micromorphological features of soils and regoliths. Elsevier.

Stringer, L.C., Mirzabaev, A., Benjaminsen, T.A., Harris, R.M.B., Jafari, M., Lissner, T.K., Stevens, N., Tirado-von Der Pahlen, C., 2021. Climate change impacts on water security in global drylands. One Earth 4, 851–864.

Stromberg, J.C., Merritt, D.M., 2016. Riparian plant guilds of ephemeral, intermittent and perennial rivers. Freshw. Biol. 61, 1259–1275. https://doi.org/10.1111/fwb.12686

Sultan, M., Sturchio, N.C., Gheith, H., Hady, Y.A., El Anbeawy, M., 2000. Chemical and isotopic constraints on the origin of Wadi El-Tarfa ground water, eastern desert, Egypt. Groundwater 38, 743–751.

Sun, Q., Miao, C., Duan, Q., Ashouri, H., Sorooshian, S., Hsu, K., 2018. A review of global precipitation data sets: Data sources, estimation, and intercomparisons. Rev. Geophys. 56, 79–107.

Sutfin, N.A., Shaw, J., Wohl, E.E., Cooper, D., 2014a. A geomorphic classification of ephemeral channels in a mountainous, arid region, southwestern Arizona, USA. Geomorphology 221, 164–175. https://doi.org/10.1016/j.geomorph.2014.06.005

Sutfin, N.A., Shaw, J.R., Wohl, E.E., Cooper, D.J., 2014b. A geomorphic classification of ephemeral channels in a mountainous, arid region, southwestern Arizona, USA. Geomorphology 221, 164–175. https://doi.org/10.1016/j.geomorph.2014.06.005

Taboada, T., Garcia, C., 1999. Smectite formation produced by weathering in a coarse granite saprolite in Galicia (NW Spain). Catena 35, 281–290.

Taniguchi, M., 1997. Subsurface water responses to land cover/use changes: an overview. Subsurf. Hydrol. responses to L. Cover L. use Chang. 1–20.

Tao, Z., Li, H., Neil, E., Si, B., 2021. Groundwater recharge in hillslopes on the Chinese Loess Plateau. J. Hydrol. Reg. Stud. 36, 100840.

Taucare, M., Daniele, L., Viguier, B., Vallejos, A., Arancibia, G., 2020. Groundwater resources and recharge processes in the Western Andean Front of Central Chile. Sci. Total Environ. 722, 137824.

Taylor, G., Eggleton, R.A., 2001. No Title. Regolith Geol. Geomorphol.

Taylor, R., 2014. When wells run dry. Nature 516, 179–180. https://doi.org/10.1038/516179a

Taylor, R., Tindimugaya, C., 2011. The impacts of climate change and rapid development on weathered crystalline rock aquifer systems in the humid tropics of sub- Saharan Africa: Evidence from south- western Uganda, Climate Change Effects on Groundwater Resources: A Global Synthesis of Findings and Recommendations. CRC Press.

Taylor, R.G., Howard, K.W.F., 1999. Lithological evidence for the evolution of weathered mantles in Uganda by tectonically controlled cycles of deep weathering and stripping. Catena 35, 65–94.

Taylor, R.G., Koussis, A.D., Tindimuguya, C., 2009. Groundwater and climate in Africa - A review. Hydrol. Sci. J. 54, 655–664. https://doi.org/10.1623/hysj.54.4.655

Taylor, R.G., Scanlon, B., Döll, P., Rodell, M., van Beek, R., Wada, Y., Longuevergne, L., Leblanc, M., Famiglietti, J.S., Edmunds, M., Konikow, L., Green, T.R., Chen, J., Taniguchi, M., Bierkens, M.F.P., MacDonald, A., Fan, Y., Maxwell, R.M., Yechieli, Y., Gurdak, J.J., Allen, D.M., Shamsudduha, M., Hiscock, K., Yeh, P.J.-F., Holman, I., Treidel, H., 2013a. Ground water and climate change. Nat. Clim. Chang. 3, 322–329. https://doi.org/10.1038/nclimate1744

Taylor, R.G., Todd, M.C., Kongola, L., Maurice, L., Nahozya, E., Sanga, H., MacDonald, A.M., 2013b. Evidence of the dependence of groundwater resources on extreme rainfall in East Africa. Nat. Clim. Chang. 3, 374–378. https://doi.org/10.1038/nclimate1731

Telvari, A., Cordery, I., Pilgrim, D., 1998. Relations between transmission losses and bed alluvium in an Australian arid zone stream. Hydrol. Chang. Environ. 2, 361–366.

Theis, C. V, 1940. The source of water derived from wells: Essential factors controlling the response of an aquifer to development. Civ. Eng. 10, 277–280.

Thomas, B.F., Behrangi, A., Famiglietti, J.S., 2016. Precipitation intensity effects on groundwater recharge in the southwestern United States. Water 8, 90.

Thomas, D.S.G., 2011. Arid zone geomorphology: process, form and change in drylands. John Wiley & Sons.

Thompson, J., Porras, I.T., Wood, E., Tumwine, J.K., Mujwahuzi, M.R., Katui-Katua, M., Johnstone, N., 2000. Waiting at the tap: changes in urban water use in East Africa over three decades. Environ. Urban. 12, 37–52.

Timms, W., Whelan, M., Acworth, I., McGeeney, D., Bouzalakos, S., Crane, R., McCartney, J., Hartland, A., 2019. A novel centrifuge permeameter to characterize flow through low permeability strata, in: ICPMG2014-Physical Modelling in Geotechnics: Proceedings of the 8th International Conference on Physical Modelling in Geotechnics 2014 (ICPMG2014), Perth, Australia, 14-17 January 2014. p. 193.

Timms, W.A., Acworth, R.I., Crane, R.A., Arns, C.H., Arns, J.-Y., McGeeney, D.E., Rau, G.C., Cuthbert, M.O., 2018. The influence of syndepositional macropores on the

hydraulic integrity of thick alluvial clay aquitards. Water Resour. Res. 54, 3122–3138.

Tooth, S., 2012. Arid geomorphology: Changing perspectives on timescales of change. Prog. Phys. Geogr. 36, 262–284. https://doi.org/10.1177/0309133311417943

Tooth, S.S., Nanson, G.C., 2011. Distinctiveness and Diversity of Arid Zone River Systems, in: Arid Zone Geomorphology: Process, Form and Change in Drylands. Wiley Blackwell, Institute of Geography and Earth Sciences, Aberystwyth University, Penglais Campus, Aberystwyth, SY23 3DB, United Kingdom, pp. 269–300.
https://doi.org/10.1002/9780470710777.ch12

Turner, R.J., Mansour, M.M., Dearden, R., Dochartaigh, B.É.Ó., Hughes, A.G., 2015. Improved understanding of groundwater flow in complex superficial deposits using three-dimensional geological-framework and groundwater models: an example from Glasgow, Scotland (UK). Hydrogeol. J. 23, 493–506.

UN, 2017. United Nations 2010-2020 Decade for Deserts and the Fight Against Desertification.

Villeneuve, S., Cook, P.G., Shanafield, M., Wood, C., White, N., 2015. Groundwater recharge via infiltration through an ephemeral riverbed, central Australia. J. Arid Environ. 117, 47–58. https://doi.org/10.1016/j.jaridenv.2015.02.009

Villholth, K.G., 2013. Groundwater irrigation for smallholders in Sub-Saharan Africa–a synthesis of current knowledge to guide sustainable outcomes. Water Int. 38, 369–391.

Vivoni, E.R., Aragón, C.A., Malczynski, L., Tidwell, V.C., 2009. Semiarid watershed response in central New Mexico and its sensitivity to climate variability and change. Hydrol. Earth Syst. Sci. 13, 715–733.

Vogel, J.C., Van Urk, H., 1975. Isotopic composition of groundwater in semi-arid regions of southern Africa. J. Hydrol. 25, 23–36. https://doi.org/10.1016/0022-1694(75)90036-0

Wada, Y., van Beek, L.P.H., van Kempen, C.M., Reckman, J.W.T.M., Vasak, S., Bierkens, M.F.P., 2010. Global depletion of groundwater resources. Geophys. Res. Lett. 37, n/a-n/a. https://doi.org/10.1029/2010GL044571

Wada, Y., van Beek, L.P.H., Wanders, N., Bierkens, M.F.P., 2013. Human water consumption intensifies hydrological drought worldwide. Environ. Res. Lett. 8, 034036. https://doi.org/10.1088/1748-9326/8/3/034036

Wade, F.B., Oates, F., 1938. An Explanation of Degree Sheet No. 52 (Dodoma). Short Pap. 17, 52_60.

Wakindiki, I.I.C., Ben-Hur, M., 2002. Soil mineralogy and texture effects on crust micromorphology, infiltration, and erosion. Soil Sci. Soc. Am. J. 66, 897–905.

Wallace, D.E., Renard, K.G., 1967. Contribution to regional water table from transmission losses of ephemeral streambeds. Trans Amer Soc Agr Eng, 10, 786–789.

Walling, D.E., 1983. The sediment delivery problem. J. Hydrol. 65, 209–237.

Walvoord, M.A., Stonestrom, D.A., Andraski, B.J., Striegl, R.G., 2004. Constraining the inferred paleohydrologic evolution of a deep unsaturated zone in the Amargosa Desert. Vadose Zo. J. 3, 502–512. https://doi.org/10.2113/3.2.502

Wang, P., Pozdniakov, S.P., Vasilevskiy, P.Y., 2017. Estimating groundwater-ephemeral stream exchange in hyper-arid environments: Field experiments and numerical simulations. J. Hydrol. 555, 68–79. https://doi.org/10.1016/j.jhydrol.2017.10.004

Wanke, H., Dünkeloh, A., Udluft, P., 2008. Groundwater recharge assessment for the Kalahari catchment of north-eastern Namibia and north-western Botswana with a regional-scale water balance model. Water Resour. Manag. 22, 1143–1158.

Warter, M.M., Singer, M.B., Cuthbert, M.O., Roberts, D., Caylor, K.K., Sabathier, R., Stella, J., 2021. Drought onset and propagation into soil moisture and grassland vegetation responses during the 2012–2019 major drought in Southern California. Hydrol. Earth Syst. Sci. 25, 3713–3729.

Wekesa, S.S., Stigter, T.Y., Olang, L.O., Oloo, F., Fouchy, K., McClain, M.E., 2020. Water Flow Behavior and Storage Potential of the Semi-Arid Ephemeral River System in the Mara Basin of Kenya. Front. Environ. Sci. 95.

West, C., Reinecke, R., Rosolem, R., MacDonald, A.M., Cuthbert, M.O., Wagener, T., 2023. Ground truthing global-scale model estimates of groundwater recharge across Africa. Sci. Total Environ. 858, 159765.

West, C., Rosolem, R., MacDonald, A.M., Cuthbert, M.O., Wagener, T., 2022. Understanding process controls on groundwater recharge variability across Africa through Recharge Landscapes. J. Hydrol. 127967.

Wheater, H., 2008. Modelling hydrological processes in arid and semi-arid areas: An introduction. Hydrol. Model. Arid Semi-Arid Areas 1–20.

Wheater, H., Sorooshian, S., Sharma, K.D., 2007. Hydrological modelling in arid and semi-arid areas, Hydrological Modelling in Arid and Semi-Arid Areas.
https://doi.org/10.1017/CBO9780511535734

Wheater, H., Sorooshian, S., Sharma, K.D. (Kapil D., 2008. Hydrological modelling in arid and semi-arid areas. Cambridge University Press.

Wilson, J.L., Guan, H., 2004. Mountain-block hydrology and mountain-front recharge. pp. 113–137. https://doi.org/10.1029/009WSA08

Winter, T.C., 1999. Relation of streams, lakes, and wetlands to groundwater flow systems. Hydrogeol. J. 7, 28–45. https://doi.org/10.1007/s100400050178

WMO, 2020. World Weather Information Service [WWW Document]. URL http://worldweather.wmo.int/en/city.html?cityId=667

Wright, E.P., Burgess, W.G., 1992. The hydrogeology of crystalline basement aquifers in Africa. Hydrogeol. Cryst. basement aquifers Africa.

Xiao, Y., Liu, K., Yan, H., Zhou, B., Huang, X., Hao, Q., Zhang, Yuqing, Zhang, Yunhui, Liao, X., Yin, S., 2021. Hydrogeochemical constraints on groundwater resource sustainable development in the arid Golmud alluvial fan plain on Tibetan plateau. Environ. Earth Sci. 80, 1–17.

Xu, Y., Beekman, H.E., 2019. Groundwater recharge estimation in arid and semi-arid southern Africa. Hydrogeol. J. 27, 929–943.

Xu, Y., Seward, P., Gaye, C., Lin, L., Olago, D.O., 2019. Preface: groundwater in sub-Saharan Africa. Hydrogeol. J. 27, 815–822.

Yair, A., Kossovsky, A., 2002. Climate and surface properties: hydrological response of small arid and semi-arid watersheds. Geomorphology 42, 43–57. https://doi.org/10.1016/S0169-555X(01)00072-1

Yair, A., Sharon, D., Lavee, H., 1978. An instrumented watershed for the study of partial area contribution of runoff in the arid zone. Z. Geomorphol. Suppl. 29, 71–82.

Yeh, H.-F., Lee, C.-H., Hsu, K.-C., Chang, P.-H., 2009. GIS for the assessment of the groundwater recharge potential zone. Environ. Geol. 58, 185–195.

Youberg, A.D., Guertin, D.P., Ball, G.L., 1998. Developing Stream Watershed Relationships for Selecting Reference Site Characteristics Using ARC/INFO, in: Proceedings of the 1998 ESRI User Conference by the Environmental Systems Research Institute, Redlands, CA.

Yu, S., Bond, N.R., Bunn, S.E., Kennard, M.J., 2019. Development and application of predictive models of surface water extent to identify aquatic refuges in eastern Australian temporary stream networks. Water Resour. Res. 55, 9639–9655.

Zarate, E., Hobley, D., MacDonald, A.M., Swift, R.T., Chambers, J., Kashaigili, J.J., Mutayoba, E., Taylor, R.G., Cuthbert, M.O., 2021. The role of superficial geology in controlling groundwater recharge in the weathered crystalline basement of semi-arid Tanzania. J. Hydrol. Reg. Stud. 36, 100833.

Zoccatelli, D., Marra, F., Armon, M., Rinat, Y., Smith, J.A., Morin, E., 2019. Contrasting rainfall-runoff characteristics of floods in desert and Mediterranean basins. Hydrol. Earth Syst. Sci. 23, 2665–2678.

Appendix A

Appendix

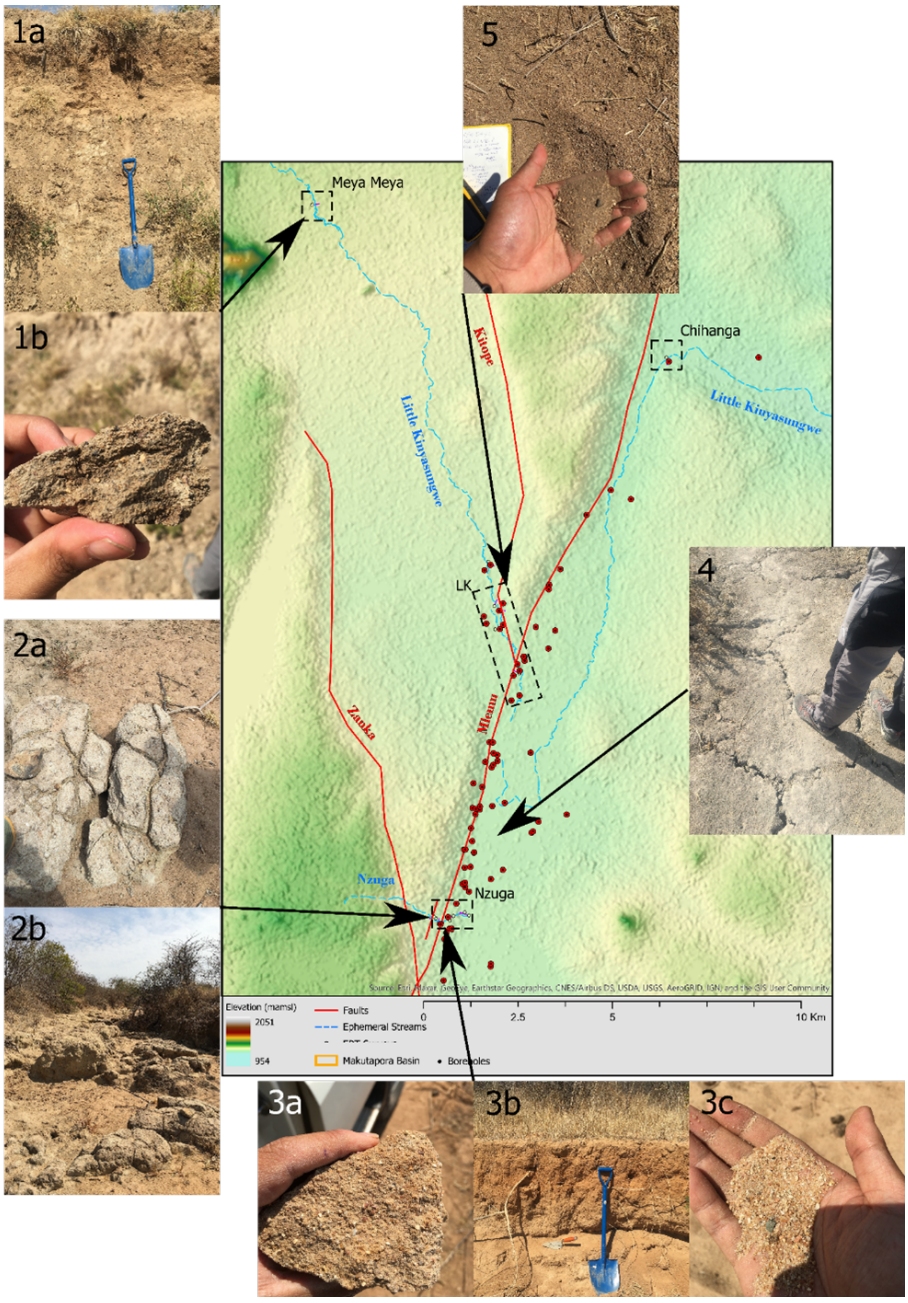

Fig. A.1 Pictures of observed outcrops at study sites. 1a) Streambed at Meya Meya 1b) Lithology of bedrock Meya Meya 2a) Weathered bedrock outcropping within Nzuga streambed at fault 2b) Fault zone with Nzuga streambed 3a) Lithology of bedrock, middle Nzuga 3b) Silt – Pedolith interface in Nzuga streambed 3c) Coarse sand within Nzuga 4) Cracked and desiccated Mbuga clay within lowlands 5) Sands within Little Kinyasungwe river at LK site

Fig. A.2 Flood discharge observed at Chihanga stream gauge (left side) in the Makutapora Basin of Tanzania on 4th April 2016 during the 2015-16 El Niño event

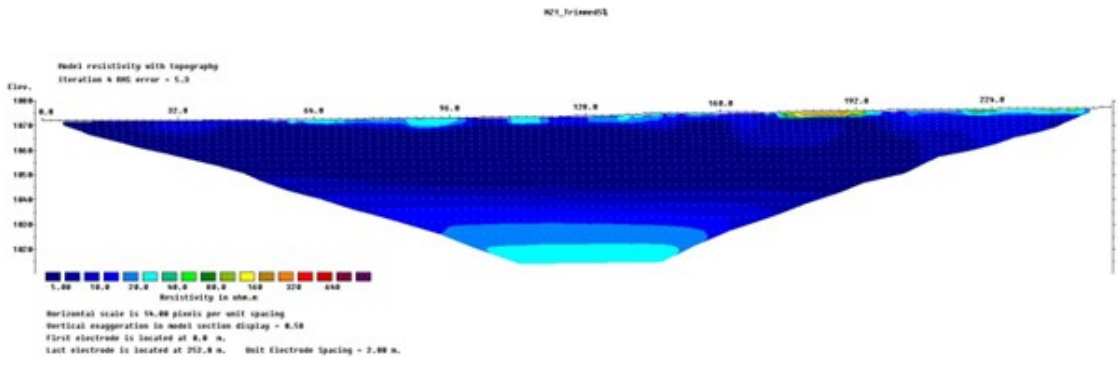

Fig. A.3 Nzuga 1 ERT Pseudosection

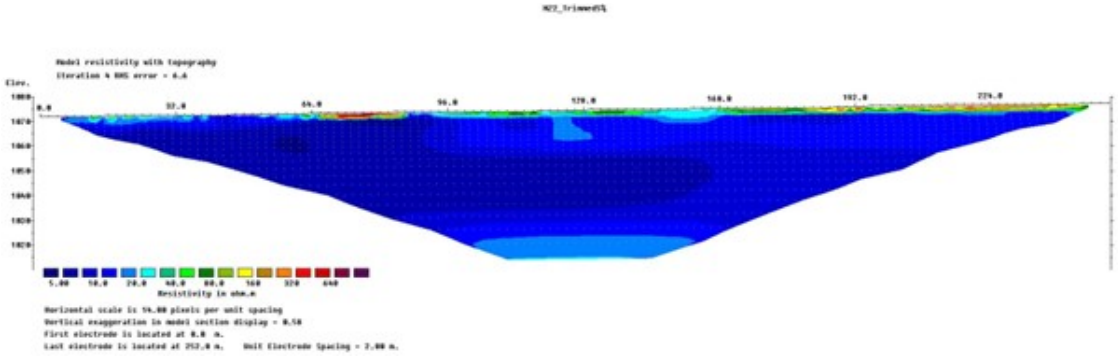

Fig. A.4 Nzuga 2 ERT Pseudosection

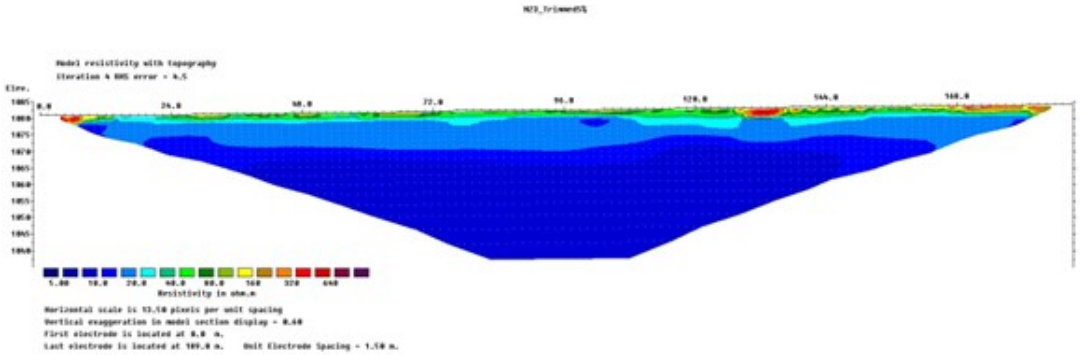

Fig. A.5 Nzuga 3 ERT Pseudosection

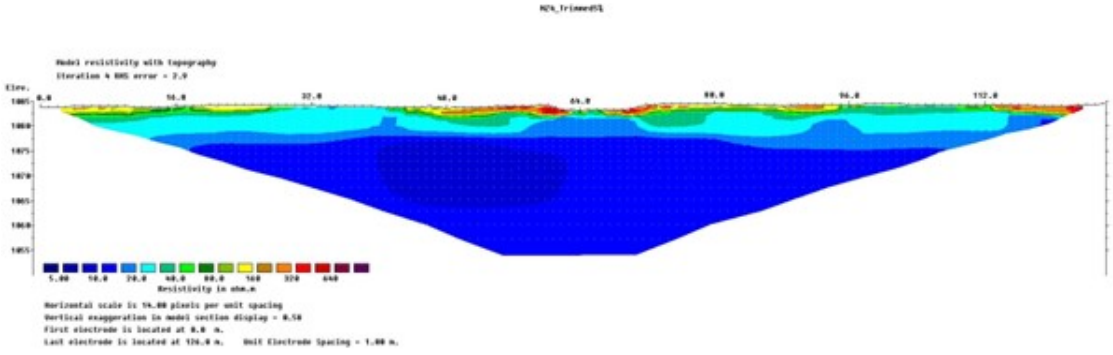

Fig. A.6 Nzuga 4 ERT Pseudosection

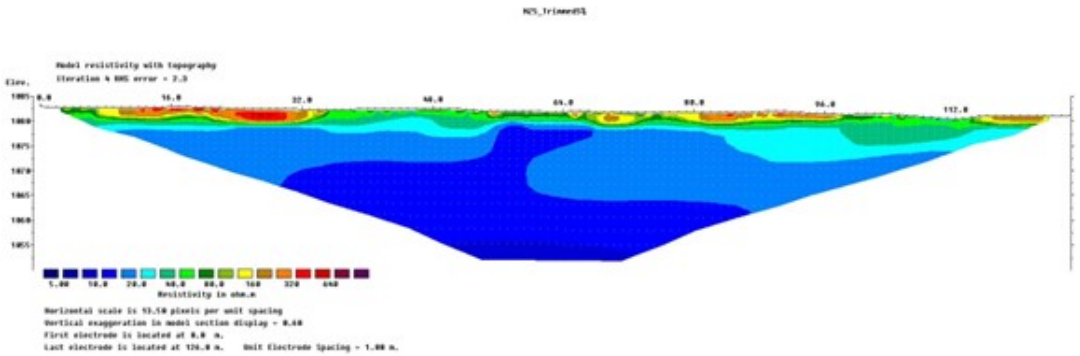

Fig. A.7 Nzuga 5 ERT Pseudosection

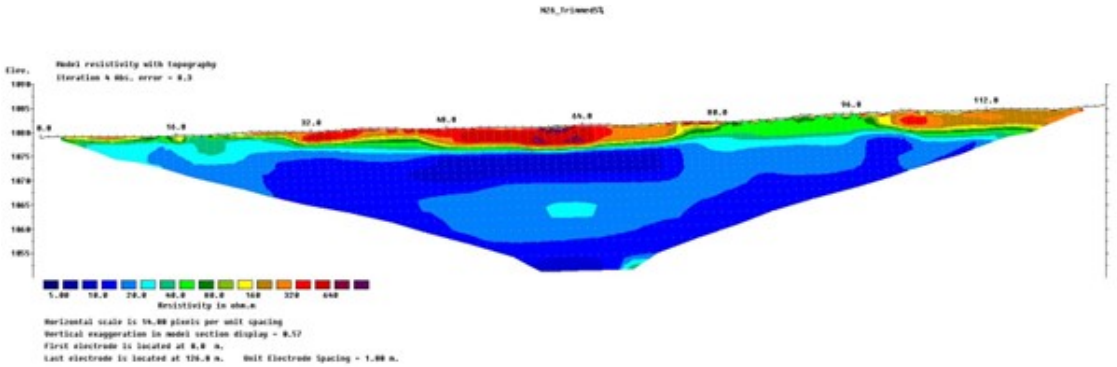

Fig. A.8 Nzuga 6 ERT Pseudosection

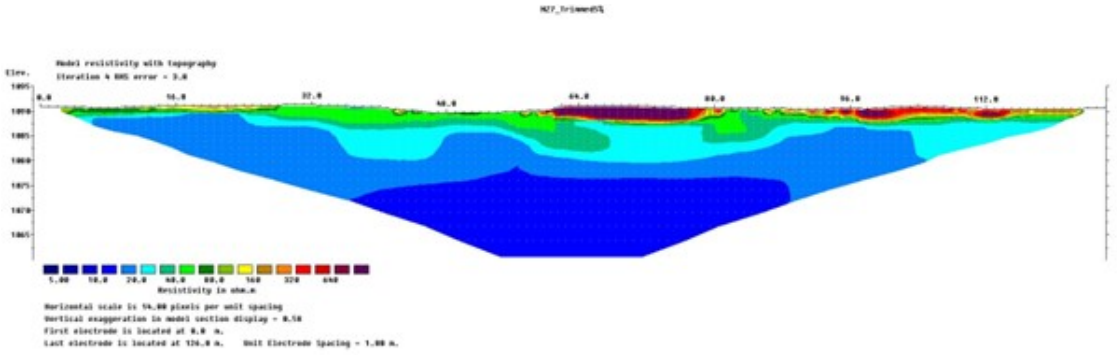

Fig. A.9 Nzuga 7 ERT Pseudosection

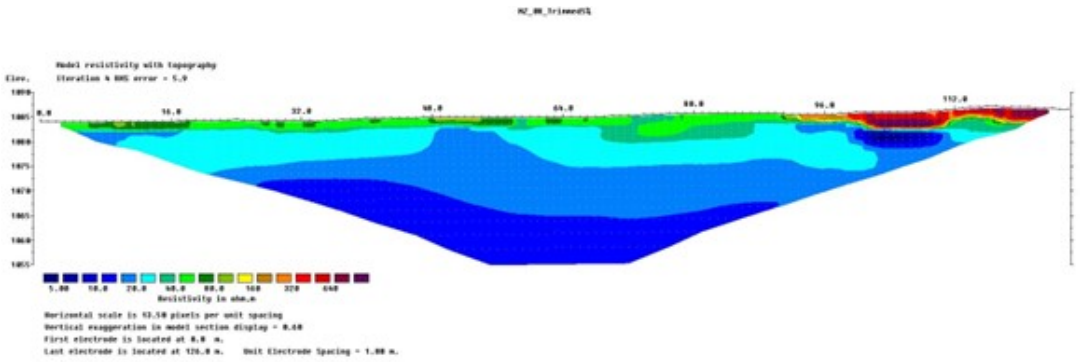

Fig. A.10 Nzuga 8 ERT Pseudosection

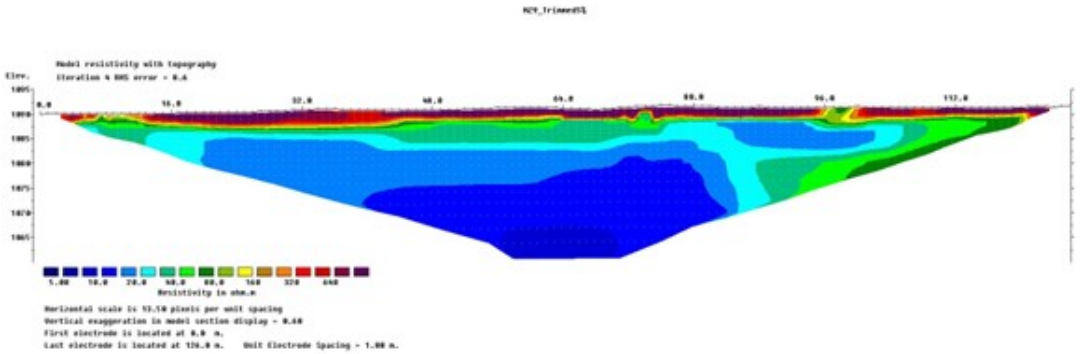

Fig. A.11 Nzuga 9 ERT Pseudosection

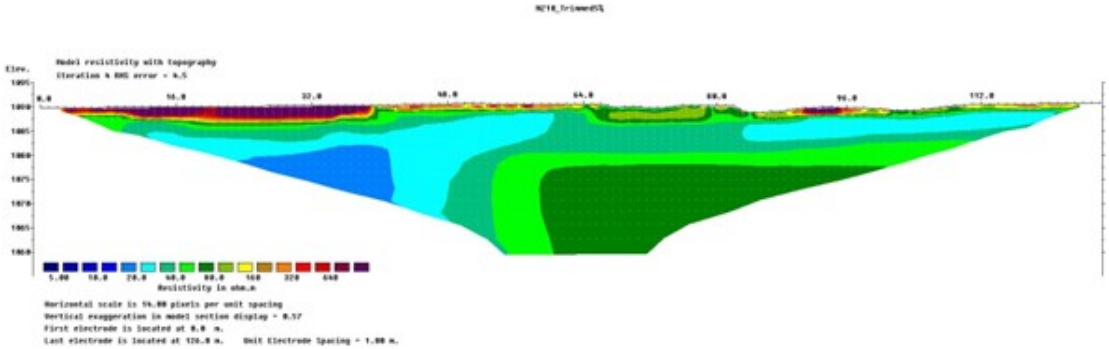

Fig. A.12 Nzuga 10 ERT Pseudosection

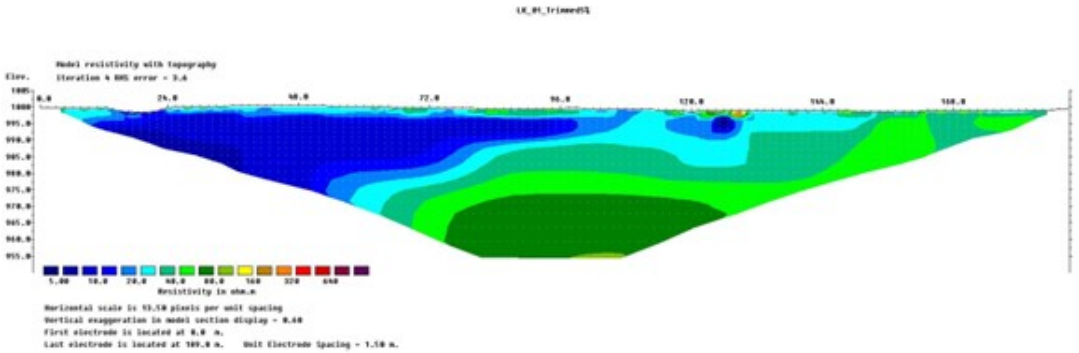

Fig. A.13 LK 1 ERT Pseudosection

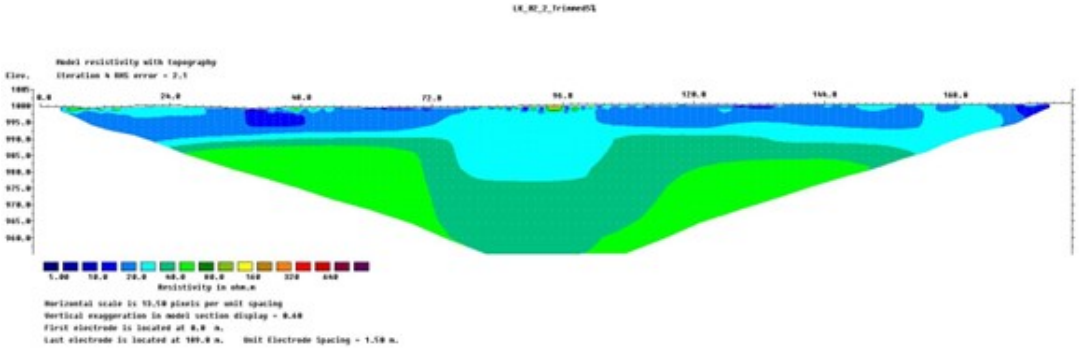

Fig. A.14 LK 2 ERT Pseudosection

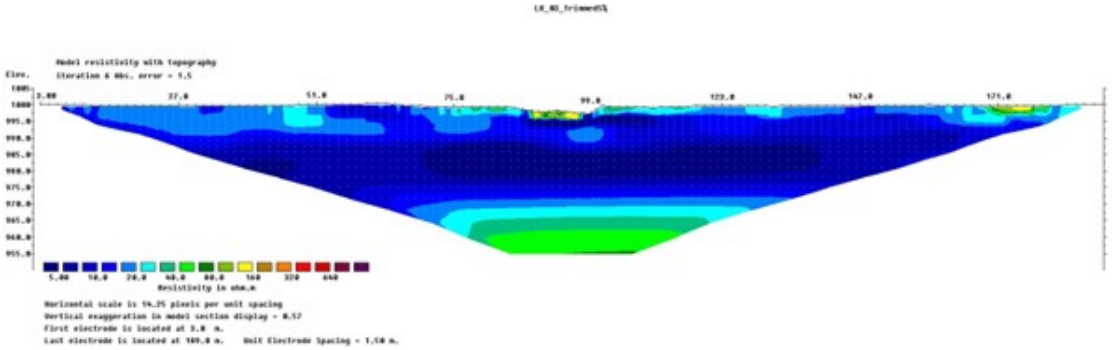

Fig. A.15 LK 3 ERT Pseudosection

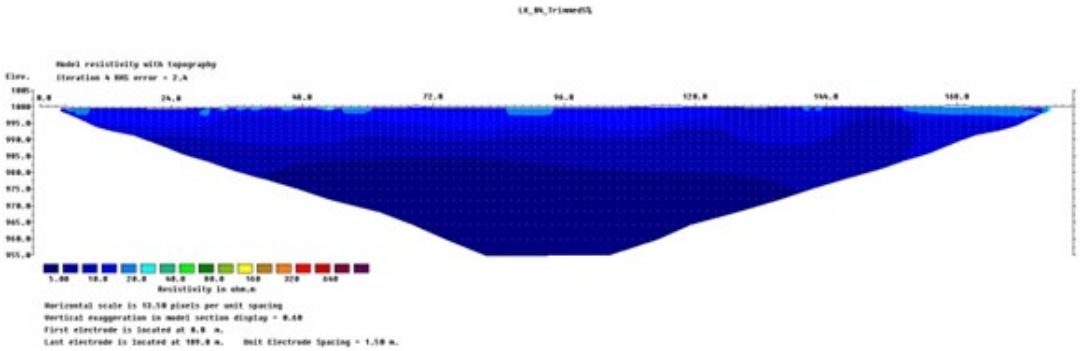

Fig. A.16 LK 4 ERT Pseudosection

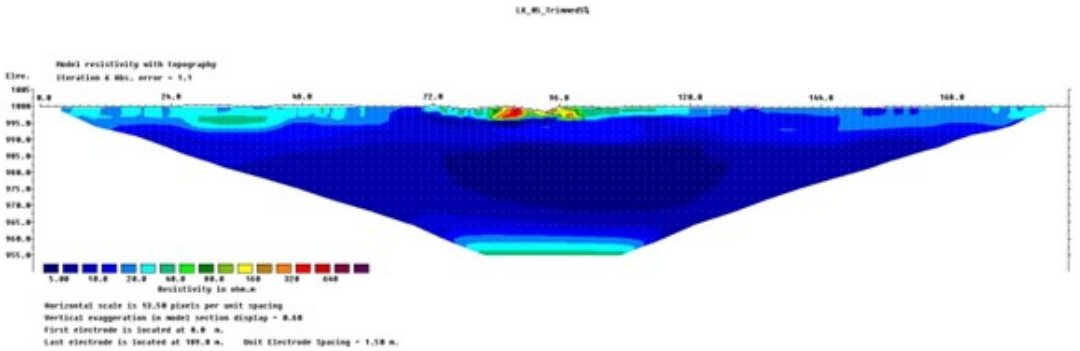

Fig. A.17 LK 5 ERT Pseudosection

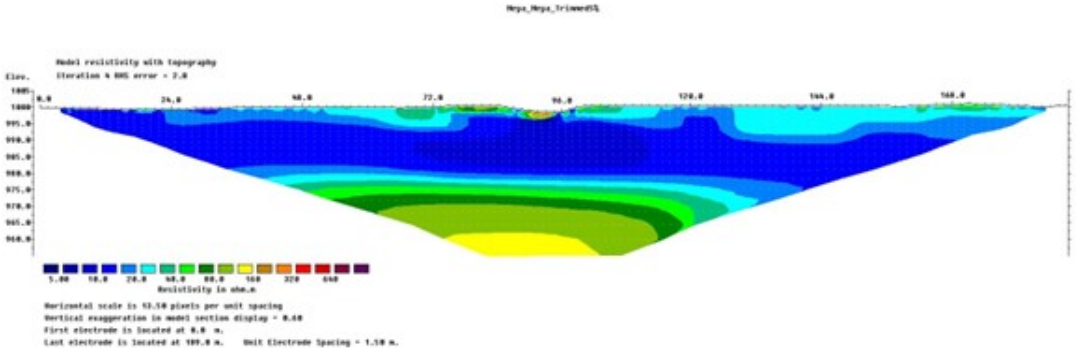

Fig. A.18 Meya Meya ERT Pseudosection

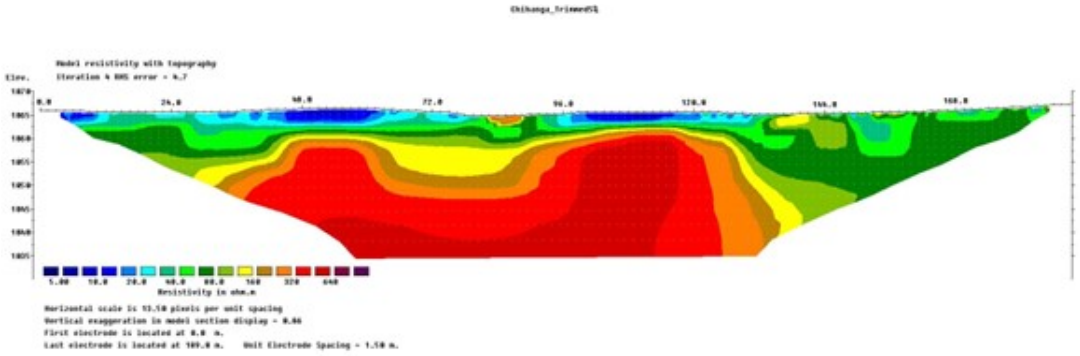

Fig. A.19 Chihanga ERT Pseudosection

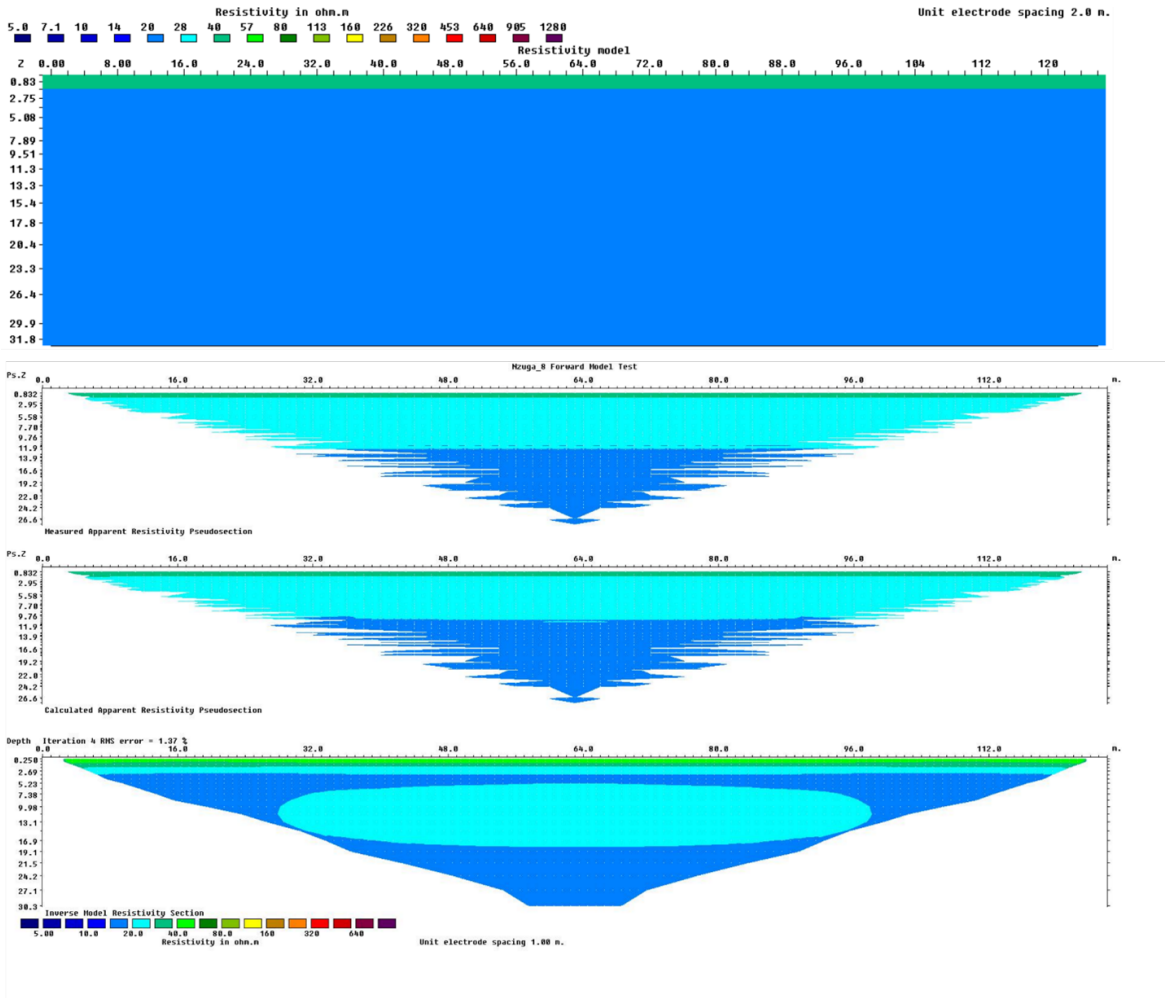

Fig. A.20 Synthetic results of simplified two layer model

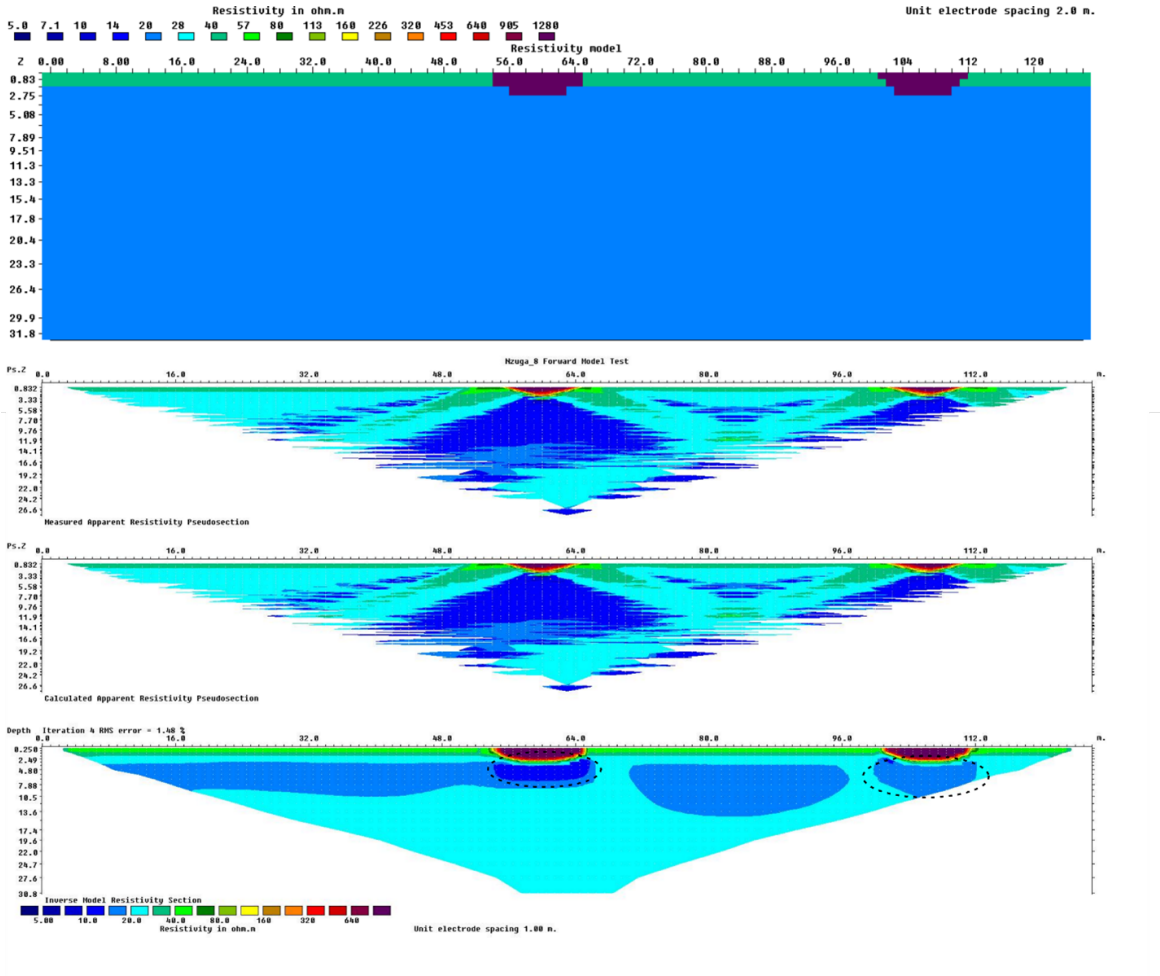

Fig. A.21 Synthetic results of two layer model with high (>1000 ω m) resistivity features surrounded by lower resistivity material. Anomalous low resistivity features beneath high resistivity features can be seen circled in black.

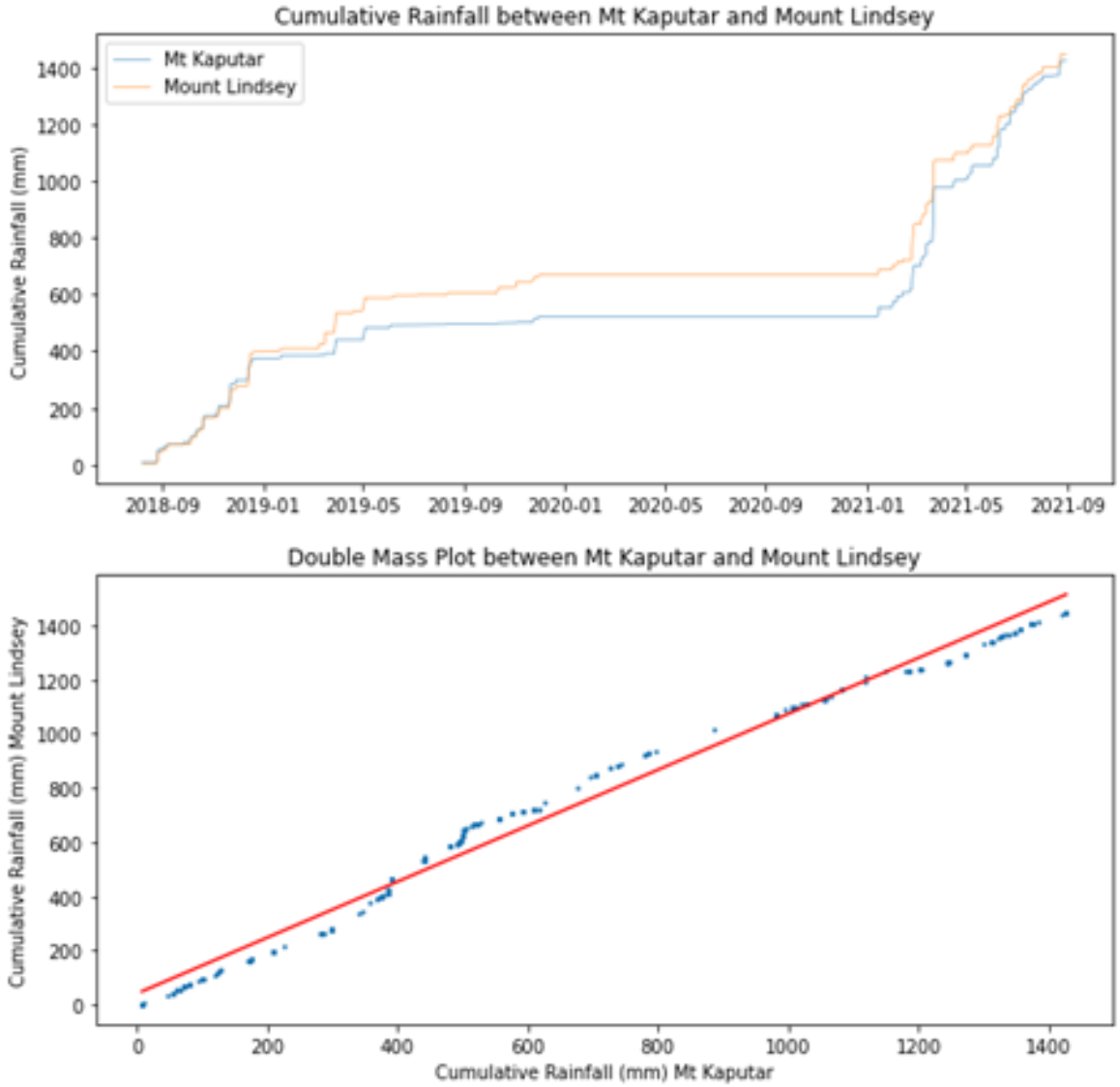

Fig. A.22 Cumulative Rainfall (mm) time series and double mass plot between Mt Kaputar and Mt Lindesay. Pearson coeff = 0.9922, gradient of best fit line = 1.03

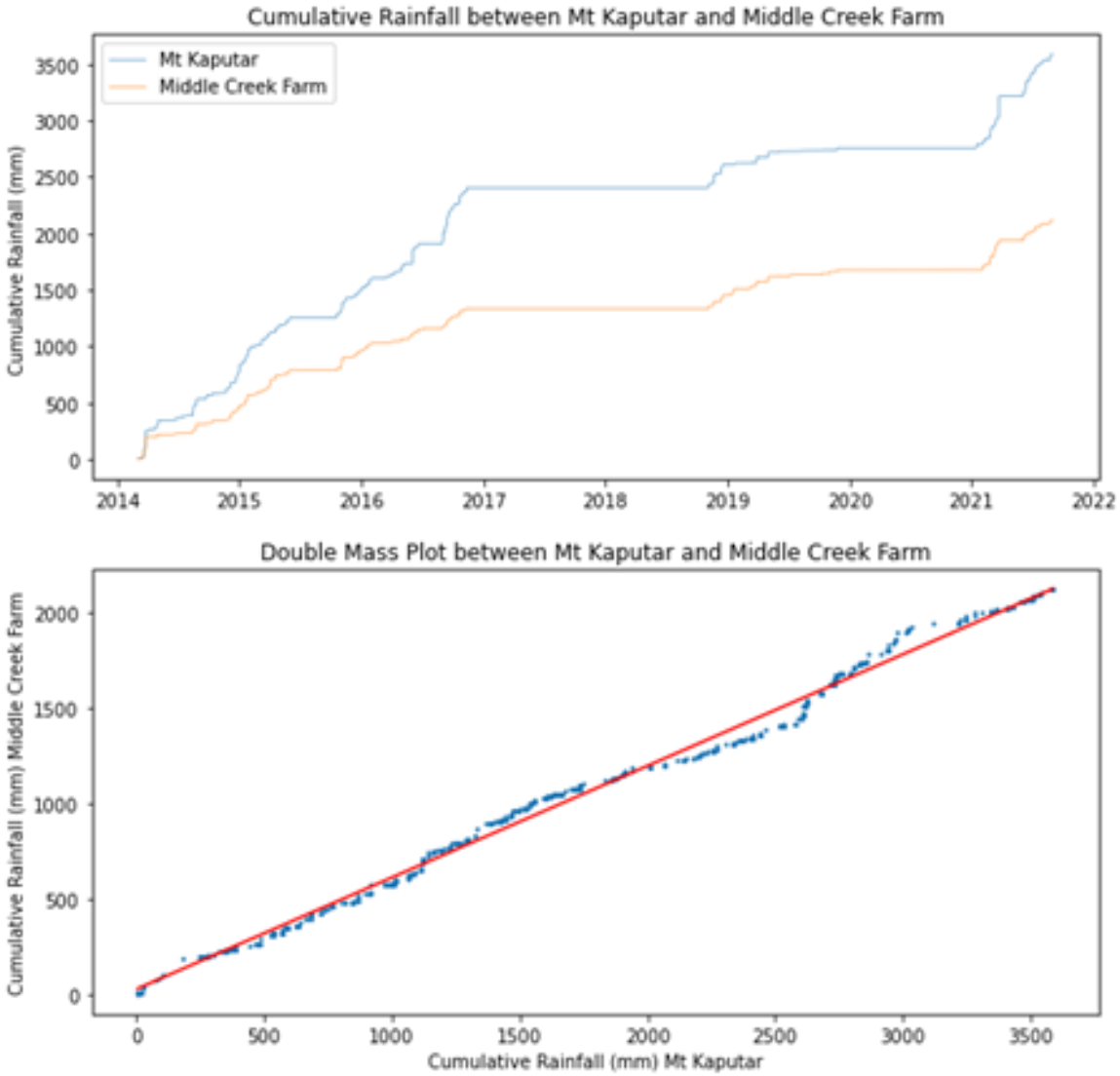

Fig. A.23 Cumulative Rainfall (mm) time series and double mass plot between Mt Kaputar and Middle Creek Farm.. Pearson coeff = 0.9966, gradient of best fit line = 0.58

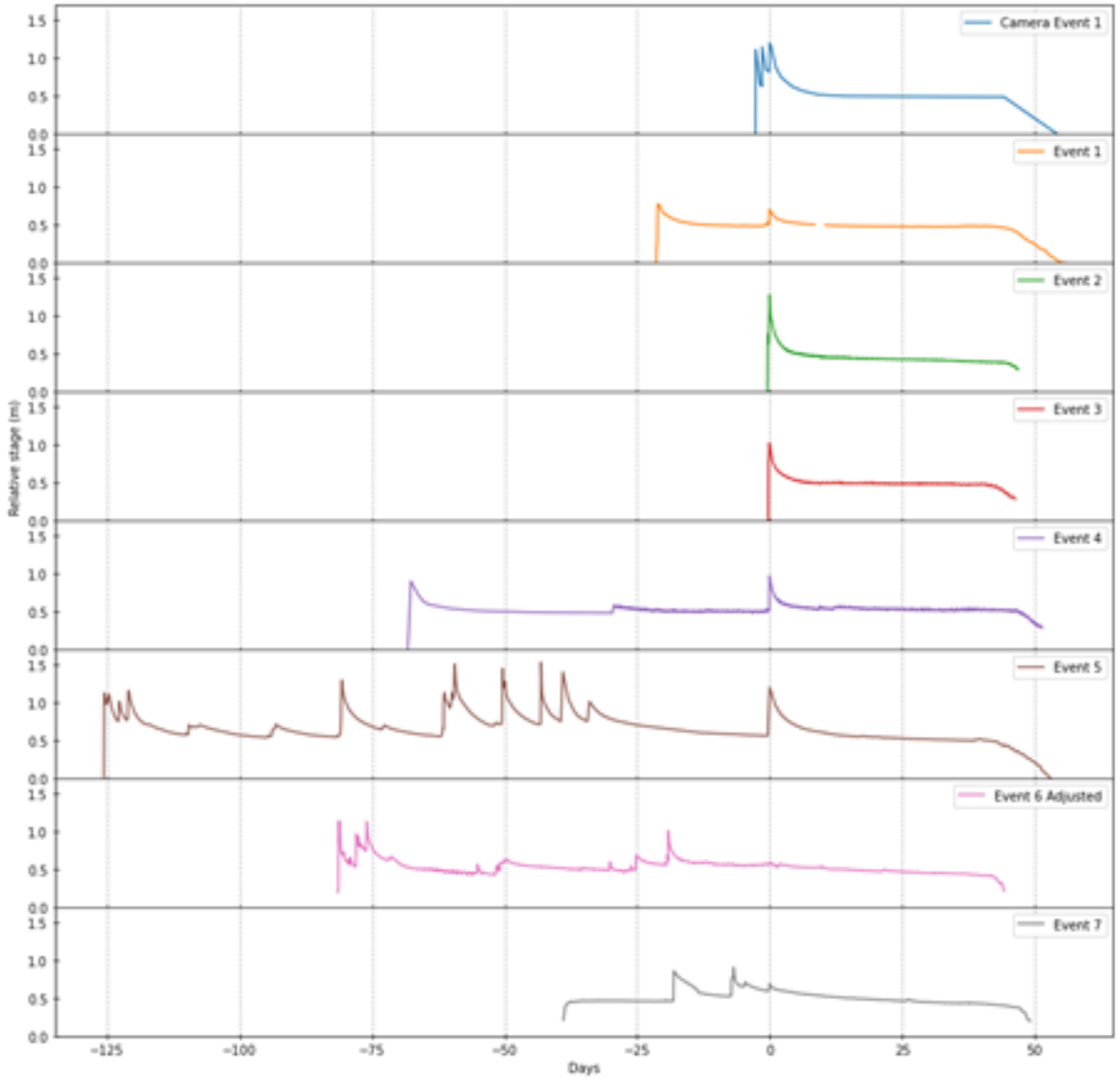

Fig. A.24 Figure S3: Streamflow events at East Lynne. Days normalised from peak of last flow event. Plot shows many events are composite events comprised of multiple runoff events in the stream.

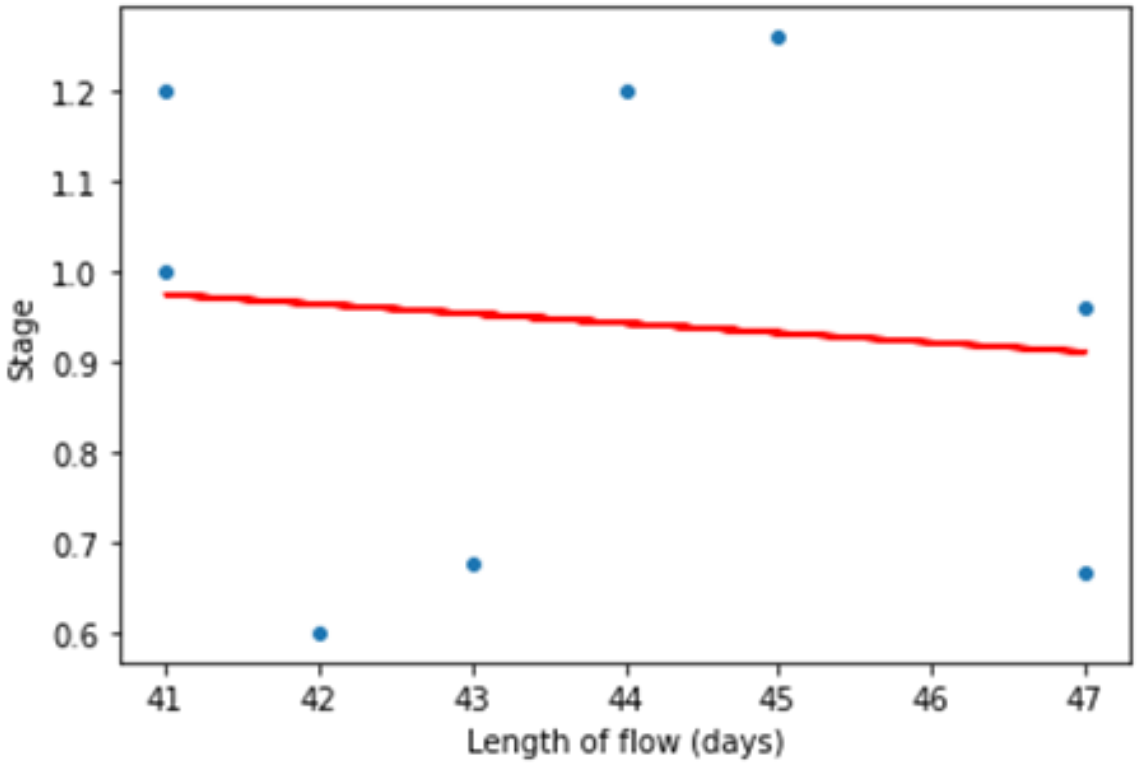

Fig. A.25 Relationship between length of flow (Days) and stream stage for flow events at East Lynne (blue dots). Red line is line of best fit, with pearson coeff of -0.1, showing little or no correlation between stream stage and length of flow

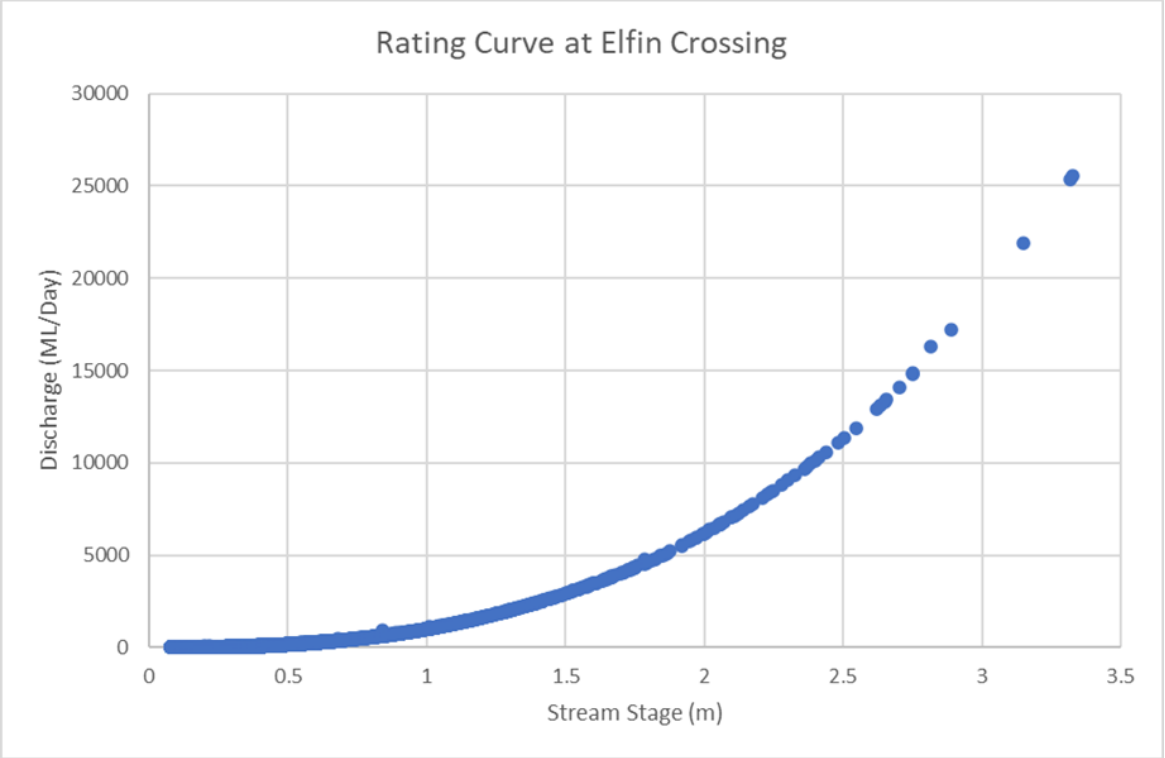

Fig. A.26 Rating Curve at Elfin Crossing

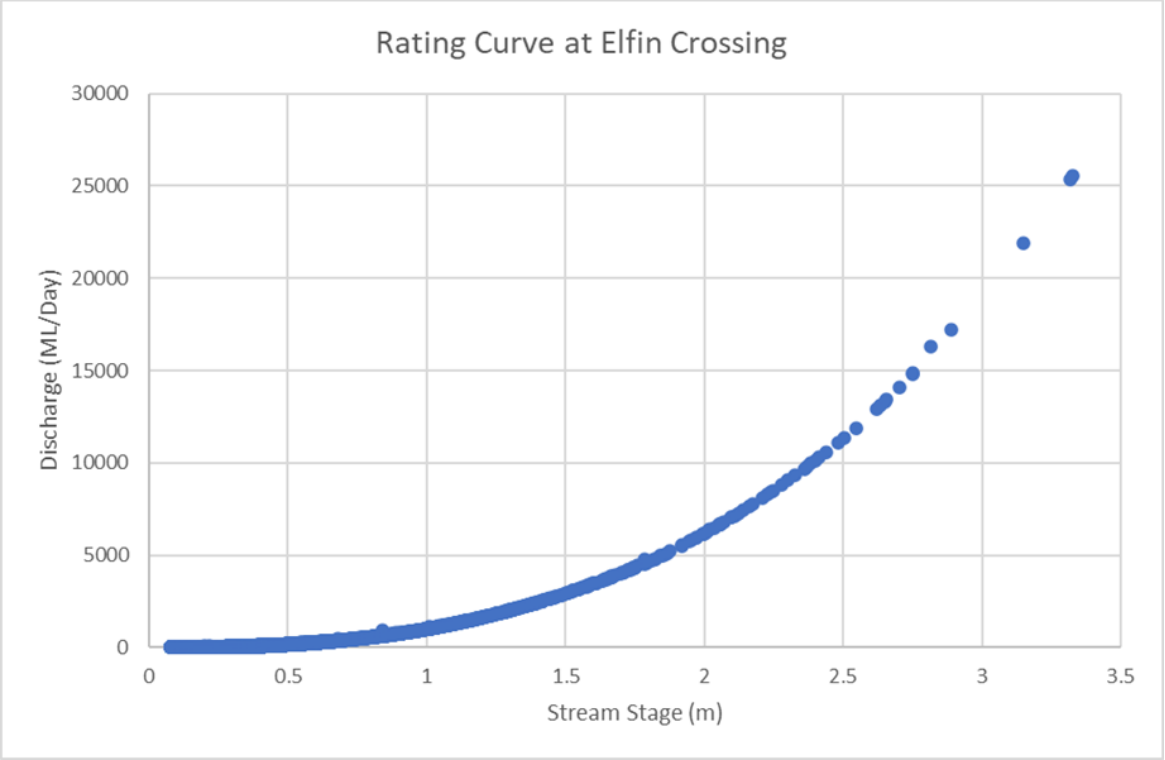

Fig. A.27 An example of typical mass balance and cumulative volumes of model runs in Chapter 5.

Borehole	Start (m)	Finish (m)	Lithology (as written on report)	Interpretation	Water Level (metres below ground level)
147/75	0	4.624 2074	Mbuga Clay	Clay	
147/75	4.624207	27.745244	Calcrete	Upper Pedolith	
147/75	27.74524	35.259581	Sand Gravel	Lower Pedolith	
147/75	35.25958	85.548594	Weathered Granite	Weathered Granite	
193/75	0	9.0766196	Silt	Silt	
193/75	9.07662	17.314923	Clay	Clay	
193/75	17.31492	25.528571	Sand	Upper Pedolith	
193/75	25.52857	35.662331	Sand Gravel	Lower Pedolith	39.624
193/75	35.66233	91.968193	Weathered Granite	Weathered Granite	
C12	0	45	Clay	Clay	
C12	45	52	Calcrete	Pedolith	
C12	52	79	Weathered Granite	Weathered Granite	
C12	79	131.22	Basement Granite	Basement Granite	
207/75	0	11.0298	Mbuga Clay	Mbuga Clay	
207/75	11.0298	23.801148	Clay	Clay	
207/75	23.80115	40.636106	Calcrete	Upper Pedolith	
207/75	40.63611	58.053101	Sand Gravel	Lower Pedolith	30
207/75	58.0531	77.789877	Weathered Granite	Weathered Granite	
207/75	77.78988	116.10544	Basement Granite	Basement Granite	
Mchemwa	0	1	Top soils	Silt	
Mchemwa	2	3	Laterite	Pedolith	
Mchemwa	3	64	Weathered Granite	Weathered Granite	
Mchemwa	64	100	Basement Granite	Basement Granite	
31/53	0	3	mbugaclay	Clay	
31/53	3	6	Claycrete	Pedolith	
31/53	6	50	Weathered alaskite	Weathered Granite	
35/53	0	12	mbugaclay	Clay	
35/53	12	24	Calcrete	Pedolith	
35/53	24	35	Decomposed Mica gneiss	Saprolite	
35/53	35	43	Weathered Gneiss	Weathered Granite	
35/53	43	65	Hornblend-biotite granite	Basement Granite	
142/76	0	8	Silt Clay	Silt	
142/76	8	57	Clay with silt	Clay	30
142/76	57	71.3	Silt with clay	Pedolith	
142/76	71.3	91.67	Clay and gravel	Saprolite	
142/76	91.67	101.68	Weathered diorite	Weathered Granite	
142/76	101.68	122.4	Diorite	Basement Granite	
94/78	0	10	Sand Clay	Pedolith	
94/78	10	40	Sand and Limestone	Saprolite	28.85
94/78	40	75	Weathered Granite	Weathered Granite	
94/78	75	140	Basement Granite	Basement Granite	
4/54	0	4	Claycrete and sandy soil	Pedolith	
4/54	4	43	Weathered granite and alaskite	Weathered Granite	36
4/54	43	53	alaskite	Basement Granite	
Chihanga	0	2	Mbuga Clay	Clay	
Chihanga	2	4	Calcrete	Pedolith	
Chihanga	4	50	Weathered granite with Schist	Weathered Granite	38

Fig. A.28 Table of actual and interpreted borehole lithologies, and water levels, for boreholes used and mentioned in conceptual models